UNIVERSITY
OF TASMANIA

From Nuna to Gondwana: A critical assessment of the early tectonic history of Tasmania

Jacob A. Mulder
Bsc. (Hons), University of Tasmania

ARC Centre of Excellence in Ore Deposits (CODES)
School of Physical Sciences (Earth Sciences)

Submitted in fulfilment of the requirements for the degree of
Doctor of Philosophy
University of Tasmania

October 2017

Table of Contents

Table of Contents

Table of Contents

List of Figures and Tables

List of Figures and Tables

List of Appendices

Abstract

The Proterozoic geology of Tasmania (southeast Australia) preserves evidence of an exotic microcontinent accreted to the Pacific margin of Gondwana in the early Paleozoic. The location of Tasmania during the Proterozoic and the tectonic setting in which its extensive Mesoproterozoic and Neoproterozoic sedimentary sequences formed are poorly understood. The goals of this study are to (1) understand the Proterozoic tectonic setting of Tasmania in the context of supercontinent cycles, (2) use the geological record of Tasmania to test and refine paleogeographic reconstructions proposed for the supercontinents Nuna and Rodinia, and (3) understand the regional tectonic setting of middle Cambrian orogenesis in Tasmania in the context of the development of the Pacific margin of Gondwana. These goals are addressed primarily through refinements to the depositional age, stratigraphy, and provenance of Mesoproterozoic and Neoproterozoic strata in Tasmania and correlative strata on continents adjacent to Tasmania during the Proterozoic.

The oldest rocks in Tasmania include an at least 10-km-thick sequence of siliciclastic strata comprising the 1450—1300 Ma lower-middle Rocky Cape Group. Detrital zircon U-Pb-Hf isotopic data demonstrate that the lower-middle Rocky Cape Group is unlikely to have been sourced from any geological terrane exposed in present-day Australia. Instead, zircon U-Pb-Hf isotopic data from basement terranes in southwest Laurentia (Proterozoic North America) and East Antarctica show striking similarities to the lower-middle Rocky Cape Group detrital zircon signature. Integrating detrital zircon and paleocurrent data indicate that the majority of sediment in the lower-middle Rocky Cape Group was sourced from Laurentia, which was to the southeast (present-day coordinates) of Tasmania. The lower-middle Rocky Cape Group is interpreted to be the sedimentary fill of a rift basin that developed on thinned continental crust between southwest Laurentia and East Antarctica during the break up Nuna.

The lower-middle Rocky Cape Group is disconformably overlain by the late Mesoproterozoic upper Rocky Cape Group, which includes a <1260 Ma carbonate-shale sequence disconformably overlain by <1170 Ma quartz arenite and siltstone. The stratigraphy of the upper Rocky Cape Group is similar to the stratigraphy of late Mesoproterozoic basins in southwest Laurentia, which comprise 1255—1230 Ma carbonate-shale sequences disconformably overlain by 1150—1100 Ma shallow marine and terrestrial siliciclastic deposits. Detrital zircon, muscovite, and biotite from late Mesoproterozoic strata in southwest Laurentia provide a key link between intracratonic basin formation and the tectonic evolution of the Grenville Orogeny. The 1255—1230 Ma carbonate-shale sequences were deposited in a regionally extensive retroarc basin system with clastic sediment sourced in part from an active continental arc along the southern margin of Laurentia. The overlying 1140—1100 Ma siliciclastic sequences were deposited in a foreland basin system during the continent-continent collisional phase of the Grenville orogen and were sourced from unroofing thrust nappes from the structurally high parts of the orogen.

Abstract

Correlation of the upper Rocky Cape Group and late Mesoproterozoic strata in southwest Laurentia is supported by similarities in stratigraphy and the U-Pb age distribution and Hf isotope compositions of detrital zircons. This correlation suggests the upper Rocky Cape Group formed part of the extensive syn-orogenic basin system associated with the Grenville Orogeny and supports a late Mesoproterozoic position for Tasmania along the southwest margin of Laurentia. The detrital zircon provenance of late Mesoproterozoic strata in Tasmania and southwest Laurentia is similar to detrital zircon ages from basement terranes in the central Transantarctic Mountains (East Antarctica), which supports a connection between southwest Laurentia and East Antarctica within Rodinia.

The late Neoproterozoic geological record of Tasmania records rift-related magmatism and basin formation during the breakup of Rodinia. The Oonah Formation is a >5-km-thick sequence of *ca.* 730 Ma turbidites and syn-sedimentary alkalic mafic rocks that are widely exposed throughout Tasmania. Detrital zircon and monazite in the Oonah Formation were derived from reworking of Mesoproterozoic successions in Tasmania and Neoproterozoic granites on King Island (~100 km to the northwest of Tasmania). Lithological similarities and a similar detrital zircon provenance support correlation of the Oonah Formation with turbidites and shallow marine conglomerate and sandstone at the base of the late Neoproterozoic Togari Group in western Tasmania. The late Neoproterozoic tectonostratigraphic record of Tasmania is similar to that preserved along the southwest margin of Laurentia and eastern margin of East Antarctica, suggesting that Tasmania occupied a broad rift-zone between these continents during the breakup of Rodinia. Mafic magmatism and sedimentation in the Oonah Formation and Togari Group reflects relatively minor lithospheric extension during a failed rifting event. A major rifting episode at *ca.* 580 Ma isolated Tasmania as a microcontinent in the paleo-Pacific Ocean during the final breakup of Rodinia.

The 515—505 Ma Tyennan Orogeny records arc-microcontinent collision and resulted in the obduction of an ophiolite over the Proterozoic crust of Tasmania. The high-grade metamorphic sole of the Tasmanian ophiolite includes strongly deformed granulite—lower amphibolite facies mafic cumulate rocks, dolerite, and basalt. Kinematic indicators in mylonitic amphibolites record the west-directed obduction of the ophiolite and suggest the metamorphic sole formed in an east-dipping subduction zone located to the east of Tasmania. Major and trace element whole rock and relict igneous spinel geochemistry indicates that the protoliths to the metamorphic sole formed at a back arc basin spreading centre. The new data supports a model in which east-dipping subduction in Tasmania was driven by collapse of a back arc basin developed above an earlier west-dipping subduction zone outboard of the pacific margin of Gondwana. The incorporation of the Tasmanian microcontinent into Gondwana occurred in a complex geodynamic environment similar to the modern southwest pacific.

Statements and Declarations

Declaration of originality

This thesis contains no material which has been accepted for a degree or diploma by the University or any other institution, except by way of background information and duly acknowledged in the thesis, and to the best of my knowledge and belief no material previously published or written by another person except where due acknowledgement is made in the text of the thesis, nor does the thesis contain any material that infringes copyright.

Signed: **Dated:** 13/10/2017

Authority of access

This thesis may be made available for loan and limited copying and communication in accordance with the Copyright Act 1968.

Signed: **Dated:** 13/10/2017

Statement regarding published work contained in this thesis

The publishers of the papers comprising Chapters 2, 3, and 6 hold the copyright for that content and access to the material should be sought from the respective journals. The remaining non published content of the thesis may be made available for loan and limited copying and communication in accordance with the Copyright Act 1968.

Signed: **Dated:** 13/10/2017

Statements and Declarations

Statement of Authorship

List of Authors

The following people and institutions contributed to the publication of work undertaken as a part of this thesis:

Candidate: Jacob Mulder, ARC Centre of Excellence in Ore Deposits (CODES), University of Tasmania

Author 1: Sebastien Meffre, Supervisor, CODES, University of Tasmania

Author 2: Jacqueline Halpin, Supervisor, Institute for Marine and Antarctica Studies, University of Tasmania

Author 3: Ron Berry, Supervisor, CODES, University of Tasmania

Author 4: Karl Karlstrom, Department of Earth and Planetary Sciences, University of New Mexico

Author 5: Nathan Daczko, ARC Centre of Excellence for Core to Crust Fluid Systems and GEMOC, Department of Earth and Planetary Sciences, Macquarie University

Author: 6: George Gehrels, Department of Geosciences, University of Arizona

Author 7: Mark Pecha, Department of Geosciences, University of Arizona

Author 8: Christopher Spencer, Department of Applied Geology, Curtin University

Author 9: Kathryn Fletcher, New Mexico Bureau of Geology and Mineral Resources, New Mexico Institute for Technology

Author 10: Matthew Heizler, New Mexico Bureau of Geology and Mineral Resources, New Mexico Institute for Technology

Author 11: J. Michael Timmons, New Mexico Bureau of Geology and Mineral Resources, New Mexico Institute for Technology

Author 12: Laura Crossey, Department of Earth and Planetary Sciences, University of New Mexico

Author 13: John Everard, Mineral Resources Tasmania

Proportion of work undertaken towards papers

Paper 1: Mesoproterozoic Tasmania: Witness to the East Antarctica-Laurentia connection within Nuna
Located in chapter 2 (Published)

Candidate was the primary author and with authors 2 and 5 contributed to the conception and design of the research and the collection and interpretation of new data. Candidate compiled data from the literature included in the analysis and wrote the paper with revision form authors 2 and 5.

Candidate contributed approximately 90% to the planning, execution, and preparation of the work for the paper.

Paper 1: Mesoproterozoic Tasmania: Witness to the East Antarctica-Laurentia connection within Nuna REPLY
Located in chapter 2 (Published)

Candidate was the primary author and wrote the reply with revision from authors 2 and 5.

Candidate contributed approximately 95% to the planning, execution and preparation of the reply.

Paper 2: The syn-orogenic sedimentary record of the Grenville Orogeny in southwest Laurentia
Located in Chapter 3 (Published)

Candidate was the primary author and with author 4 contributed to the conception and design of the research. Candidate and authors 4, 6, 7, 9, 10, 11, and 12 collected and interpreted new data included in the paper. Candidate compiled data from the literature included in the analysis and wrote the paper with revisions from author 4 and 6.

Candidate contributed to approximately 85% to the planning, execution and preparation of the work for the paper.

Paper 3: Rodinian devil in disguise: Correlation of 1.25—1.10 Ga strata between Tasmania and Grand Canyon
Located in Chapter 4 (In preparation for submission)

Candidate was the primary author and with authors 2 and 4 contributed to the conception and design of the research. Candidate and authors 2, 3, 4, 6, 7 and 8 collected and interpreted new data included in the paper. Candidate compiled data from the literature included in the analysis and wrote the paper with revisions from authors 2, 3, 4, 6, and 8

Candidate contributed approximately 90% to the planning, execution and preparation of the work for the paper.

Paper 4: Depositional age and correlation of the Oonah Formation: Refining the timing of late Neoproterozoic basin formation in Tasmania
Located in Chapter 5 (Accepted, pending minor revision)

Candidate was the primary author and with authors 1, 2, and 3 contributed to the conception and design of the research Candidate and authors 1, 2, and 13 collected and interpreted new data included in the paper Candidate wrote the paper with revisions from authors 1, 2, 3, and 13

Candidate contributed approximately 90% to the planning, execution and preparation of the work for the paper

Paper 5: The metamorphic sole of the western Tasmanian ophiolite: New insights into the Cambrian tectonic setting of the Gondwana Pacific margin
Located in Chapter 6 (Published)

Candidate was the primary author and with authors 1, 2, and 3 contributed to the conception and design of the research Candidate and authors 1, 2, and 3 collected and interpreted new data included in the paper Candidate wrote the paper with revisions from authors 1, 2, and 3

Candidate contributed approximately 90% to the planning, execution and preparation of the work for the paper

We the undersigned agree with the above stated "proportion of work undertaken" for each of the above published peer-reviewed papers (or papers in preparation) contributing to the thesis.

Signed.

Sebastien Meffre	Leonid Danyushevsky
Supervisor	Head of Discipline, Earth Sciences
School of Physical Sciences	School of Physical Sciences
University of Tasmania	University of Tasmania

Date. 13/10/17 13/10/17

Publications during the course of this thesis (2014–2017)

Journal articles:

Mulder, J. A., Halpin, J. A., and Daczko, N. R., 2015. Mesoproterozoic Tasmania: Witness to the East Antarctica-Laurentia connection within Nuna. *Geology,* v. 43*,* 759–762.

Mulder, J. A., Berry, R. F., and Scott, R. J., 2015. The structure and metamorphism of the Red Point Metamorphic Complex–A newly discovered high-pressure metamorphic complex from the south coast of Tasmania. *Australian Journal of Earth Sciences,* v. 62*,* 969–983.

Mulder, J. A., Halpin, J. A., and Daczko, N. R., 2016. Mesoproterozoic Tasmania: Witness to the East Antarctica-Laurentia connection within Nuna: REPLY. *Geology,* v. 44.

Mulder, J. A., Berry, R. F., Meffre, S., and Halpin, J. A., 2016. The metamorphic sole of the western Tasmanian ophiolite: New insights into the Cambrian tectonic setting of the Gondwana Pacific margin. *Gondwana Research,* v. 38*,* 351–369.

Mulder, J. A., Karlstrom, K. E. Fletcher, K., Heizler, M. T., Timmons, J. M., Crossey, L. J., Gehrels, G. E., and Pecha, M., 2017. The syn-orogenic sedimentary record of the Grenville Orogeny in southwest Laurentia. *Precambrian Research,* v. 294, 33–52.

Conference presentations:

Mulder, J. A., Berry, R. F., and Scott, R. J., 2014. The structure and metamorphism of the Red Point Metamorphic Complex–A newly discovered high-pressure metamorphic complex from the south coast of Tasmania. Biennial Conference of the Specialist Group for Tectonics and Structural Geology (SGTSG), Thredbo, Australia, 2–8 February, GSA Abstracts no. 109.

Mulder, J. A., Halpin, J. A., and Daczko, N. R., 2015. Mesoproterozoic Tasmania: Witness to the East Antarctica-Laurentia connection within Nuna. Biennial Conference of the Specialist Group for Tectonics and Structural Geology (SGTSG), Thredbo, Australia, 2–8 February, GSA Abstracts no. 113.

Mulder, J. A., Berry, R. F., Meffre, S., and Halpin, J. A., 2015. The metamorphic sole of the western Tasmanian ophiolite: New insights into the Cambrian tectonic setting of the Gondwana Pacific margin. Biennial Conference of the Specialist Group for Tectonics and Structural Geology (SGTSG), Thredbo, Australia, 2–8 February, GSA Abstracts no. 113.

Mulder, J. A., Karlstrom, K. E. Fletcher, K., Heizler, M. T., Timmons, J. M., Crossey, L. J., Gehrels, G. E., and Pecha, M., 2016. Provenance of the Mesoproterozoic Unkar Group and Correlates: A record of the tectonic evolution of the Grenville Orogeny in southern Laurentia. Geological Society of America Annual Meeting, Denver, Colorado, USA, 25—28 September. Geological Society of America Abstracts with Programs. v. 48, No. 7 doi: 10.1130/abs/2016AM-283468

Mulder, J. A., Karlstrom, K. E. Halpin, J. A., Jones, J. V., Holland, M. E., 2016. The Mesoproterozoic sedimentary record of long-term Australian/Antarctic,Laurentian connections (Invited Presentation). Geological Society of America Annual Meeting, Denver, Colorado, USA, 25—28 September. Geological Society of America Abstracts with Programs, v. 48, No. 7 doi: 10.1130/abs/2016AM-287780

Mulder, J.A., Karlstrom, K. E., Halpin, J. A., Spencer, C. J., Berry, R. F., Gehrels, G. E., Pecha, M., 2017. Rodinian devil in disguise: Correlation of 1.25—1.10 Ga strata between Tasmania and Grand Canyon. European Geosciences Union General Assembly. Vienna, Austria, 23—28 April.

Mulder, J. A., Karlstrom, K. E., Halpin, J. A., Spencer, C. J., Berry, R. F., Gehrels, G. E., Pecha, M., 2017. Rodinian devil in disguise: Correlation of 1.25—1.10 Ga strata between Tasmania and Grand Canyon. IGCP Project 648: Rodinia 2017 Conference, Townsville, Australia, 11—14 June.

Acknowledgements

Over the past three and a half years I've had the privilege to turn an idea that had intrigued me long before I knew anything about geology into a research project that has taken me to places I could never have imagined and let me work with the most amazing people I have met.

For this opportunity, I am indebted to my supervisors. Getting to work with such a friendly and talented group of people who have wanted nothing more than the best for me is truly humbling and something I'll always be grateful for. Sebastien, thank you for getting this project off the ground, for always making time for me, and for your infectious enthusiasm for geology. I always leave our meetings slightly overwhelmed but never disheartened. Jacqui, a special thanks for taking me under your wing early in this project, showing me what the world of research is all about, and for working so hard to open up such incredible opportunities for me. This project would never have got as far as it did without you. Thank you Ron for your enthusiasm for this project, for your amazing ability to make even the subtlest flaw in logic look glaringly obvious, and for knowing something (maybe everything?) about everything. Your rigour as a scientist is something I will always aspire to. Rob, thanks for your unquestioned support, for always challenging me to get the best out of myself, and for pointing me down the path towards a career in research from the very beginning. Thanks to Karsten, Sandrin, and Jay for your help in the lab and for always answering my questions with enthusiasm. A special thanks to all the staff and students at CODES and the School of Earth Sciences who have created such a friendly environment to work in. Thanks also to Mike Hall, John Everard, Andrew McNeill, Grace Cumming, and Clive Calver for sharing your passion and knowledge of the geology of Tasmania with me.

My sincere thanks to Karl for taking me on as a student on nothing more than a few vague emails and for giving me the opportunity to do research in the most amazing place on Earth. Working with you was as exciting an experience as it was inspiring and my year in New Mexico has helped me grow so much as a scientist and as a person. A further thanks to you and Laurie for making me feel so welcome and for encouraging me to see as much as I could— I've fallen in love with the southwest and can't wait to get back. Thanks to Mark for getting me on my feet in the States and for sharing in a beer, a game of Ping-Pong, and the struggles of working in Karl's shadow.

To my family, I can't thank you enough for your infinite support and love, and for knowing how much this project meant to me and for letting me sacrifice so much to complete it. To Rosalind, thanks for your patience and understanding, particularly over the past year. Finally, thanks to my close mates for actively showing a disinterest in geology, I wouldn't have made it through if you had let me think about rocks all day everyday.

Chapter 1

Introduction

1.0 Preamble

The assembly and dispersal of supercontinents over a ~500 million-year cycle has had a first order influence on the development of Earth's crust since the Archean (Bradley, 2011; Hawkesworth et al., 2010; Cawood et al., 2013a; Nance et al., 2014). Understanding the paleogeography of supercontinents provides key insights into the tectonic processes and time-scales over which they assemble and disperse (e.g., Hoffman, 1991; Murphy & Nance, 2008; Li et al., 2008; Stampfli et al., 2013; Merdith et al., 2017). The configuration of continents within the most recent supercontinent, Pangea, can be reconstructed in relative detail thanks to the preserved record of oceanic crust produced during its breakup (e.g., Veevers, 2004; Seton et al., 2012; Mueller et al., 2016). However, the lack of a seafloor record prior to Pangea renders the accurate paleogeographic reconstruction of older supercontinents difficult (Evans, 2013).

A critical dataset for refining the paleogeography of pre-Pangean supercontinents comes from establishing links between ancient continental blocks by identifying similarities in their geological records. Most paleogeographic reconstructions of the pre-Pangean supercontinents Nuna, Rodinia, and Gondwana (Fig. 1.1) have focused on identifying geological tie points between their largest constituent blocks (e.g., Veevers, 2004; Li et al., 2008; Zhang et al., 2012). However, the relative configurations of even large continents prior to Pangea is vigorously debated as geological connections are based on the fragmentary rock record of Earth's crust, which is rarely preserved in enough detail to establish unequivocal tie points.

In order to maximise the geological data available for testing connections between the larger continental blocks, supercontinent reconstructions should also incorporate the geological record of smaller crustal blocks such as microcontinents. The formation of microcontinents is a natural consequence of continental rifting during the breakup of supercontinents (e.g., Muller et al., 2001; Whittaker et al., 2016) and they may subsequently be incorporated into orogenic systems formed during the assembly of supercontinents (e.g., Keppie et al., 2003; von Raumer et al., 2003; Torsvik and Cocks, 2013). Therefore, the geological record of a microcontinent has the potential to provide key insight into relative changes in global paleogeography during the transition from one supercontinent into another as the tectonic history of a microcontinent must be accommodated by surrounding continental blocks (Cawood et al., 2013b). Microcontinents can also preserve a crustal record that has been strongly modified or removed from formerly adjacent continents, which further highlights their potential to provide key links between larger continents through time (e.g., Li et al., 2002; Lowry et al., 2011; Wen et al., 2017). Finally, placing a microcontinent within the paleogeographic framework of a supercontinent reconstruction can give greater insight into changes in its large-scale tectonic setting through time than can be achieved by studying the geological history of the microcontinent in isolation.

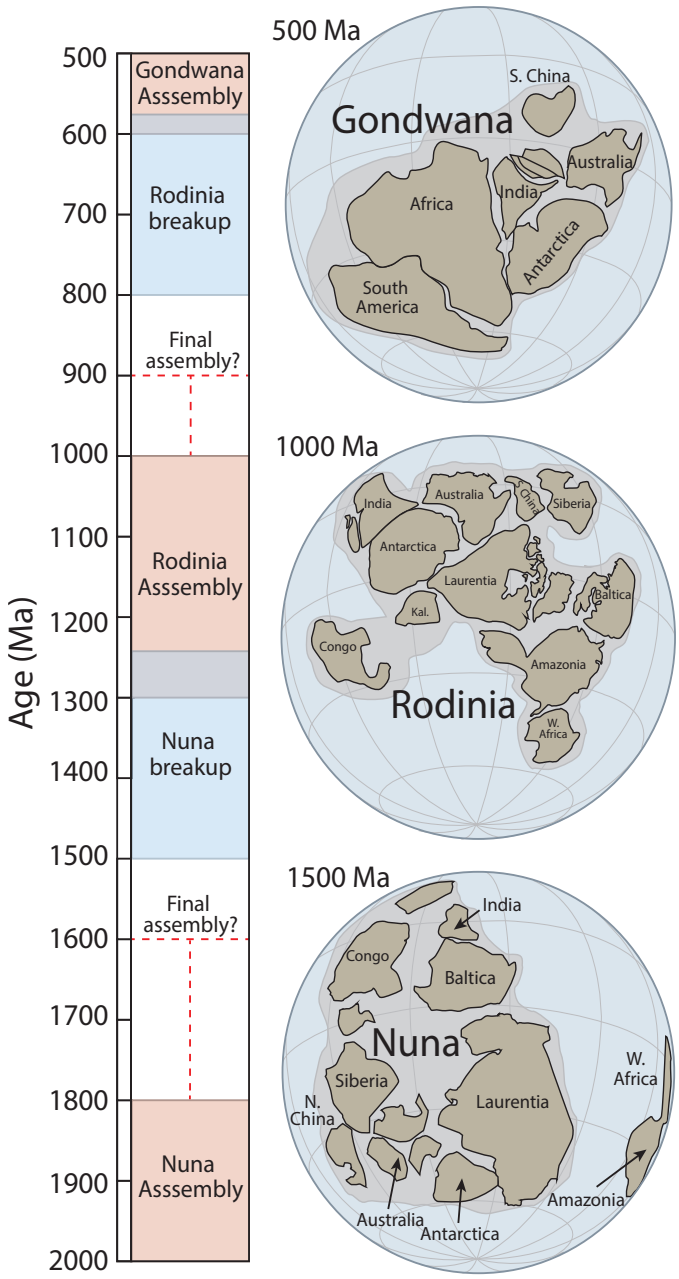

Figure 1.1: Timeline for the assembly and dispersal of pre-Pangean supercontinents. Nuna reconstruction after Pisarevsky et al. (2014), Rodinia reconstruction after Goodge et al. (2008), Gondwana reconstruction after Torsvik and Cocks (2013).

This study focuses on understanding the early tectonic history of a Proterozoic microcontinent exposed in western Tasmania (southeast Australia) in the context of pre-Pangean supercontinent cycles. The Tasmanian microcontinent lies within an extensive latest Neoproterozoic—Cambrian accretionary orogen that developed along the Pacific margin of Gondwana following the breakup of Rodinia (Fig. 1.2; Glen, 2005; Cawood, 2005). Although Tasmania had been incorporated into Gondwana and achieved its present-day position with respect to Australia by the end of the Cambrian (Li et al., 1997; Cayley, 2011), its location during the Proterozoic is less certain.

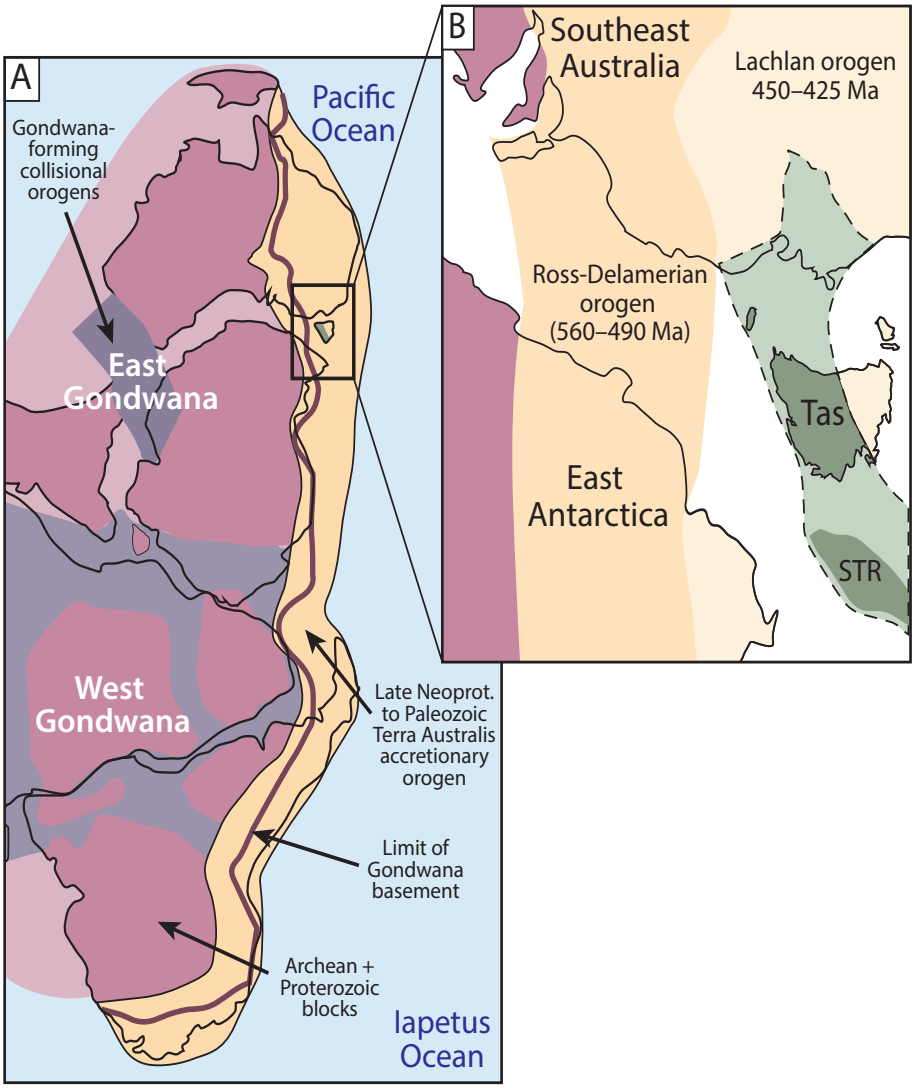

Figure 1.2: Paleogeography of the Tasmanian microcontinent in Gondwana. (A) Simplified paleogeographic reconstruction of Gondwana showing Archean and Proterozoic blocks (purple) sutured by late Neoproterozoic—early Paleozoic collisional orogens (grey) and the extensive Terra Australis accretionary orogen developed along the Pacific and Iapetus margins of the supercontinent (orange). After Cawood (2005). (B) Late Cambrian paleogeography of southeast Australia and East Antarctica showing the position of Proterozoic crust in Tasmania (green with dashed outline) embedded within late Neoproterozoic—Paleozoic accretionary orogens. After Cayley (2011). Neoprot. — Neoproterozoic, STR— South Tasman Rise.

1.1 Tasmania in pre-Pangean supercontinents

Proterozoic rocks are widely exposed throughout western Tasmania and include a volumetrically-dominant older package of siliciclastic strata comprising the marginal marine Rocky Cape Group and correlatives and laterally equivalent turbidite sequences on King Island to the northwest of Tasmania (Fig. 1.3; Spry, 1962; Gee, 1967; Brown, 1986; Turner, 1989; Calver et al., 2014). These older strata are unconformably overlain by a late Neoproterozoic sequence of carbonate, shale, and rift-related mafic rocks comprising the Togari Group and correlatives (Fig. 1.3; Turner, 1989; Everard et al., 2007; Calver et al., 2014).

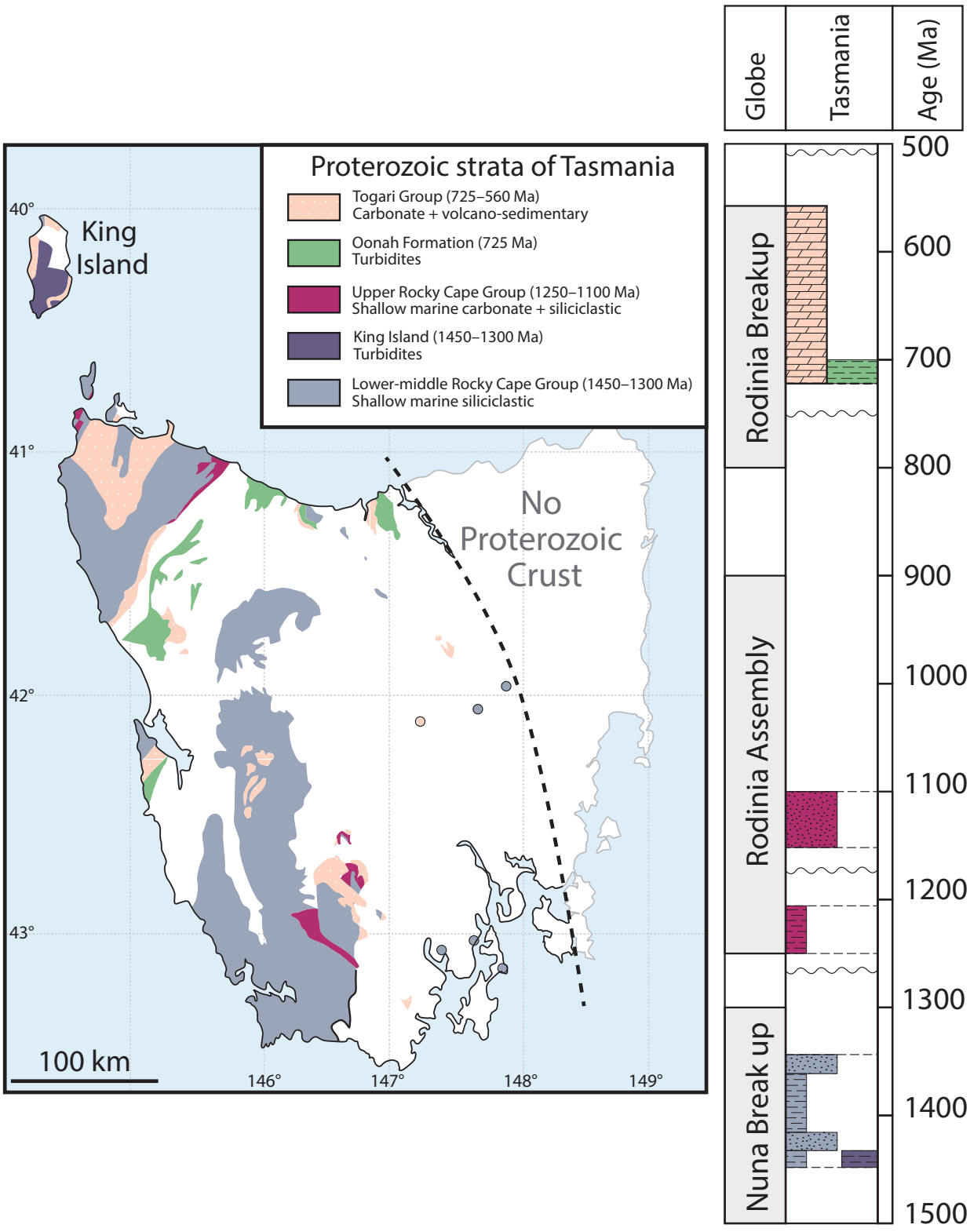

Figure 1.3: Simplified Proterozoic geology of Tasmania. Map shows distribution of exposed Proterozoic tectonostratigraphic packages, modified from Calver et al. (2014). Stratigraphic column on the right shows the age range of Proterozoic rocks in Tasmania in the context of the Nuna and Rodinia supercontinent cycles, colour of rock units as per map legend.

Early studies on the Proterozoic paleogeography of Tasmania focused on establishing links with the Neoproterozoic and early Paleozoic geology of southeast Australia (e.g., Powell et al., 1994; Calver, 1998; Preiss, 2000). Correlation of the late Neoproterozoic Togari Group in Tasmania with time-equivalent strata in the Adelaide Rift Complex of southeast Australia was proposed on the basis of lithological and chemostratigraphic similarities (Calver, 1998; Calver & Walter, 2000). The Adelaide Rift Complex formed when another continent, generally interpreted to be Laurentia (Proterozoic North America), separated from the eastern margin of the combined Australia-Antarctica landmass during the breakup of Rodinia (e.g., Preiss, 2000; Li et al., 2008). Correlation of Togari Group with the Adelaide Rift Complex therefore implied that Tasmania occupied a central location between Australia-Antarctica and western Laurentia within the supercontinent Rodinia.

Following the earlier links proposed between Tasmania and the Adelaide Rift Complex, further work in the early 2000's provided support for a Neoproterozoic position for Tasmania between Australia-Antarctica and western Laurentia, which included: (1) similarities in the detrital zircon provenance of the Rocky Cape Group, of assumed early Neoproterozoic age, to Neoproterozoic and Cambrian sandstones in southwest Laurentia (Burrett & Berry, 2000; Berry et al., 2001; Black et al., 2004), (2) cryptic evidence of late Mesoproterozoic—early Neoproterozoic metamorphism and magmatism in Tasmania (Fioretti et al. 2005; Berry et al., 2005, 2008), which was linked to the Grenville orogen in southern Laurentia and its possible continuation into central Australia or East Antarctica (e.g., Karlstrom et al., 1999; Goodge et al., 2010), and (3) evidence for late Neoproterozoic magmatism in Tasmania between *ca*. 780 and 580 Ma (e.g., Black et al., 1997; Calver et al., 2004; Meffre et al., 2004; Holm et al., 2003), which temporally overlaps with rifting in eastern Australia-Antarctica and western Laurentia attributed to the breakup of Rodinia (Li et al., 2008). In the consensus model of Rodinia produced during the International Geoscience Programme Project (IGCP) 440: Rodinia Assembly and Breakup (Fig. 1.4A), Tasmania was regarded as a Mesoproterozoic—Neoproterozoic terrane located between eastern Australia-Antarctica and western Laurentia (Fig. 1.4B; Li et al., 2008).

A major breakthrough in understanding the significance of Tasmania in Proterozoic supercontinent reconstructions was the discovery that the majority of the most widespread Proterozoic sequence in Tasmania (the Rocky Cape Group and correlatives) was deposited between 1450—1300 Ma (Calver et al., 2010; Halpin et al., 2014). The revised age of the Rocky Cape Group suggested the connection between Tasmania and Laurentia inferred from its detrital zircon provenance (e.g., Berry et al., 2001) significantly predated the assembly of Rodinia. Instead, the lower and middle parts of the Rocky Cape Group were deposited during the breakup of the supercontinent Nuna, before the formation of Rodinia. Halpin et al. (2014) showed that the detrital zircon provenance of the lower-middle Rocky Cape Group is strikingly similar to time-equivalent strata in the upper Belt-Purcell Supergroup, which supports a connection between Tasmania and western Laurentia within Nuna.

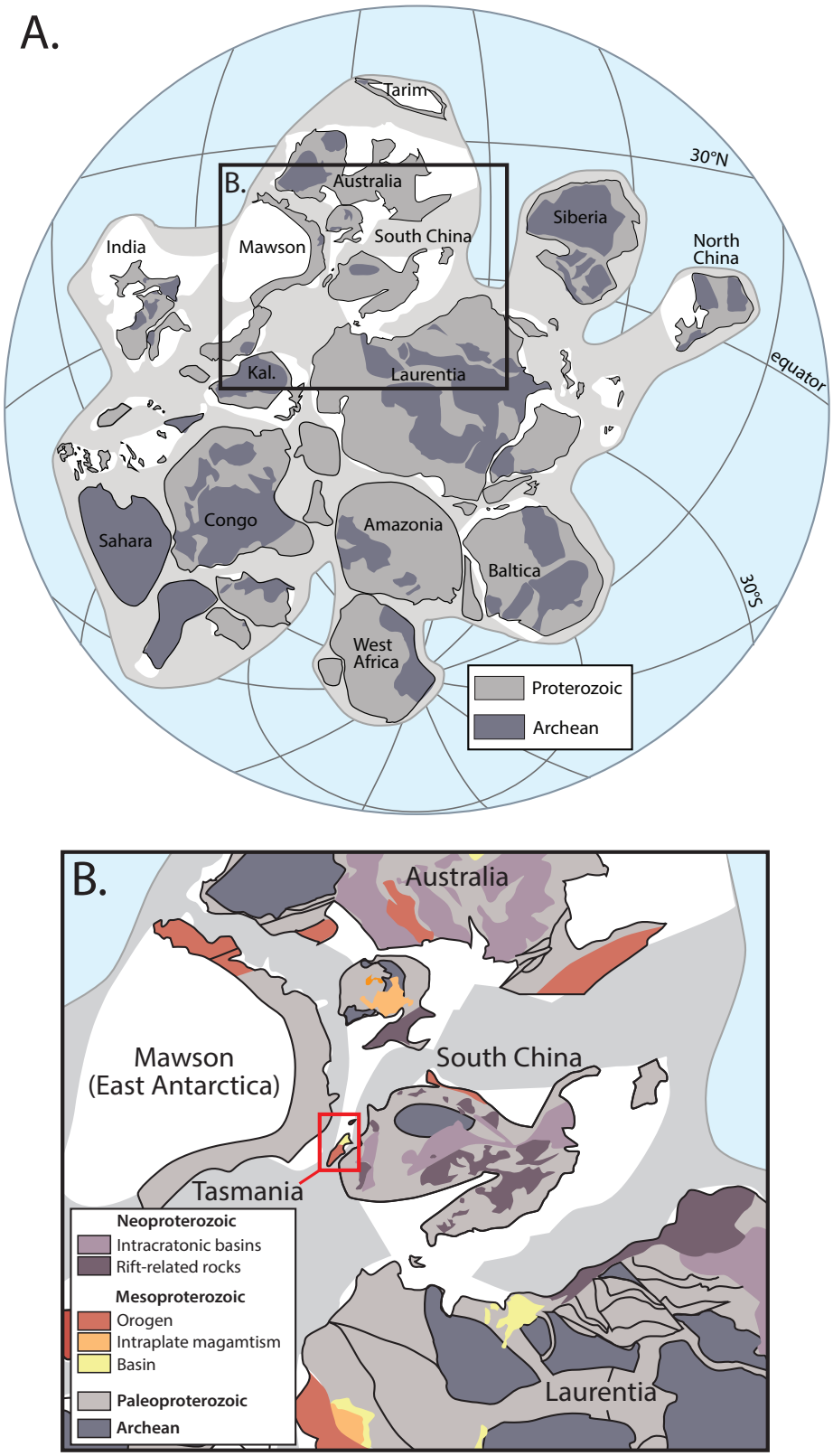

Figure 1.4: Position of Tasmania in Rodinia. (A) Consensus model of Rodinia produced during IGCP Project 440: Rodinia Assembly and Breakup. Modified from Li et al. (2008). (B) Enlargement of consensus model of Rodinia showing Tasmania as a Mesoproterozoic—Neoproterozoic terrane between eastern Australia-Antarctica and western Laurentia. Modified from Li et al. (2008).

1.2 Research aims and thesis structure

Tasmania preserves an extensive Proterozoic geological record that spans three pre-Pangean supercontinents; Nuna, Rodinia, and Gondwana. Previous work has established that Tasmania has Mesoproterozoic and Neoproterozoic affinities with both Australia-Antarctica and Laurentia, making it a key location for testing hypothesised connections between these continents within Nuna and Rodinia. The arrival of the Tasmanian microcontinent into its present-day position in southeast Australia also has the potential to provide important insight into the early development of the Pacific margin of Gondwana.

This study presents a detailed examination of the early tectonic history of Tasmania and explores its potential as a key location for testing paleogeographic reconstructions of Nuna, Rodinia, and Gondwana. The specific aims of this study are to:

(1) Understand the Proterozoic tectonic setting of Tasmania in the context of supercontinent cycles.

(2) Use the geological record of Tasmania to test and refine paleogeographic reconstructions proposed for Nuna and Rodinia.

(3) Understand the regional tectonic setting of middle Cambrian orogenesis in Tasmania in the context of the development of the Pacific margin of Gondwana.

These aims are addressed primarily through refinements to the depositional age, stratigraphy, and provenance of Mesoproterozoic and Neoproterozoic strata in Tasmania and correlative strata on continents adjacent to Tasmania during the Proterozoic.

Following this introductory chapter, the results of this study are presented in five research chapters focusing on specific rock packages that provide insight into the position and tectonic setting of Tasmania within Nuna, Rodinia, and Gondwana. The research chapters are presented in the form of papers that have been published or are being prepared for publication in peer-reviewed scientific journals. The papers have been reformatted for inclusion in this thesis but the content has not been altered from the published form. The papers include either American English or British English as required by the respective journals. A summary of the research chapters and their relevance to the overall aims of this study are as follows:

Chapter 2:
Mulder, J. A., Halpin, J. A., Daczko. N. R., (2015) 'Mesoproterozoic Tasmania: Witness to the East Antarctica-Laurentia connection within Nuna', *Geology*, v. 43, 759—762.

This paper presents new detrital zircon U-Pb-Hf isotopic data and compiled paleocurrent data from the lower-middle Rocky Cape Group with the aim of exploring Tasmania's position and wider

tectonic setting within the supercontinent Nuna. These data support the interpretation that the lower-middle Rocky Cape Group was sourced from basement terranes in southwest Laurentia and the southern parts of the Mawson Continent (East Antarctica). The lower-middle Rocky Cape Group is interpreted as an east-facing passive margin developed along the southern Mawson Continent (East Antarctica) as it rifted from southwest Laurentia during the breakup of Nuna.

A reply to a comment on this paper by Moore & Betts (2016) is included at the end of Chapter 2. The reply emphasises the geological evidence supporting the proposed position of Tasmania in Nuna and highlights the importance of the late Mesoproterozoic geology of Tasmania for understanding changes in global paleogeography during the transition into Rodinia.

Chapter 3:
Mulder, J. A., Karlstrom, K. E., Fletcher, K., Heizler, M. T., Timmons, J. M., Crossey, L. J., Gehrels, G. E., Pecha, M., (2017) 'The syn-orogenic sedimentary record of the Grenville Orogeny in southwest Laurentia', *Precambrian Research*, v. 294, 33—52.

This paper stems from research focusing on understanding the source of <1300 Ma detrital zircons in the upper parts of the Rocky Cape Group, which is specifically addressed in Chapter 4. New detrital zircon, muscovite, and biotite data are presented from a series of late Mesoproterozoic basins in southwest Laurentia that are thought to be broadly time-equivalent to the upper Rocky Cape Group. The new data support regional correlations between the late Mesoproterozoic strata of southwest Laurentia and refine the tectonic setting of these basins, which leads to a new model linking intracratonic sedimentation to the tectonic evolution of the late Mesoproterozoic Grenville orogen of southern Laurentia. This paper highlights that the late Mesoproterozoic basin system in southwest Laurentia preserves a remarkably uniform stratigraphy and detrital zircon provenance across a regionally extensive area and concludes by suggesting that extensions of this basin system should be readily identified on continents adjacent to southwest Laurentia within Rodinia.

Chapter 4:
Mulder, J. A., Karlstrom, K. E., Halpin, J. A., Spencer, C. J., Berry, R. F., Gehrels, G. E., Pecha, M. 'Rodinian devil in disguise: Correlation of 1.25—1.10 Ga strata between Tasmania and Grand Canyon', (In preparation for submission to *Geology*).

The late Mesoproterozoic tectonic setting and position of Tasmania within Rodinia are explored in this paper by proposing correlation of the upper Rocky Cape Group with the late Mesoproterozoic basins of southwest Laurentia discussed in Chapter 3. Striking similarities in stratigraphy and detrital zircon provenance support correlation of the upper Rocky Cape Group with late Mesoproterozoic strata in southwest Laurentia. This correlation supports a late Mesoproterozoic position for Tasmania along the southwest margin of Laurentia with the upper Rocky Cape Group deposited in the foreland of the Grenville orogen. The detrital zircon provenance of the westerly-derived upper parts of the

upper Rocky Cape Group is similar to basement terranes in the central Transantarctic Mountains, which supports a connection between southwest Laurentia and East Antarctica during the assembly of Rodinia.

Chapter 5:
Mulder, J. A., Berry, R. F., Halpin, J. H., Meffre, S., Everard, J. L. 'Depositional age and correlation of the Oonah Formation: Refining the timing of late Neoproterozoic basin formation in Tasmania', (Accepted, pending minor revision: *Australian Journal of Earth Science)*.

The depositional age and provenance of the enigmatic Oonah Formation is refined in this paper through U-Pb dating of magmatic apatite from syn-sedimentary mafic volcanic rocks and detrital zircon and monazite from the host sedimentary sequences. The new data are consistent with a late Neoproterozoic depositional age for the Oonah Formation and support correlation of the Oonah Formation with the lower Togari Group in western Tasmania. Rift-related magmatism and sedimentation recorded by the Oonah Formation and lower Togari Group are interpreted to reflect a failed continental rifting event in Tasmania related to the early stages of the breakup of Rodinia. The stratigraphy and provenance of the Oonah Formation-lower Togari Group are similar to late Neoproterozoic strata in southwest Laurentia and the central Transantarctic Mountains, which supports a southwest Laurentia-Tasmania-East Antarctica connection within Rodinia.

Chapter 6: Mulder, J. A., Berry, R. F., Meffre, S., Halpin, J. A. (2016). 'The metamorphic sole of the western Tasmanian ophiolite: New insights into the Cambrian tectonic setting of the Gondwana Pacific margin', *Gondwana Research*, v. 38, 351—369.

The goal of this paper is to better understand the wider geodynamic setting of the middle Cambrian Tyennan Orogeny in Tasmania in the context of the development of the Pacific margin of Gondwana. The paper presents an integrated study of the field relationships, geochemistry, petrology, pressure-temperature evolution, and structural history of the high-grade metamorphic sole of a Cambrian ophiolite in Tasmania. The detailed geological history recorded by this metamorphic sole indicates that the emplacement of the ophiolite and the incorperation of the Tasmanian microcontinent into Gondwana occurred in a complex geodynamic environment similar to the modern-day southwest Pacific region.

The final synthesis chapter (Chapter 7) summarises the progress made towards achieving the aims of this study and presents a new tectonic model for the Mesoproterozoic to early Paleozoic tectonic evolution of Tasmania. The thesis concludes by highlighting new research questions arising from this study and identifies prospective avenues for future research on the Proterozoic geology of Tasmania.

1.3 References

Bradley, D. C., 2011. Secular trends in the geologic record and the supercontinent cycle: Earth-Science Reviews, v. 108, 16–33.

Berry, R. F., Jenner, G. A., Meffre, S., and Tubrett, M. N., 2001. A North American provenance for Neoproterozoic to Cambrian sandstones in Tasmania? Earth Planetary Science Letter, v. 192, 207–222.

Berry, R. F., Holm, O. H., and Steele, D. A., 2005. Chemical U–Th–Pb monazite dating and the Proterozoic history of King Island, southeast Australia. Australian Journal of Earth Science, v. 52, 461–471.

Berry, R. F., Steele, D. A., and Meffre, S., 2008. Proterozoic metamorphism in Tasmania: implications for tectonic reconstructions. Precambrian Research, v. 166, 387–396.

Black, L. P., Seymour, D. B., Corbett, K. D., Cox S. E., Streit, J. E., Bottrill R. S., Calver C. R., Everard J. L., Green G. R., McClenaghan, M. P., Pemberton, J., Taheri, J. and Turner, N. J., 1997. Dating Tasmania's oldest geological events. Australian Geological Survey Organisation Record 1997/15, Canberra ACT.

Black, L. P., Calver, C. R., Seymour, D. B., and Reed, A., 2004. SHRIMP U–Pb detrital zircon ages from Proterozoic and Early Palaeozoic sandstones and their bearing on the early geological evolution of Tasmania. Australian Journal of Earth Science, v. 51, 885–900.

Brown A. V., 1986. Geology of the Dundas-Mt Lindsay-Mt Youngbuck region. Tasmania Department of Mines Bulletin 62.

Burrett, C., and Berry, R., 2000. Proterozoic Australia–Western United States (AUSWUS) fit between Laurentia and Australia. Geology, v. 28, 103–106.

Calver, C. R., 1998. Isotope stratigraphy of the Neoproterozoic Togari Group, Tasmania. Australian Journal of Earth Science, v. 45, 865–874.

Calver, C. R., and Walter, M. R., 2000. The late Neoproterozoic Grassy Group of King Island, Tasmania: correlation and palaeogeographic significance. Precambrian Research, v. 100, 299–312.

Calver, C. R., Black, L.P., Everard, J.L., and Seymour, D. B., 2004. U–Pb zircon age constraints on late Neoproterozoic glaciation in Tasmania. Geology, v. 32, 893–896.

Calver C. R., Grey K., and Laan, M., 2010. The 'string of beads' fossil (Horodyskia) in the mid-Proterozoic of Tasmania. Precambrian Research, v. 180, 18–25.

Calver, C. R., Everard, J. L., Berry, R. F., Bottrill, R. S., and Seymour, D. B., 2014. Proterozoic Tasmania. In: Corbett, K.D., Quilty, P.G., and Calver, C.R. (Eds.), Geological Evolution of Tasmania. Geological Society of Australia, Special Publication, v. 24. Geological Society of Australia (Tasmania Division), 34–94.

Cawood, P. A., 2005. Terra Australis Orogen: Rodinia breakup and development of the Pacific and Iapetus margins of Gondwana during the Neoproterozoic and Paleozoic. Earth-Science Reviews, v. 69, 249–279.

Cawood, P. A., Hawkesworth, C. J., and Dhuime, B., 2013a. The continental record and the generation of continental crust: Geological Society of America Bulletin, v. 125, 14–32.

Cawood, P. A., Wang, Y., Xu, Y., and Zhao, G., 2013b. Locating South China in Rodinia and Gondwana: A fragment of great India lithosphere? Geology, v. 41, 903–906.

Cayley, R. A., 2011. Exotic crustal block accretion to the eastern Gondwanaland margin in the Late Cambrian– Tasmania, the Selwyn Block, and implications for the Cambrian-Silurian evolution of the Ross, Delamerian and Lachlan Orogens. Gondwana Research, v. 19, 628–649.

Evans, D. A. D., 2013. Reconstructing pre-Pangean supercontinents. Geological Society of America Bulletin, v. 125, 1735–1751.

Everard, J. L., Seymour, D. B., Reed, A. R., McClenaghan, M. P., Green, D. C., Calver, C. R., and Brown, A. V., 2007. Regional Geology of the southern Smithton Synclinorium: Explanatory Report for the Roger, Sumac & Dempster 1:25,000 map sheets, far northwestern Tasmania, 1:25,000 Scale Digital Geological Map Series Explanatory Report 2. Mineral Resources Tasmania, Hobart, pp. 237.

Fioretti, A. M., Black L. P., Foden J. and Visona, D., 2005. Grenville-age magmatism at the South Tasman Rise (Australia): a new piercing point for the reconstruction of Rodinia. Geology, v. 33, 769–772.

Gee, R. D., 1967. The tectonic evolution of the Rocky Cape Geanticline. PhD Thesis [unpub.], University of Tasmania.

Glen, R. A., 2005. The Tasmanides of eastern Australia. In Vaughan, A. P. M., Leat, P. T., and Pankhurst, R. J. (Eds.) Terrane Processes at the Margins of Gondwana. Geological Society, London, Special Publications, v. 246, 23–96.

Goodge, J. W., Vervoort, J. D., Fanning, C. M., Brecke, D. M., Farmer, G. L., Williams, I. S., Myrow, P. M., and DePaolo, D. J., 2008. A positive test of East Antarctica–Laurentia juxtaposition within the Rodinia supercontinent: Science, v. 321, 235–240.

Goodge, J. W., Fanning, C. M., Brecke, D. M., Licht, K. J., and Palmer, E. F., 2010. Continuation of the Laurentian Grenville province across the Ross Sea margin of East Antarctica. Journal of Geology, v. 118, 601–619.

Hawkesworth, C. J., Dhuime, B., Pietranik, A. B., Cawood, P. A., Kemp, A. I. S., and Storey, C. D., 2010. The generation and evolution of the continental crust: Geological Society of London Journal, v. 167, 229–248.

Halpin, J. A., Jensen, T., McGoldrick, P., Meffre, S., Berry, R. F., Everard, J. L., Calver, C. R., Thompson, J., Goemann, K., and Whittaker, J. M., 2014. Authigenic monazite and detrital zircon dating from the Proterozoic Rocky Cape Group, Tasmania: Links to the Belt-Purcell Supergroup, North America. Precambrian Research, v. 250, 50–67.

Hoffman, P. F., 1991. Did the breakout of Laurentia turn Gondwanaland inside-out? Science, v. 252, 1409–1412.

Holm, O. H., Crawford, A. J. and Berry, R. F., 2003. Geochemistry and tectonic settings of meta-igneous rocks in the Arthur Lineament and surrounding area, northwest Tasmania. Australian Journal of Earth Sciences, v. 50, 903–918.

Karlstrom, K. E., Williams, M. L., Mclelland, J., Geissmanm J. W. and Ahall, K., 1999. Refining Rodinia: geologic evidence for the Australia–western U.S. connection in the Proterozoic. GSA Today, v. 9, 1–7.

Keppie, J. D., Nanec, R. D., Murphy, B. J., and Dostal, J., 2003. Tethyan, Mediterranean, and Pacific analogues for the Neoproterozoic—Paleozoic birth and development of peri-Gondwanan terranes and their transfer to Laurentia and Laurussia. Tectonophysics, v. 365, 195—219.

Li, Z.-X., Baillie, P. W., and Powell, C., McA., 1997. Relationship between northwestern Tasmania and East Gondwanaland in the Late Cambrian/Early Ordovician: Paleomagnetic evidence. Tectonics, v. 16, 161–171.

Li, Z.-X., Li, X.-H., Zhou, H., and Kinny, P.D., 2002. Grenvillian continental collision in south China: New SHRIMP U-Pb zircon results and implications for the configuration of Rodinia: Geology, v. 30, 163–166.

Li, Z. -X., Bogdanova, S. V., Collins, A. S., Davidson, A., De Waele, B., Ernst, R. E., Fitzsimons, I. C. W., Fuck, R. A., Gladkochub, D. P., Jacobs, J., Karlstrom, K. E., Lu, S., Natapov, L. M., Pease, V., Pisarevsky, S. A., Thrane, K., and Vernikovsky, V., 2008. Assembly, configuration, and break-up history of Rodinia: a synthesis. Precambrian Research, v. 160, 179–210.

Loewy, S. L., Dalziel, I. W. D., Pisarevsky, S., Connelly, J. N., Tait, J., Hanson, R. E., and Bullen, D., 2011. Coats Land crustal block, East Antarctica: A tectonic tracer for Laurentia? Geology, v. 39, 859–862.

Meffre, S., Direen, N. G., Crawford, A. J., and Kamenetsky, V., 2004. Mafic volcanic rocks on King Island, Tasmania: evidence for 579 Ma break-up in east Gondwana. Precambrian Research, v. 135, 177–191.

Merdith, A. S., Collins, A. S., Williams, S. E., Pisarevsky, S., Foden, J. F., Archibald, D., Blades, M. L., Alessio, B. L., Armistead, S., Plavsa, D., Clark, C., and Müller, R. D., 2017. A full-plate global reconstruction of the Neoproterozoic. Gondwana Research, In Press.

Moore, D. H., and Betts, P. G., 2016. Mesoproterozoic Tasmania: Witness to the East Antarctica–Laurentia connection within Nuna: Comment: Geology, v. 44.

Müller, R. D, Gaina, C., Roest, W. R., and Lundbek Hansen, D., 2001. A recipe for microcontinent formation. Geology, v. 29, 203–206.

Müller, R. D, Seton, M., Zahirovic, S., Williams, S. E., Matthews, K. J., Wright, N. M., Shepard, F. E., Maloney, K. T., Barnett-Moore, N., Hosseinpour, M. Bower, D. J., and Cannon, J., 2016. Ocean Basin Evolution and Global-Scale Plate Reorganization Events Since Pangea Breakup. Annual Reviews in Earth and Planetary Science, v. 44, 107–138.

Murphy, J. B., and Nance, R. D., 2008. The Pangea conundrum. Geology, v. 36, 703–706.

Nance, R. D., Murphy, J. B., and Santosh, M., 2014. The supercontinent cycle: A retrospective essay. Gondwana Research, v. 25, 4–29.

Pisarevsky, S. A., Elming, S. -Å., Pesonen, L. J., and Li, Z. -X., 2014. Mesoproterozoic paleogeography: Supercontinent and beyond: Precambrian Research, v. 244, p. 207–225.

Powell, C., McA., Preiss, W. V., Gatehouse, C. G., Krapez, B., and Li, Z. -X., 1994. South Australian record of a Rodinian epicontinental basin and its mid-Neoproterozoic breakup (~700 Ma) to for the Paleo-Pacific Ocean. Tectonophysics, v. 234, 113–140.

Preiss, W. V., 2000. The Adelaide Geosyncline of South Australia and its significance in Neoproterozoic continental reconstruction. Precambrian Research, v. 100, 21–63.

Seton, M., Müller, R. D., Zahirovic, S., Gaina, C., Torsvik, T. H., Shephard, G., Talsma, A., Gurnis, M., Turner, M., and Chandler, M., 2012. Global continental and ocean basin reconstructions since 200 Ma. Earth-Science Reviews, v. 113, 212–270.

Spry, A., 1962. Some aspects of the stratigraphy, structure and petrology of the Precambrian rocks of Tasmania. PhD Thesis [unpub.], University of Tasmania.

Stampfli, G. M., Hochard, C., Vérard, C., Wilhem, C., and von Raumer, J., 2013. The formation of Pangea. Tectonophysics, v. 593, 1–19.

Torsvik, T. H., and Cocks, L. R. M., 2013. Gondwana from top to base in space and time. Gondwana Research, v. 24, 999–1030.

Turner, N. J., 1989. Chapter 2. Precambrian. In: Burrett, C.F., Martin, E.L. (Eds.), Geology and Mineral Resources of Tasmania. Geological Society of Australia, Special Publication, 5–46.

Veevers, J. J., 2004. Gondwanaland from 650–500 Ma assembly through 320 Ma merger in Pangea to 185–100 Ma breakup: supercontinental tectonics via stratigraphy and radiometric dating. Earth-Science Reviews, v. 68, 1–132.

von Raumer, J. F., Stampfli, G. M., and Bussy, F., 2003. Gondwana-derived microcontinents — the constituents of the Variscan and Alpine collisional orogens. Tectonophysics, v. 365, 7–22.

Whittaker, J. M., Williams, S. E., Halpin, J. A., Wild, T. J., Stilwell, J. D., Jourdan, F., and Daczko, N. R., 2016. Eastern Indian Ocean microcontinent formation driven by plate motion changes. Earth and Planetary Science Letters, v. 454, 203–212.

Wen, B., Evans, D. A. D., and Li, Y. -X., 2017. Neoproterozoic paleogeography of the Tarim Block: An extended or alternative "missing-link" model for Rodinia? Earth and Planetary Science Letters, v. 458, 92–106.

Zhang, S., Li, Z. -X., Evans, D. A. D., Wu, H., Li, H., and Dong, J., 2012. Pre-Rodinia supercontinent Nuna shaping up: a global synthesis with new paleomagnetic results from North China. Earth and Planetary Science Letters, v. 353–354, 145–155.

Chapter 2

Mesoproterozoic Tasmania: Witness to the East Antarctica-Laurentia connection within Nuna

Geology, v. 43, 759–762

Jacob A. Mulder[1], Jacqueline A. Halpin[1], Nathan R. Daczko[2]

[1]ARC Centre of Excellence in Ore Deposits (CODES), School of Physical Sciences, University of Tasmania, Private Bag 79, TAS 7001, Australia

[2]ARC Centre of Excellence for Core to Crust Fluid Systems and GEMOC, Department of Earth and Planetary Sciences, Macquarie University, NSW 2109, Australia

2.0 Abstract

Most recent paleogeographic reconstructions of the supercontinent Nuna juxtapose the North Australian craton, Mawson continent (South Australia–East Antarctica), and Laurentia between 1.6 Ga and 1.3 Ga but differ in their relative positioning. The >10-km-thick siliciclastic Rocky Cape Group of Tasmania was deposited in an opening marine basin on the margin of East Antarctica during Nuna breakup. Based on a similar detrital zircon signature and depositional age, the Rocky Cape Group has been correlated with the upper Belt-Purcell Supergroup in Laurentia, thus representing a key tie point within Nuna. Here the detrital zircon age signature of Mesoproterozoic Rocky Cape Group quartzites is investigated by comparing new detrital zircon U-Pb-Hf isotopic data to an extensive compilation of zircon isotopic data from Australia, East Antarctica, and Laurentia. Our analysis demonstrates that the Rocky Cape Group is unlikely to have been sourced from any geological terrane exposed in present-day Australia. Instead, zircon U-Pb-Hf isotopic data from basement terranes in Laurentia and East Antarctica show striking similarities to the Rocky Cape Group detrital signature. Paleocurrent data indicate that the majority of sediment in the Rocky Cape Group was sourced from Laurentia, which was to the southeast (present-day coordinates) of Tasmania, supporting a SWEAT-like (southwest United States–East Antarctica) configuration for Nuna. We suggest that rifting left a thinned continental connection between East Antarctica and Laurentia onto which the lower-middle Rocky Cape Group was deposited between 1.45 and 1.30 Ga.

2.1 Introduction

Reconstructions of one of Earth's oldest supercontinents, Nuna (or Columbia), are undergoing dramatic developments based on quantitative models incorporating geological and paleomagnetic constraints (e.g., Payne et al., 2009; Evans and Mitchell, 2011; Zhang et al., 2012; Pisarevsky et al., 2014). Most recent models suggest a southwest United States–East Antarctica (SWEAT)–like configuration between Laurentia, the North Australian craton, and Mawson continent (South Australia craton–East Antarctica) between *ca.* 1.6 Ga and 1.3 Ga, although the relative positioning along the western margin of Laurentia differs considerably between models.

Tasmania (southeastern Australia) has not been considered in previous Nuna reconstructions. This crustal fragment was likely part of the eastern margin of East Antarctica (Berry et al., 2008), isolated outboard of this margin during a late Neoproterozoic rifting event before colliding with the eastern margin of Gondwana during the Cambrian (Cayley, 2011). The significance of Tasmania's position within Nuna has recently been highlighted with the discovery that the majority of a >10-km-thick marine shelfal package exposed in northwest Tasmania (Rocky Cape Group, RCG; Fig. 2.1) was deposited between 1.45 Ga and 1.3 Ga (Halpin et al., 2014). The RCG is part of the Western Tasmania terrane, which includes western Tasmania, the eastern South Tasman Rise, and King Island, and possibly extends north beneath central Victoria (Black et al., 2004; Calver et al., 2014). The detrital zircon age signatures of the RCG and correlatives are distinct from other Mesoproterozoic basins in Australia, and instead closely resemble time-equivalent upper parts of the Belt-Purcell Basin of Laurentia. A shared provenance and deposition in a marginal basin during supercontinent extension and breakup was suggested in Halpin et al. (2014). As such, the RCG basin could form a crucial tie point between Laurentia (West Nuna), and Australia and East Antarctica (East Nuna) (Fig. 2.2).

In this study, Hf and U-Pb isotopes of detrital zircon from the RCG, complemented by paleocurrent data, are compared to an extensive compilation of zircon isotopic data from the North Australian craton, Mawson continent, and Laurentia to identify possible source regions for the RCG basin. In addition to clarifying the Proterozoic position of Tasmania, this new data set provides compelling evidence for a close connection between East Antarctica and southwest Laurentia and a positive test for their juxtaposition within Nuna *ca.* 1.45 Ga.

2.2 Methods

Detrital zircons were analyzed from each of the four major quartzite units of the RCG (Fig. 2.1). Laser ablation–inductively coupled plasma–mass spectrometry (LA-ICP-MS) U-Pb zircon ages from the Jacob Quartzite were collected during this study to supplement the three lower-middle RCG samples reported in Halpin et al. (2014), following the same zircon preparation, imaging, and U-Pb isotope analysis method. Between 20 and 25 detrital zircons interpreted to be of igneous origin were selected from each sample for Lu-Hf isotopic analysis via multicollector LA-ICP-MS at Macquarie University (Sydney, Australia) following procedures outlined in Halpin et al. (2013). A spot size of

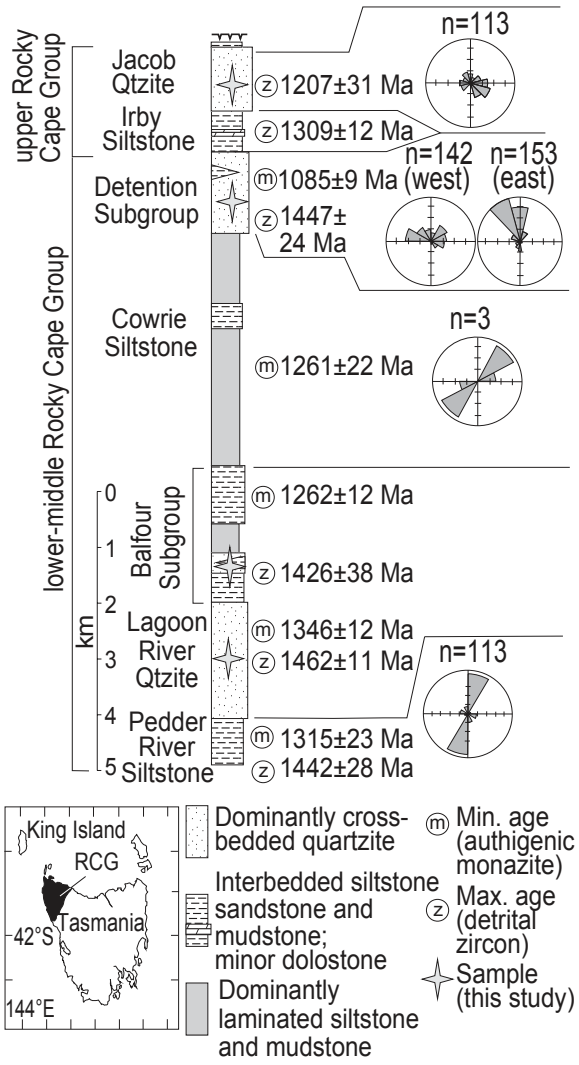

Figure 2.1: Generalized stratigraphic column with sample locations, interpretation of paleoenvironments (after Calver et al., 2014), and paleocurrent data from the Rocky Cape Group (RCG), northwest Tasmania. Authigenic monazite and detrital zircon data from the Irby Siltstone and the lower-middle RCG are from Halpin et al. (2014). Qtzite—quartzite; Min.—minimum; Max.—maximum.

40–50 μm was used to measure Lu-Hf isotopes over the same 26 μm pit used to measure the U-Pb isotopes. Initial epsilon Hf values (εHf_i) were calculated using the apparent $^{207}Pb/^{206}Pb$ age and the decay constant of Scherer et al. (2001). A compilation of paleocurrent data from the RCG from previously unpublished studies (Appendix 2.1) are summarized using rose diagrams with a sector width of 30° and plotted in increments representing 10% of the data for each unit (Fig. 2.1).

The Hf and U-Pb compilations aim to be representative of local basement terranes (Figs. 2.3 and 2.4). The Laurentian compilation is representative of the Mojave, Yavapai, and Mazatzal Provinces (southwest Laurentia), whereas the Australian and East Antarctic compilations include data from most major pre-Neoproterozoic geological provinces of the North Australian craton and Mawson continent (Appendix 2.2 and Appendix 2.3). We also follow previous work in using detrital zircons and basement clasts as a proxy for the poorly known subglacial geology of East Antarctica (e.g., Goodge et al., 2008, 2010; Wysoczanski and Allibone, 2004; Appendix 2.2 and Appendix 2.3). For the purposes of exploring the paleoposition of Tasmania, the East Antarctic data set is divided into two

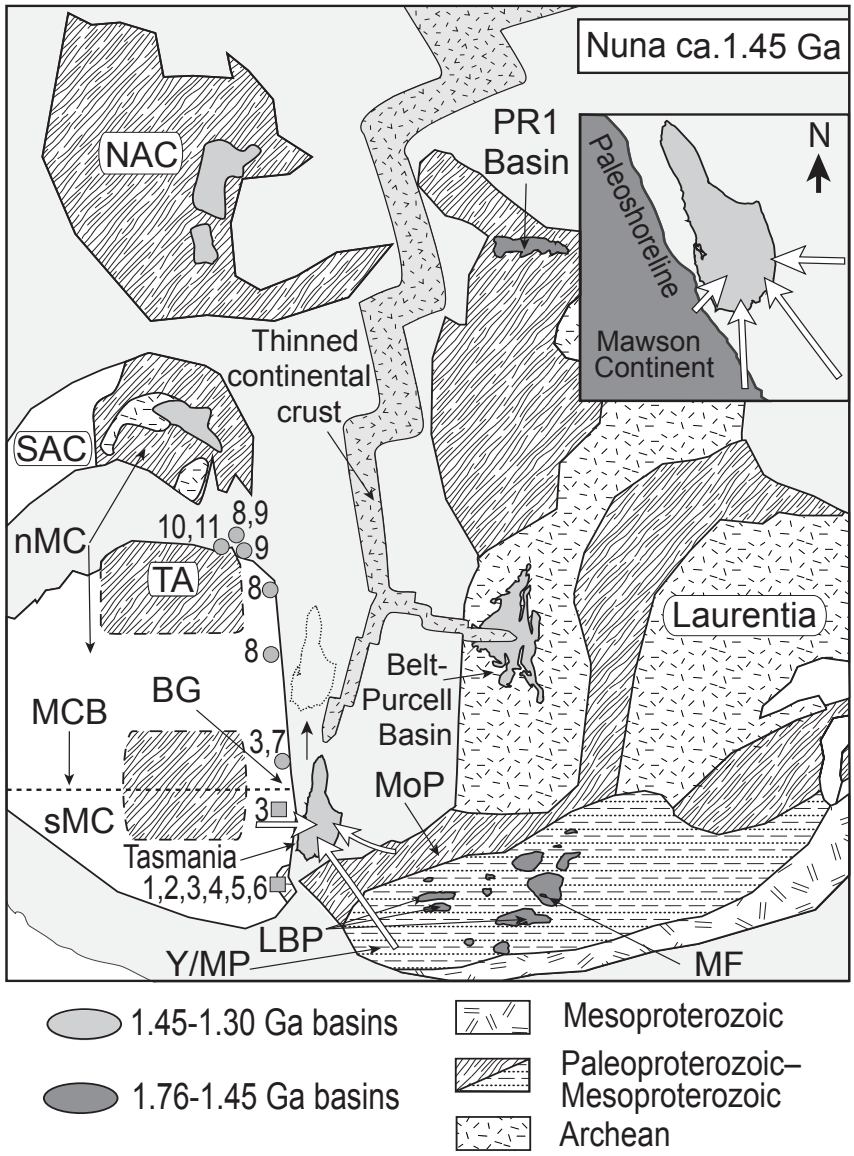

Figure 2.2: Proto–southwest United States–East Antarctica (SWEAT) paleogeographic reconstruction of Nuna *ca.* 1.45 Ga showing basement terranes and Paleoproterozoic–Mesoproterozoic sedimentary basins relevant to this study (following, e.g., Goodge et al., 2008; Medig et al., 2014). The relative positioning of the continents follows Pisarevsky et al. (2014), but rotated ~180° to reflect present-day orientations. Inset shows inferred paleoshoreline and dominant paleocurrent modes derived from cross-bedding in lower-middle Rocky Cape Group (RCG), northwest Tasmania (present-day coordinates). The paleoshoreline of the Tasmanian Mesoproterozoic basin has been rotated to parallel the orientation of the inferred margin. The exact position of Tasmania along this paleomargin is poorly constrained (dotted outline marks possible alternative position), but our detrital zircon data suggest a close link to 1.45 Ga crust in the southern Mawson continent. NAC—North, Australian craton, SAC—South Australian craton, nMC, sMC—northern and southern Mawson continent, TA—Terre Adélie, Y/MP—Yavapai-Mazatzal Province, MoP—Mojave Province, GR—Grenville Province, LBP—lower Belt-Purcell correlates, MF—Marqueñes Formation, BG—Byrd Glacier, MCB—boundary between the northern and southern Mawson continent. Paleocratonic margins are unknown and approximated by light gray fill. Circle and square symbols mark location of data assigned to northern and southern Mawson continent, respectively; numbers adjacent to symbols correspond to data sources listed in Appendix 2.4

potential source regions separated by the Byrd Glacier (Fig. 2.2; see Appendix 2.4). A northern sector (approximately north of 80°S; northern Mawson continent) includes distinctive basement rocks with ages within the North American magmatic gap (NAMG; 1.61–1.49 Ga) correlated with the

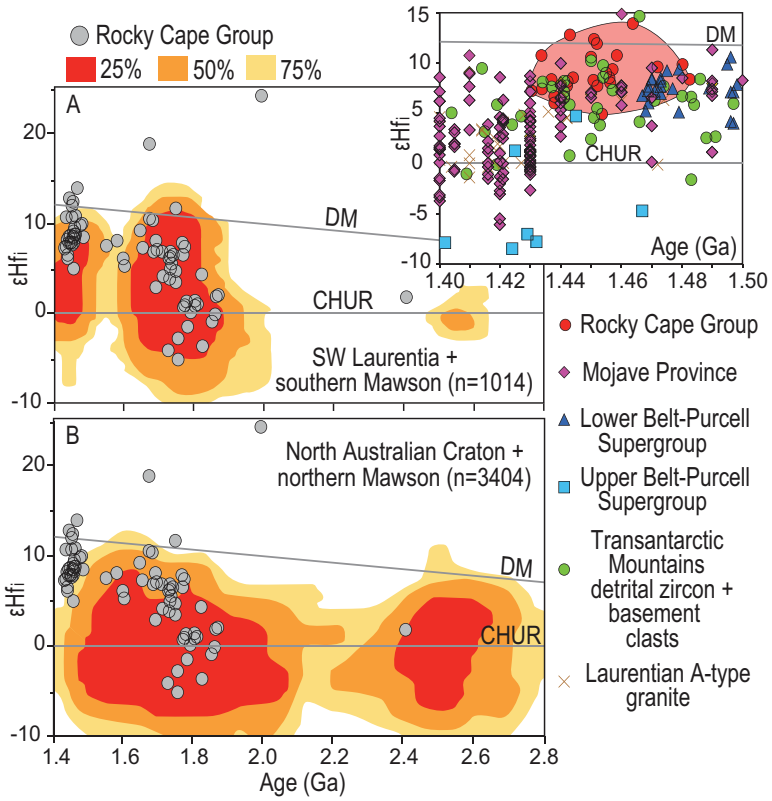

Figure 2.3: The initial epsilon Hf values (εHf_i) versus age data for Rocky Cape Group (RCG, northwest Tasmania) zircons (gray circles). Data sets are presented in Appendix 2.2. A: εHf_i compared to data contoured by percentiles from southwest (SW) Laurentia and southern Mawson continent. Inset in A compares εHf_i values for 1.50–1.40 Ga zircons from the RCG (red circles outlined by red field) with similar-aged zircons from the potential source regions. Zircons plotting below the CHUR (chondritic uniform reservoir) reference line reflect a crustal melt source, whereas those plotting at progressively more positive εHf_i values above CHUR reflect an increasing contribution from the depleted mantle (DM) to the magmas from which the zircon formed. B: εHf_i data compared to North Australian craton and northern Mawson continent.

South Australian craton. Data from the South Australian craton are also included in our definition of the northern Mawson continent. The second source region is between ~85°S and 80°S; (southern Mawson continent) and is inferred to be intruded by 1.45 Ga granites correlated with the Laurentian A-type granite belt (Goodge et al., 2008).

U-Pb probability distribution plots were constructed with Isoplot version 3.1 (Ludwig, 2003) using $^{207}Pb/^{206}Pb$ ages and their 1σ uncertainties for data <±10% discordant. Density distribution εHf_i age plots were constructed using ioGAS software (reflexnow.com/iogas/).

2.3 Results

Paleocurrent data from the RCG show variations between stratigraphic levels (Fig. 2.1). Gutter casts from the Cowrie Siltstone and Pedder River Siltstone record paleocurrents with a general northeast-southwest trend. In the eastern exposures of the Detention subgroup, cross-bedding records dominantly northwest- and north-directed modes, whereas in the western exposures, northeast-east modes are also common. Cross-bedding in the Jacob Quartzite records a variety of paleocurrent directions with southeast-directed modes dominating.

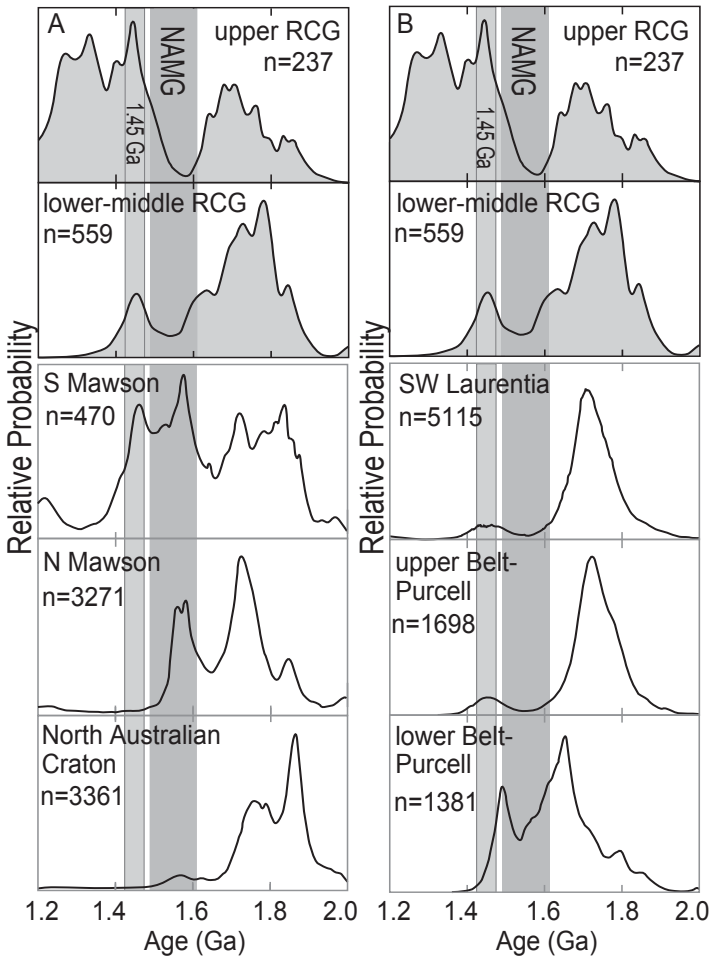

Figure 2.4: Gaussian summation probability density distribution plots of U-Pb age data for detrital zircons from the upper Rocky Cape Group (RCG, northwest Tasmania) and lower-middle RCG (includes correlatives on King Island). A: Compared to detrital zircon ages reflecting basement provinces of the North Australian craton and Mawson continent. B: Compared to detrital zircon and basement zircon ages reflecting basement of southwest Laurentia, upper Belt-Purcell Supergroup and Marqueñes Formation, lower Belt-Purcell Supergroup, and correlatives (PR1, Yankee Joe, Black Jack, Defiance, Piedra Lumbre basins). The North American magmatic gap (NAMG, 1.61–1.49 Ga, dark gray) and a reference age of 1.45 ± 0.025 Ga (light gray) are shown as bars behind each plot.

Most detrital zircons from the lower-middle RCG have ages between 1.82 Ga and 1.63 Ga, with major age peaks at 1.78 and 1.72 Ga (Fig. 2.4). Zircons with ages of 1.50–1.40 Ga represent 12% of the lower-middle RCG data set and form a prominent age peak at 1.45 Ga, which represents the maximum depositional age of the sequence. The upper RCG is characterized by an influx of grains younger than 1.40 Ga forming major age peaks *ca.* 1.33 Ga and *ca.* 1.28 Ga. A revised maximum depositional age of the upper RCG is constrained to 1.20 Ga by our data from the Jacob Quartzite. Our data set does not replicate the few grains used to derive a *ca.* 1.0 Ga maximum age by Black et al. (2004), and we suggest that these grains may have been affected by Pb loss. Zircons with ages of 1.50–1.40 Ga constitute 21% of the upper RCG data set, with 1.45 Ga representing the dominant age peak.

The εHf_i data from the RCG have a spread of values within each of the major age populations (Fig. 2.3). The oldest zircons from the RCG (1.90–1.70 Ga) have εHf_i between −5.00 and +2.00, typical of crustal melts, whereas 1.70–1.60 Ga zircons have more positive εHf_i values (+2.82 to +11.63).

The *ca.* 1.45 Ga zircons have positive εHf_i between +6.02 and +12.80, reflecting a significant mantle contribution in the source magmas.

2.4 Discussion

Comparison of the zircon age and εHf_i signatures from the RCG with regional data sets reveals key insights into the provenance and location of the RCG basin (Figs. 2.3 and 2.4). The εHf_i of RCG detrital zircons is generally more positive than similar-aged North Australian craton and northern Mawson continent sources (Fig. 2.3B), although some overlap exists, particularly for zircons older than 1.75 Ga. However, a suitable source for the 1.45 Ga zircons from the RCG is lacking (Fig. 2.3B), and the U-Pb detrital zircon age spectra are also a poor match for the RCG (Fig. 2.4A). We conclude that the North Australia craton and northern Mawson continent are unlikely to have been significant source regions for the RCG.

In contrast, the southwest Laurentia–southern Mawson continent data set shows significant overlap in εHf_i for all major age populations of detrital zircon from the RCG (Fig. 2.3A). Like the lower-middle RCG, zircon age peaks between 1.85 Ga and 1.70 Ga and distinct *ca.* 1.45 Ga populations characterize both these basement provinces (Figs. 2.4A and 2.4B). The absence in the RCG detrital zircon spectra of a prominent *ca.* 1.58 Ga peak that is in the southern Mawson continent data set (Fig. 2.4A) may reflect uncertainties in using detrital zircons as a proxy for the Mawson continent basement. This compiled East Antarctic data set is mostly from Neoproterozoic and younger successions (Appendix 2.3), and may not necessarily characterize basement rocks exposed during deposition of the RCG.

The range in U-Pb ages and εHf_i values of Paleoproterozoic zircons from the RCG is consistent with these grains having been sourced from Paleoproterozoic basement rocks in the Yavapai, Mazatzal, and Mojave Provinces of southwest Laurentia and their possible extensions in the southern Mawson continent (Fig. 2.3A). In addition, the *ca.* 1.45 Ga zircon population from the RCG has values strikingly εHf_i similar to *ca.* 1.45 Ga grains from the Transantarctic Mountains (southern Mawson continent) and the Mojave Province (Fig. 2.3A, inset).

Paleocurrent data from the RCG stratigraphy provide further insights into the location of source regions. Gutter casts in the lower-middle RCG are interpreted as storm-induced erosive channels developed perpendicular to a northwest-southeast–trending paleoshoreline. In this context, cross-bedding in the lower-middle RCG may record northwest-directed longshore currents transporting sediments from a southeastern source region.

2.5 Paleogeographic Implications

Mesoproterozoic basins across Laurentia, Australia, and East Antarctica likely formed as Nuna rifted between 1.50 Ga and 1.38 Ga (Betts and Giles, 2006; Pisarevsky et al., 2014). The northwest-southeast paleoshoreline (this study) and eastward deepening of strata (Everard, 2005; Halpin et al., 2014) are consistent with the RCG basin forming on a northwest-southeast–trending (present-day

coordinates) rift margin developed along a continental mass to the west-southwest of Tasmania. A proximal, first-cycle source region for the lower-middle RCG stratigraphy is supported by poor sorting and angular detritus (Everard, 2005). Detrital zircon isotopic data and paleocurrent indicators suggest that the RCG was dominantly sourced from Paleoproterozoic crust similar in character to southwest Laurentia, which was to the southeast of the RCG basin (Fig. 2.2). We suggest that the southern Mawson continent was the continental mass to the west-southwest of the RCG basin and was the primary source of the isotopically distinct *ca.* 1.45 Ga detrital zircons, and possibly rare NAMG-aged zircons (Fig. 2.4A).

The provenance of the RCG is consistent with a modified SWEAT-like configuration between Australia, East Antarctica, and Laurentia (Fig. 2.2). This configuration is also consistent with a proximal North Australian craton provenance for the lower PR1 basin in the Yukon (Medig et al., 2014), a southwestern source region in East Antarctica for the upper Belt-Purcell Group (Stewart et al., 2010), and the continuation of the 1.45 Ga Laurentian A-type granite belt into the central Transantarctic Mountains (e.g., Goodge et al., 2008).

The 1.47–1.45 Ga lower Belt-Purcell Supergroup is commonly interpreted as intracratonic and rapidly deposited synchronous with mafic magmatism (e.g., Evans et al., 2000), consistent with deposition within a failed rift arm (Pisarevsky et al., 2014). Basin reorganization at 1.45 Ga isolated the Belt-Purcell Basin from NAMG-aged source rocks in Australia, with a shift to a local provenance during deposition of the *ca.* 1.45–1.37 Ga upper Belt-Purcell Supergroup (Fig. 2.4B; Ross and Villeneuve, 2003; Stewart et al., 2010). The similar detrital zircon spectra and paucity of NAMG-aged detritus in the lower-middle RCG (Fig. 2.4) suggest broad correlation with the coeval upper Belt-Purcell Supergroup stratigraphy during development of a marginal sea from *ca.* 1.45 Ga (Halpin et al., 2014).

The timing of breakup in Nuna is controversial; paleomagnetic constraints are few, particularly for Australia and East Antarctica. Therefore, there is significant uncertainty in the relative positions of these continents during the transition from Nuna into a viable configuration for the successor Rodinia. Pisarevsky et al. (2014) suggested that a northward-propagating rift system led to the final separation of Laurentia from proto-Australia at 1.38 Ga. A link between southwest Laurentia and East Antarctica within Rodinia may be supported by 1.1 Ga glacial clasts from the Transantarctic Mountains (Goodge et al., 2010) that are temporally equivalent to the basement ages within the Grenville orogen (1.3–0.9 Ga). This raises the possibility that part of southwest Laurentia and East Antarctica remained connected during the Nuna to Rodinia transition. We suggest that rifting propagated southward from *ca.* 1.4 Ga, leaving a thinned continental connection between East Antarctica and southwest Laurentia onto which the lower-middle RCG was deposited prior to 1.3 Ga (Fig. 2.2). A late Mesoproterozoic connection between southwest Laurentia and East Antarctica may also be supported by the dramatic shift in provenance to Grenville-aged sources recorded in the upper RCG (Fig. 2.4), coupled with evidence for 1.3–1.0 Ga magmatism and deformation in the Western Tasmania terrane (Berry et al., 2008), and postdepositional 1.35–1.05 Ga fluid flow events recorded in both the RCG basin (Halpin et al., 2014) and the Belt-Purcell Basin (e.g., Aleinikoff et al., 2012).

2.6 Acknowledgements

We thank S. Feig and K. Goemann (Central Science Laboratory, University of Tasmania, Australia), J. Thompson (ARC [Australian Research Council] Centre of Excellence in Ore Deposits, CODES, University of Tasmania), and Yoann Gréau (ARC Centre of Excellence for Core to Crust Fluid Systems, Macquarie University, Australia) for analytical assistance. We thank J. Everard and C. Calver (Mineral Resources Tasmania) for providing samples and advice. The Hf isotope data were obtained using instrumentation funded by DEST (Department of Education, Science and Training, Australia) Systemic Infrastructure grants, the Australian Research Council (ARC) Linkage Infrastructure, Equipment and Facilities program, the National Collaborative Research Infrastructure Strategy (NCRIS)—AuScope, industry partners, and Macquarie University. This is ARC Centre of Excellence for Core to Crust Fluid Systems contribution 634 (www.CCFS. mq.edu.au) and GEMOC Key Centre contribution 1015 (www.GEMOC.mq.edu.au). ARC CODES grant CE0561595 provided financial support to conduct this research. We thank Alan Collins, John Goodge, and Ron Berry for constructive reviews and Bob Holdsworth for editorial handling.

2.7 References Cited

Aleinikoff, J.N., Hayes, T.S., Evans, K.V., Mazdab, F.K., Pillers, R.M., and Fanning, C.M., 2012, SHRIMP U-Pb ages of xenotime and monazite from the Spar Lake red bed–associated Cu-Ag deposit, western Montana: Implications for ore genesis: Economic Geology and the Bulletin of the Society of Economic Geologists, v. 107, p. 1251–1274, doi:10.2113/econgeo.107 .6.1251.

Berry, R.F., Steele, D.A., and Meffre, S., 2008, Proterozoic metamorphism in Tasmania: Implications for tectonic reconstructions: Precambrian Research, v. 166, p. 387–396, doi:10.1016/j.precamres.2007.05.004.

Betts, P.G., and Giles, D., 2006, The 1800–1100 Ma tectonic evolution of Australia: Precambrian Research, v. 144, p. 92–125, doi:10.1016/j .precamres.2005.11.006.

Black, L.P., Calver, C.R., Seymour, D.B., and Reed, A., 2004, SHRIMP U-Pb detrital zircon ages from Proterozoic and early Palaeozoic sandstones and their bearing on the early geological evolution of Tasmania: Australian Journal of Earth Sciences, v. 51, p. 885–900, doi:10.1111/j .1400-0952.2004.01091.x.

Calver, C.R., Everard, J.L., Berry, R.F., Bottrill, R.S., and Seymour, D.B., 2014, Proterozoic Tasmania, *in* Corbett, K.D., et al., eds., Geological evolution of Tasmania: Geological Society of Australia Special Publication 24, p. 34–94.

Cayley, R.A., 2011, Exotic crustal block accretion to the eastern Gondwanaland margin in the Late Cambrian—Tasmania, the Selwyn Block, and implications for the Cambrian-Silurian evolution of the Ross, Delamerian, and Lachlan orogens: Gondwana Research, v. 19, p. 628–649, doi:10.1016/j.gr.2010.11.013.

Evans, D.A.D., and Mitchell, R.N., 2011, Assembly and breakup of the core of Paleoproterozoic-Mesoproterozoic supercontinent Nuna: Geology, v. 39, p. 443–446, doi:10.1130/G31654.1.

Evans, K.V., Aleinikoff, J.N., Obradovich, J.D., and Fanning, C.M., 2000, SHRIMP U-Pb geochronology of volcanic rocks, Belt Supergroup, western Montana: Evidence for rapid deposition of sedimentary strata: Canadian Journal of Earth Sciences, v. 37, p. 1287–1300, doi:10.1139/e00-036.

Everard, J.L., 2005, Reconnaissance geology of the Norfolk Range–Sandy Cape area, northwest Tasmania: A report for the Western Tasmanian Regional Minerals Program: Tasmanian Geological Survey Record 2005/02, 82 p.

Goodge, J.W., Vervoort, J.D., Fanning, C.M., Brecke, D.M., Farmer, G.L., Williams, I.S., Myrow, P.M., and DePaolo, D.J., 2008, A positive test of East Antarctica–Laurentia juxtaposition within the Rodinia supercontinent: Science, v. 321, p. 235–240, doi:10.1126/science.1159189.

Goodge, J.W., Fanning, C.M., Brecke, D.M., Licht, K.J., and Palmer, E.F., 2010, Continuation of the Laurentian Grenville province across the Ross Sea margin of East Antarctica: Journal of Geology, v. 118, p. 601–619, doi:10.1086/656385.

Halpin, J.A., Daczko, N.R., Clarke, G.L., and Murray, K.R., 2013, Basin analysis in polymetamorphic terranes: An example from East Antarctica: Precambrian Research, v. 231, p. 78–97, doi: 10.1016/j.precamres.2013.03.015.

Halpin, J.A., Jensen, T., McGoldrick, P., Meffre, S., Berry, R.F., Everard, J.L., Calver, C.R., Thompson, J., Goemann, K., and Whittaker, J.M., 2014, Authigenic monazite and detrital zircon dating from the Proterozoic Rocky Cape Group, Tasmania: Links to the Belt-Purcell Supergroup, North America: Precambrian Research, v. 250, p. 50–67, doi:10.1016/j.precamres.2014.05.025.

Ludwig, K.R., 2003, Isoplot 3.00: A geochronological toolkit for Microsoft Excel: Berkeley, California, Berkeley Geochronological Centre Special Publication 4, 74 p.

Medig, K.P.R., Thorkelson, D.J., Davis, W.J., Rainbird, R.H., Gibson, H.D., Turner, E.C., and Marshall, D.D., 2014, Pinning northeastern Australia to northwestern Laurentia in the Mesoproterozoic: Precambrian Research, v. 249, p. 88–99, doi:10.1016/j.precamres.2014.04.018.

Payne, J.L., Hand, M., Barovich, K.M., Reid, A., and Evans, D.A.D., 2009, Correlations and reconstruction models for the 2500–1500 Ma evolution of the Mawson continent, *in* Reddy, S.M., et al., eds., Paleoproterozoic supercontinents and global evolution: Geological Society of Lon- don Special Publication 323, p. 319–355, doi: 10.1144/SP323.16.

Pisarevsky, S.A., Elming, S.-Å., Pesonen, L.J., and Li, Z.-X., 2014, Mesoproterozoic paleogeography: Supercontinent and beyond: Precambrian Research, v. 244, p. 207–225, doi:10.1016/j. precamres.2013.05.014.

Ross, G.M., and Villeneuve, M., 2003, Provenance of the Mesoproterozoic (1.45 Ga) Belt basin (western North America): Another piece in the pre-Rodinia paleogeographic puzzle: Geological Society of America Bulletin, v. 115, p. 1191–1217, doi:10.1130/B25209.1.

Scherer, E., Munker, C., and Mezger, K., 2001, Calibration of the lutetium-hafnium clock: Science, v. 293, p. 683–687, doi:10.1126/science .1061372.

Stewart, E.D., Link, P.K., Fanning, C.M., Frost, C.D., and McCurry, M., 2010, Paleogeographic implications of non-North American sediment in the Mesoproterozoic upper Belt Supergroup and Lemhi Group, Idaho and Montana, USA: Geology, v. 38, p. 927–930, doi:10.1130/G31194.1.

Wysoczanski, R.J., and Allibone, A.H., 2004, Age, correlation, and provenance of the Neoproterozoic Skelton Group, Antarctica: Grenville age detritus on the margin of East Antarctica: Journal of Geology, v. 112, p. 401–416, doi:10.1086/421071.

Zhang, S.H., Li, Z.X., Evans, D.A.D., Wu, H.C., Li, H.Y., and Dong, J., 2012, Pre-Rodinia supercontinent Nuna shaping up: A global synthesis with new paleomagnetic results from north China: Earth and Planetary Science Letters, v. 353–354, p. 145–155, doi:10.1016/j.epsl.2012.07.034.

Appendix 2.1: Compilation of Paleocurrent data from Rocky Cape Group

Unit	Type of Paleocurrent Indicators	Number	Reference
Jacob Quartzite	Cross-bedding in quartzites	113	Gee, R. D. 1967. The Tectonic Evolution of the Rocky Cape Geanticline. Unpublished PhD Thesis, University of Tasmania.
Detention Subgroup East	Cross-bedding in quartzites	153	Gee, R. D.1967. The Tectonic Evolution of the Rocky Cape Geanticline. Unpublished PhD Thesis, University of Tasmania.
Detention Subgroup West	Cross-bedding in quartzites	83	Lennox, P.G. 1976. Geology of the Upper Precambrian, Northwest Tasmania. Unpublished Honours Thesis, University of Tasmania.
		59	Scott, C. M. 1997. Sedimentology of the Arthur River Area, Northwest Tasmania. Unpublished Honours Thesis, University of Tasmania.
Cowrie Siltstone	Gutter Casts in siltstones	3	Scott, C. M. 1997. Sedimentology of the Arthur River Area, Northwest Tasmania. Unpublished Honours Thesis, University of Tasmania.
Pedder River Siltstone	Gutter Casts in siltstones	113	Britton, A.M. 1997 Structure, Stratigraphy and Mineralisation of the Temma area, North-Western Tasmania. Unpublished Honours Thesis, University of Tasmania.

Appendix 2.2: Zircon-Hf age compilation - See digital appendix

Appendix 2.3: Zircon-U-Pb age compilation - See digital appendix

Appendix 2.4: List of references for Mawson Continent data source citations in Figure 2

Data Source Number on Fig. 2	Reference	northern or southern Mawson Continent
1	Goodge, J.W., Fanning, M.C., Vickie, C.B. 2001. U–Pb evidence of ~1.7 Ga crustal tectonism during the Nimrod Orogeny in the Transantarctic Mountains, Antarctica: implications for Proterozoic plate reconstructions. Precambrian Research. 112. 261-288	southern Mawson Continent
2	Goodge, J.W., Myrow, P., Williams, I.S., Bowring, S.A. 2002. Age and Provenance of the Beardmore Group, Antarctica: Constraints on Rodinia Supercontinent Breakup, The Journal of Geology. 110. 393-406	southern Mawson Continent
3	Goodge, J.W., Williams, I.S., Myrow, P. 2004. Provenance of Neoproterozoic and lower Paleozoic siliciclastic rocks of the central Ross orogen, Antarctica: Detrital record of rift-, passive-, and active-margin sedimentation. Geological Society of America Bulletin. 116. 1253-1279	southern Mawson Continent
4	Goodge et al. 2008, A Positive Test of East Antarctica–Laurentia Juxtaposition Within the Rodinia Supercontinent, Science 321	southern Mawson Continent
5	Goodge, J.W., Fanning, M.C., Brecke, D.M., Licht, K.J., Palmer, E.F. 2010. Continuation of the Laurentian Grenville Province across the Ross Sea Margin of East Antarctica. The Journal of Geology. 118. 601-619	southern Mawson Continent
6	Elliot, D.H.,Fanning, M.C., Hulett, S.R.W. *In Press* Age provinces in the Antarctic craton: Evidence from detrital zircons in Permian strata from the Beardmore Glacier region, Antarctica, Gondwana Research (2014)	southern Mawson Continent
7	Wysoczanski, R.J., Allibone, A.H. 2004. Age, Correlation, and Provenance of the Neoproterozoic Skelton Group, Antarctica: Grenville Age Detritus on the Margin of East Antarctica. The Journal of Geology. 112. 401-416.	northern Mawson Continent
8	Veevers, J.J., Saeed., A. 2011. Age and composition of Antarctic bedrock reflected by detrital zircons, erratics, and recycled microfossils in the Prydz Bay–Wilkes Land–Ross Sea–Marie Byrd Land sector (70°–240°E). Gondwana Research. 20. 710-738	northern Mawson Continent
9	Goodge, J.W., Fanning, C.M. 2010. Composition and age of the East Antarctic Shield in eastern Wilkes Land determined by proxy from Oligocene-Pleistocene glaciomarine sediment and Beacon Supergroup sandstones, Antarctica. Geological Society of America Bulletin. 122. 1135-1159	northern Mawson Continent
10	Peucat. J.J., Menot, R.P., Monnier, O., Fanning, C.M. 1999. The Terre Ade´lie basement in the East-Antarctica Shield: geological and isotopic evidence for a major 1.7 Ga thermal event; comparison with the Gawler Craton in South Australia. Precambrian Research. 94. 205-224	northern Mawson Continent
11	Peucat. J.J., Capdevila, R., Fanning, C.M., Menot, R.P., Pecora, L., Testut, L. 2002. 1.60 Ga felsic volcanic blocks in the moraines of the Terre Adélie Craton, Antarctica: comparisons with the Gawler Range Volcanics, South Australia. Australian Journal of Earth Sciences. 49. 831-845	northern Mawson Continent

Chapter 2

Mesoproterozoic Tasmania: Witness to the East Antarctica-Laurentia connection within Nuna: REPLY

Geology, v. 44, Forum Reply

Jacob A. Mulder[1], Jacqueline A. Halpin[1], Nathan R. Daczko[2]

[1]ARC Centre of Excellence in Ore Deposits (CODES), School of Physical Sciences, University of Tasmania, Private Bag 79, TAS 7001, Australia

[2]ARC Centre of Excellence for Core to Crust Fluid Systems and GEMOC, Department of Earth and Planetary Sciences, Macquarie University, NSW 2109, Australia

2.9 Forum Reply

Our detrital zircon U-Pb-Hf isotopic data and paleocurrent indicators from the lower-middle Rocky Cape Group (RCG) of northwest Tasmania, a >10-km-thick package of marine sedimentary rocks, are consistent with a provenance including basement terranes in the southern Mawson continent (East Antarctica) and southwest Laurentia, supporting a SWEAT-like configuration for the supercontinent Nuna between 1.45 and 1.3 Ga (Mulder et al., 2015). Moore and Betts (2016) challenge our proposed paleogeographic position for Tasmania within Nuna. Instead, they champion an alternative position for Proterozoic Tasmania that they claim better fits elements of Tasmanian geology outside of the RCG (Moore et al., 2015). From the outset, we would like to reiterate that the data and paleogeographic reconstruction presented by us were discussed in the context of the Nuna supercontinent and based on the most recent reconstruction by Pisarevsky et al. (2014). We specifically addressed the interval 1.45–1.3 Ga, which encompasses the period in which Nuna started to rift and break apart. Nowhere do we address the reconstructed position of VanDieland—a microcontinent that includes rocks as young as Cambrian, and represents Tasmania (and central Victoria, South Tasman Rise, and East Tasman Plateau) just prior to incorporation into Gondwana (Cayley, 2011). Although most of the points raised by Moore and Betts are not directly relevant to the dataset and reconstruction in our paper, we welcome the opportunity to elaborate on our ongoing research on the Proterozoic tectonics of Tasmania by addressing the issues they have raised.

Moore and Betts claim that we have "failed to recognize the significance of Grenville-age orogenic and sedimentary events" in our reconstruction. Not only is this statement incorrect (see the final sentence of Mulder et al., 2015) but the magmatism and metamorphism known from the east South Tasman Rise post-dates the time period considered by us by 200–300 m.y. and therefore cannot be used as a direct constraint on Tasmania's position within Nuna.

Similarly, whether the youngest detrital zircon population in the Jacob Quartzite of *ca.* 1.2 Ga or 1 Ga is favored, the maximum depositional age of the upper RCG (and the <900 Ma Wings Sandstone)

post-dates the 1.45–1.3 Ga time frame considered by us. There is limited evidence to suggest that these strata are related to the Grenville orogenic cycle, as claimed by Moore and Betts. Only once minimum depositional ages for the upper RCG and Wings Sandstone are better understood can a source for the <1.3 Ga detrital zircons they contain be offered within the context of time-appropriate plate reconstructions. This is a current focus of our work on Proterozoic Tasmania.

Moore and Betts propose that an inferred middle to late Paleoproterozoic age for the basement of the RCG is inconsistent with our proposed reconstruction. They follow Black et al. (2010) who interpret an excess of 1.6–1.63 Ga inherited zircons in Paleozoic granites in western Tasmania relative to the overlying RCG as reflecting the age of the underlying basement. However, the most recent data (compiled in Mulder et al., 2015, our figure 2.4) demonstrate that 1.6–1.63 Ga detrital zircons are common in the RCG, and therefore inherited zircons of this age in Paleozoic granites do not necessarily reflect the age of the underlying basement.

We agree "too few Sm-Nd model ages of the basement [of Tasmania] have been determined to make statistically valid comparisons with other regions" (Moore et al., 2015). However, contrary to their assertion, we do not place Tasmania near the USA–Canada border. Our preferred position is close to modern-day Arizona in the USA, and the Miller Range in Antarctica, which is in fact consistent with a Paleoproterozoic basement age for the RCG. Given the uncertainties in the age of the basement to the RCG and hence the position of Tasmania along the margin of the Mawson continent at 1.45–1.3 Ga, we also chose to speculate on an alternative position for Tasmania (Mulder et al., 2015, our figure 2.2) to highlight geochronological commonalities in the RCG and Belt-Purcell basins (Halpin et al., 2014).

In summary, Moore and Betts refute the reconstructed position of Tasmania in Nuna at 1.45 Ga presented by us primarily because it is not constrained by geology younger than *ca.* 1.1 Ga. They suggest that the reconstruction of Moore et al. (2015) depicting Tasmania's position at 780 Ma is a more suitable model for "Nuna/Rodinia." While we consider the schematic position of Tasmania in Moore et al. (2015) as being plausible for Rodinia, their reconstruction lacks any constraints on Tasmania's position within Nuna at 1.45–1.3 Ga. We conclude by highlighting a key question arising from this discussion: why do reconstructed paleogeographies for Tasmania at both 1.45–1.3 Ga (Mulder et al., 2015) and 780 Ma (Moore et al., 2015) appear to be so similar? Answering this question will provide important insights into the tectonic transitions during the supercontinent cycle between Nuna and Rodinia, and is a subject of our ongoing work on the Proterozoic of Tasmania.

2.10 References Cited

Black, L.P., Everard, J.L., McClenaghan, M.P., Korsch, R.J., Calver, C.R., Fioretti, A.M., Brown, A.V., and Foudoulis, C., 2010, Controls on Devonian-Carboniferous magmatism in Tasmania, based on inherited zircon age patterns, Sr, Nd and Pb isotopes, and major and trace element geochemistry: Australian Journal of Earth Sciences, v. 57, p. 933–968, doi:10.1080/08120099 .2010.509407.

Cayley, R.A., 2011, Exotic crustal block accretion to the eastern Gondwanaland margin in the Late Cambrian–Tasmania, the Selwyn Block, and implications for the Cambrian–Silurian evolution of the Ross, Delamerian and Lachlan orogens: Gondwana Research, v. 19, p. 628–649, doi:10.1016/j.gr.2010.11.013.

Halpin, J. A., Jensen, T., McGoldrick, P., Meffre, S., Berry, R. F., Everard, J. L., Calver, C. R., Thompson, J., Goemann, K., and Whittaker, J. M., 2014, Authigenic monazite and detrital zircon dating from the Proterozoic Rocky Cape Group, Tasmania: Links to the Belt-Purcell Supergroup, North America: Precambrian Research, v. 250, p. 50-67, doi:10.1016/j. precamres.2014.05.025.

Moore, D.H., and Betts, P.G., 2016, Mesoproterozoic Tasmania: Witness to the East Antarctica–Laurentia connection within Nuna: Comment: Geology v. 44, p. e380, doi:10.1130/G37511C.1.

Moore, D.H., Betts, P.G., and Hall, M., 2015, Fragmented Tasmania: The transition from Rodinia to Gondwana: Australian Journal of Earth Sciences, v. 62, p. 1–35, doi:10.1080/08120099.2014.966757.

Mulder, J.A., Halpin, J.A., and Daczko, N.R., 2015, Mesoproterozoic Tasmania: Witness to the East Antarctica–Laurentia connection within Nuna: Geology, v. 43, p. 759–762, doi:10.1130/G36850.1.

Pisarevsky, S.A., Elming, S.-Å., Pesonen, L.J., and Li, Z.-X., 2014, Mesoproterozoic paleogeography: Supercontinent and beyond: Precambrian Research, v. 244, p. 207–225, doi:10.1016/j. precamres.2013.05.014.

Chapter 3

The syn-orogenic sedimentary record of the Grenville Orogeny in southwest Laurentia

Precambrian Research, v. 294, 33–52

Jacob A. Mulder[1], Karl E. Karlstrom[2], Kathryn Fletcher[3], Matthew T. Heizler[3], J. Michael Timmons[3], Laura J. Crossey[2], George E. Gehrels[4], Mark Pecha[4]

[1]ARC Centre of Excellence in Ore Deposits (CODES), School of Physical Sciences, University of Tasmania, Private Bag 79, TAS 7001, Australia

[2]Department of Earth and Planetary Sciences, University of New Mexico, Albuquerque, NM 87106, USA

[3]New Mexico Bureau of Geology and Mineral Resources, New Mexico Institute of Technology, Socorro, NM 87801, USA

[4]Department of Geosciences, University of Arizona, Tucson, AZ 85721, USA

3.0 Abstract

Late Mesoproterozoic sedimentary sequences in southwest Laurentia range in age from 1340 to 1035 Ma and record regionally extensive intracratonic sedimentation before and during the Grenville Orogeny in southern Laurentia. This paper examines the specific links between intracratonic sedimentation and orogenesis and develops a new tectonic model for basin formation throughout southwest Laurentia during the Late Mesoproterozoic. New detrital zircon, muscovite, and biotite ages refine the provenance, depositional age, and regional correlations of Late Mesoproterozoic strata throughout southwest Laurentia. These data provide a new view of the Grenville orogen in southern Laurentia as it evolved from a continental margin arc to a continent-continent collision based on the record of inboard sedimentation. Deposition of all Late Mesoproterozoic sequences in southwest Laurentia was facilitated by far-traveled, continental-scale rivers that flowed north off the developing Grenville orogen. Sediment accumulation took place during four discrete basin forming events that can be directly linked to changes in the style of convergence and collision along the southern margin of Laurentia. The oldest basin system (lower Apache and Pahrump Groups) records distal back arc basin sedimentation at 1340–1320 Ma, synchronous with widespread magmatism along the southern margin of Laurentia. Unconformably overlying shallow marine carbonate-bearing sequences (lower Unkar Group and correlatives) were deposited between 1255 and 1230 Ma in a regionally extensive retroarc basin with clastic sediment sourced in part from an active continental arc along the southern margin of Laurentia. Shallow marine and terrestrial siliciclastic sequences (upper Unkar Group and correlatives) were deposited at 1140–1100 Ma and were sourced from unroofing thrust nappes in the orogen to the south in an extensive foreland basin system during continent-continent collision. Finally, coarse-grained siliciclastic deposits of the 1060–1035 Ma Hazel Formation represent a proximal foreland basin recording the final stages of the Grenville Orogeny in southern Laurentia.

3.1 Introduction

The Late Mesoproterozoic marks one of the most active episodes of collisional tectonics in Earth's history, culminating in the amalgamation of the supercontinent Rodinia between 1300 and 900 Ma (Li et al., 2008). Laurentia (Proterozoic North America) occupied a central position within Rodinia and is bound on its eastern and southern margins by the Grenville orogen, which represents a key record of the assembly of the supercontinent (e.g. Tohver et al., 2006; Mosher et al., 2008; Li et al., 2008). The tectonic evolution of the northeastern segment of the Grenville Orogeny has been extensively studied from exposures in northeastern United States, eastern Canada, and formerly contiguous crust in Scotland and Ireland (e.g. Davidson, 1995; Rivers, 1997, 2008; Tollo et al., 2004; Storey et al., 2005; Daly and Flowerdew, 2005; McLelland et al., 2010a). The timing and geodynamic significance of the Grenville Orogeny in southern Laurentia is less well understood as this portion of the orogen is only exposed in isolated basement uplifts in central and western Texas (Mosher, 1998; Bickford et al., 2000; Mosher et al., 2008).

Although outcrops of the Late Mesoproterozoic core of the Grenville orogen in southern Laurentia are aerially limited, sedimentary basins of this age are widespread throughout southwest Laurentia (Fig. 3.1) and are interpreted to record intracratonic sedimentation in response to collision along the southern margin of Laurentia (Seeley, 1999; Timmons et al., 2005). In these models, Late Mesoproterozoic strata have been shown to be a record of north-flowing continental-scale rivers sourced from the developing Grenville orogen with basin accommodation space driven by orogen-related intracratonic tectonism. However, the specific links between intracratonic basin formation, sedimentation, and orogenesis are incompletely understood in the context of the most recent tectonic models for the Grenville Orogeny in southern Laurentia (Carlson et al., 2007; Mosher et al., 2008; Levine and Mosher, 2010; Davis and Mosher, 2015).

Syn-orogenic basins are a sensitive record of the tectonic evolution of orogens as their provenance and depositional history are fundamentally linked to major tectonic events during collision (e.g. Beaumont, 1981; Sinclair, 1997; DeCelles and Giles, 1996; Carrapa et al., 2004a; DeCelles et al., 2004; Garzanti et al., 2004; Decelles, 2012; Allen et al., 2015). This paper refines the provenance and depositional history of Late Mesoproterozoic sequences in southwest Laurentia with an extensive detrital zircon, muscovite, and biotite dataset. A detailed record of the provenance of Late Mesoproterozoic sequences in southwest Laurentia is achieved by integrating detrital zircon and mica datasets so that both the crystallization ages of rocks in the source region and the time at which metamorphic rocks cooled through the mica closure temperatures (300–350 °C) during exhumation are recorded. The goal is to further understand the relationship between intracratonic sedimentation and Late Mesoproterozoic orogenesis in southern Laurentia. This leads to a new tectonic model for Late Mesoproterozoic sedimentation in southwest Laurentia and a refined model for the southern Grenville orogen as it evolved from a continental margin arc to a continent-continent collision from *ca.* 1350 to 1000 Ma.

3.2 Geological Setting

During the Paleoproterozoic and Mesoproterozoic Laurentia was constructed by the progressive addition of dominantly juvenile crust to the Archean cratonic core of the Canadian shield by a series of southward-younging orogenic events (Karlstrom and Bowring, 1988; Hoffman, 1988; Whitmeyer and Karlstrom, 2007). Paleoproterozoic orogenic events in southwest Laurentia involved the accretion of 1800–1700 Ma island arc crust of the Yavapai province (e.g. Holland et al., 2015; Link et al., 2016) and emplacement and deformation of 1680–1600 Ma continental margin arc and back arc assemblages defining the Mazatzal province (Fig. 3.1, Karlstrom and Bowring, 1988, 1993; Wooden et al., 1988; Williams, 1991; Whitmeyer and Karlstrom, 2007; Duebendorfer, 2015). Sedimentation was closely associated with crust formation in the Yavapai and Mazatzal provinces. Most Paleoproterozoic basins were derived from a combination of newly accreted crust, post-collisional magmatic rocks, and recycling of older basement rocks (Jones et al., 2009, 2011, 2015; Shufeldt et al., 2010; Doe et al., 2012, 2013; Daniel et al., 2013; Holland et al., 2015). Following tectonic quiescence during the 1610–1490 Ma North American Magmatic Gap (Bowring and Karlstrom, 1990; Ross and Villeneuve, 2003; Karlstrom et al., 2004), accretion continued in southwest Laurentia with the docking of 1550–1400 Ma juvenile crust (Whitmeyer and Karlstrom, 2007). Accretion was accompanied by widespread 1480–1350 Ma A-type magmatism that defines the Granite-Rhyolite Province in southeastern Laurentia (Van Schmus et al., 1996; Whitmeyer and Karlstrom, 2007; Bickford et al., 2015) and also extends into the inboard Paleoproterozoic basement terranes of southwest Laurentia (e.g. Goodge and Vervoort, 2006). Deformation and exhumation of basement terranes throughout southwest Laurentia between 1480 and 1400 Ma (e.g. Nyman et al., 1994; Karlstrom and Humphreys, 1998; Shaw et al., 2005; Daniel and Pyle, 2006; Doe et al., 2012, 2013; Daniel et al., 2013) is attributed to the Picuris Orogeny, which may be a record of intracontinental deformation in response to collision along the southern margin of Laurentia (Daniel et al., 2013; Jones et al., 2015; Karlstrom et al., 2016).

The Late Mesoproterozoic Grenville Orogeny marks the culminating episode of Proterozoic accretion and termination of convergence along the long-lived (*ca.* 800 Ma) convergent margin of southwest Laurentia (Karlstrom et al., 2001). Like its continuation in northeastern Laurentia, the Grenville Orogeny in southern Laurentia records convergence, arc accretion, and continent-continent collision between *ca.* 1350 and 1000 Ma (Mosher, 1998; Bickford et al., 2000; Mosher et al., 2008). The Llano uplift in central Texas is interpreted as an exposed portion of the core of the Grenville orogen in southern Laurentia and contains high-grade metamorphic and magmatic rocks that were imbricated in a north-verging thrust stack during continent-continent collision (Mosher, 1998; Reese and Mosher, 2004; Carlson et al., 2007; Mosher et al., 2008; Levine and Mosher, 2010). The Llano uplift is divided from north to south into the Valley Springs, Packsaddle, and Coal Creek Domains (Mosher et al., 2008). Metasedimentary and metaigneous rocks of the Valley Springs and Packsaddle Domains are interpreted to represent a 1288–1232 Ma continent arc complex built on *ca.* 1360 Ma basement (Mosher, 1998; Reese et al., 2000). The 1330–1270 Ma Coal Creek Domain consists of a tonalite-diorite complex, serpentinized harzburgite, and island arc basalts of an accreted oceanic arc (Roback, 1996). Collision in the Llano uplift involved eclogite facies metamorphism

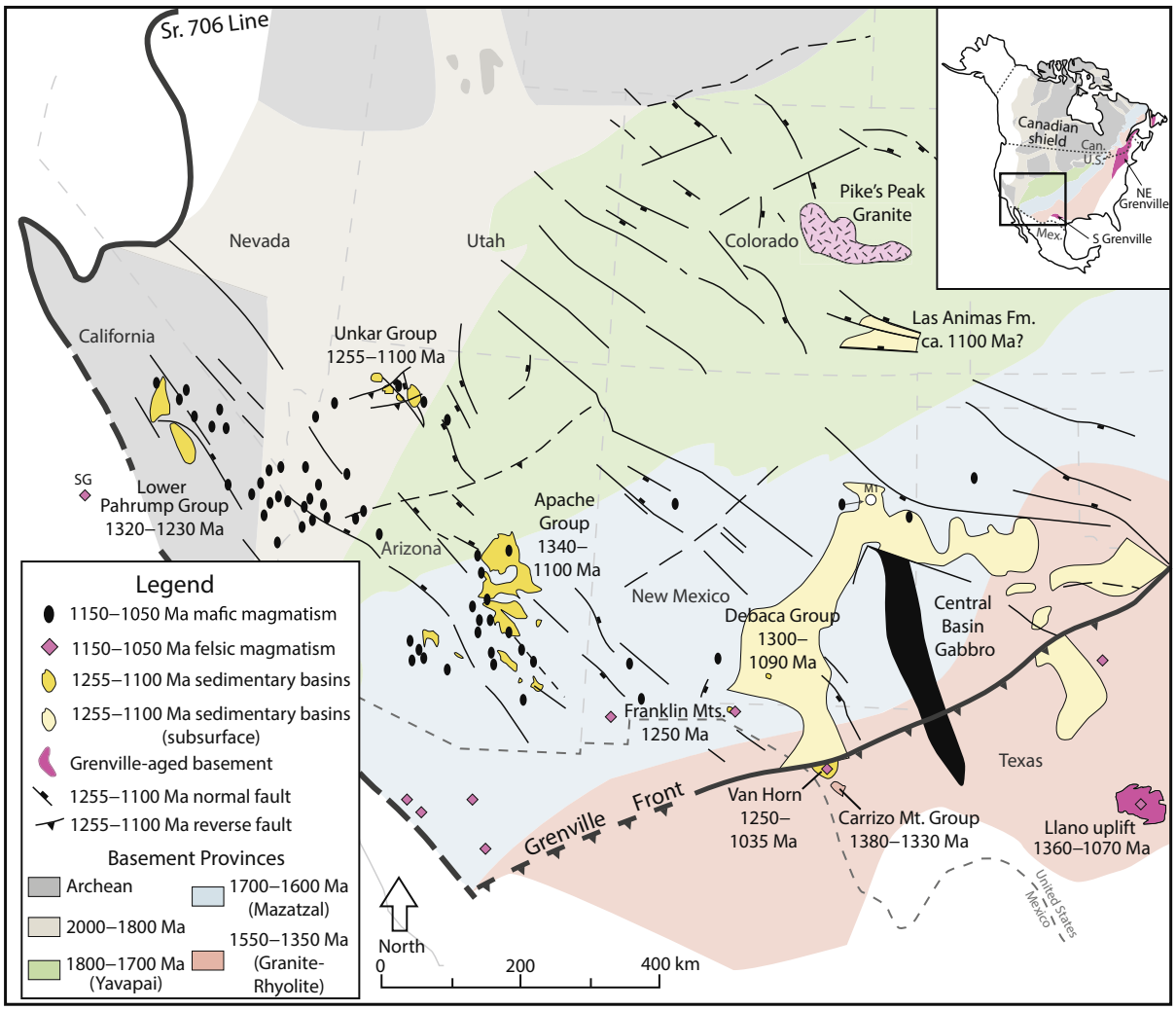

Figure 3.1: Pre-Neoproterozoic geology of southwest Laurentia showing Archean to Mesoproterozoic basement terranes (after Whitmeyer and Karlstrom, 2007), Late Mesoproterozoic fault trends and sedimentary basins (after Timmons et al., 2005), and magmatic rocks (after Bright et al., 2014). The Sr. 706 Line marks the western limit of Proterozoic crust in Laurentia. SG–San Gabriel-Eagle Mountains Anorthosite-Magnerite-Charnockite-Granite suite. M1–Mescalero 1 Well. Inset shows position of Laurentia within the North American continent (after Whitmeyer and Karlstrom, 2007): Can.–Canada, U.S.–United States, Mex.–Mexico, S Grenville–southern Grenville orogen, NE Grenville–northeastern Grenville orogen.

at 1150–1120 Ma that was followed by low- to medium-pressure regional metamorphism and the intrusion of syn-and post-collisional granitoids between 1120 and 1070 Ma (Walker, 1992; Rougive et al., 1996; Mosher, 1998; Carlson et al., 2007).

A portion of the foreland of the Grenville orogen in southern Laurentia is exposed at Van Horn, western Texas (Fig. 3.1) where amphibolite facies rocks of the 1380–1330 Ma Carrizo Mountain Group were interleaved with Mesoproterozoic cover sequences (Soegaard and Callahan, 1994; Grimes and Mosher, 2003; Davis and Mosher, 2015). Ductile deformation and metamorphism at Van Horn occurred between 1060 and 1035 Ma (Bickford et al., 2000; Grimes and Mosher, 2003; Grimes and Copeland, 2004; Davis and Mosher, 2015), followed by final movement on the frontal thrust of the southern Grenville orogen at 1000–980 Ma (Grimes and Copeland, 2004; Davis and Mosher, 2015).

The Grenville Orogeny in southern Laurentia has been interpreted in the context of arc-continent and continent-continent collision (Mosher, 1998; Carlson et al., 2007; Mosher et al., 2008; Levine and Mosher, 2010; Davis and Mosher, 2015). The Valley Springs and Packsaddle Domains in the Llano uplift are interpreted to record 1288–1232 Ma continental arc magmatism above a north-dipping subduction zone, while in the ocean basin to the south, the Coal Creek Domain oceanic arc is interpreted to have collided with an approaching continent, generally interpreted to be the Kalahari craton (e.g. Dalziel et al., 2000; Li et al., 2008; Ksienzyk and Jacobs, 2015), at 1270–1260 Ma (Mosher, 1998). Termination of continental arc magmatism in southern Laurentia likely occurred via a flip in subduction polarity from north- to south-dipping between 1232 and 1150 Ma and was followed by continent-continent collision between 1150 and 1120 Ma (Carlson et al., 2007; Mosher et al., 2008). Slab break-off following collision lead to rapid exhumation of the deeply buried margin of Laurentia and post-collisional magmatism in the Llano uplift at 1120–1070 Ma (Mosher et al., 2008). Widespread 1150–1050 Ma mafic and felsic magmatism throughout southwest Laurentia may be genetically related to slab-break off in the Llano uplift (Fig. 3.1, Hammond, 1990; Howard, 1991; Bright et al., 2014).

Deformation and metamorphism at Van Horn, western Texas post-dates tectonism in the Llano uplift by at least 60 million years, suggesting it represents a distinctly younger phase of the Grenville Orogeny in southern Laurentia (Grimes and Copeland, 2004; Davis and Mosher, 2015). The later episode of deformation and metamorphism in western Texas at 1060–980 Ma could indicate that continent-continent collision initiated earlier in central Texas (Llano uplift) and progressed westward along the southern margin of Laurentia with time (Davis and Mosher, 2015). Alternatively, the 60 million year difference in deformation and metamorphism between western and central Texas may reflect the collision of two separate blocks with the southern margin of Laurentia during the Grenville Orogeny (Mosher, 1998; Davis and Mosher, 2015).

3.3 Overview of Late Mesoproterozoic sedimentary sequences in southwest Laurentia

Late Mesoproterozoic sedimentary sequences in southwest Laurentia have been interpreted to be broadly correlative on the basis of similar lithologies and interpreted depositional environments (Fig. 3.2, Shride, 1967; Wrucke, 1989; Seeley, 1999; Timmons et al., 2005). Deposition above basement as young as 1330 Ma and crosscutting *ca.* 1100 Ma diabase dikes suggests that sedimentation was coincident with the Grenville Orogeny in southern Laurentia (Wrucke, 1989; Bickford et al., 2000; Timmons et al., 2005). A summary of the stratigraphy of the Late Mesoproterozoic basins of southwest Laurentia is presented below to provide context for new detrital mineral datasets that support new regional correlations and refined connections to the southern Grenville Orogeny (Figs. 3.1 and 3.2).

Complexly deformed pre- and syn-orogenic Late Mesoproterozoic sedimentary and volcanic rocks are exposed in the footwall of the frontal thrust of Grenville orogen at Van Horn in western Texas (Fig. 3.1). The oldest sequence is the Allamoore Formation, which comprises intertidal—supratidal stromatolitic dolostone, chert, mudstone, mafic volcanic rocks, and includes tuffs dated

between 1256 and 1250 Ma (Edwards, 1984; Roths, 1993; Bickford et al., 2000). The unconformably overlying Tumbledown Formation comprises volcaniclastic sandstone and basalt intercalated with megablocks of the Allamoore Formation and was deposited at 1243 ± 10 Ma in a tectonically active setting (Soegaard and Callahan, 1994). The youngest sequence at Van Horn comprises alluvial fan conglomerates and eolian sandstones of the Hazel Formation, which nonconformably overlies the Tumbledown Formation (Bickford et al., 2000; Spencer et al., 2014; Davis and Mosher, 2015). The Hazel Formation was derived from actively uplifting thrust sheets to the south at 1060–1035 Ma (Roths, 1993; Soegaard and Callahan, 1994; Bickford et al., 2000; Grimes and Copeland, 2004). Earlier ductile structures at Van Horn, including those in the Hazel Formation, were truncated by the frontal thrust of the southern Grenville orogen at 1000–980 Ma (King and Flawn, 1953; Grimes and Copeland, 2004; Davis and Mosher, 2015).

A second exposure of Late Mesoproterozoic sedimentary and volcanic sequences in western Texas occurs in the Franklin Mountains as a roof pendant in the 1120 ± 35 Ma Red Bluff Granite (Pittenger et al., 1994; Seeley, 1999; Bickford et al., 2000). The basal Castner Marble is a package of intertidal—subtidal stromatolitic limestone with marine $^{87}Sr/^{86}Sr$ and $\delta^{13}C$ isotopic signatures (Pittenger et al., 1994), rhythmite, conglomerate, and tuffaceous siltstone dated at 1272 ± 5, 1251 ± 47 (Bickford et al., 2000), and 1260 ± 20 Ma (Pittenger et al., 1994). Subaqueous basaltic rocks of the overlying Mundy Breccia were emplaced into unconsolidated sediments of the Castner Marble (Pittenger et al., 1994; Ballard, 1997). The Mundy Breccia is unconformably overlain by quartz arenite, subarkose, and mudstone of the Llanoria Formation, which were initially deposited in a marine shelf setting that was subsequently overlain by deltaic deposits (Seeley, 1999). North-directed paleocurrent indicators and soft sediment deformation features suggest the Llanoria Formation was deposited in a tectonically active basin sourced from the south (Seeley, 1999). Spencer et al. (2014) interpret the Llanoria Formation to be a lateral equivalent of the Hazel Formation in the Van Horn region based on similar detrital zircon populations (but see Fig. 3.2 for an alternative interpretation). The 1111 ± 48 Ma Thunderbird Group is the youngest sequence in the Franklin Mountains and comprises felsic volcaniclastic rocks, rhyolite, and ignimbrite, which may represent the extrusive equivalents of the Red Bluff Granite (Thomann, 1980; Roths, 1993; Shannon et al., 1997).

The Debaca Group occurs in the subsurface of New Mexico and Texas and is known mainly from drill hole intersections and a small exposure in the Sacramento Mountains, New Mexico (Fig. 3.1). The Debaca Group comprises dolomite, volcaniclastic siltstone, arkose, and quartzite, which are intruded by 1090 ± 4 Ma gabbro (Flawn, 1956; Pray, 1961; Amarante, 2001). Like the Debaca Group, the Las Animas Formation of southern Colorado is a subsurface sequence and consists of a lower section of greywacke, mudstone, and chert and an upper sequence of arkose, dolomite, andesite, basalt, and tuff (Tweto, 1983).

The Apache Group of eastern Arizona contains carbonate, basalt, and siliciclastic rocks intruded by diabase between 1080 and 1094 Ma (Shride, 1967; Wrucke, 1989; Bright et al., 2014). The 1340 Ma Pioneer Shale forms the base of the Apache Group and consists of a locally-present basal conglomerate overlain by tuffaceous mudstone deposited in south-flowing alluvial fans and proximal

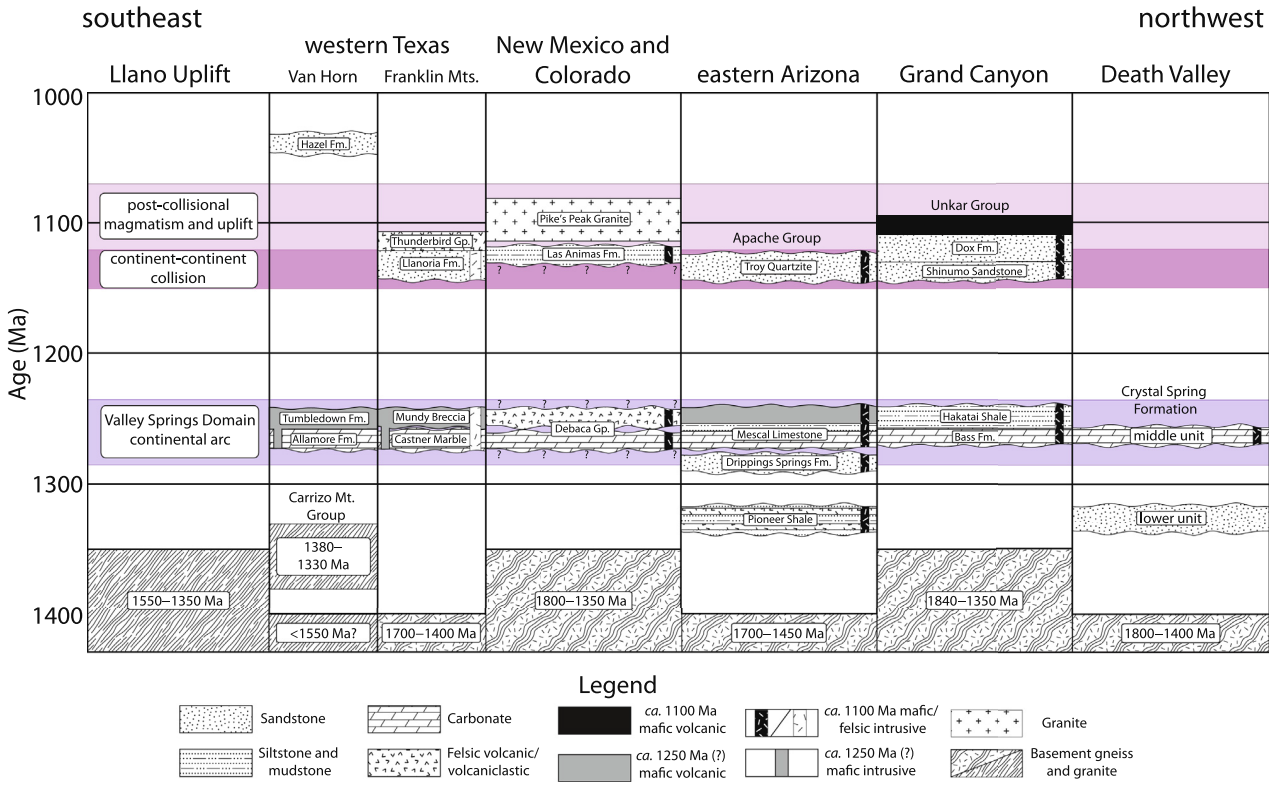

Figure 3.2: Regional correlation of Late Mesoproterozoic sedimentary and magmatic rocks in southwest Laurentia and relationship to tectonic events in the Grenville orogen of southern Laurentia modified from Timmons et al. (2005) with revised age of 1115–1066 Ma for Pike's Peak Granite from Guitreau et al. (2016), revised age of lower member of the Crystal Spring Formation from Mahon et al. (2014), age of Thunderbird Group from Bickford et al. (2000). Timing of tectonic events in Llano uplift (southern Grenville orogen) from Mosher et al. (2008). The *ca.* 1100 Ma and 1250 Ma magmatic rocks cross-cut older units so no age range is implied by the vertical orientation of the *ca.* 1100 Ma and 1250 Ma intrusive rocks in the diagram.

braided streams (Shride, 1967; Middleton and Trujillo, 1984; Cullom, 1996; Stewart et al., 2001; Doe, 2014). The unconformably overlying Dripping Springs Formation comprises arkosic sandstone and shale deposited in prograding tidal flats and distal alluvial fans derived from the south (Shride, 1967; Engel and Elmore, 1990; Middleton and Montgomery, 2001; Beraldi-Campesi et al., 2014). The lack of juvenile volcaniclastic material (e.g. glass shards) in the Dripping Springs Formation, which is abundant in the Pioneer Shale, suggests the unconformity above the Pioneer Shale represents a significant hiatus (Shride, 1967). The Mescal Limestone overlies the Dripping Springs Formation and consists of lower dolomite containing conglomerate and slump features and an upper stromatolitic dolomite overlain by mudstone and siltstone and capped by basalt flows (Shride, 1967; McConnell, 1975; Bertrand-Sarfati and Awramik, 1992). Following basaltic volcanism, the Apache Group was uplifted and gently folded prior to deposition of the Troy Quartzite (Shride, 1967; Skotnicki and Knauth, 2007). The lower Arkose Member of the Troy Quartzite was deposited in a north-northwest flowing braided stream complex and is overlain by westerly-derived quartz-rich eolian deposits (Shride, 1967; Weiss, 1986). The upper Chediski Member of the Troy Quartzite consists of conglomerate and quartz arenite deposited in southeast and southwest flowing braided streams and contains laterally extensive soft sediment deformation features that are interpreted to reflect syn-depositional seismicity (Shride, 1967; Burns, 1987; Wrucke, 1989).

The Unkar Group contains carbonate, siliciclastic, and mafic rocks exposed in a series of grabens in the eastern parts of Grand Canyon, Arizona (Sears, 1973; Timmons et al., 2005). Fig. 3.3 is a composite stratigraphic section of the Unkar Group with representative lithologies and sedimentary features that are shown in Fig. 3.3A–F. We use the Unkar Group as the basis for regional correlations as the stratigraphy of the major depositional units have been studied in detail and the lithologies and sedimentary features of the group are similar to those preserved in other Late Mesoproterozoic sequences throughout southwest Laurentia. The lowest unit of the Unkar Group is the Bass Formation, which comprises a basal conglomerate (Hotauta member) overlain by intertidal to subtidal stromatolitic dolomite, siltstone, and fine-grained sandstone (Dalton, 1972; Timmons et al., 2005). The Bass Formation is conformably overlain by marginal marine mudstone and arkose of the Hakatai Shale (Reed, 1976). Northwest-verging monoclines were active during deposition of the Bass and Hakatai sequences (Sears, 1973; Timmons et al., 2005). A low-angle unconformity separates the Hakatai Shale from cross-bedded quartz arenite comprising the Shinumo Sandstone (Fig. 3.3C). The Shinumo Sandstone was deposited in fluvial, marginal marine, and deltaic depositional environments with paleocurrent indicators recording north-directed flow (Daneker, 1975; Timmons et al., 2005). Soft sediment deformation is widespread throughout the Shinumo Sandstone and is interpreted to record syn-depositional seismic activity (Daneker, 1975; Middleton and Blakey, 1998). Deltaic and marginal marine quartz arenite, arkose, and mudstone of the Dox Formation conformably overlie the Shinumo Sandstone and were sourced from the south and west (Stevenson and Beus, 1982; Timmons et al., 2005). The upper Dox Formation interfingers with basaltic lava and volcaniclastic rocks of the 1104 Ma Cardenas Basalt, which was emplaced during northeast-southwest extension (Hendricks, 1972; Larson et al., 1994; Weil et al., 2003; Timmons et al., 2005).

The lower parts of the Pahrump Group of Death Valley, California includes the two unconformity-bound lower and middle members of the Crystal Spring Formation (Roberts, 1982; Mahon et al., 2014). The lower Crystal Spring Formation is a fluvial-marine conglomerate succession derived from the north and fines upward into intertidal-deltaic arkose and mudstone derived from the south (Roberts, 1982). The middle unit of the Crystal Spring Formation comprises stromatolitic dolomite and siliciclastic units derived from the south (Roberts, 1982). Both the lower and middle members of the Crystal Spring Formation were intruded by diabase at 1069 ± 3 and 1087 ± 3 Ma (Heaman and Grotzinger, 1992).

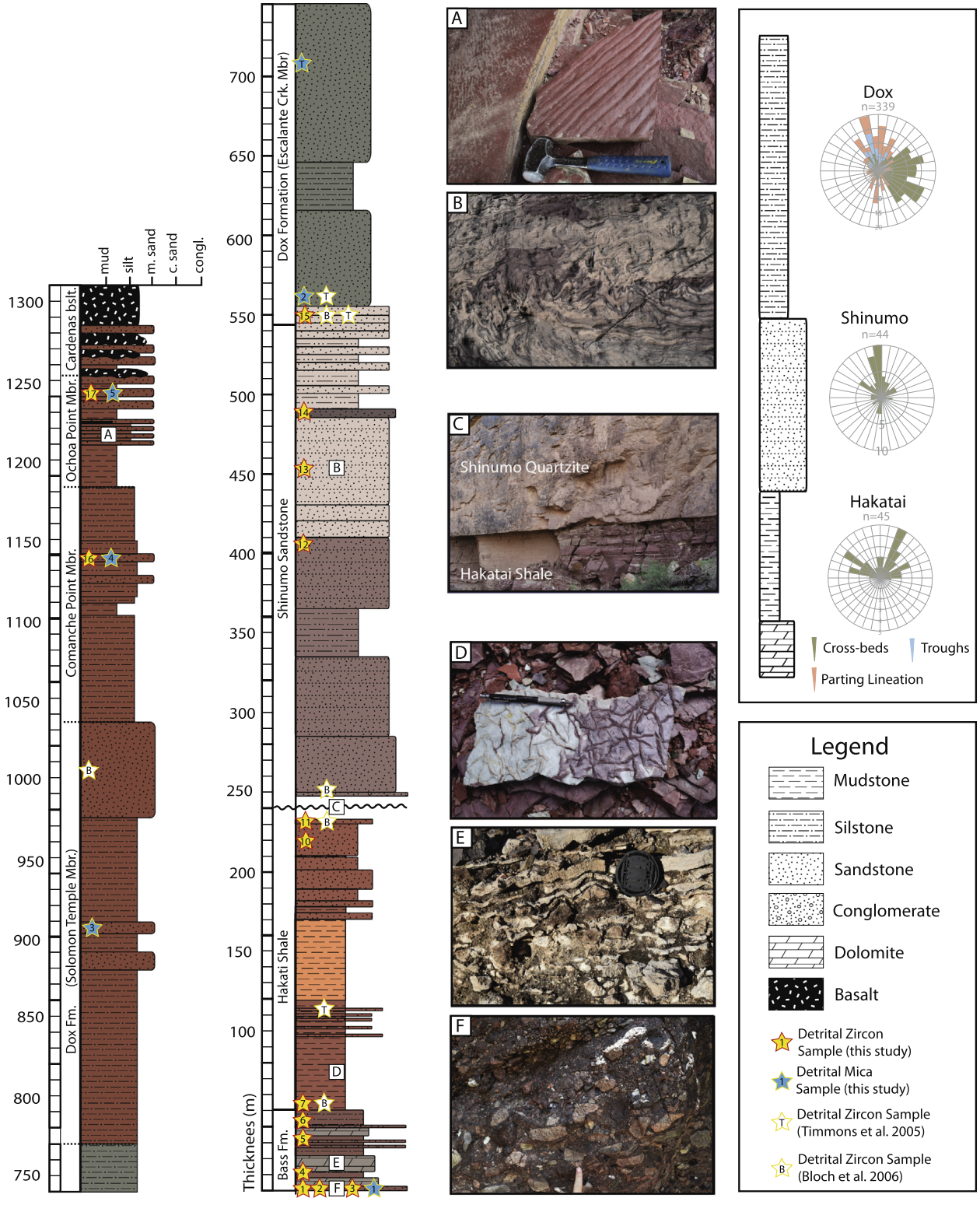

Figure 3.3: Idealized stratigraphic column of the Unkar Group, Grand Canyon, Arizona. The column is a composite of representative measured sections from each of the main depositional units and is compiled from: Dox Formation: Stevenson and Beus (1982), Hakatai Shale: Reed (1976), Bass Formation: Timmons et al. (2005). The Shinumo Sandstone section was measured during this study. Stars show approximate stratigraphic location of detrital mineral samples collected or compiled for this study, star labels correspond to sample numbers listed in Appendix 3.1 Field photographs show typical lithologies and sedimentary features of the Unkar Group: A) Ripple marks in fine-grained red sandstone, Dox Formation. B) Convoluted folds in quartz arenite produced by soft sediment deformation, Shinumo Sandstone. C) Unconformity between Shinumo Sandstone and Hakatai Shale. D) Mudcrack casts in red mudstone, Hakatai Shale. E) Stromatolitic dolomite, Bass Formation. F) Polymictic conglomerate, Hotauta Member of Bass Formation. Inset shows paleocurrent data summarized in rose diagrams with bin widths of 10°. Paleocurrent data compiled from: Dox Formation: Stevenson and Beus (1982), Timmons et al. (2005), Shinumo Sandstone: Timmons et al. (2005), Hakatai Shale: Reed (1976).

3.4 Analytical methods

Sample location information and stratigraphic context of detrital mineral samples collected during this study are presented in Appendix. 3.1.

3.4.1 Detrital zircon U-Pb analysis

Detrital zircon samples were processed by standard separation techniques and mounted in epoxy with the Sri Lanka primary standard and R33 and FC-1 secondary standards (Gehrels et al., 2008; Gehrels and Pecha, 2014). Zircons were analyzed via Laser Ablation-Inductively Couple Plasma Mass Spectrometry at the Arizona LaserChron Center following the methods outlined by Gehrels et al. (2008) and Gehrels and Pecha (2014). Approximately one hundred zircon grains from each sample were selected randomly for analysis with the placement of analysis spots aided by cathodoluminesence and Back Scattered Electron images. Analytical data are presented in Appendix. 3.2. Detrital zircon age data are plotted as probability distribution plots with Isoplot version 3.1 (Ludwig, 2003) using $^{207}Pb/^{206}Pb$ ages and 1σ uncertainties for analyses between 80 and 105% concordant (Fig. 3.4). The Unmix algorithm of Isoplot (Sambridge and Compston, 1994; Ludwig, 2003) was used to explore the distribution of ages for the youngest zircons (1350–1100 Ma) in the major depositional units of each basin (Table 3.1). Full analytical results are reported in Appendix. 3.2 and probability density plots and concordia plots for all samples analyzed during this study are included in Appendix. 3.3 and 3.4

3.4.2 Detrital muscovite and biotite $^{40}Ar/^{39}Ar$ analysis

Detrital muscovite and biotite samples were crushed, washed, and sieved, followed by hand picking of 50–100 crystals from the 60–90 sieve fraction. Step heating and total fusion experiments were conducted at the New Mexico Geochronology Research Laboratory, New Mexico Institute of Mining and Technology, using a Synrad 50 W CO2 laser beam coupled to a MAP 215-50 mass spectrometer. Full details of the instrumental set up, analytical protocols, and details of plateau age calculations and correction factors applied to the total fusion ages follow Fletcher (2004) and are outlined in Appendix. 3.5 The step heated and total fusion ages are combined in probability distribution plots using 1σ uncertainties (Fig. 3.4) and the full analytical results are reported in Appendix. 3.6 and 3.7**.** The $^{40}Ar/^{39}Ar$ ages derived from the detrital micas reflect the time at which rocks in the source region cooled through the closure temperature of Ar diffusion for the respective micas. These cooling age are a function of grain size and cooling rate and range from 300 to 420 °C for muscovite (Purdy and Jäger, 1976) and 280 to 345 °C for biotite (Harrison et al., 1985). We use 350 °C and 300 °C as the general cooling temperatures for muscovite and biotite respectively.

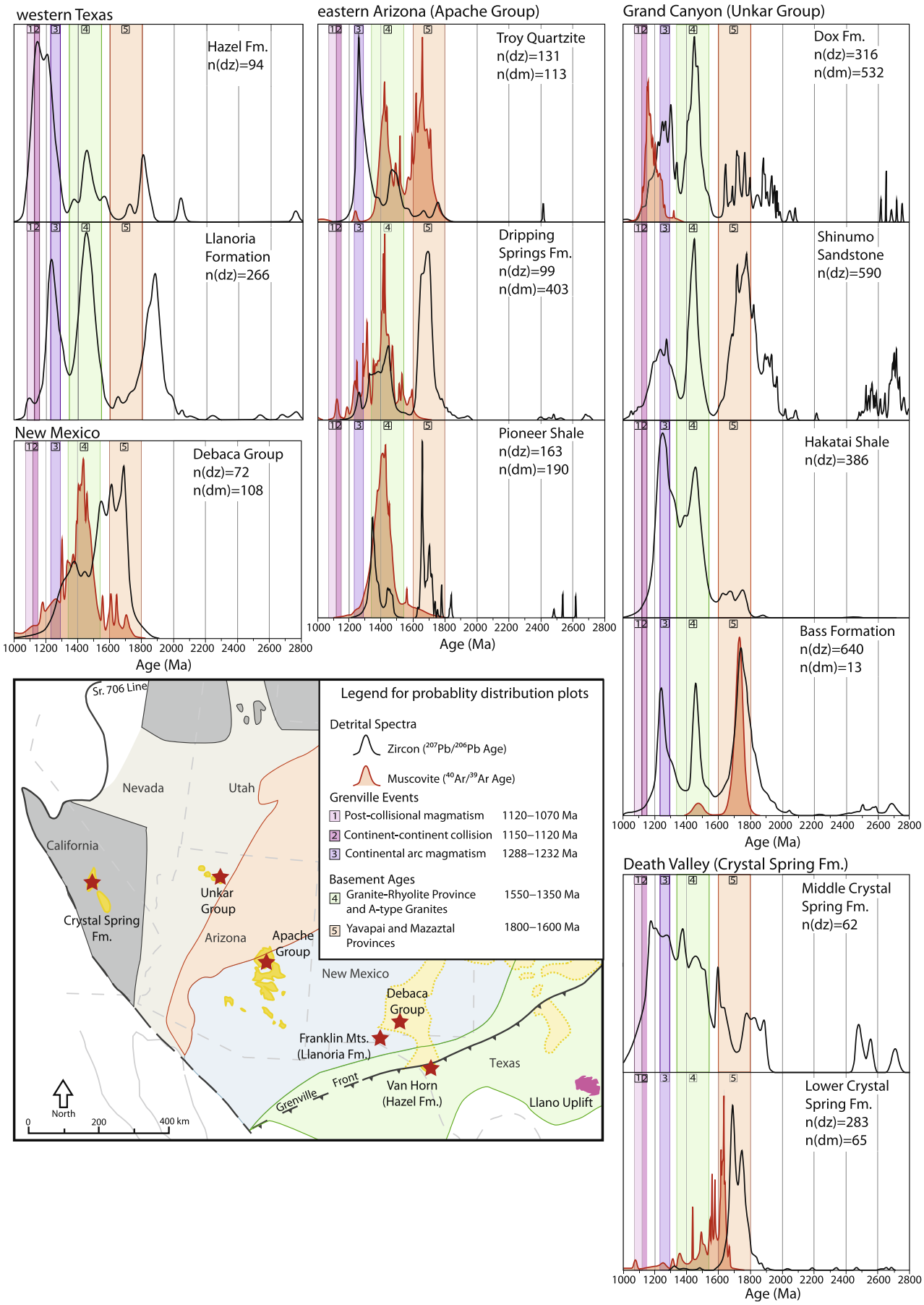

Figure 3.4: Probability distribution plots of detrital zircon and detrital muscovite data from Late Mesoproterozoic sequences of southwest Laurentia. Colored bars show age range of tectonic events in the southern Grenville Orogeny (after Mosher et al., 2008) and age ranges for basement provinces of southwest Laurentia. Inset map shows approximate location of samples (red stars) for each of the basins.

3.5 Results

Detrital mineral results for each of the Late Mesoproterozoic basins of southwest Laurentia are discussed in order of increasing distance from the Grenville orogenic front in southern Laurentia (Figs. 3.1 and 3.2) and are summarized in probability density plots that integrate new and previously published detrital zircon, muscovite, and biotite ages. Fig. 3.5 is an enlargement of the 1350–1000 Ma age window for the same data presented in Fig. 3.4, which highlights the distribution of 'Grenville-aged' (1300–1000 Ma) detritus in the Late Mesoproterozoic basins of southwest Laurentia. Color bands in Figs. 3.4 and 3.5 correspond to the duration of tectonic events in the Llano uplift during the Grenville Orogeny in southern Laurentia (after Mosher et al., 2008) and age ranges for basement provinces throughout southwest Laurentia (Fig. 3.1).

3.5.1 Detrital zircon results

3.5.1.1 Western Texas sequences

The detrital zircon dataset from the Late Mesoproterozoic sequences in western Texas includes 124 concordant analyses from 2 new samples of the Llanoria Formation in addition to the 142 analyses of the Llanoria Formation and 94 analyses of the Hazel Formation published by Spencer et al. (2014). Approximately 35% of the detrital zircons analyzed from the Llanoria Formation have Paleoproterozoic crystallization ages, which form an age peak at 1872 Ma. Mesoproterozoic zircon ages from the Llanoria Formation include age peaks at 1441 Ma, 1293, and 1229 Ma (Table 3.1 and Fig. 3.4). In contrast to Spencer et al. (2014), we interpret the small population at *ca.* 1080 Ma from the Llanoria Formation to reflect zircons affected by Pb-loss as this age is younger than the overlying 1111 Ma Thunderbird Group and crosscutting 1120 Ma Red Bluff Granite (Bickford et al., 2000). Paleoproterozoic zircon ages comprise 15% of the total analyses from the Hazel Formation with the largest age peak occurring at 1801 Ma. Approximately 20% of zircons from the Hazel Formation are assigned to an age peak at 1441 Ma, which is flanked by a minor younger peak at 1360 Ma comprising 3 analyses and an older peak at 1549 Ma comprising 4 analyses. 'Grenville-aged' zircons comprise 65% of the Hazel Formation dataset and form age peaks at 1263, 1205, and 1130 Ma (Table 3.1). Note that the age peaks quoted above for the Hazel Formation differ from those reported by Spencer et al. (2014) due to the more conservative concordance limits used in this study.

3.5.1.2 Debaca Group

The new Debaca Group dataset includes 67 concordant analyses from the exposure in the Sacramento Mountains, New Mexico. The new dataset greatly bolsters the detrital record of this poorly known sequence, which was previously restricted to 5 concordant zircons analyzed from the Mescalero 1 Well (Fig. 3.1, Barnes, 2001; Amarante, 2001). The oldest age peaks in the

Table 3.1: Youngest detrital zircon analysis

Unit/Basin	Interpreted age (Ma)	Age of young Populations (Ma)	±1σ	Number of grains in young populations	Percentage of young population of the total 1350—1000 Ma analyses
Western Texas					
Llanoria Formation	1140—1100	1229	3	57	80
		1293	8	14	20
Hazel Formation	1130—1035	1130	5	28	46
		1205	7	26	43
		1263	11	6	10
*Debaca Group**	1300—1090	1304	-	10	100
Apache Group					
Pioneer Shale*	1340	1338	-	40	100
Dripping Springs Formation	1255—1230	1256	3	15	31
		1327	2	32	69
Troy Quartzite	1140—1100	1259	3	94	96
		1325	19	4	4
Unkar Group					
Bass Formation	1255—1230	1234	1.7	129	75
		1302	4.8	43	25
Hakatai Shale	1255—1230	1243	2	149	75
		1317	3	50	25
Shinumo Sandstone	1140—1100	1111	9	4	3
		1184	5	35	27
		1230	5	36	28
		1282	2	55	43
Dox Formation	1140—1100	1201	4	33	32
		1256	5	37	36
		1309	3	32	31
Lower Pahrump Group					
Lower Crystal Springs*	1320	1323	-	3	100
Middle Crystal Springs*	1255—1230	1210	-	4	100

*Single young population, quoted age is the youngest peak on probability distribution plot.

Debaca Group dataset occur at 1686 and 1609Ma. Early Mesoproterozoic (1600–1500 Ma) crystallization ages comprise 25% of the total population and form an age peak at 1542 Ma. The youngest detrital zircon age population in the Debaca Group occurs at 1304 Ma (10 grains).

3.5.1.3 Apache Group

The probability density distribution of the 163 concordant analyses from the Pioneer Shale contains a small grouping of age peaks between 2400 and 2600 Ma, a prominent age peak at 1650 Ma, and a

smaller age peak at 1430 Ma. The youngest zircon population from the Pioneer Shale occurs at 1338 Ma and includes approximately 24% of the detrital zircons analyzed from this unit.

The Pioneer Shale dataset contains no 'Grenville-aged' (1300–1000 Ma) zircons. The Dripping Springs Formation dataset contains 383 new analyses to compliment the 20 analyses previously published by Stewart et al. (2001). Detrital zircons from the Dripping Springs Formation form populations at 2600–2400 Ma, 1800–1600 Ma, 1440 Ma, all of which closely match the age peaks found in the underlying Pioneer Shale and also contains a spread of ages between 1400 and 1300 Ma. However, unlike the Pioneer Shale, 12% of the detrital zircons from the Dripping Springs Formation have <1350 Ma crystallization ages, which form age peaks at 1327 and 1256 Ma (Table 3.1 and Fig. 3.5). The 118 new analyses from the Troy Quartzite and 13 analyses published by Stewart et al. (2001) have a minor spread of Paleoproterozoic ages (1800–1600 Ma) and a 1450 Ma age peak. The Troy Quartzite dataset is dominated by a large age peak centered on 1259 Ma, which contains nearly half of the concordant analyses from the 3 samples.

3.5.1.4 Unkar Group

All units within the Unkar Group contain a complex distribution of Paleoproterozoic zircons typically between 1800 and 1600 Ma, large age peaks at *ca.* 1450 Ma, and a young populations between 1300 and 1200 Ma (Figs. 3.4 and 3.5). Approximately 70% of the 640 concordant detrital zircons from the Bass Formation analyzed during this study have crystallization ages >1400 Ma, which form two age peaks at 1450 Ma and 1732 Ma, and a minor distribution of ages between 2675 and 2450 Ma. The youngest detrital zircon population from the Bass Formation forms an age peak at 1234 Ma with a shoulder of older ages extending between 1285 and 1354 Ma with an age peak at 1302 Ma (Table 3.1 and Fig. 3.5). The detrital zircon dataset from the Hakatai Shale includes 256 new analyses in addition to the 77 analyses published by Timmons et al. (2005) and 53 analyses published by Bloch et al. (2006). Detrital zircons from the Hakatai Shale form a relatively simple probability distribution that includes a minor group of Paleoproterozoic grains between 1600 and 1800 Ma and a major age peak at 1452 Ma, which forms 52% of the total analyses. The youngest zircons in the Hakatai Shale form an age peak at 1243 Ma and a second smaller peak at 1317 Ma (Table 3.1 and Fig. 3.5).

The Shinumo Sandstone dataset includes 334 new analyses collected during this study to compliment the 88 analyses published by Timmons et al. (2005) and 168 analyses published by Bloch et al. (2006). Unlike the lower units of the Unkar Group, the Shinumo Sandstone contains abundant Late Archean—Early Paleoproterozoic zircons forming a complex age distribution between 2400 and 2800 Ma (Fig. 3.4). The majority of Paleoproterozoic detrital zircons from the Shinumo Sandstone have crystallization ages between 1600 and 2000 Ma, which represent 42% of the total population from this unit. Mesoproterozoic zircons from the Shinumo Sandstone form an age peak at 1440 Ma and a complex distribution of age peaks between 1183 and 1305 Ma, the largest of which occurs at 1282 Ma (Table 3.1). Ages between 1000 and 1180 Ma are interpreted to be derived from zircons affected by Pb-loss as they generally have low precision and form only a single minor age peak at

1111 Ma, which consists of only 4 zircons (Table 3.1). Over half (55%) of the 1000–1180 Ma analyses from the Shinumo Sandstone come from a single sample (T01-75-7) that also yields detrital zircons with ages younger than the 1104 Ma depositional age of the overlying Cardenas Basalt, which supports the interpretation that zircons in sample T01-75-7 have experienced Pb-loss. Our preferred youngest age peak in the Shinumo Sandstone dataset occurs at 1184 Ma and consists of 35 individual analyses representing 27% of the total ages between 1100 and 1350 Ma from this unit (Table 3.1 and Fig. 3.5). We present 152 new analyses from the Dox Formation in addition to the 92 analyses published by Timmons et al. (2005) and the 72 analyses of Bloch et al. (2006). The Dox Formation dataset contains a small population of Late Archean to Early Paleoproterozoic zircons between 2400 and 2600 Ma, a broad distribution of ages at 1600–2000 Ma, and a prominent 1440 Ma population. Detrital zircons with crystallization ages <1350 Ma comprise 33% of the total analyses from the Dox Formation and form a cluster of age peaks at 1201 Ma, 1256 Ma, and 1309 Ma (Table 3.1).

3.5.1.5 Lower Pahrump Group

The two detrital zircon samples from the lower member of the Crystal Spring Formation reported by Mahon et al. (2014) are dominated by Paleoproterozoic zircons with 96% of the analyses having ages between 1600 and 1900 Ma and a minor scatter of ages between 2000 and 2700 Ma. The youngest detrital zircons from the lower member of the Crystal Spring Formation form a small age peak at 1323 Ma (3 grains). Detrital zircon data from the middle member of the Crystal Spring Formation collected during this study (62 concordant analyses) form a complicated age distribution, which includes age peaks between 2450 and 2880 Ma, and a grouping of Paleoproterozoic peaks between 1700 and 1900 Ma. Mesoproterozoic detrital zircons form an age peak at 1596 Ma and include 25 grains that form a broad spread of ages between 1100 and 1350 Ma, with a possible age peak at 1210 Ma comprising 4 analyses.

3.5.2 Detrital mica results

Detrital muscovite was analyzed from almost all of the major stratigraphic units from each of the Late Mesoproterozoic basins of southwest Laurentia with the exception of the sequences in western Texas. Approximately 1001 new analyses of detrital muscovite grains from 24 samples are summarized (in red) along with the detrital zircon probability distribution plots in Figs. 3.4 and 3.5. The muscovite data include analyses from both step heating and total fusion experiments. The spread in ages derived from the two different methods generally overlap, so that the sharp peaks from the higher precision step heated ages are superimposed over broader peaks from the lower precision total fusion method. Therefore, although the majority of ages quoted from the probability density plots in Figs. 3.4 and 3.5 reflect discrete populations of step heated data, these age peaks are also representative of the total fusion results for a given sample (Apendix 3.5).

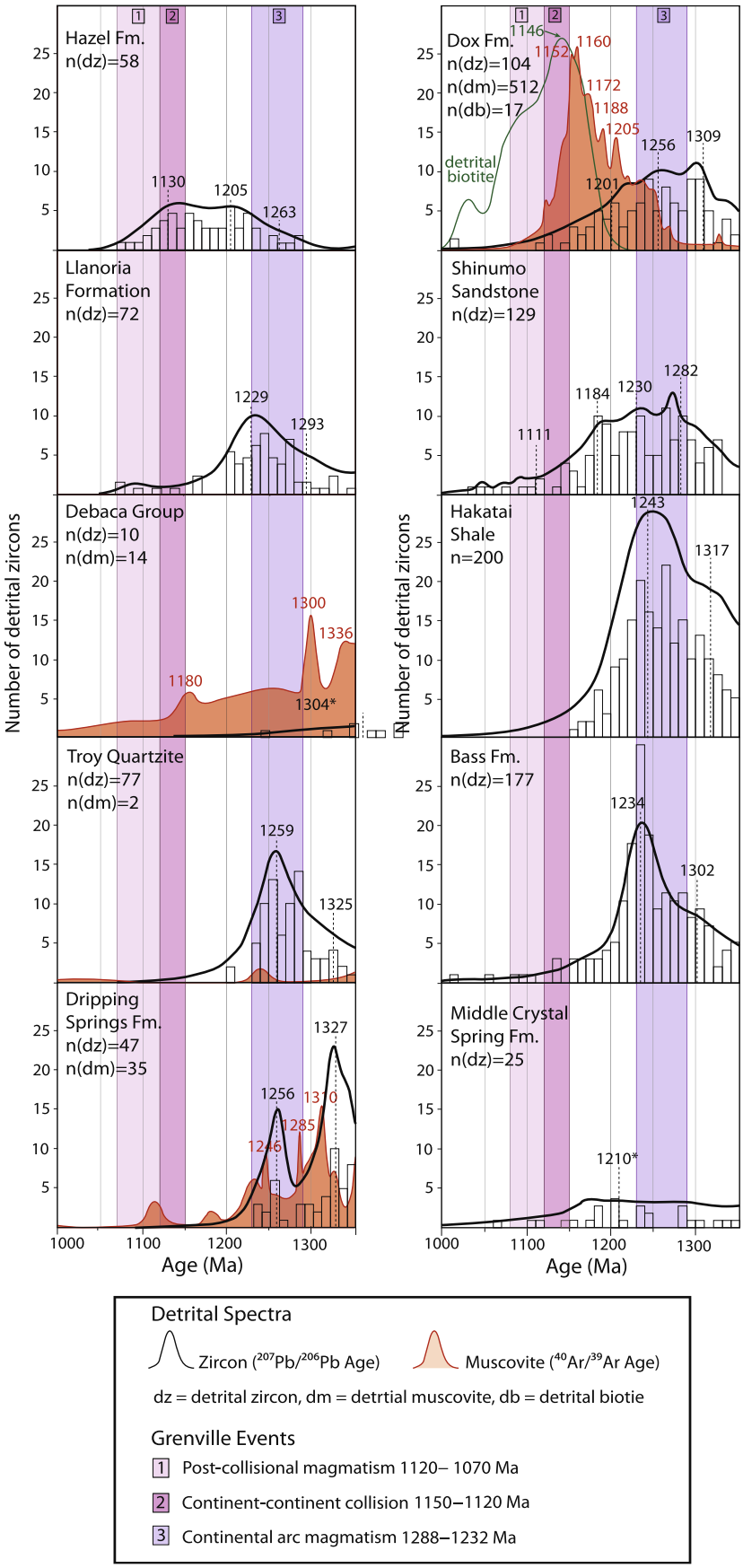

Figure 3.5: Probability distribution plots and histograms of the young populations (1350–1100 Ma) of detrital zircon, muscovite, and biotite ages from Late Mesoproterozoic basins of southwest Laurentia. Detrital zircon age peaks were derived from Unmix algorithm of Isoplot (Table 3.1). Colored bars show age ranges for tectonic events in the southern Grenville Orogeny (after Mosher et al., 2008).

3.5.2.1 Debaca Group

The Debaca Group detrital muscovite ages are spread between 1000 and 1530 Ma and are dominated by a cluster of age peaks between 1000 and 1460 Ma (Fig. 3.4). Paleoproterozoic cooling ages are rare (7 of 108 analyses) and form minor peaks between 1600 and 1700 Ma. The youngest cooling ages form a broad distribution between 1000 and 1400 Ma, which includes peaks at 1180 Ma, 1300 Ma, 1336 Ma, and 1370 Ma. Approximately 20% of the analyses from the Debaca Group produce a spread of low-precision ages from 100 Ma to 1000 Ma, which are interpreted to represent crystals affected by Ar-loss.

3.5.2.2 Apache Group

Detrital muscovite cooling age distributions throughout the Apache Group stratigraphy are characterized by the persistence of a large 1450 Ma cooling age peak and a scarcity of <1400 Ma cooling ages. Cooling ages from the Pioneer Shale form a cluster of age peaks between 1370 and 1450 Ma and a minor, broad distribution between 1500 and 1800 Ma. Detrital muscovite from the Dripping Springs Formation has a complex cooling age spectrum characterized by a prominent double peak at 1410–1420 Ma, which is flanked by clusters of smaller peaks between 1510 and 1590 Ma and a second cluster of peaks between 1440 and 1470 Ma. Younger cooling ages from the Dripping Springs Formation include peaks between 1230 and 1320 Ma and two minor peaks at 1110 and 1180 Ma. An influx in detrital muscovite with Paleoproterozoic cooling ages is recorded in the upper most Apache Group by the Troy Quartzite and form a spread of ages between 1600 and 1710 Ma with a prominent age peak at 1660 Ma. As with the underlying stratigraphy of the Apache Group, <1400 Ma cooling ages are rare in the Troy Quartzite with a minor peak at 1230 Ma reflecting a single total fusion analysis.

3.5.2.3 Unkar Group

Detrital muscovite cooling ages from the basal conglomerate (Hotauta Member) of the Bass Formation (lower Unkar Group) define a relatively simple probability density distribution characterized by a prominent peak at 1710 Ma and a small peak derived from a single total fusion analysis at 1450 Ma (Fig. 3.4). In contrast to the Bass Formation, the Dox Formation (upper Unkar Group) contains abundant Late Mesoproterozoic detrital muscovite with 97% of analyses producing cooling ages <1300 Ma. The probability distribution plot for the Dox Formation contains 450 analyses obtained during this study in addition to the 82 analyses reported by Timmons et al. (2005) and is dominated by two large age peaks at 1152 Ma and 1160 Ma and spread of older ages up to 1250 Ma including peaks at 1172 Ma, 1188 Ma, and 1205 Ma. A minor peak occurs at 1123 Ma and comprises 13 analyses that may represent the youngest detrital muscovite population for the Dox Formation. However, only 1 of the 10 analyses obtained during this study assigned to the

Table 3.2: Number of detrital muscovite analyses by method and major cooling age peaks for each member of the Dox Formation, Unkar Group (data from this study only).

Member	Total Fusion analyses	Step heated analyses	Age peaks (Ma)
Escalante Creek	103	55	1160, 1200, 1220
Solomon Temple	55	10	1150, 1160, 1200, 1220
Comanche Point	75	0	1160
Ochoa Point	92	11	1160, 1230

1123 Ma peak is a precise step heated age. We prefer a more conservative estimate of the youngest detrital muscovite population in this sample derived from the next youngest peak at 1152 Ma, which contains 66 individual analyses, including 15 step heated ages. There is no appreciable difference in the muscovite ages derived from each of the members of the Dox Formation with both total fusion and step heated data from the individual members containing the 1150–1250 Ma spread of ages observed in the combined probability density plot (Table 3.2 and Figs. 3.4 and 3.5). The major 1140 Ma detrital muscovite age peak reported by Timmons et al. (2005) from the basal member of the Dox Formation was not reproduced in any of the new samples analyzed during this study but forms a prominent shoulder on the 1152 Ma peak in the combined probability density plot (Fig. 3.5). Detrital biotite from the Solomon Temple Member of the Dox Formation has a spread of ages between 1030 and 1190 Ma, forming a broad age peak centered on 1146 Ma. We interpret this 1146 Ma peak to be the youngest reliable detrital mica cooling age peak from the Dox Formation, which agrees with the 1140 Ma maximum depositional age for the Dox Formation based on the detrital muscovite data reported by Timmons et al. (2005).

3.5.2.4 Lower Pahrump Group

Detrital muscovite from the lower member of the Crystal Spring Formation define a complex cooling age spectrum with a spread of ages from 1080 to 1670 Ma. Paleoproterozoic cooling ages comprise 57% of the analyses and form a large age peak at 1620 Ma. Mesoproterozoic cooling ages include peaks at 1440 Ma, 1560 Ma, and 1580 Ma and series of small broad peaks extending from 1080 to 1300 Ma.

3.6 Discussion

3.6.1 Provenance of Late Mesoproterozoic sequences

Integrating the detrital zircon and mica datasets refines the correlation of sedimentary successions and provenance of the Late Mesoproterozoic basins of southwest Laurentia by revealing the crystallization age of rocks in the source region as indicated by detrital zircon ages and the time at which source regions most recently passed through the closure temperature for muscovite (300–420 °C, Purdy and Jäger, 1976) and biotite (280–345 °C, Harrison et al., 1985).

3.6.1.1 Detrital zircon provenance

The detrital zircon record of Late Mesoproterozoic basins of southwest Laurentia show broad similarities to one another; most of the major depositional units are characterized by 1600–1800 Ma distributions, prominent age peaks at 1440–1450 Ma, and Late Mesoproterozoic populations that typically form age peaks between 1230 and 1250 Ma (Fig. 3.5). We suggest the overall similarity of the detrital zircon populations of Late Mesoproterozoic strata in southwest Laurentia reflects derivation of these sequences from broadly similar sources, which are discussed on a regional basis below.

Of the 3457 concordant zircons analyses included in this study, 14% have Archean or pre-1800 Ma Paleoproterozoic ages and 32% have ages between 1600 and 1800 Ma. We interpret the source of the 1600–1800 Ma detrital zircons to be metaigneous and metasedimentary sequences of the Yavapai and Mazatzal terranes (Fig. 3.1). Archean and pre-1800 Ma Early Paleoproterozoic detrital zircons are less common in the Late Mesoproterozoic southwest Laurentian basins but form notable age distributions in the Llanoria Formation, upper Unkar Group, and middle Crystal Spring Formation (Fig. 3.4). The >1800 Ma detrital zircons in the middle member of the Crystal Spring Formation were likely derived from local Paleoproterozoic metasedimentary sequences in the Mojave province, which contain 1800–1900 Ma and Archean zircons (e.g. Wooden et al., 2012). We suggest the >1800 Ma zircons in the upper Unkar Group were sourced locally from recycling of the Paleoproterozoic Vishnu Schist, which contains an approximately bimodal detrital zircon age distribution with broad age peaks at 2400–2800 Ma and 1740–2000 Ma and was likely derived from the Mojave province (Shufeldt et al., 2010; Holland et al., 2015). A similar source in the Mojave province, or sedimentary sequences derived from the Mojave province, may account for the 1872 Ma age population in the Llanoria Formation.

Only the sample of the Debaca Group contains appreciable (25% of the total population) 1500–1600 Ma detrital zircons (Fig. 3.4). The 1500–1600 Ma interval is defined as the North American Magmatic Gap as crust of this age is rare in exposed Laurentian basement terranes (Bowring and Karlstrom, 1990; Ross and Villeneuve, 2003; Karlstrom et al., 2004). However, 1500–1600 Ma detrital zircons are found in the 1500–1450 Ma Yankee Joe Formation of central Arizona (Doe et al., 2012, 2013) and Trampas Group of New Mexico (Daniel et al., 2013) and are interpreted to have been derived from basement terranes outside of Laurentia (perhaps Australia). Although more data are required, we interpret at least part of the 1300–1090 Ma Debaca Group to have been derived from recycling of the Yankee Jo Formation and Trampas Group successions.

Approximately 19% of the total zircon population has ages between 1400 and 1500 Ma and there are major age peaks between 1440 and 1450 Ma in most samples. The 1400–1500 Ma zircons were likely sourced from voluminous A-type granites in the southern Granite-Rhyolite Province and from granites that intrude Paleoproterozoic basement terranes throughout southwest Laurentia. Only 4% of the detrital zircons in the total dataset have ages between 1400 and 1350 Ma, which may have been derived from felsic igneous rocks in southern Granite-Rhyolite Province or the 1380–1330 Ma Carrizo Mountain Group (Figs. 3.1 and 3.2). The remaining 28% of detrital zircons in

the dataset have <1350 Ma ages that generally form age peaks at 1230—1300 Ma (Table 3.1). A plausible source region for these younger zircons is the southern Granite-Rhyolite Province, which although dominated by >1350 Ma plutons, records magmatism as young as 1320 Ma (Bickford et al., 2015). A second source region for <1350 Ma zircons is the 1288–1232 Ma continental arc complex preserved in the Valley Springs and Packsaddle Domains of the Llano uplift (Mosher et al., 2008). The continental arc rocks in the Llano uplift may also account for the 1230–1250 Ma detrital zircon populations, which are common in the Late Mesoproterozoic basins of southwest Laurentia. Detrital zircons with crystallization ages between the end of continental arc activity at 1232 Ma and the onset of syn-collisional magmatism in the Llano uplift at 1150 Ma are rare in the Late Mesoproterozoic basins of southwest Laurentia (Table 3.1 and Fig. 3.5). Units with notable 1150–1232 Ma age peaks include the Hazel Formation (1205 Ma), Dox Formation (1201 Ma), and Shinumo Sandstone (1184 Ma). The 1180–1200 Ma detrital zircons from these three units could have been derived from rocks formed during continued (i.e. post-1232 Ma) magmatism along the southern margin of Laurentia, but which are no longer exposed. An alternative source is 1200–1180 Ma Anorthosite-Magnerite-Charnockite-Granite suites in the San Gabriel and Eagle Mountains of California (Fig. 3.1, Barth et al., 2001; Wooden et al., 2012).

3.6.1.2 Detrital muscovite provenance

As with the detrital zircon dataset, detrital muscovite data from most of the Late Mesoproterozoic sequences throughout southwest Laurentia show broad similarities between basins and are interpreted to have been derived from similar source regions. Detrital muscovite from Late Mesoproterozoic strata throughout southwest Laurentia are dominated by >1400 Ma cooling ages (Fig. 3.4). Approximately 54% of the >1400 Ma cooling ages occur between 1400 and 1500 Ma and form major age peaks between 1420 and 1450 Ma in most samples. The *ca.* 1450 Ma detrital muscovite is likely derived from the basement terranes of southwest Laurentia, which preserve widespread 1400–1500 Ma muscovite cooling ages reflecting magmatism and the exhumation associated with the Picuris Orogeny (Shaw et al., 2005; Daniel et al., 2013; Jones et al., 2015). The common 1600–1700 Ma detrital muscovite ages likely reflect unroofing of basement terranes in southwest Laurentia that were less affected by 1400–1500 Ma thermal overprinting (e.g. Shaw et al., 2005).

Detrital muscovite with 1500–1600 Ma cooling age peaks occur in the Debaca Group, Pioneer Shale, and lower member of the Crystal Spring Formation (Fig. 3.4). Similar to our interpretation for the 1500–1600 Ma detrital zircons in the Debaca Group, these detrital muscovites may have been recycled from the Early Mesoproterozoic Yankee Jo Formation and Trampas Group, which contain 'exotic' 1500–1600 Ma detritus, possibly derived from outside of Laurentia.

In contrast to the other Late Mesoproterozoic sequences, the detrital muscovite dataset from the Dox Formation (upper Unkar Group) is dominated by <1400 Ma cooling ages, which are mostly between 1160 and 1200 Ma (Fig. 3.5). Mica with cooling ages <1400 Ma are uncommon in the

basement terranes of southwest Laurentia (Shaw et al., 2005), which suggests that the Grenville orogen of southern Laurentia is the probable source for detrital muscovite and biotite in the Dox Formation. Detrital muscovite and biotite in the Dox Formation are unlikely to have been derived from the core of the Grenville orogen as the Dox Formation contains few detrital zircons with ages coincident with 1120–1150 Ma high-grade metamorphic and plutonic rocks exposed in the Llano uplift. Instead, detrital mica in the Dox Formation are interpreted to have been sourced from the structurally high parts of the orogen, which may have consisted of imbricated thrust sheets of the southern margin of Laurentia (i.e. 1232–1288 Ma continental arc rocks). Exhumation of 1232–1288 Ma crust from depths of approximately 10–15 km (i.e. depths corresponding to the 280–450 °C closure temperatures of biotite and muscovite) by thrust stacking during the early stages of continent–continent collision (i.e. before the onset of 1150–1120 Ma high-grade metamorphism and magmatism) therefore provides a suitable source for Late Mesoproterozoic detrital zircon, muscovite, and biotite in the Dox Formation (Fig. 3.5).

Interestingly, the Troy Quartzite, which is broadly time-equivalent to the Dox Formation (Fig. 3.2), contains abundant 1200–1300 Ma detrital zircons but few detrital muscovites with <1400 Ma cooling ages (Fig. 3.4). The detrital muscovite record of the Troy Quartzite is instead dominated by *ca.* 1450 Ma and 1600–1700 Ma cooling ages (Fig. 3.4). The Troy Quartzite is interpreted to have been sourced in part from Paleoproterozoic muscovite-rich, zircon-poor pelitic metasedimentary rocks, which can account for the abundance of 1600–1700 Ma detrital muscovite and scarcity of Paleoproterozoic detrital zircons in the dataset (Fig. 3.4). The abundance of 1200–1300 Ma detrital zircon in the Troy Quartzite suggests a source within the Grenville orogen to the south. However, unlike the Dox Formation, the Troy Quartzite did not receive abundant 1160–1200 Ma detrital muscovite from the Grenville orogen. We suggest that in addition to local Paleoproterozoic and Mesoproterozoic basement, the Troy Quartzite was sourced in part from a zircon-rich, muscovite-poor source within the Grenville orogen, possibly a metaluminous granitic or volcanic suite.

In summary, the detrital mineral record of Late Mesoproterozoic sedimentary sequences in southwest Laurentia is consistent with a combination of source regions including local Paleoproterozoic and Mesoproterozoic basement terranes and more distal sources in the Grenville orogen to the south. The provenance of the Late Mesoproterozoic basins highlights a complex interplay between local and distal transport systems that in some cases resulted in detrital zircon being derived from a distinctly different source region than detrital muscovite in the same sample.

3.6.2 A new tectonic model for Late Mesoproterozoic basin formation in southwest Laurentia

Integration of the new detrital mineral dataset, basin sedimentology and stratigraphy, and recent models for the tectonic evolution of the Grenville Orogeny in southern Laurentia (e.g. Carlson et al., 2007; Mosher et al., 2008; Levine and Mosher, 2010; Davis and Mosher, 2015), allows us to refine the depositional age and correlation of Late Mesoproterozoic basins in southwest Laurentia. The refinements to the depositional age and correlation of Late Mesoproterozoic basins in southwest

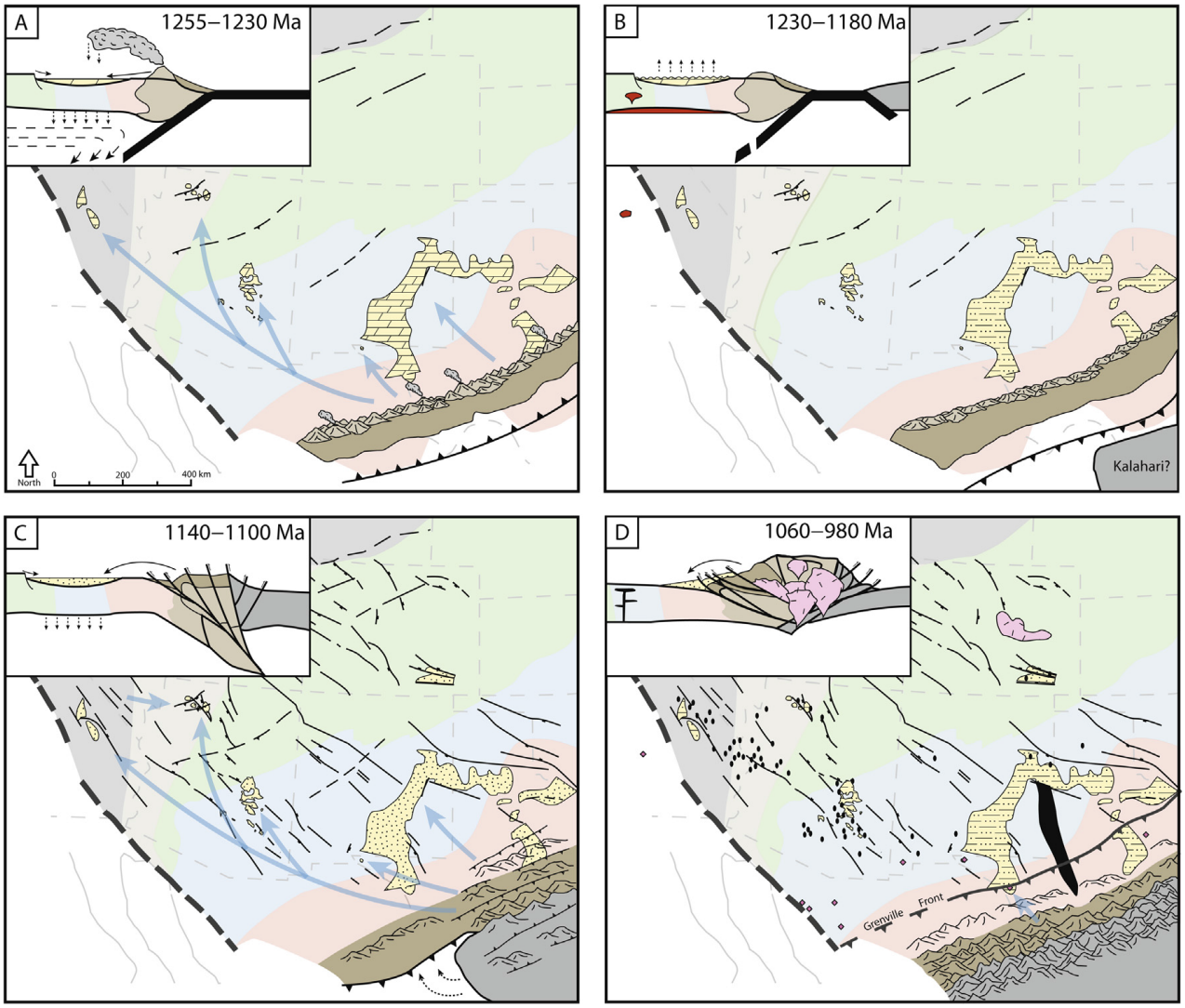

Figure 3.6: Tectonic evolution of southwest Laurentia from 1255 Ma to 1070 Ma highlighting the relationship between tectonic events in the Grenville orogen and intracratonic sedimentary basins. Symbols and colors for basement terranes, faults, and magmatic rocks as for Fig. 3.1. Blue arrows show approximate sedimentary dispersal patterns based on provenance and paleocurrent data (see text for details). Insets show schematic southeast—northwest trending cross sections through Grenville orogen and intracratonic basins: A) 1255–1230 Ma: retroarc basin formation, accommodation space created by coupling of convecting mantle above subduction zone and upper plate (cartoon modified from DeCelles, 2012), sediments sourced from local basement and continental margin arc. B) 1230–1180: slab break off, uplift of 1255–1230 Ma carbonate sequences, subduction zone reversal, mafic underplating leads to emplacement of Anorthosite-Magnerite-Charnockite-Granite suites in California. C) 1140–1100 Ma: Foreland basin sedimentation during early stages of continent–continent collision in Llano uplift (central Texas), regional northeast-southwest directed extension, accommodation space produced by loading of upper plate by thrust nappes, sediments sourced from local basement and structurally high parts of Grenville orogen. Subduction continues in western Texas leading to clockwise rotation of colliding continent (Davis and Mosher, 2015). D) 1100–980 Ma: post-collisional magmatism and uplift in the Llano uplift, 1150–1050 Ma mafic magmatism throughout southwest Laurentia. Continent-continent collision in western Texas at 1060–980 Ma. Proximal foreland basin sedimentation in Hazel Formation at 1060–1035 Ma, cross section of collisional orogen modified from Garzanti et al (2004; for the Alps).

Laurentia help to place this widespread episode of sedimentation into a regional tectonic framework. The new tectonic model for Late Mesoproterozoic basin formation in southwest Laurentia is depicted in map and cross sectional views in Fig. 3.6. Time periods in Fig. 3.6 are keyed to the color bands in

Figs. 3.4 and 3.5 and include the four key tectonic intervals during the southern Grenville Orogeny (adapted from Mosher et al., 2008 and Davis and Mosher, 2015) and the sedimentary response in the continental interior.

3.6.2.1 1340–1320 Ma basin evolution

The earliest phase of sedimentation considered in this study is preserved in the Pioneer Shale (Apache Group) and the lower member of the Crystal Spring Formation of the Pahrump Group (Figs. 3.1 and 3.2). Both formations are northerly-derived fluvial successions and were previously correlated based on lithological similarities and stratigraphic position (Shride, 1967; Wrucke, 1989; Seeley, 1999). Detrital zircon data provide further support for correlation as both sequences share large age peaks between 1600 and 1800 Ma and youngest detrital zircon populations at 1320–1340 Ma (Fig. 3.4). The 1320–1340 Ma zircon population is interpreted to reflect the depositional age of the Pioneer-lower Crystal Spring sequences as the Pioneer Shale contains abundant tuffaceous mudstone, which we interpret to have been derived from a syn-sedimentary volcanic source that contributed to the youngest detrital zircon age peak at *ca.* 1340 Ma (Fig. 3.4). The 1340–1320 Ma age range coincides with back arc basin sedimentation and magmatism in the 1380–1330 Ma Carrizo Mountain Group in western Texas (Bickford et al., 2000). The Pioneer Shale-lower Crystal Spring Formation may therefore be distal equivalents of the Carrizo Mountain Group and together represent a once extensive back arc basin system associated with convergence along the southern margin of Laurentia at 1380–1320 Ma.

3.6.2.2 1255–1230 Ma retroarc basin sedimentation

The Pioneer Shale is unconformably overlain by the Dripping Springs Formation, which has a maximum depositional age of 1250 Ma based on our new detrital zircon data. This indicates that a hiatus of at least 70 million years followed deposition of the 1340–1320 Ma distal back arc basin sequences of the Pioneer Shale and lower member of Crystal Spring Formation. Uplift and erosion during this hiatus may have removed much of the 1340–1320 Ma back arc basin system and was followed by a change in the sedimentary regime to widespread shallow water carbonate sedimentation. Distinctive 100–500m-thick sequences of intertidal to subtidal, stromatolitic dolomite occur in all Late Mesoproterozoic basins in southwest Laurentia except the poorly known Debaca Group and Las Animas Formation (Fig. 3.2). Despite lacking the characteristic stromatolitic intervals, we interpreted the thick dolomite units in the lower Debaca Group to be correlative with the Late Mesoproterozoic carbonate-bearing sequences elsewhere in southwest Laurentia. These widespread carbonate sequences are likely correlative with the Bass Formation in the Unkar Group, which was deposited between 1255 and 1230 Ma based on the new detrital zircon ages from sandstones in the upper Bass Formation, which overlie a 1254.8 ± 1.6 Ma tuff (Timmons et al., 2005). The 1250– 1240 Ma tuffs in the carbonate sequences of western Texas (Allamoore Formation and Castner Marble) provide further support for correlating the Late Mesoproterozoic carbonate-bearing sequences of southwest Laurentia. Sedimentary structures indicating episodic sub-aerial exposure and marine

$^{87}Sr/^{86}Sr$ isotopic signatures from the Castner Marble in western Texas (Pittenger et al., 1994) indicate that deposition of the 1255–1230 Ma carbonate sequences occurred in restricted marine basins. Intraformational conglomerates, syn-sedimentary monoclines, and mafic magmatism indicate a tectonically active setting for the carbonate basins (Sears, 1973; Timmons et al., 2005). The age of 1255–1230 Ma carbonate successions overlaps with 1288–1232 Ma continental arc magmatism along the southern margin of Laurentia and suggests deposition in an extensive retroarc basin system as depicted in Fig. 3.6A.

Retroarc basins form by a combination of lithospheric flexure due to development of a continental arc and lithospheric subsidence induced by coupling of the upper plate with convecting asthenosphere above the subducting slab (Fig. 3.6A, Mitrovica et al., 1989; Gurnis, 1992; DeCelles and Giles, 1996). The dynamic mantle effect can cause subsidence in the upper plate thousands of kilometers from the arc front producing regional-scale, generally shallow water depositional settings (e.g. Gurnis, 1992; DeCelles, 2012). The extensive distribution of 1255–1230 Ma shallow marine carbonate sequences throughout southwest Laurentia is therefore consistent with deposition in a retroarc basin setting (Fig. 3.6A cross section).

3.6.2.3 1200–1180 Ma slab breakoff and subduction reversal

Continental arc magmatism along the southern margin of Laurentia appears to have ceased by 1232 Ma and was followed by a reversal in subduction zone polarity (Mosher et al., 2008). We speculate that the end of 1255–1230 Ma carbonate sedimentation throughout southwest Laurentia coincided with uplift following slab break off and termination of north-dipping subduction along the southern margin of Laurentia (Fig. 3.6B). Subduction zone reversal is interpreted to have occurred between 1232 and 1150 Ma based on the absence of magmatism of this age in the Llano uplift (Mosher et al., 2008). However, our data suggest a younger age for slab break off and subduction zone reversal as indicated by the presence of 1180–1200 Ma detrital zircons in the upper Unkar Group (Table 3.1), which unconformably overlie the Bass Formation (a part of the 1255–1230 Ma retroarc basin system; Figs. 3.3 and 3.5). A possible source for 1180–1200 Ma zircons in the upper Unkar Group is the Anorthosite-Magnerite-Charnockite-Granite complex in the San Gabriel and Eagle Mountains of California, which was emplaced between 1200 and 1180 Ma (Fig. 3.1 and Section 3.6.1.1). McLelland et al. (2010b) note that Anorthosite-Magnerite-Charnockite-Granite suites form in post- or late-tectonic settings with one plausible mechanism for their generation being asthenospheric upwelling and ponding at the base of the crust following slab break off. Slab breakoff along the southern margin of Laurentia at *ca.* 1200–1180 Ma can explain the shutdown of continental arc magmatism, uplift and erosion of 1255–1230 Ma carbonate sequences, and emplacement of Anorthosite-Magnerite-Charnockite-Granite suites in California, which may have been the source of enigmatic 1180–1200 Ma detrital zircons in the siliciclastic sequences deposited during the next phase of Late Mesoproterozoic sedimentation throughout southwest Laurentia (Fig. 3.6B).

3.6.2.4 1140–1100 Ma distal foreland basin sedimentation

The unconformity above the 1255–1230 Ma carbonate sequences (Fig. 3.3C) represents a hiatus of at least 40 million years and was followed by deposition of siliciclastic sediments of the upper Unkar Group and correlative units of the Troy Quartzite, Llanoria Formation, and possibly the Las Animas Formation (Fig. 3.2). The depositional age of these siliciclastic sequences is best constrained in the upper Unkar Group where the Dox Formation has a maximum depositional age of 1140 Ma based detrital mica ages (Table 3.1 and Timmons et al., 2005) and a minimum depositional age of 1104 Ma from the Cardenas Basalt, which was emplaced during deposition of the upper parts of the Dox Formation (Timmons et al., 2005). The 1140–1100 Ma siliciclastic sequences were deposited in widespread shallow marine and fluvial settings across southwest Laurentia (Fig. 3.1). Previous correlation of these sequences highlighted lithological similarities, including the presence of soft-sediment deformation features (Shride, 1967; Wrucke, 1989; Seeley, 1999; Timmons et al., 2005). Correlation is further supported by the new detrital zircon dataset, which shows that the siliciclastic sequences typically contain abundant 1600–1800 Ma zircons likely derived from the Yavapai and Mazatzal Provinces, a high proportion of *ca.* 1450 Ma detrital zircons sourced from local A-type granite plutons, and 'Grenville-aged' zircons derived from the eroded remnants of the 1288–1232 Ma continental arc along the southern margin of Laurentia or reworked from lower units (Table 3.1 and Figs. 3.4 and 3.5). The 1140–1100 Ma siliciclastic deposits temporally overlap with syn- and post-collisional events in the Llano uplift (1150–1070 Ma) and we interpret these sedimentary units to have been deposited in a series of distal foreland basins during continent-continent collision along the southern margin of Laurentia (Fig. 3.6C). The lack of 1070–1150 Ma detrital zircon in these distal foreland basin sequences suggests that the high-grade core of the southern Grenville orogen was not extensively exposed between 1140 and1100 Ma. Instead, we suggest the 1140–1100 Ma basins were derived from relatively low-grade rocks in the structurally high parts of the orogen.

The 1140–1100 Ma distal foreland basins of southwest Laurentia have a provenance and sedimentary history that is similar in character to the early phases of sedimentation in foreland basins of the Alpine and Himalayan continent-continent collisions. Foreland basins in the Alps and Himalaya were initially sourced from local basement and low-grade cover sequences imbricated by thrust stacking in the developing orogen, whereas in the later phases of the orogeny, sequences were sourced predominantly from the high-grade core of the orogen (Alps: Sinclair, 1997; Spiegel et al., 2000; Carrapa et al., 2004b; Kuhlemann et al., 2006; Jourdan et al., 2013; Himalaya: DeCelles et al., 1998, 2004; Najman and Garzanti, 2000; White et al., 2002; Ravikant et al., 2011). The post-collisional stages of foreland basin sedimentation observed from the Alpine and Himalayan orogens are apparently not widely preserved in Late Mesoproterozoic foreland basins of southwest Laurentia with only the Hazel Formation containing abundant detrital zircons (20 out of 94 analyses, Fig. 3.5) interpreted to be derived from the 1150–1070 Ma high-grade core of the southern Grenville orogen (Fig. 3.6D, Bickford et al., 2000; Spencer et al., 2014).

Accommodation space in foreland basins is a response to lithospheric flexure driven by loading of thrust nappes onto the upper plate, the effects of which can extend for hundreds of kilometers perpendicular to the orogenic front (e.g. DeCelles and Giles, 1996; DeCelles, 2012). These flexural loading effects decrease away from the orogenic front such that distal foreland basin deposits produced by lithospheric flexural alone are predicted to be relatively thin (<600 m, DeCelles and Giles, 1996; DeCelles, 2012). The presence of approximately 2 km of foreland basin strata in the upper Unkar Group, located some 600 km from the orogenic front (Fig. 3.1), therefore requires a mechanism in addition to flexural loading to produce the required accommodation space for Late Mesoproterozoic foreland basin sedimentation in southwest Laurentia.

3.6.2.5 1140–1100 Ma intracratonic extension and magmatism

Timmons et al. (2005) interpret syn-sedimentary extensional faulting in the upper Unkar Group to record a regional northeast-southwest extensional regime throughout southwest Laurentia, which developed perpendicular to the orogenic front during continent-continent collision. Syn-orogenic rift basins striking at a high angle to orogenic fronts (i.e. the "Impactogens" of Şengör et al., 1978; Şengör, 1995) are recognized in many collisional settings (e.g. Ingersoll, 2012; Allen et al., 2015) and are interpreted to form in response to extension that is kinematically linked to collision at the plate margin. The most comprehensively studied examples of "Impactogens" related to continent-continent collisions are the late Cenozoic Baikal Rift (Siberia) and the Cenozoic Rhine graben (Europe). The Baikal Rift represents a distal portion of an extensive system of transtentional and transpressional syn-orogenic basins developed throughout the continental interior of Asia during the Himalayan Orogeny (e.g. Molnar and Tapponnier, 1975; Allen et al., 1999; Yin and Harrison, 2000). The Baikal Rift consists of a series of sub-basins with a complex depositional history, the most recent phase of which occurred during the collision of India with Asia in a transtensional setting approximately 3000 km from the orogenic front (e.g. Polyansky, 2002; Petit and Déverchère, 2006; Mats, 2012; Buslov, 2012). The Rhine graben has a similarly complex depositional history associated with transtension related to the Alpine Orogeny and was sourced from basement uplifts adjacent to the rift and more distally from the developing orogen (Şengör et al., 1978; Sissingh, 1998; Hagedorn and Boenigk, 2008; Reiter et al., 2013, 2015). The structural history, extensive distribution, and provenance of 1140–1100 Ma siliciclastic sequences in southwest Laurentia are therefore similar to analogue "Impactogens" associated with geologically recent continent-continent collisions. We suggest these similarities also highlight the important influence that regional extension driven by continent-continent collision had in the development of Late Mesoproterozoic foreland basins in southwest Laurentia.

3.6.2.6 1060–1035 Ma proximal foreland basin sedimentation

The youngest episode of sedimentation associated with the Grenville orogeny in southern Laurentia is recorded by the proximal foreland basin deposits of the Hazel Formation at Van Horn, western Texas (Figs. 3.1 and 3.2). The Llanoria Formation in Franklin Mountains of western Texas may also have been deposited during the 1060–1035 Ma deformation in western Texas if correlation with the Hazel Formation is favoured (Spencer et al., 2014). However, we propose an alternative interpretation in which the Llanoria Formation is correlated with the 1140–1100 Ma siliciclastic sequences throughout southwest Laurentia based on the scarcity of <1150 Ma detrital zircons (5 out of 266 analyses, Fig. 3.5) and minimum depositional age indicated by the overlying 1111 Ma Thunderbird Group and crosscutting 1120 Ma Red Bluff Granite. The Hazel Formation was deposited synchronously with northwest-directed thrusting in the Van Horn region at 1060–1035 Ma (Soegaard and Callahan, 1994; Bickford et al., 2000; Grimes and Mosher, 2003; Spencer et al., 2014). The youngest episode of Late Mesoproterozoic deformation at Van Horn is recorded by movement on the frontal thrust of the southern Grenville orogen at 1000–980 Ma (Grimes and Mosher, 2003; Grimes and Copeland, 2004; Davis and Mosher, 2015). Deformation in the Van Horn region at 1060–980 Ma therefore post-dates the end of continent-continent collision in the Llano uplift by at least 60 million years (Bickford et al., 2000; Grimes and Copeland, 2004; Davis and Mosher, 2015). Davis and Mosher (2015) propose that collision of a continent with the southern margin of Laurentia during the Grenville Orogeny first occurred at 1150–1120 Ma in the Llano uplift, while subduction of ocean crust continued in the Van Horn region to the east (Fig. 3.6C). Closure of the small ocean basin to the east of the Llano uplift lead to clockwise rotation of the colliding continent and eventual collision with the southern margin of Laurentia at 1060–980 Ma in western Texas (Fig. 3.6D). The sedimentary record of the Hazel Formation is therefore interpreted to reflect continent-continent collision during the final phase of the Grenville Orogeny in southern Laurentia.

3.6.3 Comparison with syn-orogenic basins in the northeastern Grenville orogen

The southern Grenville orogen represents a portion of the larger Grenville orogenic system, which is widely exposed throughout northeast Laurentia in the northeastern United States and eastern Canada (Fig. 3.1, Rivers, 1997, 2008; Davidson, 1995, 2008). Portions of the Grenville orogen are also exposed in formerly contiguous crust in Scotland (Storey et al., 2005) and Ireland (Daly and Flowerdew, 2005). The Sveconorwegian orogen of Norway and Sweden was likely continuous with the Grenville orogen of northeast Laurentia but appears to be a predominantly accretionary orogen and is not considered further here (Bingen et al., 2002, 2008; Slagstad et al., 2013). Sedimentary basins formed during the Grenville Orogeny occur throughout northeastern Laurentia and are well exposed in the foreland of the orogen in Scotland (e.g. Cawood et al., 2007). These basins provide a key record of the Grenville Orogeny in northeast Laurentia as it evolved from a convergent margin dominated by accretionary processes at *ca.* 1300–1100 Ma to a continent–continent collisional orogen at 1080–980 Ma (Rivers, 1997, 2008; Rivers and Corrigan, 2000; Gower and Krogh, 2002; Tollo et al., 2004; Cawood et al., 2007; Davidson, 2008; Hynes and Rivers, 2010).

The Late Mesoproterozoic basins of northeast Laurentia and Scotland can be broadly divided into basins formed during the accretionary stages of the Grenville Orogeny prior to continent-continent collision and those formed during continent-continent collision (Cawood et al., 2007; Spencer et al., 2015). Late Mesoproterozoic basins that formed prior to continent-continent collision in northeast Laurentia comprise *ca.* 1300–1250 Ma carbonate, siliciclastic, and bimodal volcanic rocks and include the Grenville supergroup and related inliers in the Appalachian orogen (Wynne-Edwards, 1972; Easton, 1992; Chiarenzelli et al., 2015). Similar-aged sequences in Ontario and Labrador include the Simarnekh Formation (Spencer et al., 2015), the western Wakeham Supergroup (Rivers and Corrigan, 2000), and the Seal Lake Group (van Nostrand and Lowe, 2010). The 1300–1250 Ma volcano-sedimentary successions of northeast Laurentia are interpreted to be back arc and marginal basins deposited inboard of an accretionary margin (Rivers and Corrigan, 2000). A younger series of predominantly siliciclastic sedimentary sequences were deposited throughout northeast Laurentia at *ca.* 1150–1090 Ma and include the Flinton Group (Sager-Kinsman and Parrish, 1993), Twelve Mile quartzite (Wodicka et al., 1996), St. Boniface quartzite (Corrigan and van Breemen, 1997), and psammite on Battle Island, Labrador (Kamo et al., 2011). The 1150–1090 Ma basins likely formed in response to extension associated with continued accretionary orogenesis along the eastern margin of Laurentia (Cawood et al., 2007). The 1150–1090 Ma basins contain abundant 1350–1150 Ma detrital zircons, which were likely derived from local arc-related plutons and voluminous Anorthosite-Magnerite-Charnockite-Granite suites, consistent with deposition inboard of an accretionary margin (Sager-Kinsman and Parrish, 1993; Cawood et al., 2007). In Scotland, the 1180 Ma Stoer Group may represent a failed continental rift basin that pre-dates continent-continent collision during Grenville Orogeny (Rainbird et al., 2001; Cawood et al., 2007; Parnell et al., 2011) and was sourced exclusively from local Archean and Paleoproterozoic basement (Rainbird et al., 2001). The provenance of the Stoer Group may indicate the absence of arc-related magmatism in the Scottish sector of the Grenville Orogeny or isolation of the Stoer Group basin from contemporaneous arc sources (Cawood et al., 2007).

The main phase of continent-continent collision in the Grenville Orogeny in northeast Laurentia at 1080–980 Ma was accompanied by deposition of up to 8 km of predominantly fluvial sediments in the Midcontinent Rift in the Lake Superior region (Craddock et al., 2013; Stein et al., 2015; Malone et al., 2016) and in the East Continent Rift System of Indiana, Kentucky, and Ohio (Santos et al., 2002; Baranoski et al., 2009). The Midcontinent Rift and East Continent Rift formed in a complex tectonic setting related to both continental rifting and mantle plume activity, which occurred within the foreland of the Grenville orogen (e.g. Hutchinson et al., 1990; Baranoski et al., 2009; Craddock et al., 2013; Bright et al., 2014; Stein et al., 2015; Malone et al., 2016). Sediments deposited during the continent-continent collisional phase of the Grenville Orogeny in Scotland include up to 12 km of predominantly clastic strata comprising the *ca.* 1020–980 Ma Torridon, Morar, and Sleat Groups (Stewart, 2002; Kinnaird et al., 2007; Cawood et al., 2007; Krabbendam et al., 2008, 2014; Krabbendam et al., in review). The 1080–980 Ma basins of northeast Laurentia and Scotland likely represent proximal foreland basins formed primarily in response to orogenic loading of the Laurentian margin during continent-continent collision (Rainbird et al., 2001; Kinnaird et al., 2007; Krabbendam et al., in review, but see Williams and Foden, 2011 for an alternative interpretation).

The three episodes of basin formation in northeast Laurentia and Scotland at 1300–1250 Ma, 1150–1090 Ma, and 1080–980 Ma, broadly overlap in time with the four phases of Late Mesoproterozoic basin formation in southwest Laurentia. Although similar in age, important differences exist in the tectonic setting of some Late Mesoproterozoic basins in southwest Laurentia compared to those in northeast Laurentia and Scotland. The tectonic setting of the earliest phases of syn-orogenic sedimentation in southwest Laurentia and northeast Laurentia share the closest similarities. The 1300–1250 Ma volcano-sedimentary sequences of northeast Laurentia were deposited in back arc or marginal basins, analogous to the tectonic setting inferred for the 1340–1320 Ma Pioneer Shale-lower Crystal Spring Formation and 1255–1230 Ma carbonate sequences of southwest Laurentia. Together, these *ca.* 1350–1230 Ma sedimentary and volcanic sequences represent a series of back arc and marginal basins developed inboard of an accretionary orogen extending along the entire southern and eastern margins of Laurentia (e.g. Rivers and Corrigan, 2000; Whitmeyer and Karlstrom, 2007).

A distinct change in the tectonic setting of the Grenville Orogeny from an accretionary orogen to a collisional orogen is recorded by the foreland basins of southwest Laurentia, northeast Laurentia, and Scotland. Foreland basin deposition was widespread throughout southwest Laurentia at 1140–1100 Ma during the initial stages of continent–continent collision along the margin to the south (Fig. 3.6C). In contrast, 1150–1090 Ma basins in northeast Laurentia formed in an accretionary orogenic setting that pre-dates continent–continent collision in the northeastern Grenville Orogeny. Continent-continent collision in northeast Laurentia at 1080–980 Ma is recorded by clastic sediments deposited in the Midcontinent Rift and East Continent Rift in the foreland of the Grenville orogen and proximal foreland basin sediments in Scotland. The syn-collisional sedimentary basins in northeast Laurentia and Scotland were deposited at the same time as the 1060–1035 Ma proximal foreland deposits of the Hazel Formation in western Texas. Despite similarities in age and tectonic setting, the Hazel Formation formed in response to a different continent-continent collision to time-equivalent sequences in northeast Laurentia and Scotland. The continent-continent collisional phase of the Grenville Orogeny in northeast Laurentia and Scotland records collision of the Amazonia craton with northeast Laurentia (e.g. Hoffman, 1991; Tohver et al., 2006; Li et al., 2008), whereas in southern Laurentia, the colliding block is generally interpreted to be the Kalahari craton (e.g. Dalziel et al., 2000; Li et al., 2008; Ksienzyk and Jacobs, 2015).

In summary, the Late Mesoproterozoic sedimentary basins of southwest Laurentia, northeast Laurentia, and Scotland are an important record of convergence, accretion, and collision along the southern and eastern margins of Laurentia during the Grenville Orogeny. Late Mesoproterozoic basins in southwest and northeast Laurentia record a shared history of back arc basin sedimentation associated with a convergent margin that extended from southern Laurentia to northeastern Laurentia from *ca.* 1350–1230 Ma (Whitmeyer and Karlstrom, 2007). The syn-collisional sedimentary record of Late Mesoproterozoic basins in southwest Laurentia and northeast Laurentia differs markedly, with foreland basin sedimentation in southwest Laurentia initiating earlier (1140 Ma) than in northeast Laurentia and Scotland (1080 Ma). This contrasting record of Late Mesoproterozoic foreland basin sedimentation reflects the collision of two separate continents at different times and along different segments of the Laurentian margin (e.g. Hoffman, 1991; Li et al., 2008).

3.6.4 Paleogeographic implications

The Grenville orogen represents one of several Late Mesoproterozoic orogenic belts worldwide that record the assembly of the supercontinent Rodinia. As Laurentia occupied a central position in Rodinia (e.g. Dalziel, 1991; Hoffman, 1991), identifying the extension of the Grenville orogen on formerly adjacent continents is critical for refining the paleogeographic configuration of the supercontinent. One particularly controversial challenge for refining the paleogeographic configuration of Rodinia is identifying the continuation of the southern Grenville orogen into continents formerly to the west of Laurentia (e.g. Moores, 1991; Dalziel, 1991; Karlstrom et al., 1999, 2001; Burrett and Berry, 2000; Sears and Price, 2000; Wingate et al., 2002; Fioretti et al., 2005; Li et al., 2008; Goodge et al., 2008). Both the southern Grenville orogen and the associated Late Mesoproterozoic syn-orogenic basins are truncated by the western Neoproterozoic rift margin of Laurentia (Fig. 3.1). Therefore, in addition to matching 'Grenville-aged' magmatic and metamorphic events, identifying possible correlates of the Late Mesoproterozoic basins of southwest Laurentia on formerly contiguous continents will assist in locating the western continuation of the Grenville orogen within Rodinia. The Late Mesoproterozoic basins of southwest Laurentia represent a particularly promising piercing point to test paleogeographic reconstructions of Rodinia as the stratigraphy and provenance of the basins are remarkably consistent across a regionally extensive area.

3.7 Conclusion

Detrital zircon, muscovite, and biotite data from Late Mesoproterozoic sequences throughout southwest Laurentia provide a powerful combination of datasets to refine depositional ages, regional correlations, and a better understanding of the tectonic context for this widespread phase of sedimentation. We highlight the episodic nature of basin formation throughout southwest Laurentia during the Late Mesoproterozoic, which is characterized by four syn-orogenic basin forming episodes that correspond to different stages of convergence and collision during the Grenville Orogeny in southern Laurentia.

Deposition of 1340–1320 Ma fluvial deposits of the Pioneer Shale and lower member of the Crystal Spring Formation are remnants of a distal back arc basin system development inboard of the southern convergent margin of Laurentia. Following an approximately 70 million year hiatus, the next phase of basin formation is recorded by 1255–1230 Ma shallow marine carbonate sequences. The 1255–1230 Ma carbonate sequences contain detrital zircon and muscovite sourced from local Paleoproterozoic and Mesoproterozoic basement and an active continental arc system along the southern margin of Laurentia. These widespread carbonate sequences were deposited in an extensive retroarc basin system that was uplifted and eroded following termination of north-dipping subduction along the southern margin of Laurentia at 1230–1180 Ma. A hiatus of at least 40 million years was followed by shallow marine and terrestrial siliciclastic sedimentation throughout southwest Laurentia at 1140–1100 Ma. The 1140–1100 Ma siliciclastic strata contain detrital zircon and muscovite derived largely from

local basement provinces and from the erosion of thrust nappes exhumed during the early stages of continent-continent collision along the southern margin of Laurentia. The 1140–1100 Ma siliciclastic sequences likely represent an extensive foreland basin system developed during the first phase of continent-continent collision during the Grenville Orogeny in southern Laurentia. Accommodation space for the 1140–1100 Ma foreland basins was driven in part by regional intracratonic extension throughout southwest Laurentia driven by continent-continent collision along the margin to the south. The final episode of Late Mesoproterozoic sedimentation in southwest Laurentia is recorded in the Hazel Formation, which was deposited in a proximal foreland basin as continent-continent collision migrated westward along the southern margin of Laurentia.

The Late Mesoproterozoic sedimentary record of southwest Laurentia refines models proposed for the geodynamic evolution of the southern margin of Laurentia during the Mesoproterozoic by providing evidence for an extensive *ca.* 1300–1230 Ma continental margin arc that pre-dated continent-continent collision. We also revise the timing of the reversal from north-dipping to south-dipping subduction zone polarity along the southern margin of Laurentia to between 1230 and 1180 Ma. The combination of detrital mica and detrital zircon data provide a critical dataset for unraveling the unroofing record of structurally high levels of the hinterland of the Grenville orogen in southern Laurentia, which are no longer exposed. The record of Late Mesoproterozoic back arc basin sedimentation in southwest Laurentia at 1340–1320 Ma and 1255–1230 Ma is similar to that preserved in the northeastern sector of the Grenville Orogeny and supports the existence of an extensive accretionary orogen along the southern and eastern margins of Laurentia prior to continent-continent collision. Foreland basin sedimentation in southwest Laurentia initiated at least 60 million years earlier than in northeast Laurentia and Scotland, suggesting the southern and northeastern Grenville orogens record the collision of two different continents with the margin of Laurentia during the Late Mesoproterozoic. Identifying remnants of the distinctive Late Mesoproterozoic basin system of southwest Laurentia on the continent(s) formerly adjacent to western Laurentia would provide an important piercing point for improving paleogeographic reconstructions of Rodinia.

3.8 Acknowledgements

We gratefully acknowledge Grand Canyon National Park for permission to undertake research and sampling within Grand Canyon. J. Hagadorn and C. Dehler are thanked for assistance in the field. Field work was supported by NSF grant EAR-1144521 and analytical work at the Arizona LaserChron center is supported by NSF grant EAR-1338583. Mike Doe is thanked for providing unpublished detrital zircon data from the Pioneer Shale. This research was made possible through an Australian Government Endeavour Postgraduate Exchange Scholarship award to J. Mulder. We thank Randy Parrish for editorial handling and Maarten Krabbendam and two anonymous reviews for constructive reviews that improved the manuscript. Maarten Krabbendam is further thanked for insightful comments on the tectonic evolution and sedimentary record of the Grenville Orogeny in Scotland.

3.9 References

Allen, M.B., Vincent, S.J., Wheeler, P.J., 1999. Late Cenozoic tectonics of the Kepingtage thrust zone: interactions of the Tien Shan and Tarim basin, northwest China. Tectonics 18, 639–654.

Allen, P.A., Eriksson, P.G., Alkmim, F.F., Betts, P.G., Catuneanu, O., Mazumder, R., Meng, Q., Young, G.M., 2015. Classification of basins, with special reference to Proterozoic examples. In: Mazumder, R., Eriksson, P.G. (Eds.), Precambrian Basins of India, Stratigraphic and Tectonic Context, pp. 5–28.

Amarante, J.F.A., 2001. Characteristic of the basement rocks in the Mescalero 1 well, Guadalupe County, New Mexico (M.S. thesis). New Mexico Institute of Mining and Technology, Socorro, p. 73.

Ballard, J.L.W., 1997. The depositional history of the Mundy Breccia and lowermost member of the Lanoria Formation (M.S. thesis). University of Texas, El Paso, p. 360.

Baranoski, M., Dean, S., Wicks, J., Brown, V., 2009. Unconformity-bounded seismic reflection sequences define Grenville-age rift system and foreland basins beneath the Phanerozoic in Ohio. Geosphere 5, 140–151.

Barnes, M.A., 2001. The Petrology and Tectonics of the Mesoproterozoic margin of southern Laurentia (Ph.D. thesis). Texas Tech University, Lubbock, p. 287. Barth, A.P., Wooden, J.L., Coleman, D.S., 2001. SHRIMP-RG U-Pb zircon geochronology of Mesoproterozoic metamorphism and plutonism in the southwesternmost United States. J. Geol. 109 (3), 319–327. Beaumont, C., 1981. Foreland basins. Geophys. J. Int. 65, 291–329.

Beraldi-Campesi, H., Farmer, J.D., Garcia-Pichel, F., 2014. Modern terrestrial sedimentary biostructures and their fossil analogs in mesoproterozoic subaerial deposits. Palaios 29, 45–54. Bertrand-Sarfati, J., Awramik, S.M., 1992. Stromatolites of the mescal limestone (Apache Group, Middle Proterozoic, Central Arizona) – taxonomy, biostratigraphy, and paleoenvironments. Geol. Soc. Am. Bull. 104, 1138–1155.

Bickford, M.E., Soegaard, K., Nielsen, K.C., McLelland, J.M., 2000. Geology and geochronology of Grenville-age rocks in the Van Horn and Franklin Mountains area, west Texas; implications for the tectonic evolution of Laurentia during the Grenville. Geol. Soc. Am. Bull. 112, 1134–1148.

Bickford, M.E., Van Schmus, W.R., Karlstrom, K.E., Mueller, P.A., Kamenov, G.D., 2015. Mesoproterozoic-trans-Laurentian magmatism: a synthesis of continent-wide age distributions, new SIMS U-Pb ages, zircon saturation temperatures, and Hf and Nd isotopic compositions. Precambr. Res. 265, 286–312.

Bingen, B., Mansfield, J., Sigmond, E.M.O., Stein, H., 2002. Baltica-Laurentia link during the Mesoproterozoic: 1.27 Ga development of continental basins in the Sveconorwegian Orogen, southern Norway. Can. J. Earth Sci. 39, 1425–1440.

Bingen, B., Andersson, J., Söderlund, U., Möller, C., 2008. The Mesoproterozoic in the Nordic countries. Episodes 31, 29–34.

Bloch, J., Timmons, M., Crossey, L.J., Gehrels, G.E., Karlstrom, K.E., 2006. Mudstone petrology of the Mesoproterozoic Unkar Group, Grand Canyon, U.S.A.: Provenance, weathering, and sediment transport on intracratonic Rodinia. J. Sediment. Res. 76, 1106–1119.

Bowring, S.A., Karlstrom, K.E., 1990. Growth, stabilization, and reactivation of Proterozoic lithosphere in the southwestern United States. Geology 18, 1203– 1206.

Bright, R.M., Amato, J.M., Denyszyn, S.W., Ernst, R.E., 2014. U-Pb geochronology of 1.1 Ga diabase in the southwestern United States: Testing models for the origin of a post-Grenville large igneous province. Lithosphere 6, 135–156.

Burns, B.A., 1987. The Sedimentology and Significance of a Middle Proterozoic braidplain; Chediski Sandstone Member of the Troy Quartzite, central Arizona (M.S. thesis). Northern Arizona University, Flagstaff, p. 143.

Burrett, C., Berry, R., 2000. Proterozoic Australia-Western United States (AUSWUS) fit between Laurentia and Australia. Geology 28, 103–106.

Buslov, M.M., 2012. Geodynamic nature of the Baikal Rift Zone and its sedimentary filling in the Cretaceous-Cenozoic: the effect of the far-range impact of the Mongolo-Okhotsk and Indo-Eurasian collisions. Russ. Geol. Geophys. 53, 955–962.

Carlson, W.D., Anderson, S.D., Mosher, S., Davidow, J.S., Crawford, W.D., Lane, E.D., 2007. High-pressure metamorphism in the Texas Grenville orogen: Mesoproterozoic subduction of the southern Laurentian continental margin. Int. Geol. Rev. 49, 99–119.

Carrapa, B., Di Giulio, A., Wijbrans, J., 2004a. The early stages of the Alpine collision: an image derived from the upper Eocene-lower Oligocene record in the Alps- Apennines junction area. Sed. Geol. 171, 181–203.

Carrapa, B., Wijbrans, J., Bertotti, G., 2004b. Detecting provenance variations and cooling patterns within the western Alpine orogen through $^{40}Ar/^{39}Ar$ geochronology on detrital sediments: the Tertiary Piedmont Basin, northwest Italy. In: Bernet, M., Spiegel, C. (Eds.), Detrital Thermochronology-Provenance Analysis, Exhumation, and Landscape Evolution of Mountain Belts. Geological Society of America Special Paper, Boulder, Colorado, p. 378.

Cawood, P.A., Nemchin, A.A., Strachan, R., Prave, T., Krabbendam, M., 2007. Sedimentary basin and detrital zircon record along East Laurentia and Baltica during assembly and breakup of Rodinia. J. Geol. Soc., Lond. 164, 257–275.

Chiarenzelli, J., Kratzmann, D., Selleck, B., deLorraine, W., 2015. Age and provenance of Grenville supergroup rocks, Trans-Adirondack Basin, constrained by detrital zircons. Geology 43 (2), 183–186.

Corrigan, D., van Breemen, O., 1997. U-Pb age constraints for the lithotectonic evolution of the Grenville Province along the Mauricie transect, Quebec. Can. J. Earth Sci. 34, 299–316.

Craddock, J.P., Konstantinou, A., Vervoort, J.D., Wirth, K.R., Davidson, C., Finley-Blast, L., Juda, N.A., Walker, E., 2013. Detrital zircon provenance of the Mesoproterozoic Midcontinent Rift, Lake Superior Region, U.S.A. J. Geol. 121, 57–73.

Cullom, C.R., 1996. Sedimentology and Petrology of the Pioneer Formation, Middle Proterozoic, Central Arizona (M.S. thesis). Northern Arizona University, Flagstaff, p. 120.

Dalton Jr., R.O., 1972. Stratigraphy of the Bass Formation (Late Precambrian, Grand Canyon, Arizona) (M.S. thesis). Northern Arizona University, Flagstaff, p. 140.

Daly, J.S., Flowerdew, M.J., 2005. Grampian and late Grenville events recorded by mineral geochronology near a basement–cover contact in north Mayo. Irel. J. Geol. Soc. 162, 163–174.

Dalziel, I.W.D., 1991. Pacific margins of Laurentia and East Antarctica-Australia as a conjugate rift pair: evidence and implications for an Eocambrian supercontinent. Geology 19, 598–601.

Dalziel, I.W.D., Mosher, S., Gahagan, L.M., 2000. Laurentia-Kalahari collision and the assembly of Rodinia. J. Geol. 108, 499–513.

Daneker, T.M., 1975. Sedimentology of the Precambrian Shinumo Sandstone, Grand Canyon, Arizona (M.S. thesis). Northern Arizona University, Flagstaff, p. 195.

Daniel, C.G., Pyle, J.M., 2006. Monazite-xenotime thermochronometry and Al2SiO5 reaction textures in the Picuris Range, northern New Mexico, USA: new evidence for a 1450–1400 Ma orogenic event. J. Petrol. 47 (1), 97–118.

Daniel, C.G., Pfeifer, L.S., Jones III, J.V., McFarlane, C.M., 2013. Detrital zircon evidence for non-Laurentian provenance, Mesoproterozoic (ca. 1490–1450 Ma) deposition and orogenesis in a reconstructed orogenic belt, northern New Mexico, USA: defining the Picuris orogeny. Geol. Soc. Am. Bull. 125 (9–10), 1423–1441.

Davidson, A., 1995. A review of the Grenville orogen in its North American type area. J. Aust. Geol. Geophys. 16, 3–24.

Davidson, A., 2008. Late Paleoproterozoic to mid-Neoproterozoic history of northern Laurentia; an overview of central Rodinia. Precambr. Res. 160, 5–22.

Davis, B.R., Mosher, S., 2015. Complex structural and fluid flow evolution along the Grenville Front, west Texas. Geosphere 11, 868–898.

DeCelles, P.G., 2012. Foreland basin systems revisited: variations in response to tectonic settings. In: Busby, C.J., Azor, A. (Eds.), Tectonics of Sedimentary Basins: Recent Advances. 2nd ed. Wiley-Blackwell, Oxford, pp. 405–426.

DeCelles, P.G., Giles, K.N., 1996. Foreland basin systems. Basin Res. 8, 105–123. DeCelles, G., Gehrels, G.E., Quade, J., Ojha, T.P., 1998. Eocene-early Miocene foreland basin development and the history of Himalayan thrusting, western and central Nepal. Tectonics 17, 741–765.

DeCelles, P.G., Gehrels, G.E., Najman, Y., Martin, A.J., Carter, A., Garzanti, E., 2004. Detrital geochronology and geochemistry of Cretaceous-Early Miocene strata of Nepal: implications for timing and diachroneity of initial Himalayan orogenesis. Earth Planet. Sci. Lett. 227, 313–330.

Doe, M.F., 2014. Reassessment of Paleo- and Mesoproterozoic Basin Sediments of Arizona: Implications for Tectonic Growth of Southern Laurentia and Global Tectonic Configurations (Ph.D. thesis). Colorado School of Mines, Golden, Colorado, p. 649.

Doe, M.F., Jones, J.V., Karlstrom, K.E., Thrane, K., Frei, D., Gehrels, G., Pecha, M., 2012. Basin formation near the end of the 1.60–1.45 Ga tectonic gap in southern Laurentia: Mesoproterozoic Hess Canyon Group of Arizona and implications for ca. 1.5 Ga supercontinent configurations. Lithosphere 4 (1), 77–88.

Doe, M.F., Jones, J.V., Karlstrom, K.E., Dixon, B., Gehrels, G., Pecha, M., 2013. Using detrital zircon ages and Hf isotopes to identify 1.48–1.45 Ga sedimentary basins and fingerprint sources of exotic 1.6–1.5 Ga grains in southwestern Laurentia. Precambr. Res. 231, 409–421.

Duebendorfer, E.M., 2015. Refining the early history of the Mojave-Yavapai boundary zone: rifting versus Arc accretion as mechanisms for Paleoproterozoic crustal growth in southwestern Laurentia. J. Geol. 123, 21–37.

Easton, R.M., 1992. The Grenville Province and the Proterozoic history of central and southern Ontario. In: Thurston, P.C. (Ed.), Geology of Ontario: Ontario Geological Survey Special Volume 4, Part 2, pp. 714–964.

Edwards, G., 1984. Petrography and Geochemistry of the Allamoore Formation, Culberson and Hudspeth counties, Texas (Ph.D. thesis). University of Texas at El Paso, p. 284.

Engel, M.H., Elmore, R.D., 1990. Assessments of the Hydrocarbon Generation Potential of Selected North American Proterozoic Rock Sequences. Progress Report for the U.S. Department of Energy.

Fioretti, A.M., Black, L.P., Foden, J., Visona, D., 2005. Grenville-age magmatism at the South Tasman Rise (Australia): a new piercing point for the reconstruction of Rodinia. Geology 33, 769–772.

Flawn, P.T., 1956. Basement Rocks of Texas and Southeast New Mexico The University of Texas Publication number 5605, p. 261.

Fletcher, K.E., 2004. Geochronology and Provenance of Four Mesoproterozoic Basins across the Southwest United States: Evidence from $^{40}Ar/^{39}Ar$ Dating of Detrital Muscovite (M.S. thesis). New Mexico Institute of Mining and Technology, Socorro, New Mexico, p. 277.

Garzanti, E., Vezzoli, G., Lombardo, B., Ando, S., Mauri, E., Monguzzi, S., Russo, M., 2004. Collision-orogen provenance (Western Alps): Detrital signatures and unroofing trends. J. Geol. 112, 145–164.

Gehrels, G., Pecha, M., 2014. Detrital zircon U-Pb geo-chronology and Hf isotope geochemistry of Paleozoic and Triassic passive margin strata of western North America. Geosphere 10 (1), 49–65.

Gehrels, G.E., Valencia, V.A., Ruiz, J., 2008. Enhanced precision, accuracy, efficiency, and spatial resolution of U-Pb ages by laser ablation-multicollector-inductively coupled plasma mass spectrometry. In: Geochem. Geophys. Geosyst. 9.

Goodge, J.W., Vervoort, J.D., 2006. Origin of Mesoproterozoic A-type Granites in Laurentia: Hf isotope evidence. Earth Planet. Sci. Lett. 243, 711–731.

Goodge, J.W., Vervoort, J.D., Fanning, C.M., Brecke, D.M., Farmer, G.L., Williams, I.S., Myrow, P.M., DePaolo, D.J., 2008. A positive test of East Antarctica-Laurentia juxtaposition within the Rodinia supercontinent. Science 321, 235–240.

Gower, C.F., Krogh, T.E., 2002. A U-Pb geochronological review of the Proterozoic history of the eastern Grenville Province. Can. J. Earth Sci. 39, 795–829.

Grimes, S.W., Copeland, P., 2004. Thermochronology of the Grenville Orogeny in west Texas. Precambr. Res. 131, 23–54.

Grimes, S.W., Mosher, S., 2003. Structure of the Carrizo Mountain Group, southeastern Carrizo Mountains, west Texas: a transpressional zone of the Grenville orogeny. Tectonics, 795–829. 3-1–3-20.

Guitreau, M., Mukasa, S.B., Blichert-Toft, J., Fahnestock, M.F., 2016. Pikes Peak batholith (Colorado, USA) revisited: a SIMS and LA-ICP-MS study of zircon U-Pb ages combined with solution Hf isotopic compositions. Precambr. Res. 280, 179–194.

Gurnis, M., 1992. Rapid continental subsidence following the initiation and evolution of subduction. Science 255, 1556–1558.

Hagedorn, E.M., Boenigk, W., 2008. The Pliocene and Quaternary sedimentary and fluvial history in the Upper Rhine Graben based on heavy mineral analyses. Neth. J. Geosci. 87, 21–32.

Hammond, J.G., 1990. Middle Proterozoic diabase intrusions in the southwestern U. S.A. as indicators of limited extensional tectonism. In: Gower, C.F., Rivers, T., Ryan, B. (Eds.), Mid-Proterozoic Laurentia-Baltica. Geological Association of Canada Special Paper 38, pp. 517–531.

Harrison, M.T., Duncan, I., McDougall, I., 1985. Diffusion of 40Ar in biotite: Temperature, pressure and compositional effects. Geochim. Cosmochim. Acta 49 (11), 2461–2468.

Heaman, L.M., Grotzinger, J.P., 1992. 1.08 Ga diabase sills in the Pahrump Group, California: Implications for development of the Cordilleran miogeocline. Geology 20, 637–640.

Hendricks, J.D., 1972. Younger Precambrian Basaltic Rocks of the Grand Canyon, Arizona (M.S. thesis). Northern Arizona University, Flagstaff, p. 122.

Hoffman, P.F., 1988. United Plates of America, the birth of a Craton: Early Proterozoic assembly and growth of Laurentia. Annu. Rev. Earth Planet. Sci. 16, 543–603.

Hoffman, P.F., 1991. Did the breakout of Laurentia turn Gondwanaland inside out? Science 252, 1409–1412.

Holland, M.E., Karlstrom, K.E., Doe, M.F., Gehrels, G.E., Pecha, M., Shufeldt, O.P., Begg, G., Griffin, W.L., Belousova, E., 2015. An imbricate midcrustal suture zone: the Mojave-Yavapai Province boundary in Grand Canyonm, Arizona. Geol. Soc. Am. Bull. 127, 1391–1410.

Howard, K.A., 1991. Intrusion of horizontal dikes: tectonic significance of Middle Proterozoic diabase sheets widespread in the upper crust of the southwestern United States. J. Geophys. Res. 96, 12461–12478.

Hutchinson, D.R., White, R.S., Cannon, W.F., Schulz, K.J., 1990. Keweenaw hot spot: geophysical evidence for a Ga mantle plume beneath the Midcontinent rift system. J. Geophys. Res. 95, 10869.

Hynes, A., Rivers, T., 2010. Protracted continental collision—evidence from the Grenville orogen. Can. J. Earth Sci. 47, 591–620.

Ingersoll, R.V., 2012. Tectonics of sedimentary basins, with revised nomenclature. In: Busby, C.J., Azor, A. (Eds.), Tectonics of Sedimentary Basins. second ed. Wiley-Blackwell, Oxford, pp. 3–43.

Jones, J.V., Connelly, J.N., Karlstrom, K.E., Williams, M.L., Doe, M.F., 2009. Age, provenance, and tectonic setting of Paleoproterozoic quartzite successions in the southwestern United States. Geol. Soc. Am. Bull. 121 (1–2), 247–264.

Jones, J.V., Daniel, C.G., Frei, D., Thrane, K., 2011. Revised regional correlations and tectonic implications of Paleoproterozoic and Mesoproterozoic metasedimentary rocks in northern New Mexico, USA: new findings from detrital zircon studies of the Hondo Group, Vadito Group, and Marqueñas Formation. Geosphere 7 (4), 974–991.

Jones, J.V., Daniel, C.G., Doe, M.F., 2015. Tectonic and sedimentary linkages between the Belt-Purcell basin and southwestern Laurentia during the Mesoproterozoic, ca. 1.60–1.40 Ga. Lithosphere 7, 465–472.

Jourdan, S., Bernet, M., Tricart, P., Hardwick, E., Paquette, J.L., Guillot, S., Dumont, T., Schwartz, S., 2013. Short-lived, fast erosional exhumation of the internal western Alps during the late early Oligocene: constraints from geothermochronology of pro- and retro-side foreland basin sediments. Lithosphere 5, 211–225.

Kamo, S.L., Heaman, L.M., Gower, C.F., 2011. Evidence for post-1200 Ma – pre-Grenvillian supracrustal rocks in the Pinware terrane, eastern Grenville Province at Battle Harbour. Can. J. Earth Sci. 48, 371–387.

Karlstrom, K.E., Bowring, S.A., 1988. Early Proterozoic assembly of tectonostratigraphic terranes in south- western North America. J. Geol. 96, 561–576.

Karlstrom, K.E., Bowring, S.A., 1993. Proterozoic orogenic history in Arizona. In: Reed, J.C., Jr. (Ed.), Precambrian: Conterminous U.S., C-2. Geological Society of America, Geology of North America, Boulder, Colorado, pp. 188–211.

Karlstrom, K.E., Humphreys, G., 1998. Influence of Proterozoic accretionary boundaries in the tectonic evolution of western North America: interaction of cratonic grain and mantle modification events. Rocky Mountain Geol. 33, 161–179.

Karlstrom, K.E., Harlan, S.S., Williams, M.L., McLelland, J., Geissman, J.W., Ahall, K.I., 1999. Refining Rodinia: geologic evidence for the Australia – Western U.S. connection for the Proterozoic. GSA Today 9 (10), 1–7.

Karlstrom, K.E., Ahall, K.I., Harlan, S.S., William, M.L., McLelland, J., Geissman, J.W., 2001. Long-lived (1.8–0.8 Ga) convergent orogen in southern Laurentia, its extensions to Australia and Baltica, and implications for refining Rodinia. Precambr. Res. 111, 5–30.

Karlstrom, K.E., Amato, J.M., Williams, M.L., Heizler, M., Shaw, C.A., Read, A.S., Bauer, P., 2004. Proterozoic tectonic evolution of the New Mexico region. In: Mack, G. H., Giles, K.A. (Eds.), The Geology of New Mexico: A Geological History, 11. New Mexico Geological Society Special Publication, pp. 1–34.

Karlstrom, K.E., Williams, M.L., Heizler, M.T., Holland, M.E., Grambling, T.A., Amato, J.M., 2016. U-Pb monazite and 40Ar/39Ar data supporting polyphase tectonism in the Manzano Mountains: a record of both the Mazatzal (1.66–1.60 Ga) and Picuris (1.45 Ga) orogenies. In: Frey, B, A., Karlstrom, K.E., Lucas, S.G., Williams, S., Zeigler, K., McLemore, V., Ulmer-Scholle, D.S. (Eds.), The Geology of the Belen Area, Guidebook, 67th Field Conference. New Mexico Geological Society, pp. 177–184.

King, P.B., Flawn, P.T., 1953. Geology and mineral deposits of Precambrian rocks of the Van Horn area, Texas University of Texas Bureau of Economic Geology Bulletin. 5301, p. 218.

Kinnaird, T., Prave, A.R., Horstwood, M., Parrish, R.R., 2007. The late Mesoproterozoic-Early Neoproterozoic tectonostratigraphic evolution of Northwest Scotland: the Torridonian revisited. J. Geol. Soc., Lond. 164, 541–551.

Krabbendam, M., Prave, A.P., Cheer, D., 2008. A fluvial origin for the Neoproterozoic Morar Group, NW Scotland; implications for Torridon-Morar group correlation and the Grenville Orogen Foreland Basin. J. Geol. Soc., Lond. 165, 379–394.

Krabbendam, M., Leslie, A.G., Goodenough, K.M., 2014. Structure and stratigraphy of the Morar Group in Knoydart, NW Highlands: implications for the history of the Moine Nappe and stratigraphic links between the Moine and Torridonian successions. Scott. J. Geol. 50, 125–142.

Krabbendam, M., Bonsor, H., Horstwood, M.S.A., Rivers, T. (in review). Tracking the evolution of the Grenvillian Foreland Basin: constraints from sedimentology and detrital zircon and rutile in the Sleat and Torridon groups, Scotland. Precambr. Res.

Ksienzyk, A.K., Jacobs, J., 2015. Western Australia-Kalahari (WAlahari) connection in Rodinia: Not supported by U-Pb detrital zircon data from the Maud Belt (East Antarctica) and the Northampton Complex (Western Australia). Precambr. Res. 259, 207–221.

Kuhlemann, J., Dunkl, I., Brugel, A., Spiegel, C., Frisch, W., 2006. From source terrains of the Eastern Alps to the Molasse Basin: Detrital record of non-steady-state exhumation. Tectonophysics 413, 301–316.

Larson, E.E., Patterson, P.E., Mutschler, F.E., 1994. Lithology, chemistry, age, and origin of the Proterozoic Cardenas Basalt, Grand Canyon, Arizona. Precambr. Res. 65 (1–4), 255–276.

Levine, J.S.F., Mosher, S., 2010. Contrasting Grenville-age tectonic histories across the Llano Uplift, Texas: new evidence for deep-seated high-temperature deformation in the western uplift. Lithosphere 2, 399–410.

Li, Z.X., Bogdanova, S.V., Collins, A.S., Davidson, A., De Waele, B., Ernst, R.E., Fitzsimons, I.C.W., Fuck, R.A., Gladkochub, D.P., Jacobs, J., Karlstrom, K.E., Lu, S., Natapov, L.M., Pease, V., Pisarevsky, S.A., Thrane, K., Vernikovsky, V., 2008. Assembly, configuration, and break-up history of Rodinia: a synthesis. Precambr. Res. 160, 179–210.

Link, P.K., Stewart, E.D., Steel, T., Sherwin, J-A., Hess, L.T., McDonald, C., 2016. Detrital zircons in the Mesoproterozoic upper Belt Supergroup in the Pioneer, Beaverhead and Lemhi Ranges, Montana and Idaho: the Big White arc. In: Maclean, J.S., Sears, J.W. (Eds.), Belt Basin: Window to Mesoproterozoic Earth. Geological Society of America Special Paper 522, pp. 163–183.

Ludwig, K.R., 2003. Isoplot 3.00: A Geochronological Toolkit for Microsoft Excel. Berkeley Geochronological Centre Special Publication 4, Berkeley, California, p. 74.

Mahon, R.C., Dehler, C.M., Link, P.K., Karlstrom, K.E., Gehrels, G.E., 2014. Detrital zircon provenance and paleogeography of the Pahrump Group and overlying strata, Death Valley, California. Precambr. Res. 251, 102–117.

Malone, D.H., Stein, C.A., Craddock, J.P., Kley, J., Stein, S., Malone, J.E., 2016. Maximum depositional age of the Neoproterozoic Jacobsville Sandstone, Michigan: Implications for the evolution of the Midcontinent Rift. Geosphere 12 (4), 1–12.

Mats, V.D., 2012. The sedimentary fill of the Baikal Basin: implications for rifting age and geodynamics. Russ. Geol. Geophys. 53, 1382–1383.

McConnell, R.L., 1975. Biostratigraphy and depositional environment of algal stromatolites from the Mescal Limestone (Proterozoic) of central Arizona. Precambr. Res. 2, 317–328.

Mclelland, J.M., Selleck, B.W., Bickford, M.E., 2010a. Review of the Proterozoic evolution of the Grenville Province, its Adirondack outlier, and the Mesoproterozoic inliers of the Appalachians. From Rodinia to Pangea: The Lithotectonic Record of the Appalachian Region, 20, pp. 21–49.

McLelland, J.M., Selleck, B.W., Hamilton, M.A., Bickford, M.E., 2010b. Late- to post-tectonic setting of some major Proterozoic anorthosite–mangerite– charnockite–granite (AMCG) suites. Can. Mineral. 48, 729–750.

Middleton, L.T., Blakey, R.C., 1998. Seismically induced liquefaction in late Proterozoic strata, northern and central Arizona; implications for tectonic setting and regional correlations: Geological Society of America Abstracts with Programs, 30(2), p. 399.

Middleton, L.T., Montgomery, M.W., 2001. Sedimentary responses to changing tectonic patterns, Mesoproterozoic Apache Group/Troy Quartzite, Central Arizona, in Rocky Mountain (53rd) and South-Central (35th) Sections, Geological Society of America, Joint Annual Meeting; April 29–May 2, 2001; Albuquerque, New Mexico, Session No. 11.

Middleton, L.T., Trujillo, A.P., 1984. Sedimentology and depositional setting of the upper Proterozoic Scanlan Conglomerate, central Arizona. In: Koster, E.H., Steel, R.H. (Eds.), Sedimentology of Gravels and Conglomerates. Canadian Society of Petroleum Geologists Memoir 10, pp. 189–201.

Mitrovica, J.X., Beaumont, C., Jarvis, G.T., 1989. Tilting of continental interiors by the dynamical effects of subduction. Tectonics 8, 1079–1094.

Molnar, P., Tapponnier, P., 1975. Cenozoic tectonics of Asia: effects of a continental collision. Science 189, 419–426.

Moores, E.M., 1991. The Southwest U.S.–East Antarctica (SWEAT) connection: a hypothesis. Geology 19, 425–428.

Mosher, S., 1998. Tectonic evolution of the southern Laurentian Grenville orogenic belt. Geol. Soc. Am. Bull. 110, 1357–1375.

Mosher, S., Levine, J.S.F., Carlson, W.D., 2008. Mesoproterozoic plate tectonics: a collisional model for the Grenville-aged orogenic belt in the Llano uplift, central Texas. Geology 36, 55–58.

Najman, Y., Garzanti, E., 2000. Reconstructing early Himalayan tectonic evolution and paleogeography from Tertiary foreland basin sedimentary rocks, northern India. Geol. Soc. Am. Bull. 112, 435–449.

Nyman, M.W., Karlstrom, K.E., Kirby, E., Graubard, C., 1994. 1.4 Contractional orogeny in western North America: Evidence from ca. 1.4 Ga plutons. Geology 22, 901–904.

Parnell, J., Mark, D., Fallick, T.E., Boyce, A., Thackrey, S., 2011. The age of the Mesoproterozoic Stoer Group sedimentary and impact deposits, NW Scotland. J. Geol. Soc., Lond. 168, 349–358.

Petit, C., Déverchère, J., 2006. Structure and evolution of the Baikal rift: a synthesis. Geochem. Geophys. Geosyst. 7.

Pittenger, M.A., Marsaglia, K.M., Bickford, M.E., 1994. Depositional history of the Middle Proterozoic Castner Marble and basal Mundy Breccia, Franklin Mountains, west Texas. J. Sediment. Res. B64, 282–297.

Polyansky, O.P., 2002. Dynamic causes for the opening of the Baikal Rift Zone: a numerical modelling approach. Tectonophysics 351, 91–117.

Pray, L.C., 1961. Geology of the Sacramento Mountains Escarpment, Otero County, New Mexico: New Mexico Bureau of Mines and Mineral Resources, Bulletin 35, 144 p.

Purdy, J., Jäger, E., 1976. K-Ar ages on rock-forming minerals from the central Alps. Memorie degli Istituti di Geologia e Mineralogia dell' Uni- versità di Padova 30, 31.

Rainbird, R.H., Hamilton, M.A., Young, G.M., 2001. Detrital zircon geochronology and provenance of the Torridonian, NW Scotland. J. Geol. Soc., Lond. 158, 15–27.

Ravikant, V., Wu, F.Y., Ji, W.Q., 2011. U-Pb age and Hf isotopic constraints of detrital zircons from the Himalayan foreland Subathu sub-basin on the Tertiary palaeogeography of the Himalaya. Earth Planet. Sci. Lett. 304, 356–368.

Reed, V.S., 1976. Stratigraphy and Depositional Environment of the upper Precambrian Hakatai Shale, Grand Canyon, Arizona (M.S. thesis). Northern Arizona University, Flagstaff, p. 163.

Reese, J.F., Mosher, S., 2004. Kinematic constraints on Rodinia reconstructions from the core of the Texas Grenville orogen. J. Geol. 112, 185–205.

Reese, J.S., Mosher, S., Connelly, J., Roback, R., 2000. Mesoproterozoic chronostratigraphy of the southeastern Llano Uplift, central Texas. Geol. Soc. Am. Bull. 112, 278–291.

Reiter, W., Elfert, S., Bernet, M., Glotzbach, C., Spiegel, C., 2013. Relations between denudation, glaciation, and sediment deposition: implications from the Plio-Pleistocene Central Alps. In: Basin Res. 25, 1–16.

Reiter, W., Elfert, S., Glotzbach, C., Spiegel, C., 2015. Plio-Pleistocene evolution of the north Alpine drainage system: new constraints from detrital thermochronology of foreland deposits. Int. J. Earth Sci. 104, 891–907.

Rivers, T., 1997. Lithotectonic elements of the Grenville province: review and tectonic implications. Precambr. Res. 86, 117–154.

Rivers, T., 2008. Assembly and preservation of lower, mid, and upper orogenic crust in the Grenville Province-Implications for the evolution of large hot long-duration orogens. Precambr. Res. 167, 237–259.

Rivers, T., Corrigan, D., 2000. Convergent margin on southeastern Laurentia during the Mesoproterozoic: tectonic implications. Can. J. Earth Sci. 37, 359–383. Roback, R.C., 1996. Characterization and tectonic evolution of a Mesoproterozoic island arc in the southern Grenville Orogen, Llano uplift, central Texas. Tectonophysics 265, 29–52.

Roberts, M.T., 1982. Depositional environments and tectonic setting of the Crystal Spring Formation, Death Valley, California. In: Cooper, J.D., Troxel, B.W., Wright, L.A. (Eds.), Geology of Selected Areas in the San Bernardino Mountains, Western Mojave Desert, and Southern Great Basin, California: Volume and Guidebook for Field Trip no. 9, 78th Anniversary Meeting of Cordilleran Section. Geological Society of America. Death Valley Publishing Company, Shoshone, CA, pp. 165– 170.

Ross, G.M., Villeneuve, M.E., 2003. Provenance of the Mesoproterozoic (1.45 Ga) Belt basin (western North America): another piece in the pre-Rodinia paleogeographic puzzle. Geol. Soc. Am. Bull. 115, 1191–1217.

Roths, P.J., 1993. Geochemical and geochronological studies of the Grenville-age (1,250–1,000 Ma) Allamoore and Hazel Formations, Hudspeth and Culberson counties, west Texas. In: Soegaard, K. et al. (Eds.), Precambrian Geology of the Franklin Mountains and Van Horn Area, Trans-Pecos Texas. Geological Society of America South Central Section, University of Texas, Dallas, Texas, pp. 11–35.

Rougive, J.R., Carlson, W.D., Connelly, J.N., Roback, R.C., Copeland, P., 1996. Late thermal evolution of Proterozoic rocks in the northeastern Llano uplift, central Texas. Geological Society of America Abstracts with Programs 28 (7), A376.

Sager-Kinsman, E.A., Parrish, R.R., 1993. Geochronology of detrital zircons from the Elzevir and Frontenac terranes, Central Metasedimentary Belt, Grenville Province, Ontario. Can. J. Earth Sci. 30, 465–473.

Sambridge, M.S., Compston, W., 1994. Mixture modeling of multi-component data sets with application to ion-probe zircon ages. Earth Planet. Sci. Lett. 128, 373– 390.

Santos, J.O.S., Hartmann, L.A., McNaughton, N.J., Easton, R.M., Rea, R.G., Potter, P.E., 2002. Sensitive high resolution ion microprobe (SHRIMP) detrital zircon geochronology provides new evidence for a hidden Neoproterozoic foreland basin to the Grenville Orogen in the eastern Midwest, USA. Can. J. Earth Sci. 39, 1505–1515.

Sears, J.W., 1973. Structural Geology of the Precambrian Grand Canyon Series, Arizona (M.S. thesis). University of Wyoming, Laramie, p. 112.

Sears, J.W., Price, R.A., 2000. New look at the Siberian connection: No SWEAT. Geology 28, 423–426.

Seeley, J., 1999. Studies of the Proterozoic Tectonic Evolution of the Southwestern United States (Ph.D. thesis). University of Texas, El Paso, p. 321.

Şengör, A.M.C., 1995. Sedimentation and tectonics of fossil rifts. In: Busby, C.J., Ingersoll, R.V. (Eds.), Tectonics of Sedimentary Basins. Blackwell Science, Oxford, pp. 53–117.

Şengör, A.M.C., Burke, K., Dewey, J.F., 1978. Rifts at high angles to orogenic belts; tests for their origin and the Upper Rhine Graben as an example. Am. J. Sci. 278 (1), 24–40.

Shannon, W.M., Barnes, C.G., Bickford, M.E., 1997. Grenville magmatism in west Texas: petrology and geo-chemistry of the Red Bluff granite suite. J. Petrol. 38, 1279–1305.

Shaw, C.A., Heizler, M.T., Karlstrom, K.E., 2005. $^{40}Ar/^{39}Ar$ thermochronologic record of 1.45-1.35 Ga intracontinental tectonism in the southern Rocky Mountains: Interplay of conductive and advective heating with intracontinental deformation. In: Kalstrom, K.E., Keller, G.R. (Eds.), The Rocky Mountain Region: An Evolving Lithosphere; Tectonics, Geochemistry, and Geophysics. American Geophysical Union Geophysical Monograph 154, pp. 163–184.

Shride, A.F., 1967. Younger Precambrian geology in southern Arizona. U.S. Geol. Surv. Prof. Pap. 566, 88.

Shufeldt, O.P., Karlstrom, K.E., Gehrels, G.E., Howard, K.E., 2010. Archean detrital zircons in the Proterozoic Vishnu Schist of the Grand Canyon, Arizona: implications for crustal architecture and Nuna supercontinent reconstructions. Geology 38 (12), 1099–1102.

Sinclair, H.D., 1997. Tectonostratigraphic model for underfilled peripheral foreland basins: an Alpine perspective. Geol. Soc. Am. Bull. 109, 324–346.

Sissingh, W., 1998. Comparative tertiary stratigraphy of the Rhine Graben, Bresse Graben and Molasse Basin: correlation of Alpine foreland events. In: Tectonophysics 300, 249–284.

Skotnicki, S.J., Knauth, L.P., 2007. The middle Proterozoic Mescal paleokarst, central Arizona, USA: karst development, silicification, and cave deposits. J. Sediment. Res. 77, 1046–1062.

Slagstad, T., Roberts, N.M.W., Marker, M., Røhr, T.S., Schiellerup, H., 2013. A non-collisional, accretionary Sveconorwegian orogen. Terra Nova 25, 30–37.

Soegaard, K., Callahan, D.M., 1994. Late Middle Proterozoic Hazel Formation near Van Horn, trans-Pecos Texas: evidence for transpressive deformation in Grenvillian basement. Geol. Soc. Am. Bull. 106, 413–423.

Spencer, C.J., Prave, A.R., Cawood, P.A., Roberts, N.M.W., 2014. Detrital zircon geochronology of the Grenville/Llano foreland and basal Sauk Sequence in west Texas, USA. Geol. Soc. Am. Bull. 126, 1117–1128.

Spencer, C.J., Cawood, P.A., Hawkesworth, C.J., Prave, A.R., Roberts, N.M.W., Horstwood, M.S.A., Whitehouse, M.J., et al., 2015. Generation and preservation of continental crust in the Grenville Orogeny. Geosci. Front. 6, 357–372.

Spiegel, C., Kuhlemann, J., Dunkl, I., Frisch, W., Von Eynatten, H., Balogh, K., 2000. The erosion history of the Central Alps: evidence from zircon fission track data of the foreland basin sediments. Terra Nova 12, 163–170.

Stein, C.A., Kley, J., Stein, S., Hindle, D., Keller, G.R., 2015. North America's Midcontinent Rift: when rift met LIP. Geosphere 11 (5), 1607–1616.

Stevenson, G.M., Beus, S.S., 1982. Stratigraphy and depositional setting of the upper precambrian dox formation in grand-canyon. Geol. Soc. Am. Bull. 93, 163–173. Stewart, A.D., 2002. The Later Proterozoic Torridonian Rocks of Scotland: Their Sedimentology, Geochemistry and Origin Geological Society Memoir, 24. The Geological Society, London.

Stewart, J.H., Gehrels, G.E., Barth, A.P., Link, P.K., Christie-Blick, N., Wrucke, C.T., 2001. Detrital zircon provenance of Mesoproterozoic to Cambrian arenites in the western United States and northwestern Mexico. Geol. Soc. Am. Bull. 113, 1343–1356.

Storey, C.D., Brewer, T.S., Temperly, S., 2005. P-T conditions of Grenville-age eclogite facies metamorphism and amphibolite facies retrogression of the Glenelg-Attadale Inlier, NW Scotland. Geol. Mag. 142, 605–615.

Thomann, W.F., 1980. Ignimbrites, trachytes, and sedimentaiy rocks of the Precambrian Thunderbird Group, Franklin Mountains, El Paso, Texas. Geol. Soc. Am. Bull. 92, 94–100.

Timmons, J.M., Karlstrom, K.E., Heizler, M.T., Bowring, S.A., Gehrels, G.E., Crossey, L. J., 2005. Tectonic inferences from the ca. 1255–1100 Ma Unkar Group and Nankoweap Formation, Grand Canyon: intracratonic deformation and basin formation during protracted Grenville orogenesis. Geol. Soc. Am. Bull. 117, 1573–1595.

Tohver, E., Teixeira, W., Van Der Pluijm, B., Geraldes, M.C., Bettencourt, J.S., Rizzotto, G., 2006. Restored transect across the exhumed Grenville orogen of Laurentia and Amazonia, with implications for crustal architecture. Geology 34, 669–672.

Tollo, R.P., Corriveau, L., McLelland, J.M., Bartholomew, M.J. (Eds.), 2004. Proterozoic tectonic evolution of the Grenville orogen in North America: Geological Society of America Memoir 197, p. 820.

Tweto, O., 1983. Las Animas Formation (Upper Precambrian) in the Subsurface of Southeastern Colorado U.S. Geological Survey Bulletin 1529-G, p. 20.

van Nostrand, T., Lowe, D., 2010. Geology of the Seal Lake area, central Labrador (parts of NTS map sheets 13K/3,4,5 and 6). In Current Research, Newfoundland and Labrador Department of Natural Resources, Geological Survey, Report 10-1. pp. 1–20.

Van Schmus, W.R., Bickford, M.E., Turek, E., 1996. Proterozoic geology of the east-central mid-continent basement. In: van der Pluijm, B.A., Catacosinos, P.A. (Eds.), Basement and basins of eastern North America: Geological Society of America Special Paper 308, pp. 7–32.

Walker, N., 1992. Middle Proterozoic geologic evolution of Llano Uplift, Texas: evidence from U-Pb zircon geochronometry. Geol. Soc. Am. Bull. 104, 494–504.

Weil, A.B., Geissman, J.W., Heizler, M., Van der Voo, R., 2003. Paleomagnetism of Middle Proterozoic mafic intrusions and Upper Proterozoic (Nankoweap) red beds from the Lower Grand Canyon Supergroup, Arizona. Tectonophysics 375, 199–220.

Weiss, G.C., 1986. A depositional Analysis of the Arkose Member (middle Proterozoic) of the Troy Quartzite in Central Arizona (M.S. thesis). Northern Arizona University, Flagstaff, p. 382.

White, N.M., Pringle, M., Garzanti, E., Bickle, M., Najman, Y., Chapman, H., Friend, P., 2002. Constraints on the exhumation and erosion of the High Himalayan Slab, NW India, from foreland basin deposits. Earth Planet. Sci. Lett. 195, 29–44.

Whitmeyer, S.J., Karlstrom, K.E., 2007. Tectonic model for the Proterozoic growth of North America. Geosphere 3 (4), 220–259.

Williams, M.L., 1991. Overview of Proterozoic metamorphism in Arizona. In: Karlstrom, K.E. (Ed.), Proterozoic geology and ore deposits of Arizona: Arizona Geological Society Digest, 19, pp. 11–26.

Williams, G.E., Foden, J., 2011. A unifying model for the Torridon Group (early Neoproterozoic), NW Scotland: Product of post-Grenvillian extensional collapse. Earth Sci. Rev. 108, 34–49.

Wingate, M.T.D., Pisarevsky, S.A., Evans, D.A.D., 2002. Rodinia connections between Australia and Laurentia: no SWEAT, no AUSWUS? Terra Nova 14, 121–128.

Wodicka, N., Parrish, R.R., Jamieson, R.A., 1996. The Parry Sound domain: a far travelled allochthon? New evidence from U-Pb zircon geochronology. Can. J. Earth Sci. 33, 1087–1104.

Wooden, J.L., Stacey, J.S., Howard, K.A., Doe, B.R., Miller, D.M., 1988. Pb isotopic evidence for the formation of Proterozoic crust in the southwestern United States. In: Ernst, W.G. (Ed.), Metamorphism and Crustal Evolution of the Western United States. Prentice-Hall, Englewood Cliffs, New Jersey, pp. 68–86.

Wooden, J.L., Barth, A.P., Mueller, P.A., 2012. Crustal growth and tectonic evolution of the Mojave crustal province: insights from hafnium isotope systematics in zircons. Lithosphere 5, 17–28.

Wrucke, C.T., 1989. The middle Proterozoic Apache Group, Troy Quartzite, and associated diabase of Arizona: Arizona Geological Society Digest, 17, pp. 239– 258.

Wynne-Edwards, H.R., 1972. The Grenville Province. In: Price, R.A., Douglas, R.J.W. (Eds.), Variations in Tectonic Styles in Canada: Geological Association of Canada Special Paper 11, pp. 263–334.

Yin, A., Harrison, T.M., 2000. Geologic evolution of the Himalayan-Tibetan orogen. Annu. Rev. Earth Planet. Sci. 29, 211–280.

Appendix 3.1: Sample locations - See digital appendix

Appendix 3.2: Detrital zircon U-Pb data - See digital appendix

Appendix 3.3: Detrital zircon probability distribution plots - See digital appendix

Appendix 3.4: Detrital zircon concordia plots - See digital appendix

Appendix 3.5: Muscovite step heated data - See digital appendix

Appendix 3.6: Muscovite total fusion data - See digital appendix

Chapter 4

Rodinian devil in disguise: Correlation of 1.25—1.10 Ga strata between Tasmania and Grand Canyon

In preparation for submission to *Geology*

Jacob A. Mulder[1], Karl E. Karlstrom[2], Jacqueline A. Halpin[3], Christopher J. Spencer[4], Ron F. Berry[1], George E. Gehrels[5], Mark Pecha[5]

[1]ARC Centre of Excellence in Ore Deposits (CODES), School of Physical Sciences, University of Tasmania, Private Bag 79, TAS 7001, Australia

[2]Department of Earth and Planetary Sciences, University of New Mexico, Albuquerque, NM 87106, USA

[3]Institute for Marine and Antarctic Studies, University of Tasmania, Hobart, Tasmania 7001, Australia

[4]Department of Applied Geology, Curtin University, Perth, Western Australia 6845, Australia

[5]Department of Geosciences, University of Arizona, Tucson, AZ 85721, USA

4.0 Abstract

Paleogeographic reconstructions of the supercontinent Rodinia typically place Australia or East Antarctica adjacent to the southwestern margin of Laurentia. Of critical importance to these reconstructions is a linkage of the 1.30—1.00 Ga Grenville orogen in southern Laurentia to late Mesoproterozoic orogens in Australia or East Antarctica. Here we emphasize a correlation of late Mesoproterozoic foreland sedimentary basins that, prior to truncation by Neoproterozoic rift margins, may have extended west of Laurentia within Rodinia. We propose a correlation of the Unkar Group (Grand Canyon, Arizona) and upper Rocky Cape Group (Tasmania) based on their similar stratigraphy, 1.25—1.15 Ga depositional age, and detrital zircon age spectra and Hf isotope composition. Both successions were dominantly derived from 1.8—1.4 Ga crust similar to Paleoproterozoic—Mesoproterozoic basement terranes and the hinterland of the Grenville orogen in southwest Laurentia. However, east-directed paleocurrents in the <1.17 Ga upper parts of the upper Rocky Cape Group suggest the Tasmanian strata were partly sourced from a landmass west of Laurentia. We demonstrate that the most suitable westerly source for the upper Rocky Cape Group in a paleomagnetically-viable reconstruction of Rodinia is Precambrian basement in the central Transantarctic Mountains (East Antarctica). A position of Tasmania along the southwestern margin of Laurentia and source within the central Transantarctic Mountains supports a *ca.* 1.15 Ga connection between southwest Laurentia and East Antarctica within Rodinia.

4.1 Introduction

An enduring controversy surrounding the paleogeography of the supercontinent Rodinia is the configuration of continents west of Laurentia (Li et al., 2008). A key geological constraint for refining reconstructions of Rodinia is identifying the continuation of the 1.30—1.00 Ga Grenville orogen, which extends for >6000 km along the southeast margin of Laurentia before being truncated by the Neoproterozoic rift margin of the craton in the southwest. Many reconstructions of Rodinia favour continuity between the Grenville orogen and late Mesoproterozoic orogens in Australia (Karlstrom et al., 1999; Wingate et al., 2002) or East Antarctica (Moores, 1991; Dalziel, 1991; Goodge et al., 2010) based on the similar timing of magmatism and high-grade metamorphism in the hinterland of these orogens.

An additional constraint yet to be fully exploited in Rodinia reconstructions is an extensive 1.25—1.10 Ga basin system that developed in the foreland of the Grenville orogen in southwest Laurentia (Timmons et al., 2005). This basin system preserves similar stratigraphy and detrital zircon provenance over and area of ~900,000 km^2 and is also truncated by the western rift margin of Laurentia produced during the breakup of Rodinia (Fig. 4.1; Mulder et al., 2017). Locating fragments of this distinctive foreland basin system in Australia or Antarctica has not been considered in previous reconstructions of Rodinia and could be a key constraint for locating the westerly continuation of the Grenville orogen.

Here we identify late Mesoproterozoic strata comprising the upper Rocky Cape Group (uRCG) in Tasmania (southeast Australia) that share striking similarities in age and stratigraphy to the late Mesoproterozoic Grenville foreland basins of southwest Laurentia. New detrital zircon U-Pb-Hf data from the uRCG and late Mesoproterozoic strata in southwest Laurentia demonstrate that both the Tasmanian and Laurentian successions were derived from similar Paleoproterozoic—late Mesoproterozoic sources. We interpret the uRCG as part of the Grenville foreland basin system, which places Tasmania adjacent to southwest Laurentia in the late Mesoproterozoic, providing a new opportunity to refine the paleogeography of Rodinia.

4.2 Geological setting and stratigraphy

The Grenville foreland basin system in southwest Laurentia comprises a series of correlative 1.25—1.10 Ga basins that rest unconformably on 1.80—1.40 Ga basement or 1.38—1.32 Ga volcano-sedimentary sequences (Fig. 4.1; Timmons et al., 2005; Mulder et al., 2017). The Unkar Group of Grand Canyon, Arizona is the most completely preserved Grenville foreland basin sequence and its distinctive stratigraphy is recognized in most correlative basins throughout southwest Laurentia (Mulder et al., 2017). The Unkar Group comprises a lower 1.25—1.23 Ga succession of conglomerate, sandstone, siltstone, and stromatolitic dolomite (Bass Formation and Hakatai Shale) disconformably overlain by the <1.14 Ga Shinumo Sandstone. The Shinumo Sandstone includes cross-bedded quartz arenite recording north-directed paleocurrents, contains conspicuous soft-sedimentary deformation features (Fig. 4.1), and grades upwards into the siltstone-rich Dox Formation.

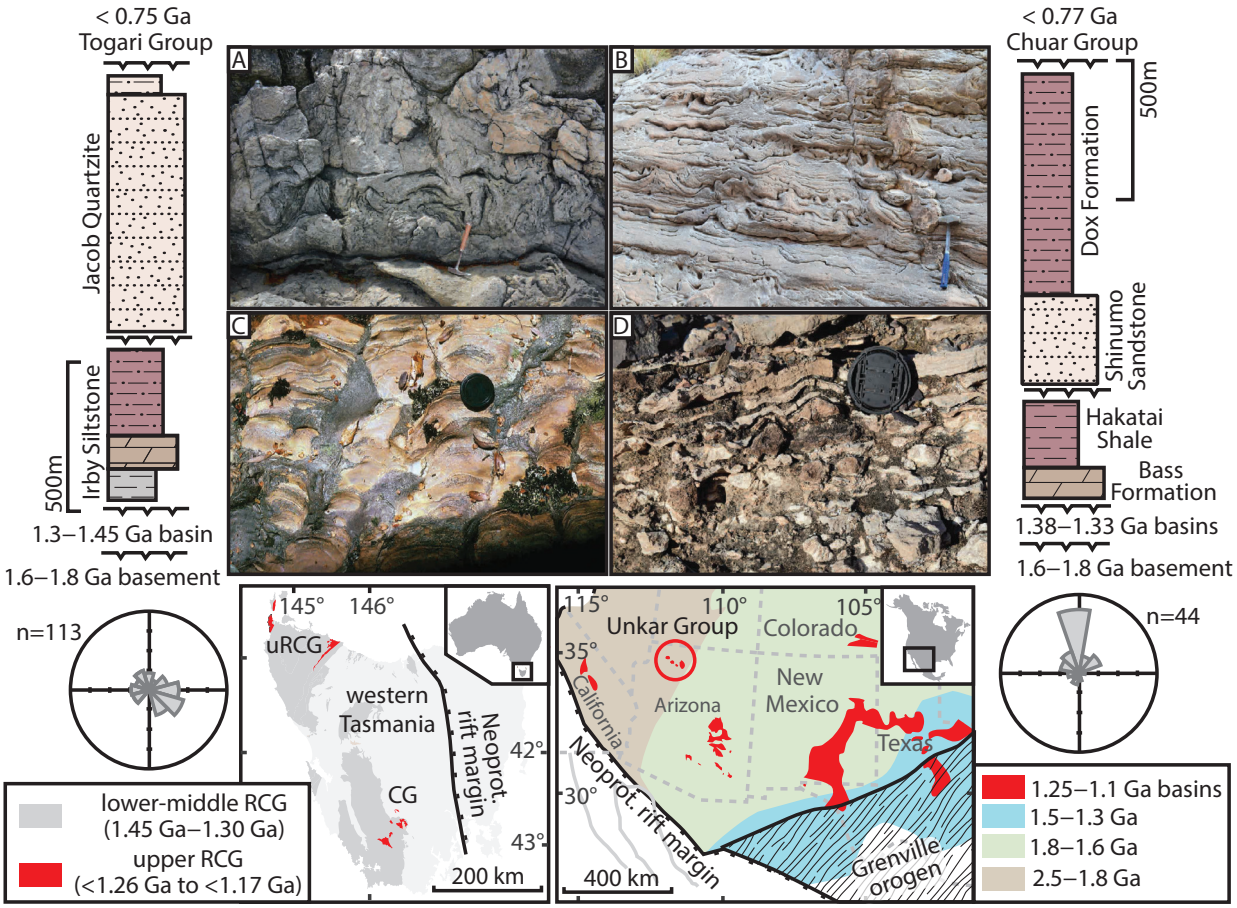

Figure 4.1: Regional geology, simplified stratigraphy, and field photographs of the upper Rocky Cape Group and Unkar Group. For upper Rocky Cape Group (left panels) geological map and stratigraphy follow Halpin et al. (2014), paleocurrent data are from Jacob Quartzite (summarized in Mulder et al. 2015). For Unkar Group (right panels), geological map and stratigraphy from Mulder et al. (2017), paleocurrent data from Shinumo Sandstone are from Timmons et al. (2005). Field photographs A and B show soft-sediment deformation in Jacob Quartzite and Shinumo Sandstone respectively. Field photographs C (Calver et al., 2014) and D show stromatolitic dolostones from Irby Siltstone and Bass Formation respectively. Paleocurrent rose diagrams have 30° sector width and scale on axes represents increments comprising 10% of total dataset. Neoprot.—Neoproterozoic; uRCG—upper Rocky Cape Group; CG— Clark Group.

The upper Dox Formation is interlayered with 1.10 Ga Cardenas Basalt and is unconformably overlain by the <0.78 Ga Chuar Group, which was deposited during the formation of Laurentia's western rift margin (Dehler et al., 2017).

The Proterozoic geology of Tasmania represents an exotic microcontinent accreted to the southeastern margin of Australia in the early Paleozoic (Berry et al., 2008; Cayley, 2011). The oldest rocks in Tasmania are 1.45—1.30 Ga marginal marine sequences of the lower-middle Rocky Cape Group (Halpin et al., 2014), which overlie an unexposed basement with Nd model ages of 1.80—1.60 Ga (Berry et al., 2008). The lower-middle Rocky Cape Group is disconformably overlain by the uRCG (Fig. 4.1, Halpin et al., 2014). The uRCG comprises a lower unit of siltstone, shale, and stromatolitic dolostone (Irby Siltstone) disconformably overlain by the Jacob Quartzite— a succession of cross-bedded quartz arenite with soft-sediment deformation features conformably overlain by an unnamed siltstone unit. Cross-beds in the Jacob Quartzite record predominantly east-directed paleocurrents

(Fig. 4.1). The uRCG is unconformably overlain by the <0.75 Ga Togari Group, which was deposited during formation of an east-facing rift margin in Tasmania (Calver et al., 2014). To the south of Tasmania, late Mesoproterozoic rocks dredged from the South Tasman Rise include 1.12—1.05 Ga granitoids, which experienced high-grade metamorphism at 0.92 Ga (Fioretti et al., 2005; Berry et al., 2008).

4.3 New detrital zircon geochronology and Hf isotopes

We present new detrital zircon U-Pb age and Hf isotope data from the uRCG to complement the dataset of Mulder et al. (2015) and new Hf isotope data from previously dated detrital zircons from the Unkar Group and correlative strata in eastern Arizona (Apache Group) and western Texas (Llanoria Formation; Spencer et al., 2014; Mulder et al., 2017). U-Pb and Hf isotope measurements were conducted via Laser ablation-inductively coupled plasma mass spectrometry at the University of Tasmania, University of Arizona, and Curtin University (Western Australia). Full analytical results and methods are presented in Appendix 4.1 and 4.2.

The new detrital zircon ages from the uRCG refine the maximum depositional age of the Irby Siltstone to 1.26 ± 0.02 Ga and the Jacob Quartzite to 1.17 ± 0.02 Ga (2σ errors, Appendix 4.1). Detrital zircons from the uRCG include minor 3.30 Ga—2.20 Ga grains (5% of total population) and abundant 1.90—1.60 Ga zircons (54%) forming age peaks at 1.85 Ga, 1.78 Ga, and 1.71 Ga (Fig. 4.2). Mesoproterozoic detrital zircons in the uRCG include rare 1.60—1.50 Ga grains (4%), a large age peak at 1.46 Ga (16%), and a spread of ages between 1.38 and 1.29 Ga (10%). The youngest age peak occurs at 1.22 Ga (7%).

To explore the provenance of the uRCG with respect to late Mesoproterozoic Rodinia-forming orogens, we restrict our discussion of detrital zircon Hf isotopic data to Mesoproterozoic age populations (Fig. 4.2, see Appendix 4.2 for Hf isotope data from Paleoproterozoic zircons). The *ca.* 1.45 Ga detrital zircons from the uRCG have initial epsilon hafnium values (εHf_i, calculated with decay constant of Scherer et al., 2001) between +12.53 and +4.03, 1.40—1.30 Ga detrital zircons have εHf_i ranging from +12.47 to +1.33, and the youngest population (1.25—1.20 Ga) has εHf_i of +10.10 to -6.26 (Fig. 4.2). The *ca.* 1.45 Ga detrital zircons from the Unkar Group and correlates have εHf_i of +12.95 to +3.73, 1.40—1.30 Ga zircons have εHf_i of +11.89—+1.16, and the youngest population (*ca.* 1.24 Ga) has εHf_i between +12.74 and -3.00 (Fig. 4.2).

4.4 Correlating late Mesoproterozoic strata in Tasmania and Grand Canyon

Correlation of the uRCG and Unkar Group is supported by similarities in age, stratigraphy, and detrital zircon provenance (Fig. 4.1 and Fig. 4.2; Appendix 4.3). The lower carbonate-shale unit in the uRCG (Irby Siltstone) was deposited after *ca.* 1.26 Ga and is correlated with 1.25—1.23 Ga carbonate-shale strata of the lower Unkar Group (Bass Formation and Hakatai Shale). In the uRCG, the Irby Siltstone is disconformably overlain by <1.17 Ga quartz arenite (Jacob Quartzite) and siltstone.

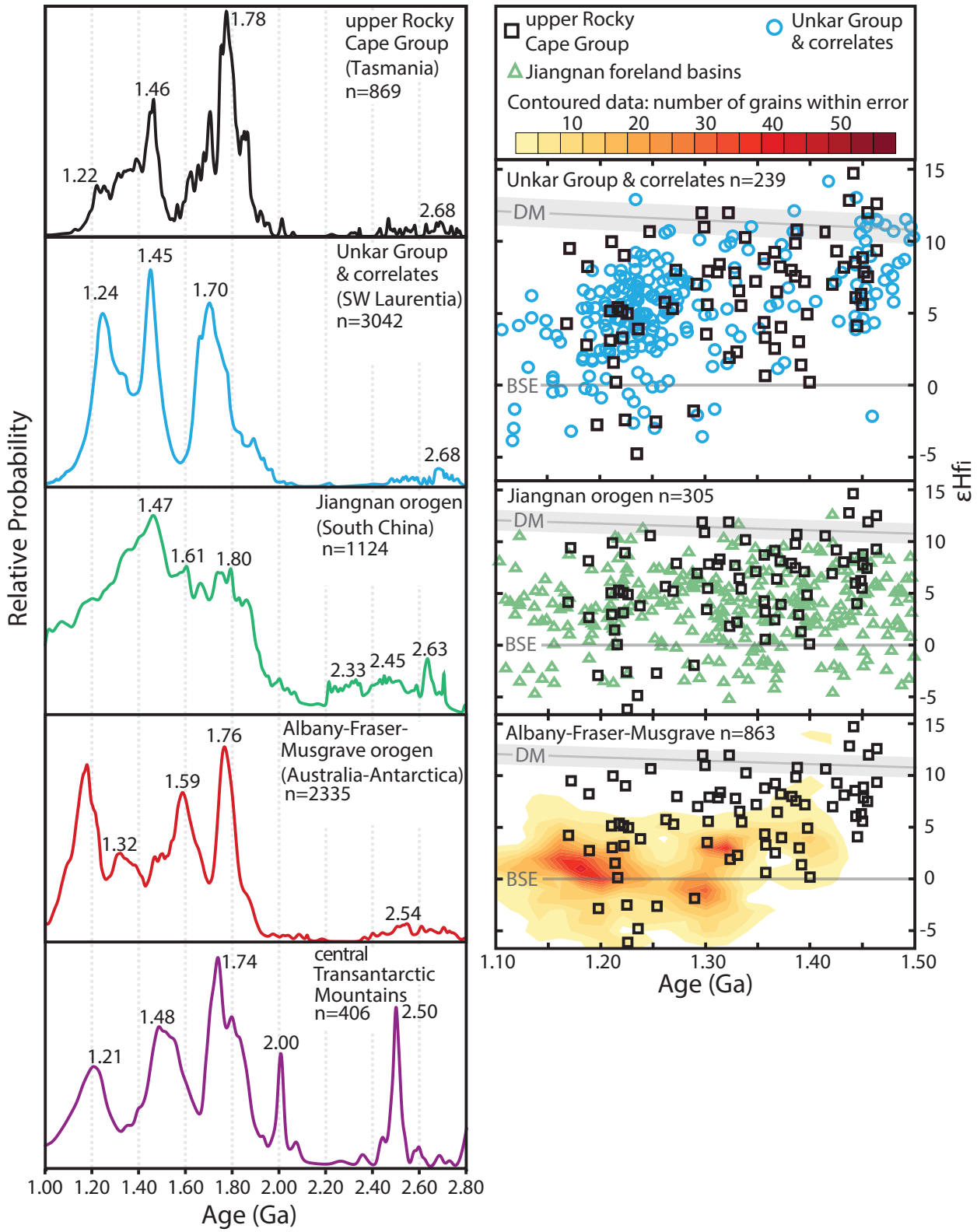

Figure 4.2: Detrital zircon U-Pb probability distribution plots (left) and εHf_i vs. age plots (right) from the upper Rocky Cape Group, Unkar Group and correlates, and compiled data from late Mesoproterozoic orogens west of Laurentia within Rodinia. Labels in probability distribution plots (left panels) mark age of prominent >1.20 Ga age populations (in Ga). See Appendix 4.1 and Appendix 4.2 for all data and references to compiled data sources. Probability density plots constructed with $^{207}Pb/^{206}Pb$ ages (and 1σ errors) for analyses <±10% discordant and density distribution εHf_i vs age plots were constructed with surfer 8.0 (www.goldensoftware.com/products/surfer) using grid dimensions of 1 εHf unit and 20 Ma.

A similar stratigraphic relationship is preserved in Grand Canyon where the Bass Formation and Hakatai Shale are disconformably overlain by quartz arenite and siltstone of the 1.14—1.10 Ga Shinumo Sandstone and Dox Formation. We suggest the Jacob Quartzite and overlying siltstone unit are correlative with the Shinumo Sandstone and Dox Formation and were deposited at 1.14— 1.10 Ga. Correlation of the uRCG and Unkar Group suggests Tasmania formed part of the Grenville foreland basin system and was located along the southwest margin of Laurentia at 1.25—1.10 Ga (Fig. 4.3).

The uRCG and Unkar Group also share a similar detrital zircon provenance with both sequences sourced predominantly from 1.80—1.60 Ga, 1.45 Ga, and 1.25—1.20 Ga crust (Fig. 4.2). Detrital zircon εHf_i data are consistent with Mesoproterozoic crust in the source region(s) of both basins developing through the addition of juvenile mantle melts and reworking of older crust (Fig. 4.2). The detrital zircon age spectrum and paleocurrent data from the Unkar Group and correlates are consistent with a provenance in local Paleoproterozoic—Mesoproterozoic basement terranes and the hinterland of the Grenville orogen in southwest Laurentia (Fig. 4.1; Mulder et al., 2017). The detrital zircon provenance of the uRCG is consistent with a source similar to that of the Unkar Group (Fig. 4.2). However, east-directed paleocurrent indicators suggest that during deposition of the Jacob Quartzite (1.14—1.10 Ga) the source of the uRCG was west of Laurentia (Fig. 4.1). Given Tasmania's position along the southwest margin of Laurentia during the late Mesoproterozoic, we suggest the westerly source of the uRCG at 1.14—1.10 Ga was the continuation of the Grenville orogen on the continent(s) adjacent to Laurentia within Rodinia.

4.5 uRCG provenance and implications for Rodinia paleogeography

Figure 4.3 shows our preferred late Mesoproterozoic position for Tasmania along the southwest margin of Laurentia and is similar to the location of Tasmania at 0.78 Ga proposed by Moore et al. (2015). This position aligns the 1.8—1.6 Ga Nd model ages of the Tasmanian basement with the juvenile 1.8—1.6 Ga basement in southwest Laurentia (Moore et al., 2015), places the uRCG adjacent to correlative strata in southwest Laurentia (Fig. 4.1), juxtaposes 1.12—0.92 Ga igneous and metamorphic rocks from the South Tasman Rise against the southern extension of the Grenville orogen (Fioretti et al., 2005), and aligns opposing Neoproterozoic rift margins of Tasmania and southwest Laurentia.

High-quality paleomagnetic data support the Figure 4.3 reconstruction that places Australia and East Antarctica west of Laurentia at 1.14 Ga (Pisarevsky et al., 2014). Both Australia and East Antarctica contain late Mesoproterozoic orogens developed on Paleoproterozoic and Mesoproterozoic crust that are plausible continuations of the Grenville orogen and hence possible westerly sources regions for uRCG at 1.14—1.10 Ga. An alternative westerly source for the uRCG is the Jiangnan orogen of South China, which is placed between Australia and Laurentia in the 'Missing-link' reconstruction of Rodinia (Li et al., 2002). Figure 4.2 includes U-Pb-Hf data compiled from late Mesoproterozoic orogens in South China, Australia, and East Antarctica in order to test these regions as possible

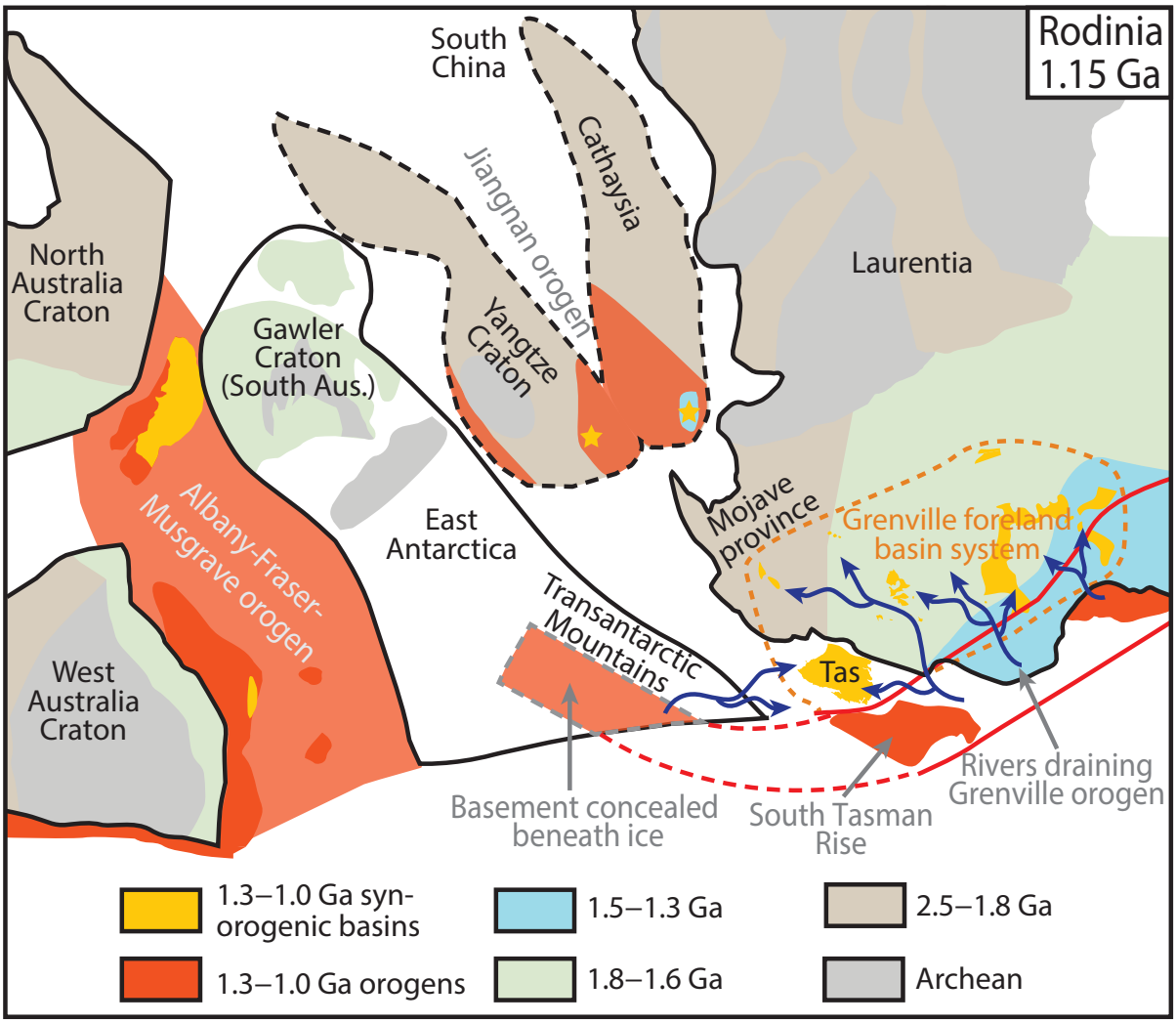

Figure 4.3: Paleogeographic reconstruction of Rodinia at 1.15 Ga showing preferred position of Tasmania and late Mesoproterozoic orogenic belts. Reconstruction follows Whitmeyer & Karlstrom (2007), Li & Evans (2011), Moore et al. (2015), Aitken et al. (2016), Goodge & Fanning (2016), and Yao et al. (2017). Dark blue arrows show inferred transport direction of sediment into the upper Rocky Cape and Unkar Groups. Dashed red lines show inferred westerly continuation of the Grenville orogen.

westerly sources for the uRCG. The compilations include data from late Mesoproterozoic and Neoproterozoic strata derived from these orogens and are representative of the source rocks exposed during deposition of the uRCG (see Appendix 4.1 and 4.2 for a list of compiled data and references).

In the 'Missing-link' reconstruction of Rodnia, the Jiangnang orogen is interpreted as a late Mesoproterozoic to early Neoproterozoic suture between the Yangtze Craton and Cathaysia that led to the final amalgamation of the South China Craton (Li et al., 2002). Mesoproterozoic detrital zircons from the Jiangnang orogen have εHf_i values that are broadly similar to time-equivalent grains from the uRCG (Fig 4.2; Yao et al., 2017). However, the nearly continuous distribution of detrital zircon ages between 2.0 Ga and 1.0 Ga from the Jiangnan orogen is unlike the detrital provenance of the uRCG (Fig. 4.2). Although the new data do not refute the 'Missing-link' reconstruction of Rodinia, we suggest the Jiangnan orogen was not the westerly source of the uRCG.

The Albany-Fraser-Musgrave orogen is exposed in central Australia, western Australia, and formerly contiguous crust in Wilkes Land, Antarctica and records collision of the South Australia Craton and its extension into East Antarctica with the West Australian Craton at 1.29—1.08 Ga (e.g., Aitken et al. 2016). Although the age distribution of Archean and Paleoproterozoic detrital zircons in the uRCG and Albany-Fraser-Musgrave orogen are similar, the latter contains abundant 1.60—1.50 Ga detrital zircons, which are rare in the uRCG (Fig. 4.2). Furthermore, the εHf_i values of Mesoproterozoic detrital zircons from the Albany-Fraser-Musgrave orogen are a poor match for similar-aged grains from the uRCG (Fig. 4.2). We conclude that the Albany-Fraser-Musgrave orogen was not the source of the uRCG and is not the westerly continuation of the Grenville orogen.

Neoproterozoic strata in the central Transantarctic Mountains are interpreted to have been derived from a proximal late Mesoproterozoic orogen developed in Archean—Mesoproterozoic crust concealed beneath the adjacent ice cap (e.g., Goodge & Fanning, 2016). The detrital zircon provenance of Neoproterozoic strata in the central Transantarctic Mountains shows close similarities with the uRCG with both sequences sharing age populations at 1.80—1.70 Ga, 1.45 Ga, and *ca.* 1.20 Ga (Fig. 4.2). Unfortunately, relatively few Hf isotopic data are currently available from central Transantarctic Mountains to allow for a detailed comparison with the uRCG. In the context of the reconstruction in Figure 4.3, we suggest the late Mesoproterozoic orogen in the central Transantarctic Mountains is the most plausible westerly source region for the uRCG at 1.14—1.10 Ga. Our preferred late Mesoproterozoic position for Tasmania and the provenance of the uRCG is consistent with the interpretation that the Grenville orogen extends into the central Transantarctic Mountains (Goodge et al., 2010) and supports a paleomagnetically-viable connection between southwest Laurentia and East Antarctica within Rodinia at *ca.* 1.15 Ga

4.6 Conclusions

Similarities in age, stratigraphy, and detrital zircon provenance support correlation of the uRCG of Tasmania with the Unkar Group (Grand Canyon) and correlative late Mesoproterozoic strata throughout southwest Laurentia. We suggest the uRCG represents a displaced fragment of the extensive foreland basin system that developed throughout southwest Laurentia during the Grenville Orogeny, and that Tasmania was located along the southwest margin of Laurentia during the assembly of Rodinia. The westerly-derived 1.14—1.10 Ga Jacob Quartzite in the uRCG has a detrital zircon provenance similar to a late Mesoproterozoic orogenic belt concealed beneath ice cover in the central Transantarctic Mountains. The position of Tasmania along the southwest margin of Laurentia and a westerly provenance in the central Transantartic Mountains supports a paleomagnetically-viable connection between southwest Laurentia and East Antarctica within Rodinia at *ca.* 1.15 Ga

4.7 Acknowledgements

We gratefully acknowledge Grand Canyon National Park for permission to undertaken research and sampling in Grand Canyon. J. Thompson, S. Meffre, K. Goemann, S. Feig (University of Tasmania) and D. Giesler and C. White (University of Arizona) are thanked for analytical assistance. This research was funded by the ARC Centre of Excellence in Ore Deposits (CODES), School of Physical Sciences, University of Tasmania and NSF grant EAR-1338583. We thank XX and XX for reviews and XX for editorial handling. This is a contribution to IGCP Project 648.

4.8 References cited

Aitken, A.R.A., Betts, P.G., Young, D.A., Blankenship, D.D., Roberts, J.L., and Siegert, M.J., 2015, The Australo-Antarctic Columbia to Gondwana transition: Gondwana Research, v. 29, p. 136—152.

Berry, R.F., Steele, D.A., and Meffre, S., 2008, Proterozoic metamorphism in Tasmania: Implications for tectonic reconstructions: Precambrian Research, v. 166, p. 387–396.

Calver, C.R., Everard, J.L., Berry, R.F., Bottrill, R.S., and Seymour, D.B., 2014, Proterozoic Tasmania, in Corbett, K.D., et al., (eds.). Geological evolution of Tasmania: Geological Society of Australia Special Publication 24, p. 34–94

Cayley, R.A., 2011, Exotic crustal block accretion to the eastern Gondwanaland margin in the Late Cambrian—Tasmania, the Selwyn Block, and implications for the Cambrian-Silurian evolution of the Ross, Delamerian, and Lachlan orogens: Gondwana Research, v. 19, p. 628–649.

Dalziel, I.W.D., 1991, Pacific margins of Laurentia and East Antarctica as a conjugate rift pair: Evidence and implications for an Eocambrian supercontinent: Geology, v. 19, p. 598–601.

Dehler, C., Gehrels, G. E., Porter, S., Heizler, M. T., Karlstrom, K.E., Cox, G., Crossey, L.J., and Timmons, J.M., 2017, Synthesis of the 780–740 Ma Chuar, Uinta Mountain, and Pahrump (ChUMP) groups, western USA: Implications for Laurentia-wide cratonic marine basins. Geological Society of America Bulletin.

Fioretti, A.M., Black, L.P., Foden, J., and Visona, D., 2005, Grenville-age magmatism at the South Tasman Rise (Australia): a new piercing point for the reconstruction of Rodinia. Geology, v. 33, p. 769–772.

Goodge, J.W., and Fanning, C.M., 2016, Mesoarchean and Paleoproterozoic history of the Nimrod Complex: central Transantarctic Mountains, Antarctica: Stratigraphic revisions and relation to the Mawson Continent in East Gondwana. Precambrian Research, v 285, p. 242–271.

Goodge, J.W., Fanning, C.M., Brecke, D.M., Licht, K.J., and Palmer, E.F., 2010, Continuation of the Laurentian Grenville province across the Ross Sea margin of East Antarctica: Journal of Geology, v. 118, p. 601–619.

Halpin, J.A., Jensen, T., McGoldrick, P., Meffre, S., Berry, R.F., Everard, J.L., Calver, C.R., Thompson, J., Goemann, K., and Whittaker, J.M., 2014, Authigenic monazite and detrital zircon dating from the Proterozoic Rocky Cape Group, Tasmania: Links to the Belt-Purcell Supergroup, North America: Precambrian Research, v. 250, p. 50–67.

Karlstrom, K.E., Williams, M.L., McLelland, J., Geissman, J.W., and Åhäll, K.I., 1999, Refining Rodinia: Geological evidence for the Australia–western U.S. connection in the Proterozoic: GSA Today, v. 9, no. 10, p. 1–7

Li, Z.-X., and Evans, D.A.D., 2011, Late Neoproterozoic 40° intraplate rotation within Australia allows for a tighter-fitting and longer-lasting Rodinia: Geology, v. 39, p. 39–42.

Li, Z.-X., Li, X.H., Zhou, H., and Kinny, P.D., 2002, Grenvillian continental collision in South China: new SHRIMP U–Pb zircon results and implications for the configuration of Rodinia. Geology, v. 30, p. 163–166.

Li, Z.-X., Bogdanova, S.V., Collins, A.S., Davidson, A., De Waele, B., Ernst, R.E., Fitzsimons, I.C.W., Fuck, R., Gladkochub, D.P., Jacobs, J., Karlstrom, K.E., Lu, S., Natapov, L.M., Pease, V., Pisarevsky, S.A., Thrane, K., and Vernikovsky, V., 2008. Assembly, configuration, and break-up history of Rodinia: a synthesis. Precambrian Research 160, 179–210.

Moore, D.H., Betts, P.G., and Hall, M., 2015, Fragmented Tasmania: The transition from Rodinia to Gondwana: Australian Journal of Earth Sciences, v. 62, p. 1–35.

Moores, E.M., 1991, Southwest U.S–East Antarctica (SWEAT) connection: A hypothesis: Geology, v. 19, p. 425–428.

Mulder, J.A., Halpin, J.A., and Daczko, N.R., 2015. Mesoproterozoic Tasmania: Witness to the East Antarctica-Laurentia connection within Nuna. Geology 43, 759–762.

Mulder, J.A., Karlstrom, K.E. Fletcher, K., Heizler, M.T., Timmons, J.M., Crossey, L.J., Gehrels, G.E., and Pecha, M., 2017, The syn-orogenic sedimentary record of the Grenville Orogeny in southwest Laurentia. Precambrian Research, v. 294, 33–52.

Pisarevsky, S.A., Wingate, M.T.D., Li, Z.-X., Wang, X.C., Tohver, E., and Kirkland, C.L., 2014, Age and paleomagnetism of the 1210 Ma Gnowangerup–Fraser dyke swarm, Western Australia, and implications for late Mesoproterozoic paleogeography. Precambrian Research, v. 246, p. 1—15.

Scherer, E., Munker, C., and Mezger, K., 2001, Calibration of the lutetium-hafnium clock: Science, v. 293, p. 683–687.

Spencer, C.J., Prave, A.R., Cawood, P.A., and Roberts, N.M.W., 2014. Detrital zircon geochronology of the Grenville/Llano foreland and basal Sauk Sequence in west Texas, USA. Geological Society of America Bulletin, v. 126, p. 1117–1128.

Timmons, J.M., Karlstrom, K.E., Heizler, M.T., Bowring, S.A., Gehrels, G.E., and Crossey, L.J., 2005, Tectonic inferences from the ca. 1255–1100 Ma Unkar Group and Nankoweap Formation, Grand Canyon: intracratonic deformation and basin formation during protracted Grenville orogenesis. Geological Society of America Bulletin, v. 117, p. 1573–1595.

Whitmeyer, S.J., and Karlstrom, K.E., 2007. Tectonic model for the Proterozoic growth of North America. Geosphere 3 (4), 220–259.

Wingate, M.T.D., Pisarevsky, S.A., and Evans, D.A.D., 2002. Rodinia connections between Australia and Laurentia: no SWEAT, no AUSWUS? Terra Nova 14, 121–128.

Yao, W., Li, Z.-X., Li, W.X., and Li, X.H., 2017. Proterozoic tectonics of Hainan Island in supercontinent cycles: new insights from geochronological and isotopic results. Precambrian Research, v. 290, p. 86–100.

Appendix 4.1: Zircon-Hf age compilation - See digital appendix

Appendix 4.2: Zircon-U-Pb age compilation - See digital appendix

Appendix 4.3: Detailed stratigraphy of late Mesoproterozoic basins in Tsmania and southwest Laurentia

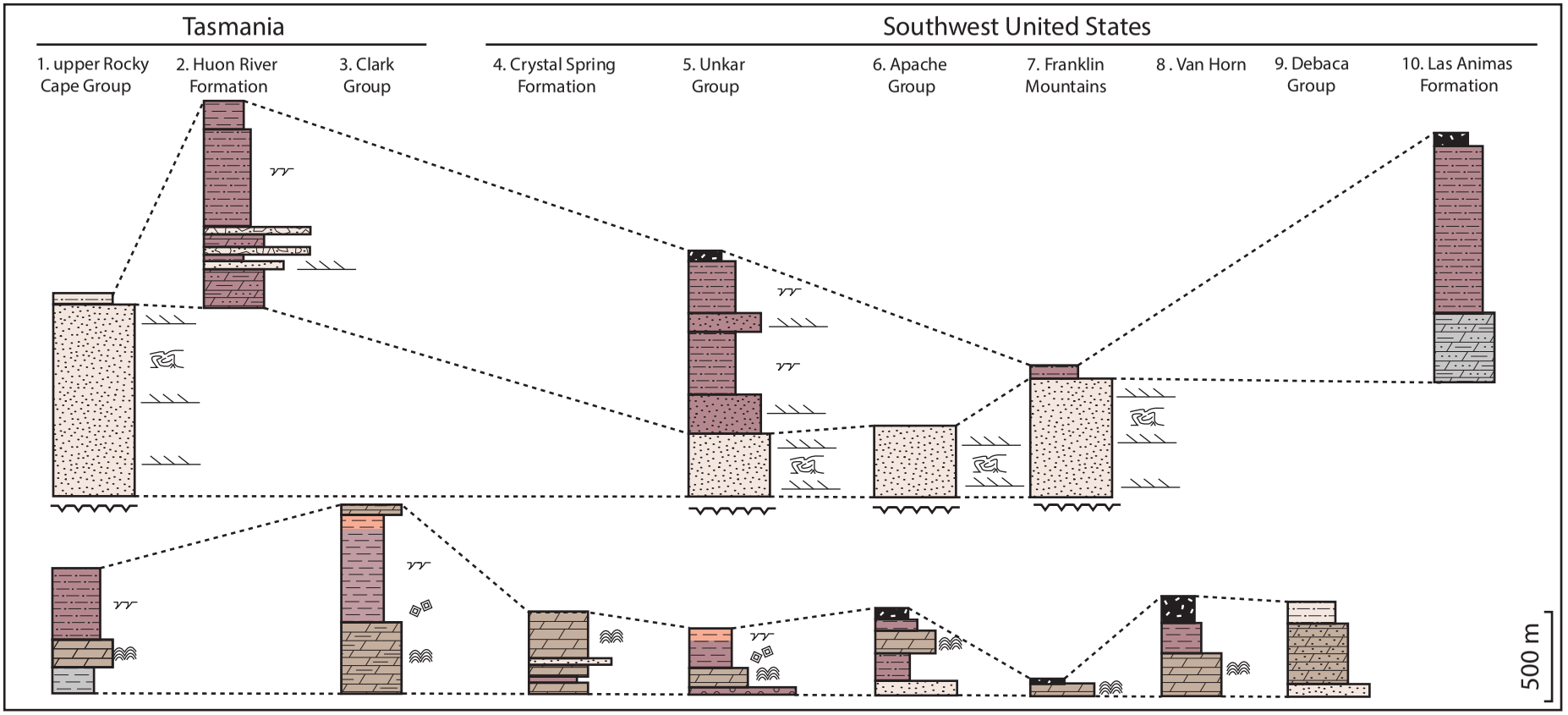

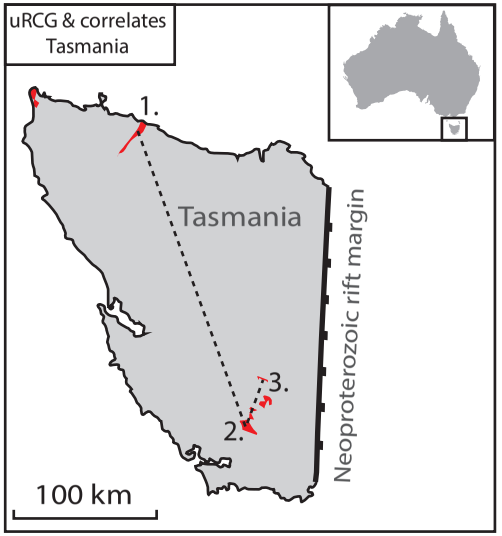

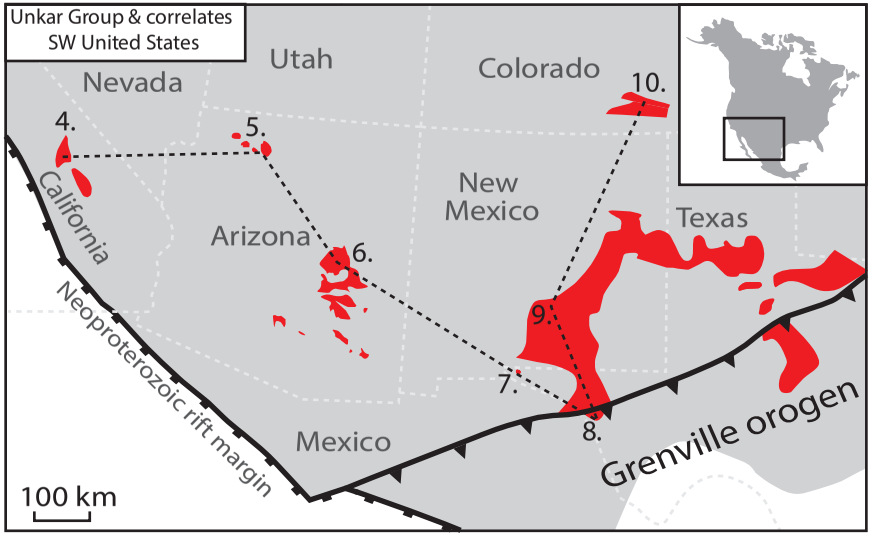

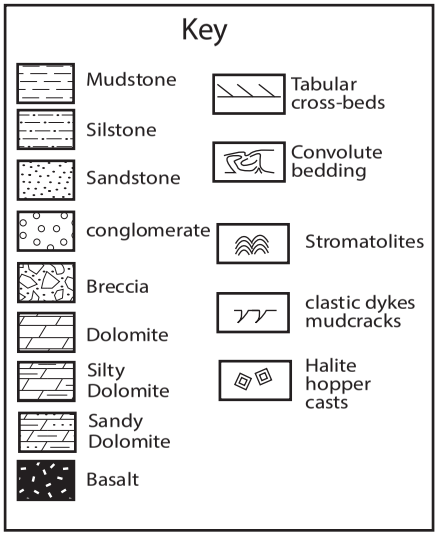

upper Rocky Cape Group, northwest Tasmania

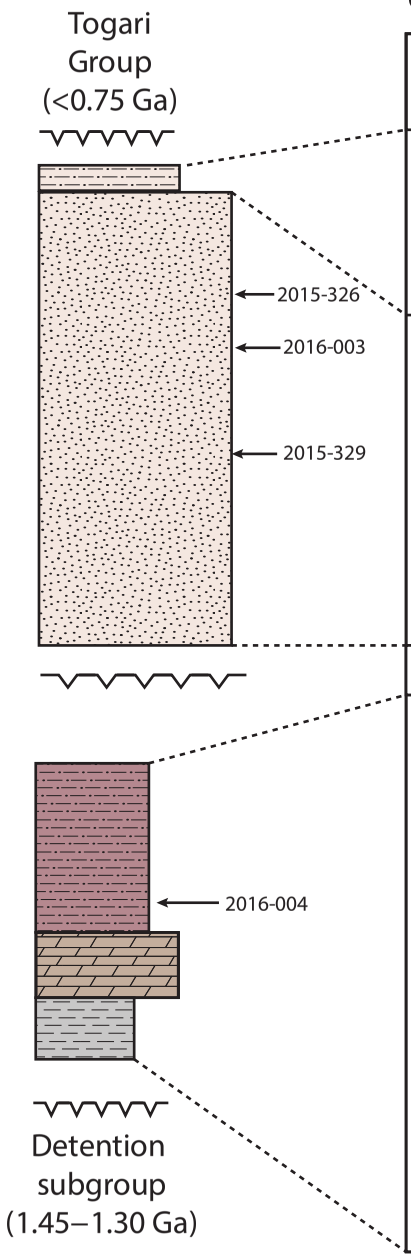

Name	Age Constraints	Thickness	Lithologies	Sedimentary Structures	Depositional Environments	References
Silstone Unit (unamed)	Conformable with underlying Jacob Quartzite	60 m (minimum)	Thinly interbedded, light brown to tan micaceous quartz silstone, and quartz sandstone	Planar lamination	Shallow marine	Gee (1967)
Jacob Quartzite	Max: 1170 ± 16 Ma (Youngest detrital zircon population) Min: <750 Ma from overlying Togari Group	1100 m	<1 m tabular beds of medium–coarse quartz arenite. tabular cross-bedding common throughout. <0.5 m-thic beds of micaceous silstone in upper parts	Tabular cross-beds, convolute folding, ripple marks	Shallow marine, high-energy, nearshore	Gee (1967)
Disconformity inferred from abrupt change in depositional setting and shift in detrital zircon provenance						
Irby Siltstone	Max: 1258 ± 16 Ma (Youngest detrital zircon population) Min: <750 Ma from overlying Togari Group	680 m	Black mudstone, maroon-grey-green silstone, quartz sandstone, dolomitic mudstone, dolomitic, silstone, dolostone, stromatolitic dolomite	Slump folds sandstones: planar lamination, cross-bedding, climbing ripple lamination, ripple marks. Silstone: clastic dykes, polygonal cracks Dolomite: microbial lamination, stromatolites, ooids, peloids, molar tooth structure	Shallow marine, periodically subaerial, low energy possibly, a sub- tidal to supra-tidal mudflat	Gee (1967) Calver & Baillie (1990) Seymour (2002)

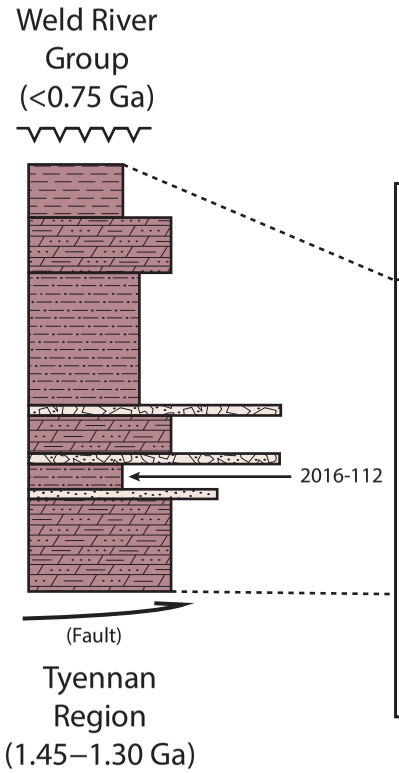

Huon River Formation, southern Tasmania

Name	Age Constraints	Thickness	Lithologies	Sedimentary Structures	Depositional Environments	References
Huon River Formation	Max: 1179 ± 13 Ma (Youngest detrital zircon population) Min: <750 Ma from overlying Weld River Group	(?)3000 m (disrupted by faulting)	red-purple-green mudstone and silstone, quartz arenite, intra-clastic breccia, dolostone	Clastic dykes, cross-bedding, ripple marks, chert nodules.	Shallow marine, periodically subaerial, mostly low energy, possibly a sub- to supra-tidal mudflat. Abundant breccia beds in lower parts suggest syn-depositional tectonism	Calver (1990)

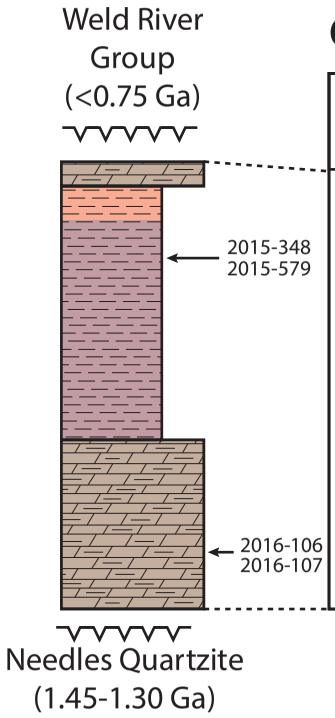

Clark Group, southern Tasmania

Name	Age Constraints	Thickness	Lithologies	Sedimentary Structures	Depositional Environments	References
Humboldt Formation	Max: 1329 ± 20 Ma (Youngest detrital zircon population) Min: <750 Ma from overlying Weld River Group	(?)2000 m (disrupted by faulting)	Dolomitic mudstone, dolostone, stromatolitic dolomite, shale, red and orange mudstone, red siltstone, chert, flat-pebble conglomerate, quartz arenite	Clastic dykes, halite hopper casts, molar tooth structure, (?)anhydrite nodules, oolites, stromatolites	Shallow marine, periodically subaerial, low energy possibly a sub- tidal to supra-tidal mudflat	Calver et al. (2006)

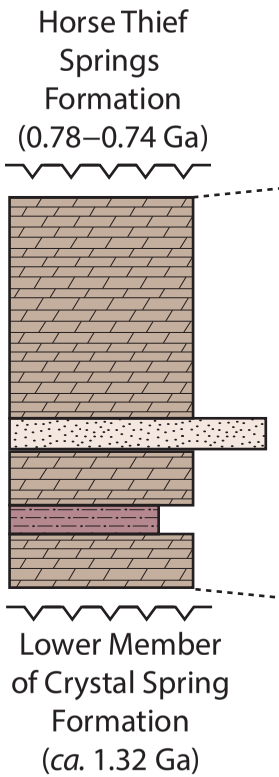

Crystal Spring Formation (Pahrump Group), Death Valley, California, USA

Name	Age Constraints	Thickness	Lithologies	Sedimentary Structures	Depositional Environments	References
Middle Member	Max: *ca.* 1210 Ma (Youngest detrital zircon population) Min: 1069 ± 3 Ma (cross-cutting diabse)	135–400 m	Dolomitic limestone, stromatolitic dolomite, quartz sandstone, silstone, mudstone	Stromatolites	Shallow marine	Roberts (1982) Heaman & Grotzinger (1992) Mahon et al. (2014) Mulder et al. (2017)

Unkar Group, Grand Canyon, Arizona, USA

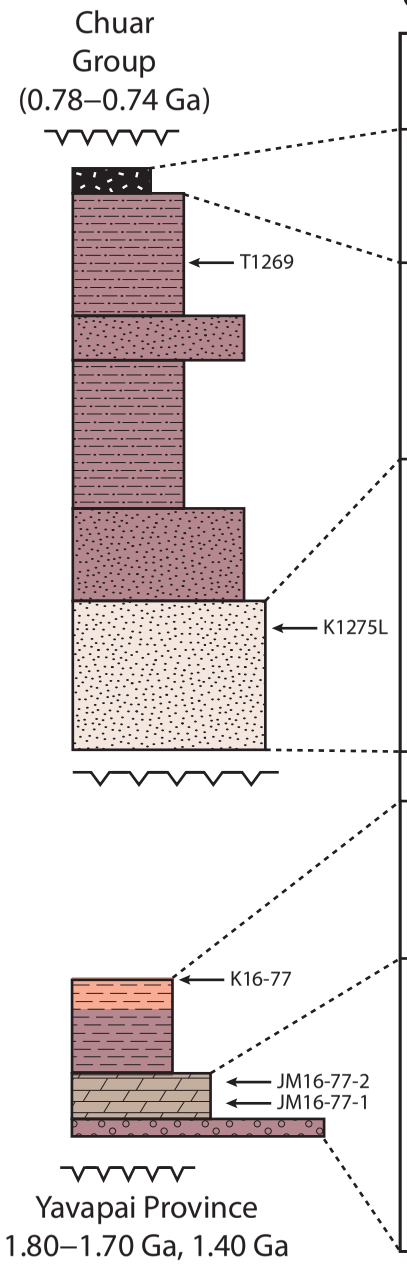

Name	Age Constraints	Thickness	Lithologies	Sedimentary Structures	Depositional Environments	References
Cardenas Basalt	1104 Ma	300 m	Basaltic lava flows and asscoiated volcani-clastic rocks		Intracratonic rift	Hendricks (1972) Larson et al. (1994) Weil et al. (2003) Timmons et al. (2005)
Dox Formation	Upper parts interlayered with 1104 Ma Cardenas Basalt	1000–1500 m	Red and maroon quartz sandstone, arkose, micaceous sandstone, and mudstone	Tabular cross-bedding, partling lineations, trouchs, clastic dykes, ripples marks	Deltaic and shallow marine	Stevenson and Beus (1982) Timmons et al. (2005) Mulder et al. (2017)
Shinumo Sandstone	Max: 1184 ± 5 Ma (Youngest detrital zircon population)	200–300 m	<2 m thick beds of medium-coarse quartz arenite, minor silstone and mudstone Tabular cross-bedding common throughout	Tabular cross-bedding, ripple marks, convolute folding	High energy shallow marine, supra-tidal mudflat, fluvial, deltaic	Daneker (1975) Middleton and Blakey (1998) Timmons et al. (2005) Mulder et al. (2017)
Disconformity inferred from abrupt change in depositional setting and shift in detrital zircon provenance						
Hakatai Shale	Max: 1243 ± 2 Ma (Youngest detrital zircon population)	100–300 m	Red and orange mudstone, arkose	Clastic dykes, polygonal cracks, ripple marks, halite hopper casts	Sub- to supra-tidal mudflats, shallow marine	Reed (1976) Timmons et al. (2005) Bloch et al. (2006) Mulder et al. (2017)
Bass Formation	Lower parts interlayered with a felsic tuff dated at 1254.8 ± 1.6 Ma	60–100 m	Stromatolitic dolomite, quartz sandstone, arkose, silstone, mudstone, felsic tuff, conglomer-ates in lower parts and at base	Tabular cross-bedding, ripple marks, clastic dykes, polygonal cracks, microbial lamination, stromatolites	Low energy shallow marine, sub- to supra-tidal mudflats, conglomerates record syn-depositional seismicity	Dalton (1972) Timmons et al. (2005) Mulder et al. (2017)

Apache Group, eastern Arizona, USA

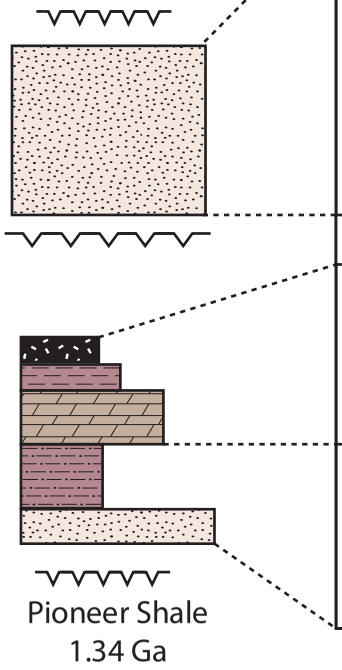

Name	Age Constraints	Thickness	Lithologies	Sedimentary Structures	Depositional Environments	References
Troy Quartzite	Max: 1259 ± 1.7 Ma (Youngest detrital zircon population) Min: 1080 Ma (cross-cutting dolerite dyke)	365 m (minimum)	Tabular bedded arkose, quartz-arenite, silstsone, mudstone, conglomerate	Cross-bedding (tabular and trough), ripplemarks, convolute folding	Fluvial floodplain and braided stream complex, eolian, high energy shallow marine	Schride (1967) Weiss (1986) Burns (1987) Wrucke (1989) Mulder et al. (2017)
Unconformity inferred from, minor folding of Mescal Limestone, abrupt change in depositional setting						
Mescal Limestone	Min: 1080 Ma (cross-cutting dolerite dyke)	75–130 m	Laminated dolomite, stromatolitic dolomite, chert, conglomerate, mudstone, silstone, basaltic lava	Stromatolites, slump folds	Low energy shallow marine	Schride (1967) McConnel (1975) Bertrand-Sarfati and Awramik (1992)
Dripping Springs Formation	Max: 1256 ± 3 Ma (Youngest detrital zircon population)	170–215 m	Arkose, siltstone, mudstone	Tabular cross-bedding, scour and fill structures	sub- to supra-tidal mud flats, distal alluvial fans	Shride (1967) Engel and Elmore (1990) Middleton and Montgomery (2001) Beraldi-Campesi et al. (2014)

Franklin Mountains, western Texas, USA

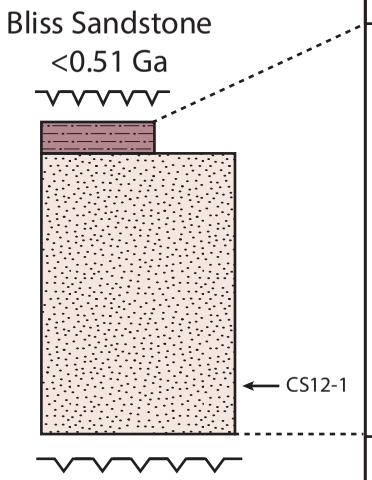

Name	Age Constraints	Thickness	Lithologies	Sedimentary Structures	Depositional Environments	References
Llanoria Formation	Max: 1229 ± 3 Ma (Youngest detrital zircon population from Mulder et al. 2017) Max: 1130 Ma (Youngest detrital zircon population from Spencer et al. 2014) Min: 1120 ± 35 Ma (cross-cutting Red Bluff Granite)	739 m	Tabular bedded quartz arenite, sub arkose, and mudstone red-maroon sandstone and silstone in upper parts	Tabular cross-bedding, ripple marks, convulte folding	High-energy, tidally dominated shallow marine shelf. Upper parts deltaic	Seeley (1999) Spencer et al. (2014) Mulder et al. (2017)
Disconformity inferred from abrupt change in depositional setting						
Mundy Breccia	Synchronous with Castner Marble	70 m	Basaltic breccia, massive basalt, agglomerate	Megablocks of Castner Marble	subaqueous gravity flows	Pittenger et al. (1994)
Castner Marble	Interbedded with felsic tuffs dated at 1251 ± 47 Ma, 1260 ± 20 Ma, 1272 ± 5 Ma	100 m (minimum)	Limestone, rhythmite, flat-pebble conglomerate, tuffaceous silstone, felsic tuffs	Stromatolites	Sub-tidal to supra -tidal carbonate ramp	Pittenger et al. (1994)

Van Horn, western Texas, USA

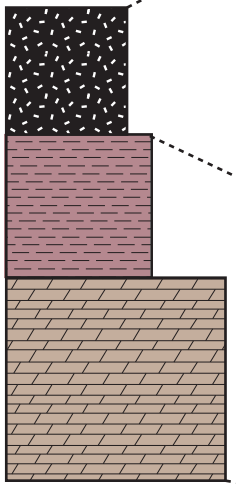

Name	Age Constraints	Thickness	Lithologies	Sedimentary Structures	Depositional Environments	References
Tumbledown Formation	Max: 1243 ± 10 Ma (rhyolite clast in basal lithic arenite) Min: <510 Ma disconformably overlying Bliss Sandstone	168 m	Volcanic lithic arenite, pillow basalt, basaltic breccia, agglomerate, and flows		Intracontinental rift	Soegaard and Callahan (1994) Bickford et al. (2000) Spencer et al.(2014)
Allamoore Formation	Interbedded with felsic tuffs dated at 1253 ± 15 Ma, 1256 ± 5 Ma, 1250 + 20/ -27 Ma	324 m	Interbedded dolostone and chert, talc rock, mudstone, felsic tuff, pillow basalt, basalt flows and hyaloclastic breccia	Stromatolites, halite hopper casts	Sub- to supra-tidal mudflats	King & Flawn (1953) Edwards (1984) Soegaard and Callahan (1994) Roths (1993) Bickford et al. (2000)

Debaca Group, Texas and New Mexico, USA

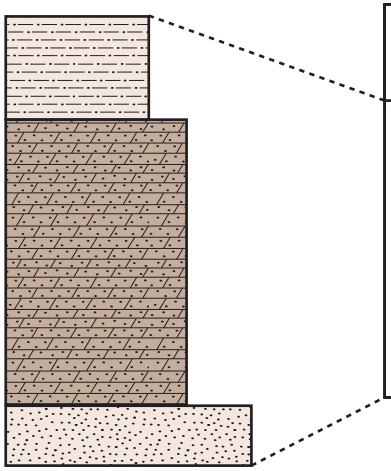

Name	Age Constraints	Thickness	Lithologies	Sedimentary Structures	Depositional Environments	References
Debaca Group	Max: 1334 ± 52 Ma (underlying basement) Min: 1090 ± 4 Ma (cross-cutting gabbro intrusive)	500 m (approximate)	Arkose, quartzite, micaceous silstone, shale, quartz-rich dolomite, dolomitic quartzite, felsic volcaniclastic silt-stone and sandstone, rhyolite	Tabular cross-bedding, clastic dykes, polygonal cracks	Shallow marine	Pary (1961) Amarante (2001)

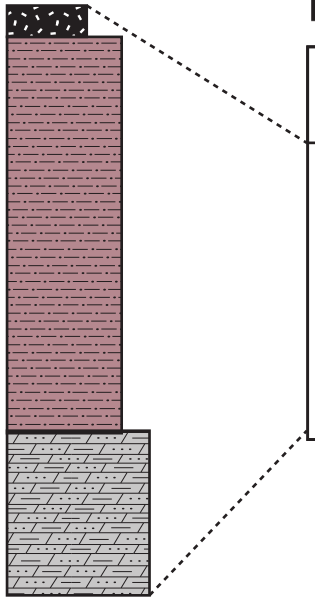

Las Animas Formation, Colorado, USA

Name	Age Constraints	Thickness	Lithologies	Sedimentary Structures	Depositional Environments	References
Las Animas Formation	Max: *ca.* 1400 Ma (underlying basement)	1700 m	Greywacke, mudstone, chert, red-maroon arkose, dolomite, conglomerate, andesitic and basaltic lava and tuffs		Shallow marine	Tweto (1983)

Appendix 4.3 References

Amarante, J.F.A., 2001. Characteristic of the basement rocks in the Mescalero 1 well, Guadalupe County, New Mexico (M.S. thesis). New Mexico Institute of Mining and Technology, Socorro, p. 73.

Beraldi-Campesi, H., Farmer, J.D., Garcia-Pichel, F., 2014. Modern terrestrial sedimentary biostructures and their fossil analogs in mesoproterozoic subaerial deposits. Palaios 29, 45–54.

Bertrand-Sarfati, J., Awramik, S.M., 1992. Stromatolites of the mescal limestone (Apache Group, Middle Proterozoic, Central Arizona) – taxonomy, biostratigraphy, and paleoenvironments. Geol. Soc. Am. Bull. 104, 1138–1155.

Bickford, M.E., Soegaard, K., Nielsen, K.C., McLelland, J.M., 2000. Geology and geochronology of Grenville- age rocks in the Van Horn and Franklin Mountains area, west Texas; implications for the tectonic evolution of Laurentia during the Grenville. Geol. Soc. Am. Bull. 112, 1134–1148.

Bloch, J., Timmons, M., Crossey, L.J., Gehrels, G.E., Karlstrom, K.E., 2006. Mudstone petrology of the Mesoproterozoic Unkar Group, Grand Canyon, U.S.A.: Provenance, weathering, and sediment transport on intracratonic Rodinia. J. Sediment. Res. 76, 1106–1119.

Burns, B.A., 1987. The Sedimentology and Significance of a Middle Proterozoic braidplain; Chediski Sandstone Member of the Troy Quartzite, central Arizona (M.S. thesis). Northern Arizona University, Flagstaff, p. 143.

Calver C. R.. 1990. Huon River Formation. In: Calver, C.R. , Turner, N.J. , McClenaghan, M.P. , McClenaghan, J. Pedder,Tasmania. 1:50,000 Sheet 80(8112S). Geological Survey of Tasmania.

Calver, C. R., and Baillie, P. W., 1990. Early diagenetic concretions associated with intrastratal shrinkage cracks in an upper Proterozoic dolomite, Tasmania, Australia. Journal of Sedimentary Petrology, v. 60, 293—305.

Calver, C. R., Forsyth, S. M., Everard, J. L., 2006. Geology of the Skeleton, Nevada, Weld and Picton 1:25 000 scale map sheets. Tasmanian Geological Survey Record 2006/4.

Dalton Jr., R.O., 1972. Stratigraphy of the Bass Formation (Late Precambrian, Grand Canyon, Arizona) (M.S. thesis). Northern Arizona University, Flagstaff, p. 140.

Daneker, T.M., 1975. Sedimentology of the Precambrian Shinumo Sandstone, Grand Canyon, Arizona (M.S. thesis). Northern Arizona University, Flagstaff, p. 195.

Engel, M.H., Elmore, R.D., 1990. Assessments of the Hydrocarbon Generation Potential of Selected North American Proterozoic Rock Sequences. Progress Report for the U.S. Department of Energy.

Gee, R.D., 1967. The tectonic evolution of the Rocky Cape Geanticline. PhD Thesis [unpub.], University of Tasmania.

Heaman, L.M., Grotzinger, J.P., 1992. 1.08 Ga diabase sills in the Pahrump Group, California: Implications for development of the Cordilleran miogeocline. Geology 20, 637–640.

Hendricks, J.D., 1972. Younger Precambrian Basaltic Rocks of the Grand Canyon, Arizona (M.S. thesis). Northern Arizona University, Flagstaff, p. 122.

Larson, E.E., Patterson, P.E., Mutschler, F.E., 1994. Lithology, chemistry, age, and origin of the Proterozoic Cardenas Basalt, Grand Canyon, Arizona. Precambr. Res. 65 (1–4), 255–276.

Mahon, R.C., Dehler, C.M., Link, P.K., Karlstrom, K.E., Gehrels, G.E., 2014. Detrital zircon provenance and paleogeography of the Pahrump Group and overlying strata, Death Valley, California. Precambr. Res. 251, 102–117.

McConnell, R.L., 1975. Biostratigraphy and depositional environment of algal stromatolites from the Mescal Limestone (Proterozoic) of central Arizona. Precambr. Res. 2, 317–328.

Middleton, L.T., Blakey, R.C., 1998. Seismically induced liquefaction in late Proterozoic strata, northern and central Arizona; implications for tectonic setting and regional correlations: Geological Society of America Abstracts with Programs, 30(2), p. 399.

Middleton, L.T., Montgomery, M.W., 2001. Sedimentary responses to changing tectonic patterns, Mesoproterozoic Apache Group/Troy Quartzite, Central Arizona, in Rocky Mountain (53rd) and South-Central (35th) Sections, Geological Society of America, Joint Annual Meeting; April 29–May 2, 2001; Albuquerque, New Mexico, Session No. 11.

Pittenger, M.A., Marsaglia, K.M., Bickford, M.E., 1994. Depositional history of the Middle Proterozoic Castner Marble and basal Mundy Breccia, Franklin Mountains, west Texas. J. Sediment. Res. B64, 282–297.

Pray, L.C., 1961. Geology of the Sacramento Mountains Escarpment, Otero County, New Mexico: New Mexico Bureau of Mines and Mineral Resources, Bulletin 35, 144 p.

Reed, V.S., 1976. Stratigraphy and Depositional Environment of the upper Precambrian Hakatai Shale, Grand Canyon, Arizona (M.S. thesis). Northern Arizona University, Flagstaff, p. 163.

Roberts, M.T., 1982. Depositional environments and tectonic setting of the Crystal Spring Formation, Death Valley, California. In: Cooper, J.D., Troxel, B.W., Wright, L.A. (Eds.), Geology of Selected Areas in the San Bernardino Mountains, Western Mojave Desert, and Southern Great Basin, California: Volume and Guidebook for Field Trip no. 9, 78th Anniversary Meeting of Cordilleran Section. Geological Society of America. Death Valley Publishing Company, Shoshone, CA, pp. 165– 170.

Roths, P.J., 1993. Geochemical and geochronological studies of the Grenville-age (1,250–1,000 Ma) Allamoore and Hazel Formations, Hudspeth and Culberson counties, west Texas. In: Soegaard, K. et al. (Eds.), Precambrian Geology of the Franklin Mountains and Van Horn Area, Trans-Pecos Texas. Geological Society of America South Central Section, University of Texas, Dallas, Texas, pp. 11–35.

Seeley, J., 1999. Studies of the Proterozoic Tectonic Evolution of the Southwestern United States (Ph.D. thesis). University of Texas, El Paso, p. 321.

Seymour, D. B. compiler 2002. Marrawah West, Tasmania. Digital Geological Atlas 1:25000 Series Map Sheet. Mineral Resources Tasmania.
Shride, A.F., 1967. Younger Precambrian geology in southern Arizona. U.S. Geol. Surv. Prof. Pap. 566, 88.

Soegaard, K., Callahan, D.M., 1994. Late Middle Protero- zoic Hazel Formation near Van Horn, trans-Pecos Texas: evidence for transpressive deformation in Grenvillian basement. Geol. Soc. Am. Bull. 106, 413–423.

Spencer, C.J., Prave, A.R., Cawood, P.A., Roberts, N.M.W., 2014. Detrital zircon geochronology of the Grenville/Llano foreland and basal Sauk Sequence in west Texas, USA. Geol. Soc. Am. Bull. 126, 1117–1128.

Stevenson, G.M., Beus, S.S., 1982. Stratigraphy and depositional setting of the upper precambrian dox formation in grand-canyon. Geol. Soc. Am. Bull. 93, 163–173.

Timmons, J.M., Karlstrom, K.E., Heizler, M.T., Bowring, S.A., Gehrels, G.E., Crossey, L. J., 2005. Tectonic inferences from the ca. 1255–1100 Ma Unkar Group and Nankoweap Formation, Grand Canyon: intracratonic deformation and basin formation during protracted Grenville orogenesis. Geol. Soc. Am. Bull. 117, 1573–1595.

Tweto, O., 1983. Las Animas Formation (Upper Precambrian) in the Subsurface of Southeastern Colorado U.S. Geological Survey Bulletin 1529-G, p. 20.

Weil, A.B., Geissman, J.W., Heizler, M., Van der Voo, R., 2003. Paleomagnetism of Middle Proterozoic mafic intrusions and Upper Proterozoic (Nankoweap) red beds from the Lower Grand Canyon Supergroup, Arizona. Tectonophysics 375, 199–220.

Weiss, G.C., 1986. A depositional Analysis of the Arkose Member (middle Proterozoic) of the Troy Quartzite in Central Arizona (M.S. thesis). Northern Arizona University, Flagstaff, p. 382.

Wrucke, C.T., 1989. The middle Proterozoic Apache Group, Troy Quartzite, and associated diabase of Arizona: Arizona Geological Society Digest, 17, pp. 239– 258.

Chapter 5

Depositional age and correlation of the Oonah Formation: Refining the timing of late Neoproterozoic basin formation in Tasmania

Accepted, pending minor revision:
Australian Journal of Earth Science

Jacob A. Mulder[1], Ron F. Berry[1], Jacqueline A. Halpin[2], Sebastien Meffre[1], John L. Everard[3]

[1]ARC Centre of Excellence in Ore Deposits (CODES), School of Physical Sciences, University of Tasmania, Private Bag 79, TAS 7001, Australia

[2]Institute for Marine and Antarctic Studies, University of Tasmania, Hobart, Tasmania 7001, Australia

[3] Mineral Resources Tasmania, PO Box 56, Rosny Park, Tasmania 7018, Australia

5.0 Abstract

The Proterozoic Oonah Formation is a >5-km-thick sequence of turbidites with minor alkalic mafic rocks that are widely exposed throughout western and northern Tasmania. The regional significance of sedimentation and magmatism recorded in the Oonah Formation is poorly understood as contacts with other Proterozoic rocks in Tasmania are typically faulted and previous depositional age estimates range from *ca.* 1450 Ma to *ca.* 700 Ma. Here we refine the depositional age of the Oonah Formation and clarify its relationship to other Proterozoic sequences in Tasmania. Magmatic apatite from syn-sedimentary mafic intrusions (Cooee Dolerite) has a ^{207}Pb-corrected ^{238}U/^{206}Pb age of 733 ± 9 Ma and provides a robust estimate of the age of deposition of the Oonah Formation. Detrital zircons from the Oonah Formation include major age populations at 1800—1700 Ma, minor Mesoproterozoic age populations at 1590 Ma and 1450 Ma, and rare 3100—2000 Ma grains, all of which were likely recycled from Mesoproterozoic strata in western Tasmania. Detrital monazite age spectra from the Oonah Formation are dominated by *ca.* 750 Ma grains, which were likely sourced from Neoproterozoic granites on King Island. On the basis of lithological similarity and a shared detrital zircon provenance, the Oonah Formation is interpreted to be laterally equivalent to the base of the late Neoproterozoic—early Cambrian Togari Group and correlates in western Tasmania. These refinements to the late Neoproterozoic stratigraphy of Tasmania do not support previous correlations with the Adelaide Rift Complex of southeast Australia. Instead, late Neoproterozoic strata in Tasmania share similarities in age, lithology, and detrital zircon provenance to late Neoproterozoic strata in the Pahrump Group in Death Valley, California and the Cobham Formation in the central Transantarctic Mountains, which supports a late Neoproterozoic position for Tasmania between southwest Laurentia (Proterozoic North America) and East Antarctica within the supercontinent Rodinia.

5.1 Introduction

Proterozoic sedimentary rocks are widely exposed in western Tasmania and record a protracted history of basin formation and continental rifting spanning the middle Mesoproterozoic (1450 Ma) to latest Neoproterozoic (Figs. 5.1 and 5.2). The oldest Proterozoic strata are marginal marine siliciclastic sequences of the 1450—1300 Ma lower-middle Rocky Cape Group in northwest Tasmania and time-equivalent turbidite sequences exposed on King Island (Figs. 5.1 and 5.2; Black et al., 2004; Calver et al., 2010; 2014; Halpin et al., 2014). A second cycle of Mesoproterozoic sedimentation is preserved in the upper Rocky Cape Group (Black et al., 2004; Calver et al., 2014; Halpin et al., 2014), which was deposited after 1300 Ma (Fig. 5.2; Halpin et al., 2014; Mulder et al., 2015a). The Mesoproterozoic strata of Tasmania are overlain with low-angle unconformity by the (?)750 Ma to early Cambrian volcano-sedimentary Togari Group and correlates (Figs. 5.1 and 5.2; Calver, 1998; Meffre et al., 2004; Everard et al., 2007).

The Oonah Formation is an enigmatic Proterozoic sequence that is exposed in fault-bound inliers throughout western and northern Tasmania and comprises at least 5 km of turbidites and mafic volcanic rocks (Fig. 5.1; Gee, 1977; Brown, 1986; Black et al., 1997; Crawford & Berry, 1992; Calver et al., 2014). The relationship of the widespread episode of sedimentation and magmatism recorded in the Oonah Formation to other Proterozoic sequences in Tasmania is uncertain as contacts are either faulted or ambiguous (Brown, 1986; Calver et al., 2014) and existing radiometric dates are consistent with a wide range of depositional ages including middle Mesoproterozoic (<1450 Ma), latest Mesoproterozoic (<1070 Ma), or late Neoproterozoic (*ca.* 700 Ma).

In this study we refine the depositional age of the Oonah Formation through U-Pb dating of detrital zircon and detrital monazite from turbiditic sandstones and magmatic apatite from syn-sedimentary mafic intrusive rocks. The new data support a *ca.* 730 Ma depositional age for the Oonah Formation. On the basis of lithological similarity and shared detrital zircon provenance, the Oonah Formation is likely to be a lateral equivalent to the base of the Togari Group and correlates in western Tasmania. To refine Tasmania's position within the supercontinent Rodinia, we explore correlations between the late Neoproterozoic strata of Tasmania and late Neoproterozoic sequences in southeast Australia, East Antarctica, and southwest Laurentia (Proterozoic North America).

5.2 Regional geology

5.2.1 Proterozoic geology of western Tasmania

The Rocky Cape Group is the oldest basin system exposed in Tasmania and is a >10-km-thick sequence of quartz arenite and mudstone deposited on a tidally-dominated shelf (Fig. 5.1; Everard, 2005; Calver et al., 2010, 2014; Halpin et al., 2014). The Rocky Cape Group is divided into a lower-middle succession deposited between 1450 and 1300 Ma (Halpin et al., 2014) and an upper succession deposited after 1300 Ma (Halpin et al., 2014; Mulder et al., 2015a). Siliciclastic turbidities on King Island to the northwest of Tasmania (Fig. 5.1; Surprise Bay and Fraser Formations) are probable

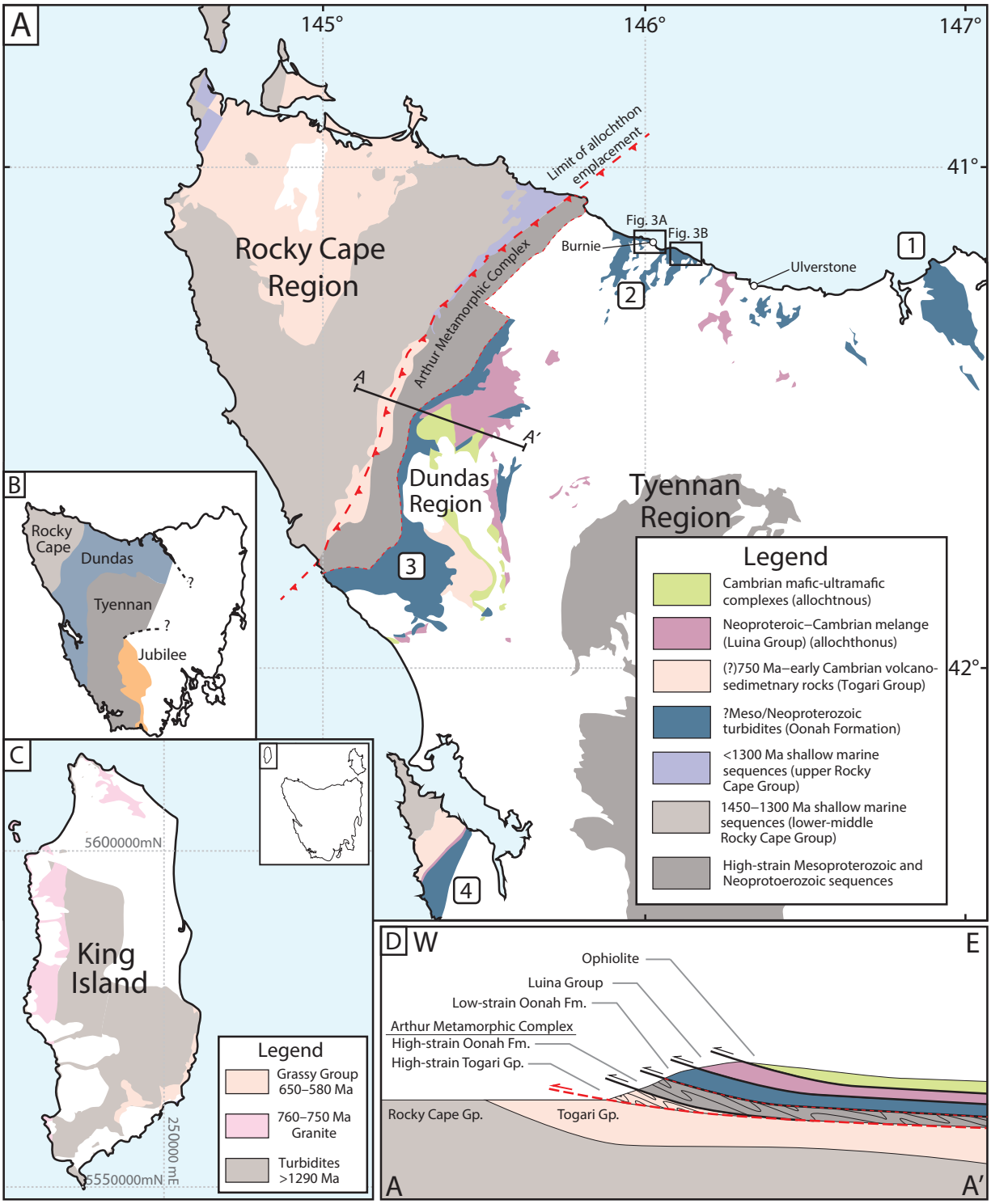

Figure 5.1: Pre-middle Cambrian geology of northwest Tasmania. (A) shows distribution of Proterozoic basin sequences and Neoproterozoic—Cambrian allochthonous sequences emplaced during the middle Cambrian Tyennan Orogeny. Inliers of the Oonah Formation are labeled: (1) Badger Head, (2) Burnie, (3) Western Tasmania, (4) Cape Sorell . Modified from Calver et al. (2014). (B) Tectonostratigraphic elements of Tasmania, modified from Seymour and Calver (1995). (C) Proterozoic Geology of King Island. Modified from Calver et al. (2014) (D) Simplified cross-section through western Tasmania showing interpreted structural architecture following the Tyennan Orogeny, modified from Holm and Berry (2002) and Berry (2014).

lateral equivalents of the lower-middle Rocky Cape Group (Black et al., 2004; Halpin et al., 2014) and record low-pressure greenschist—amphibole facies metamorphism and tight folding at 1287 ± 18 Ma (Berry et al., 2005; Calver & Everard, 2014).

Mesoproterozoic strata on King Island are intruded by A-type granite plutons including the 760 ± 12 Ma Cape Wickham Granite and 748 ± 2 Ma Loorana Granite (Cox, 1989; Black et al., 1997), and sills of quartz-feldspar porphyry dated at *ca.* 775 Ma (Calver et al., 2013a). A 777 ± 7 Ma granitoid lens in the allochthonous Bowry Formation of the Arthur Metamorphic Complex (Fig. 5.2; Black et al., 1997, Holm et al., 2003) and a 777 ± 7 Ma granite clast in late Neoproterozoic conglomerate of the Port Sorell Formation in northern Tasmania (Henson, 2002) may also be related to Neoproterozoic plutonism on King Island. Intrusion of granites on King Island at *ca.* 780—750 Ma and the development of a low angle unconformity above Mesoproterozoic strata in western Tasmania have been interpreted to be expressions of a regional orogenic event termed the Wickham Orogeny (Turner et al., 1998). The significance of the Wickham Orogeny is uncertain as deformation associated with this event on King Island is restricted to the contact aureoles of Neoproterozoic granites (Berry et al., 2005) and the low angle unconformity in western Tasmania may reflect fault-block rotation during extension associated with early stages of Neoproterozoic sedimentation (Everard et al., 2007).

Neoproterozoic sequences in Tasmania comprise predominantly shallow marine dolomitic and siliciclastic strata and mafic volcano-sedimentary sequences (Figs. 5.1 and 5.2). The Togari Group in the Rocky Cape Region of northwest Tasmania is the most completely preserved Neoproterozoic sequence in Tasmania and includes a locally developed basal conglomerate-quartz sandstone unit (Forest Conglomerate and Quartzite) conformably overlain by dolostone, black shale, chert, and diamictite of the Black River Dolomite (Everard et al., 2007). A latest Tonian (1000—800 Ma) to Cryogenian (720—635 Ma) age for the Black River Dolomite is supported by vase-shaped microfossils in the lower parts of the unit (Saito et al., 1998; Everard et al., 2007), which are interpreted to be a global *ca.* 740 Ma biostratigraphic marker (Strauss et al., 2014). The Black River Dolomite is overlain by a glacial diamictite (Julius River Member) correlated with the Sturtian Glaciation (Calver, 1998; Calver et al., 2004), and is in turn overlain by black shale with a 641 ± 5 Ma whole rock Re-Os age (Kendall et al., 2009). The Black River Dolomite is conformably overlain by shale, siltstone, diamictite and mafic volcanic rocks of the Kanunnah Subgroup (Fig. 5.2). Mafic rocks within the Kanunnah Subgroup (Spinks Creek Volcanics) and correlates elsewhere in Tasmania were emplaced at *ca.* 580 Ma (Calver et al., 2004; Meffre et al., 2004) and include voluminous rift-tholeiites and lesser alkali basalt and picrite (Brown, 1986; Holm et al., 2003; Meffre et al., 2004; Everard et al., 2007). The Kanunnah Subgroup is conformably overlain by shallow marine dolostone of the Ediacaran Smithton Dolomite (Calver, 1998) and the early Cambrian Salmon River Siltstone (Everard et al., 2007).

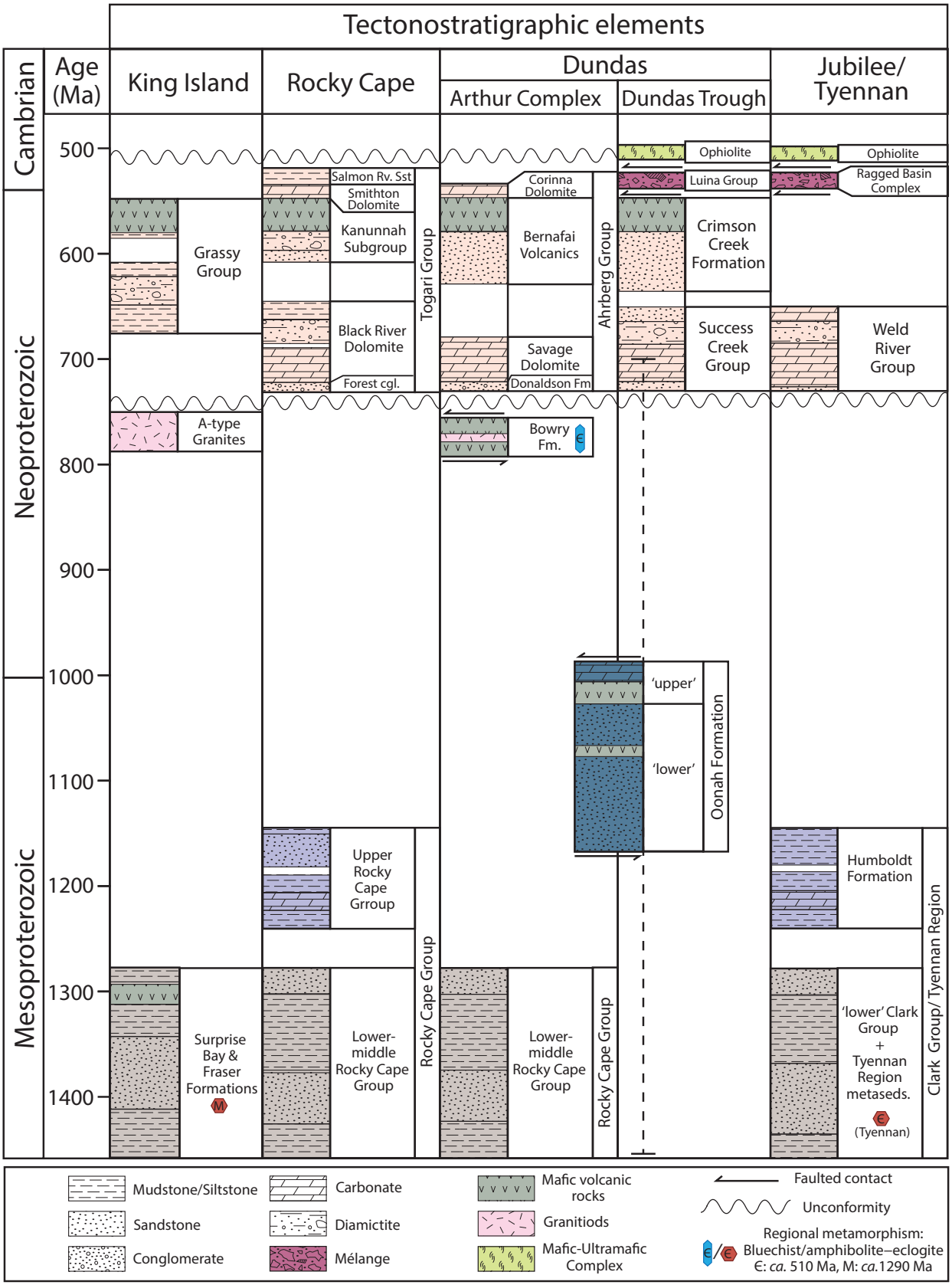

Figure 5.2: Time-space diagram from Mesoproterozoic—middle Cambrian geology of Tasmania. Modified from Calver et al. (2014). Location of tectonostratigraphic elements is shown in Figure 5.1.

5.2.2 Paleozoic tectonism

The Proterozoic crust of Tasmania experienced major deformation during the middle Cambrian Tyennan and Devonian Tabberabberan orogenies. The Tyennan Orogeny is interpreted to record the collision of Tasmania with an intraoceanic island arc and involved high-pressure metamorphism and polyphase deformation between 515 and 505 Ma (Berry & Crawford, 1988; Crawford & Berry, 1992; Turner et al., 1998; Meffre et al., 2000; Foster et al., 2005; Berry et al., 2007; Chmielowski & Berry, 2012; Mulder et al., 2015b). Allochthonous sequences including mélange units composed of deep marine mudstone, chert, and basalt (Luina Group) and a suprasubduction zone ophiolite were emplaced southward and westward over Tasmania during the Tyennan Orogeny with the westerly limit of major Cambrian deformation and metamorphism being defined by the eastern margin of the Rocky Cape Region (Figs. 5.1A and 5.1D; Berry, 1989; Turner & Bottrill, 2001; Holm & Berry, 2002; Mulder et al., 2016). The Devonian Tabberabberan Orogeny involved reactivation of Cambrian structures, regional-scale folding, and granite emplacement at *ca.* 400—351 Ma (Black et al., 2010; Seymour et al., 2014; Hong et al., 2017).

5.3 Geology of the Oonah Formation

5.3.1 Stratigraphy

Fault-bound sequences of Proterozoic turbidites on mainland Tasmania include the Oonah Formation in western Tasmania (Blissett, 1962; Spry, 1962; Brown, 1986) and lithologically similar sequences near Burnie (Fig. 5.3; Gee, 1977) and Badger Head (Gee & Legge, 1979) in northern Tasmania (Fig. 5.1). The following summary is based on the synthesis of Calver et al. (2014). Original names from some inliers such as Burnie Formation (Burnie inlier) and Badger Head Group (Badger Head inlier) have been superseded and we follow Calver et al. (2014) in referring to all of these fault-bound turbidite sequences as Oonah Formation.

The Oonah Formation is at least 3 km thick in western Tasmania and over 5 km thick in northern Tasmania and has a lower subdivision dominated by siliciclastic turbidites and an upper subdivision of pelite, carbonate, conglomerate, and mafic volcanic rocks. The Oonah Formation is generally of sub- or lower greenschist facies and experienced polyphase deformation during the Tyennan and Tabberabberan orogenies (e.g., Berry & Grey, 2001). The lower turbidite-rich subdivision includes texturally immature, fine-grained quartz sandstone, quartz siltstone, mudstone, and minor conglomerate (Blissett, 1962; Gee, 1977; Brown, 1986). Sedimentary structures are typical of deposition from turbidity flows and include Bouma sequences, scour marks, load structures, and cross bedding (Gee, 1977; Brown, 1986). The upper pelite-rich subdivision of the Oonah Formation comprises fine—coarse grained, cross-bedded quartz sandstone, black, green, and purple mudstone, beds and lenses of recrystallised dolomite, and thin layers of crystal and lithic tuff (Brown, 1986).

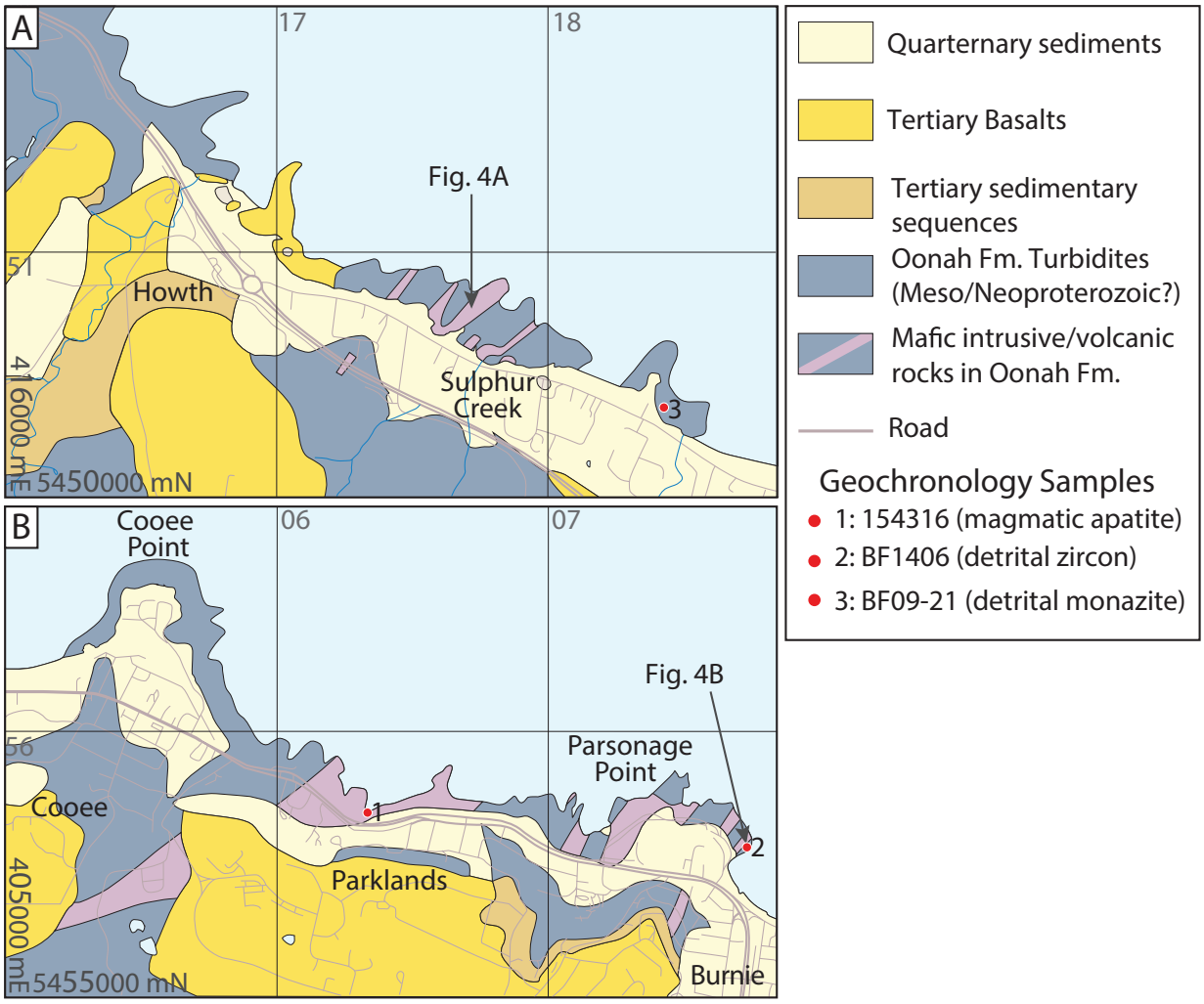

Figure 5.3: Geology of the Oonah Formation exposed along the north coast of Tasmania (Burnie inlier) showing distribution of siliciclastic turbidites and mafic igneous rocks at (A) Sulphur Creek and (B) Parsonage Point. Modified from Vicary (2004).

Mafic rocks in the lower subdivision of the Oonah Formation on the north coast of Tasmania include pillow basalts at Sulphur Creek (Figs. 5.3 and 5.4A) and sills of the nearby Cooee Dolerite (Fig. 5.3). The Cooee Dolerite locally contains amygdales and has peperitic contacts, which are consistent with shallow-level emplacement into unconsolidated sediments (Fig. 5.4B—D; Gee, 1977; Crook, 1979). The upper subdivision of the Oonah Formation includes a series of basaltic lava flows, pillow basalts, and mafic volcaniclastic rocks. Near Zeehan (western Tasmania) this association is called the Montana volcanics. The mafic rocks within the Oonah Formation are enriched in immobile trace elements such as Ti, Zr, Nb, P, and Y and have ratios of these elements that are typical of alkali basalts from within-plate tectonic settings (Fig. 5.5A; Appendix 5.1; Brown, 1986; Crawford & Berry, 1992; Black et al., 1997; Calver & Everard, 2014). The alkalic geochemistry of these mafic rocks is also reflected in their primary mineralogy, which includes titaniferous augite, kaersutitic amphibole, and abundant accessory apatite (Fig. 5.5B and 5.5C).

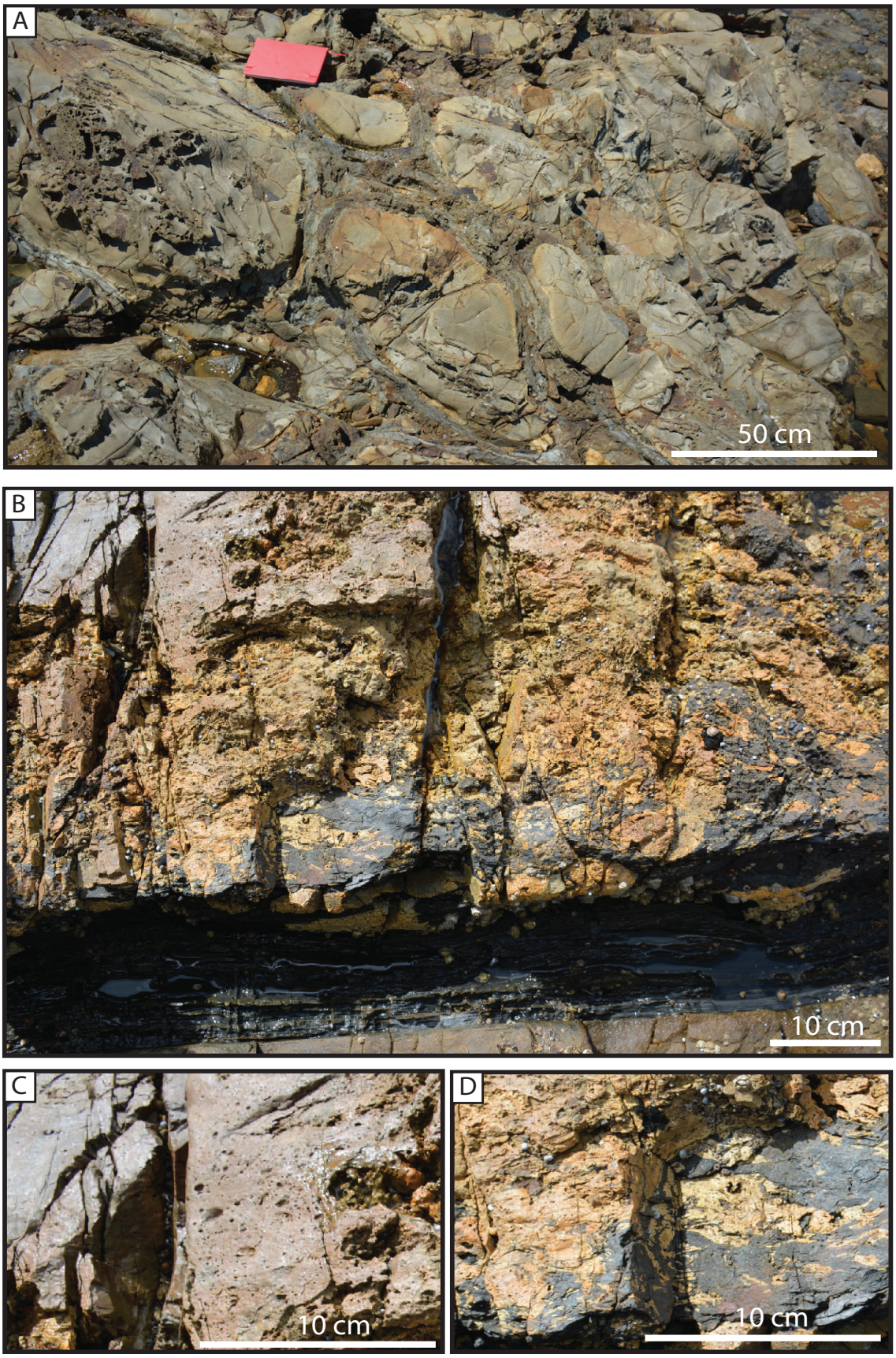

Figure 5.4: Field photographs of mafic rocks in the Oonah Formation in northern Tasmania. (A) Pillow basalts in the Oonah Formation at Sulphur Creek (B) Peperitic contact between the Cooee Dolerite and turbidites of the Oonah Formation at Parsonage Point. (C) Enlargement of Cooee Dolerite near (D) Enlargement of peperitic contact showing chaotic mixing of basalt (light) and mudstone (dark).

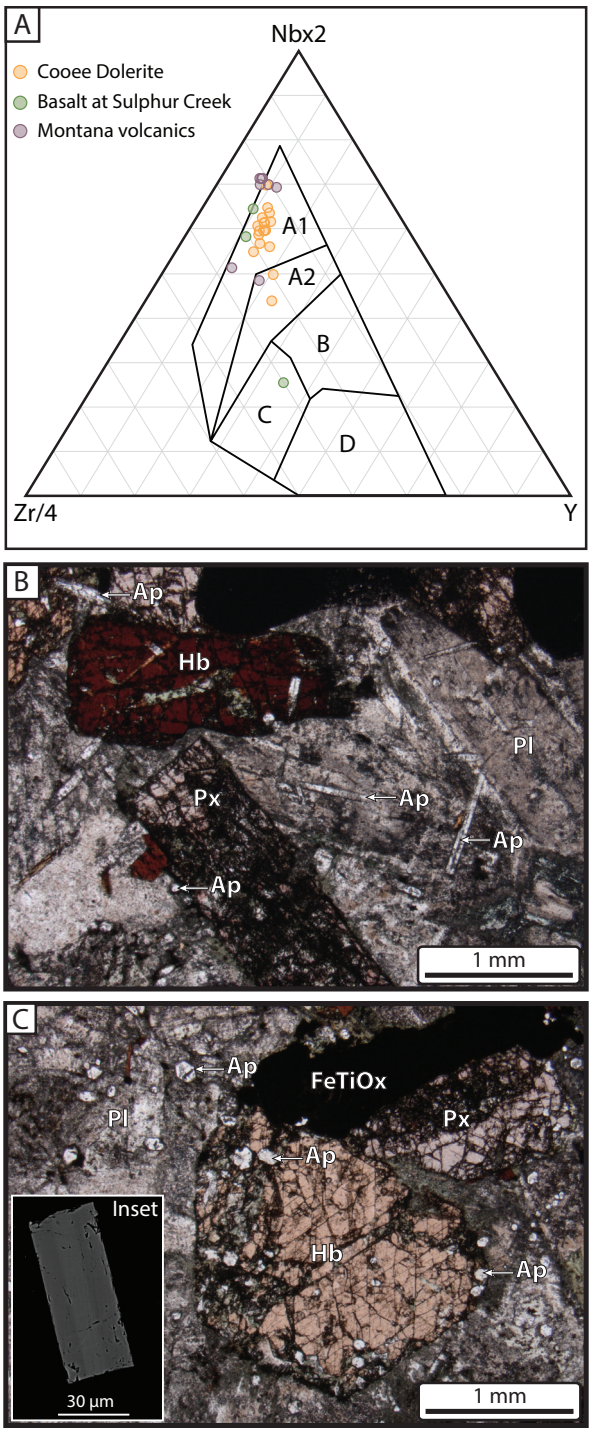

Figure 5.5: Geochemistry and petrography of mafic rocks in the Oonah Formation. (A) Zr-Nb-Y plot of Cooee Dolerite and related mafic igneous rocks in the Oonah Formation. Location of Cooee Dolerite and basalts at Sulphur Creek is shown in Figure 5.3. Montana volcanics include basaltic rocks exposed in inliers of the Oonah Formation in western Tasmania. A1: within-plate alkali basalts, A2: within-plate alkali basalts and within-plate tholeiites, B: E-MORB, C: within-plate tholeiites and volcanic arc basalts, D: N-MORB and volcanic arc basalts (Meschede, 1986). (B) Photomicrograph of Cooee Dolerite showing pale pink titaniferous augite (Tiau), dark brown kaersutitic amphibole (Hb), sericitised plagioclase (Pl), and abundant needles of apatite (Ap). (C) Photomicrograph of Cooee Dolerite including an iron-titanium oxide phase (FeTiOx) and abundant euhedral sections of apatite. Inset shows a BSE image of apatite with faint simple compositional zoning.

5.3.2 Previous age constraints and correlation

The maximum depositional age of the Oonah Formation has previously been estimated from detrital zircon studies from inliers in western Tasmania and Badger Head (Fig. 5.1). Two samples of the Oonah Formation in western Tasmania include detrital zircons with individual and often low precision ages as young as *ca.* 1000 Ma (Black et al., 2004; Cumming et al., 2016). A more conservative maximum depositional age for the Oonah Formation inliers in western Tasmania is taken from the next youngest populations at *ca.* 1450 Ma (Black et al., 2004). Unlike other exposures of the Oonah Formation, the detrital zircon age spectra from the Badger Head inlier includes a prominent age peak at *ca.* 1240 Ma (Black et al., 2004). A Neoproterozoic (*ca.* 700 Ma) depositional age for the Oonah Formation was inferred from K/Ar data, including a 690 ± 10 Ma whole rock age (Adams et al., 1985), a 708 ± 6 Ma detrital muscovite age (Turner et al., 1998), and a 711 ± 16 Ma magmatic biotite age from the Cooee Dolerite (McDougall & Leggo, 1965).

The relationship of the Oonah Formation to other Proterozoic sequences in Tasmania is uncertain as contacts are either faulted or ambiguous (Fig. 5.6). On the basis of lithological similarity, Turner et al. (1998) favoured correlation of the Oonah Formation with siliciclastic proximal turbidite deposits at the base of the Ahrberg Group— a correlate of the Togari Group exposed further to the south and in the Arthur Metamorphic Complex (Fig. 5.2). Alternatively, on the basis of similarities in composition and detrital zircon provenance, the Oonah Formation could be time-equivalent to the Mesoproterozoic Rocky Cape Group or be a younger sequence reworked from the Rocky Cape Group (Gee, 1977; Holm, 2003; Black et al., 2004). Correlating the Oonah Formation with the <1300 Ma upper Rocky Cape Group is favoured by the age of the youngest reported individual detrital zircon ages of *ca.* 1000 Ma (Black et al., 2004; Cumming et al., 2016). Alternatively, if a more conservative maximum depositional age for the Oonah Formation is taken from the detrital zircon populations at *ca.* 1450 Ma, the Oonah Formation could be correlative with the 1450—1300 Ma lower-middle Rocky Cape Group (Fig. 5.2). A *ca.* 1450 maximum depositional age for the Oonah Formation supports correlation with 1450—1290 Ma siliciclastic turbidites on King Island (*c.f.* Calver & Everard, 2014).

5.4 Methods

5.4.1 U-Pb apatite geochronology

Heavy minerals were separated from a 500 g sample of a coarse-grained, hornblende-bearing phase of the Cooee Dolerite using standard crushing, milling, and separation techniques. Apatite was identified from the heavy mineral separate using automated mineral identification software on a FEI Quanta 600 Scanning Electron Microscope (SEM) following the method outlined in Halpin et al. (2014). High-resolution back scattered electron (BSE) images of apatite were acquired on an Hitachi Field Emission-SEM to characterise chemical and textural zoning prior to analysis. Approximately 50 apatite grains were selected for U-Pb analysis via laser ablation-inductively coupled plasma mass spectrometry (LA-ICPMS) using an Agilent 7900 quadrupole ICPMS coupled to a 193 nm Coherent

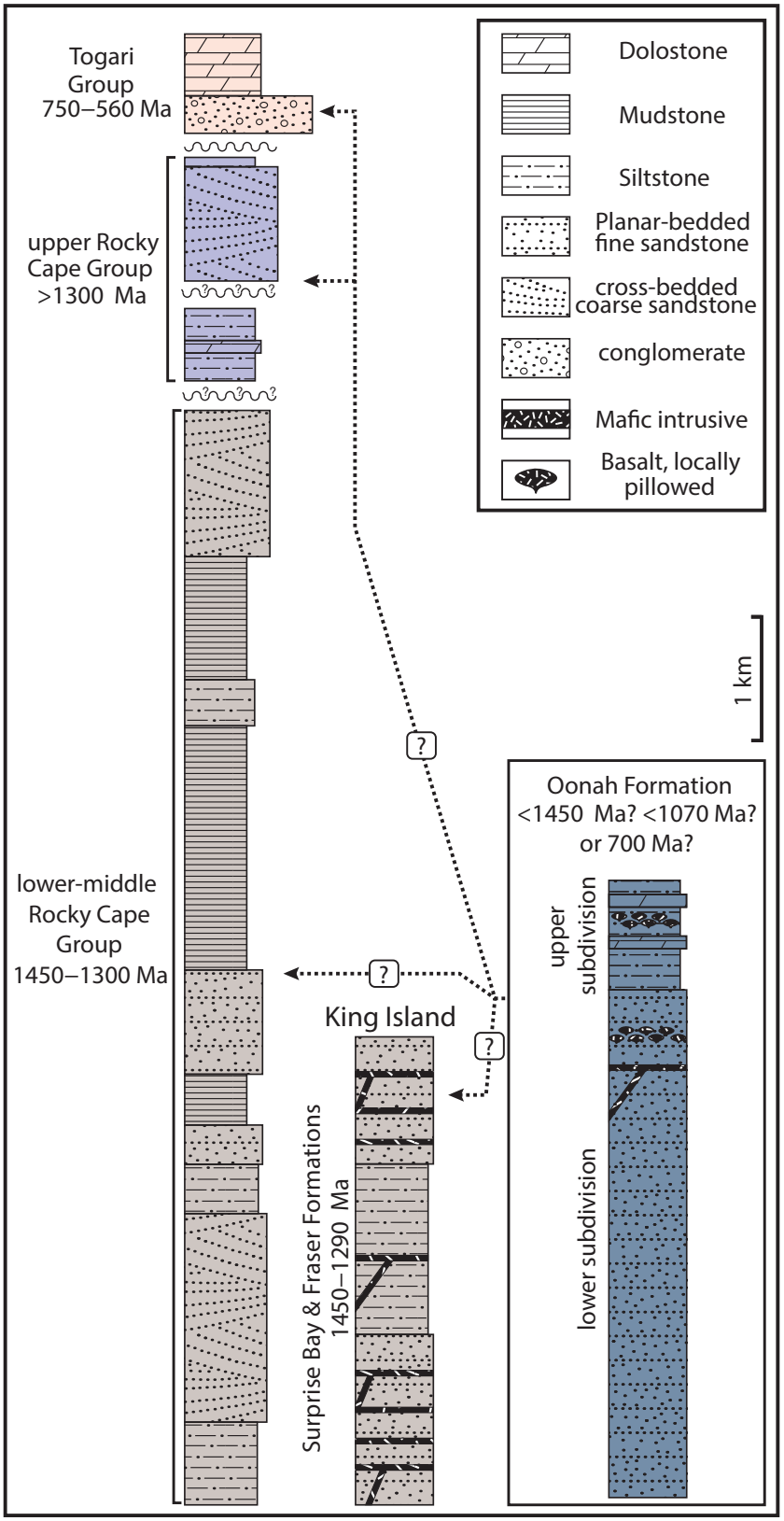

Figure 5.6: Summary of previous correlations proposed between the Oonah Formation and other Proterozoic sequences in western Tasmania and King Island. Stratigraphic columns modified from Halpin et al. (2014), Calver et al. (2014), and Calver & Everard (2014).

Ar-F excimer laser and a Resonetics S155 ablation cell at the University of Tasmania. Instrumental setup and analytical procedures follow Meffre et al. (2008) and Halpin et al. (2014). Downhole fractionation, instrument drift, and Pb/U mass bias correction factors were calculated using the primary standard OD306 (Thompson et al., 2016) and secondary standards McClure Mt. (Schoene & Bowring, 2006) and Otter Lake (Barford et al., 2005; Chew et al., 2011). NIST610 was used to calculate absolute Pb isotopic abundances using the values of Baker et al. (2004) and to correct for common Pb in the primary standard following the method of Chew et al. (2014). Full analytical results and sample locations are presented in Appendix 5.2 and 5.3 respectively.

5.4.2 Detrital zircon geochronology

Detrital zircons were separated from a medium-grained quartz sandstone from the margin of the Cooee Dolerite (Fig. 5.3) and a sample of the Forest Conglomerate and Quartzite (Fig. 5.2) using standard crushing, milling, and separation techniques. Cathodoluminescence images of detrital zircons were acquired on a FEI Quanta 600 SEM to characterise internal zoning and to guide placement of analysis spots. Approximately 200 zircon grains were randomly selected from each sample for analysis via LA-ICPMS following the same analytical procedures and instrument setup detailed in Meffre et al. (2008) and Halpin et al. (2014). Downhole fractionation, instrument drift, and mass bias were corrected using the primary standard 91500 (Wiedenbeck et al., 1995) and secondary standards TEMORA 1 (Black et al., 2003), GJ-1 (Jackson et al., 2004), Mudtank (Black & Gulson, 1978), and Plesŏvice (Sláma et al., 2008). Full analytical results are presented in Appendix 5.4.

5.4.3 Detrital monazite geochronology

Detrital monazites were separated from a medium-grained quartz sandstone near Sulphur Creek (Fig. 5.3) using standard crushing, milling, and separation techniques. U-Pb isotopes were measured via LA-ICPMS using the same instrumental and analytical procedures used for detrital zircon analysis. Placement of 29 μm analysis spots was guided by high-resolution BSE images to avoid inclusions, cracks, and overlapping of distinct chemical or textural zones. Downhole fractionation, instrument drift, and mass bias corrections were made using the primary standard 14971 Monazite (in-house standard) and secondary standards RGL4B (Rubatto et al., 2001) and Banaeira (Gonçalves et al., 2016). Full analytical results are presented in Appendix 5.5

5.5 Results

5.5.1 U-Pb apatite geochronology

Apatite in the Cooee Dolerite occurs as pristine, euhedral crystals, up to 1 mm long that are intergrown with magmatic phases including pyroxene, plagioclase, and hornblende (Figs. 5.5B and 5.5C). The apatite grains typically display faint simple zoning in BSE images (inset, Fig. 5.5C) and are interpreted to be a magmatic phase.

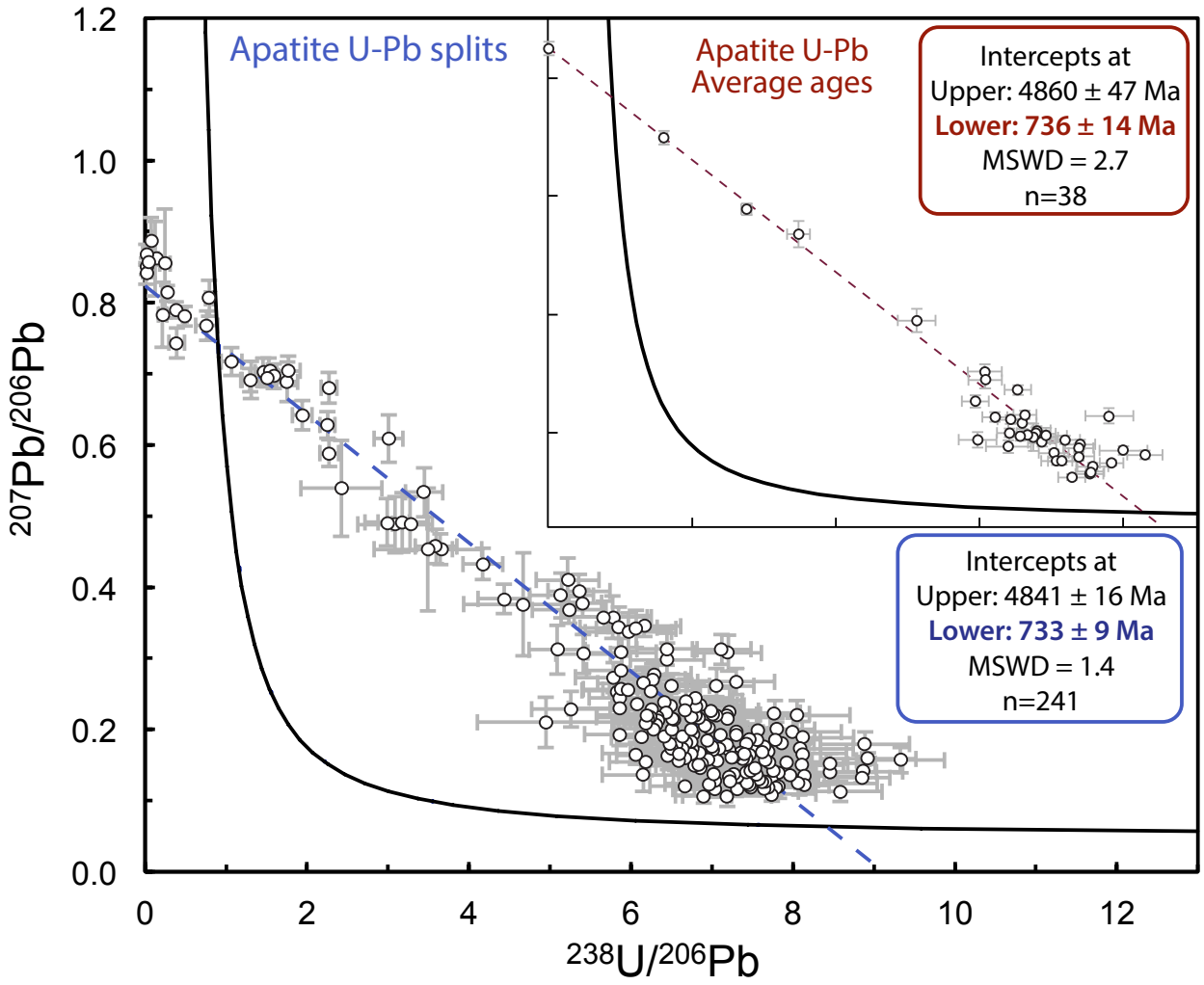

Figure 5.7: Terra-Wasserberg plots of U-Pb data from magmatic apatite from the Cooee Dolerite. Main diagram shows U-Pb composition of analyses split into 8 segments of equal time, inset shows average U-Pb composition for each analysis. Error bars are 1 sigma.

Apatite can incorporate significant amounts of common Pb in its crystal structure, which can result in the calculation of discordant U-Pb ages (e.g., Chew et al., 2011). Time-resolved analysis of U and Pb isotopes of apatite analysed during this study indicates that common Pb is heterogeneously distributed both within the ablation volume of individual analyses and throughout the population of grains analysed. To better visualise the full spectrum of mixing between common Pb and radiogenic Pb within the population of grains analysed, each analysis is split into 8 equal-time segments and shown on the Tera-Waserburg Plot in Figure 5.7. This approach has the benefit of increasing the dispersion of data points along the common Pb-radiogenic Pb mixing line, which improves the precision of the calculated age (e.g., Davidson et al., 2007; Kamenetsky et al., 2016). Data from 241 splits derived from 38 individual apatite grains show variable mixing of radiogenic and common Pb and define a discordia array with a lower intercept age of 733 ± 9 Ma (Fig. 5.7). Using the average $^{207}Pb/^{206}Pb$ and $^{238}U/^{206}Pb$ composition of analysis spots yields a similar intercept age of 736 ± 14 Ma that is also consistent with our interpretations (inset, Fig. 5.7).

5.5.2 Detrital zircon geochronology

A total of 175 detrital zircons from the Oonah Formation with analyses between 80% and 105% concordant are presented as a probability distribution diagram in Figure 5.8, which was constructed using Isoplot version 3.1 (Ludwig, 2003). For grains older than 1000 Ma the $^{207}Pb/^{206}Pb$ ages are plotted in Figure 5.8 whereas ^{207}Pb corrected $^{238}U/^{206}Pb$ ages are used for grains younger than 1000 Ma (*c.f.* Gehrels et al., 2008). The majority of detrital zircons analysed during this study have Paleoproterozoic ages (75% of total analyses) forming age peaks between 1800 and 1700 Ma. Archean detrital zircons include ages between 3100 and 2500 Ma and form a small age peak at 2990 Ma (3 grains). Mesoproterozoic ages comprise 16% of the new data set and form age peaks at 1590 Ma and 1435 Ma. The youngest detrital zircon has a moderately concordant (85%) age of 728 ± 10 Ma. Reanalysis of this grain in a separate analytical session produced a similar moderately concordant (89%) age of 723 ± 6 Ma. Combining the most concordant intervals of this grain from both analytical sessions produces a ^{207}Pb corrected $^{206}Pb/^{238}U$ age of 730 ± 8 Ma. Two additional Neoproterozoic detrital zircons analysed during this study have ages of 738 ± 11 Ma (94% concordant) and 767 ± 8 Ma (100% concordant) respectively.

New detrital zircon data from the Forest Conglomerate and Quartzite includes 183 analyses with ages between 80% and 105% concordant (Fig. 5.9). The detrital zircons from the Forest Conglomerate and Quartzite include abundant Paleoproterozoic grains with ages between 1800 and 1600 Ma (80% of total population), which form a prominent age peak at 1790 Ma. Archean ages comprise 6% of the total dataset and form a scatter of small age peaks between 2800 and 2500 Ma. Mesoproterozoic detrital zircons include 3 analyses at *ca.* 1550 Ma and a cluster of ages between 1490 and 1415 Ma (13% of total analyses). Neoproterozoic detrital zircons from the Forest Conglomerate and Quartzite include two grains with ages of 725 ± 7 Ma (98% concordant) and 729 ± 8 Ma (97% concordant) respectively.

5.5.3 Detrital monazite geochronology

Detrital monazites from the Oonah Formation are mostly rounded or subhedral grains between 20 and 100 μm that typically have homogenous or faint patchy zoning in BSE images. All 51 detrital monazite grains analysed fall within the concordance limits used in this study (80—105% concordant), with 70% of the analysed grains having ages between 95% and 105% concordant. The probability distribution plot of detrital monazite ^{207}Pb corrected $^{206}Pb/^{238}U$ ages is dominated by a large age peak at 750 Ma, which includes 49% of the total analyses (Fig. 5.9). The remainder of the detrital monazite dataset have mostly <1400 Ma ages (47% of total analyses) that form age peaks at 1270 Ma, 1220 Ma, 1170 Ma, and 1065 Ma (Fig. 5.9). Older grains include individual analyses at 1630 Ma and 1410 Ma.

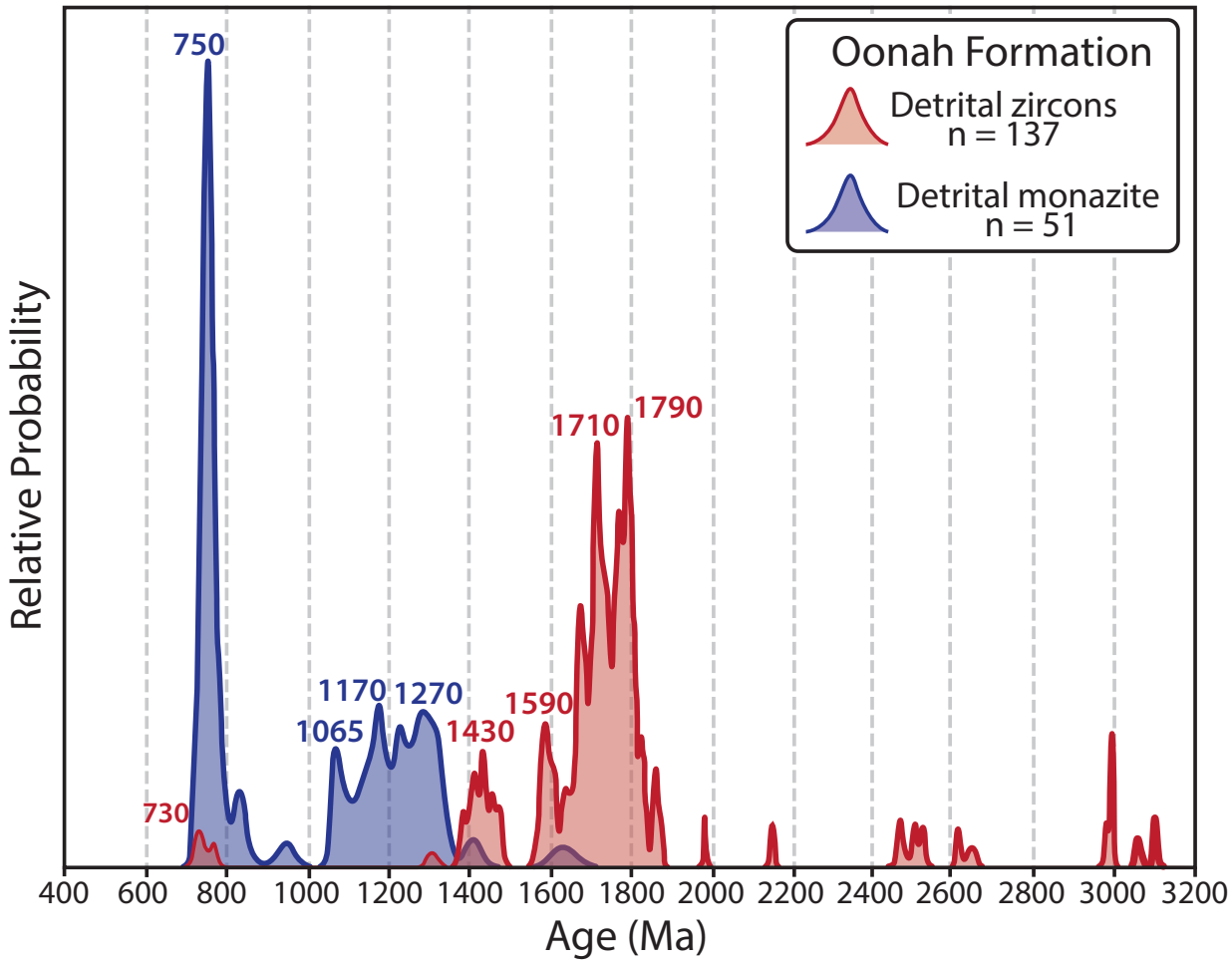

Figure 5.8: Probability distribution plots for detrital zircon and detrital monazite ages from the Oonah Formation. Detrital zircon probability distribution plot uses $^{207}Pb/^{206}Pb$ ages for grains >1000 Ma and ^{207}Pb-corrected $^{238}U/^{206}Pb$ for grains <1000 Ma. Detrital monazite probability distribution plot uses ^{207}Pb-corrected $^{238}U/^{206}Pb$ ages for all grains. All data are between 80% and 105 % concordant.

5.6 Discussion

5.6.1 Depositional age and provenance of the Oonah Formation

The field relationships of the Cooee Dolerite and related igneous rocks in northern Tasmania are interpreted to reflect mafic magmatism being contemporaneous with deposition of the Oonah Formation turbidites (Fig. 5.4; Gee, 1977; Crook, 1979). The *ca.* 730 Ma magmatic apatite age from the Cooee Dolerite is therefore considered a robust estimate of the depositional age of the Oonah Formation. The *ca.* 730 Ma emplacement age of the syn-sedimentary Cooee Dolerite is compatible with the maximum depositional age of the host sedimentary rocks inferred from the youngest detrital zircon and detrital monazite ages of 730 Ma and 750 Ma respectively (Fig. 5.8).

Detrital zircon data from the Oonah Formation is dominated by late Paleoproterozoic grains, with lesser Archean populations—early Paleoproterozoic and Mesoproterozoic (Fig. 5.8, see also Black et al., 2004; Cumming et al., 2016). The major detrital zircon age peaks in the Oonah Formation closely

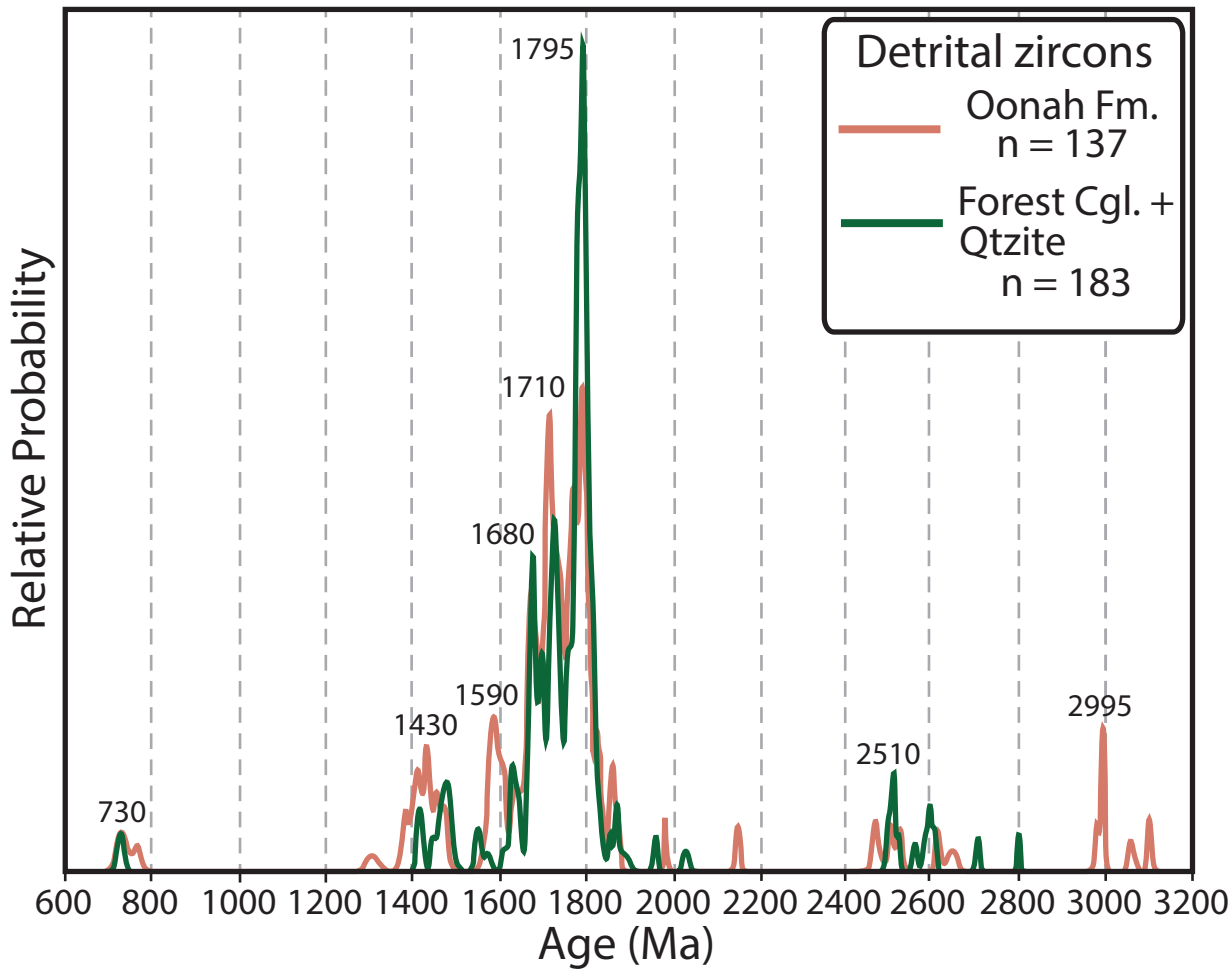

Figure 5.9: Comparison of detrital zircon age probability distribution plots from the Oonah Formation and Forest Conglomerate and Quartzite (data from this study only). Probability distribution plot uses $^{207}Pb/^{206}Pb$ ages for grains >1000 Ma and ^{207}Pb-corrected $^{238}U/^{206}Pb$ for grains <1000 Ma. All data are between 80% and 105 % concordant.

match major detrital zircon age populations of Mesoproterozoic sedimentary rocks in Tasmania such as the 1450—1300 Ma lower-middle Rocky Cape Group and 1450—1290 Ma turbidites on King Island (Black et al., 2004; Halpin et al., 2014, Mulder et al., 2015a). Although not recorded in the new detrital zircon dataset, *ca.* 1240—1070 Ma detrital zircons occur in exposures of the Oonah Formation in western Tasmania and at Badger Head (Black et al., 2004; Cumming et al., 2016). These late Mesoproterozoic detrital zircon ages overlap with *ca.* 1300—1100 Ma detrital zircon ages in the <1300 Ma upper Rocky Cape Group (Black et al., 2004; Halpin et al., 2014; Mulder et al., 2015a). We therefore suggest Archean—Mesoproterozoic detrital zircons in the Oonah Formation were recycled from Mesoproterozoic strata in western Tasmania. Neoproterozoic detrital zircons in the Oonah Formation analysed during this study include a single *ca.* 770 Ma grain that may have been derived from Neoproterozoic granites exposed on King Island (Figs. 5.1 and 5.2) and two *ca.* 730 Ma grains, which post-date the youngest Neoproterozoic granite on King Island at 748 Ma (Black et al., 1997). The *ca.* 730 Ma zircons may represent volcanic grains derived from felsic magmatism contemporaneous with emplacement of the Cooee Dolerite.

Detrital monazite from the Oonah Formation include abundant *ca.* 750 Ma grains, which may have been derived from Neoproterozoic granites on King Island. The 1270 Ma population of detrital monazite may also have a source on King Island where Berry et al. (2005) dated metamorphic monazite at 1287 ± 18 Ma in amphibolite facies turbidities of the Surprise Bay Formation (Figs. 5.1 and 5.2). The *ca.* 1250—1065 Ma detrital monazite populations may have been recycled from the upper Rocky Cape Group, which contains common detrital zircons of this age (Black et al., 2004; Halpin et al., 2014; Mulder et al., 2015a).

5.6.2 Correlation of the Oonah Formation and significance to the Neoproterozoic development of Tasmania

The refined Neoproterozoic depositional age and new provenance data provide a new opportunity to test previously proposed correlations between the Oonah Formation and other Proterozoic sequences in Tasmania. A Neoproterozoic age for the Oonah Formation does not support the interpretation that these turbidities are a deeper water lateral-equivalent of the Mesoproterozoic Rocky Cape Group (e.g., Holm & Berry, 2002). The revised depositional age of the Oonah Formation also precludes correlation with lithologically similar Mesoproterozoic turbidities exposed on King Island. Instead, the new data support the interpretation of Turner (1993), who correlated the Oonah Formation with proximal turbidite fan deposits in the Donaldson Formation in the Ahberg Group (Fig. 5.2). The Donaldson Formation is a correlate of the Forest Conglomerate and Quartzite, which forms the base of the (?)750 Ma to early Cambrian Togari Group in western Tasmania (Fig. 5.2). Correlation of the Oonah Formation and the Forest Conglomerate and Quartzite is also supported by their very similar detrital zircon provenance, which includes youngest age populations at *ca.* 730 Ma (Fig. 5.9).

The Oonah Formation and lower Togari Group mark the start of a widespread episode of sedimentation in Tasmania, which continued through to the early Cambrian. Deposition of the Oonah Formation and lower Togari Group closely followed *ca.* 780—750 Ma A-type granitic magmatism on King Island, which Holm et al. (2003) interpret to have occurred in a continental rift setting, possibly associated with the arrival of a mantle plume north of Tasmania (Li et al., 2003). Granitic magmatism on King Island is interpreted to be broadly coeval with development of a regional low-angle unconformity separating Mesoproterozoic sequences from the Togari Group and correlates throughout Tasmania (Fig. 5.2; Turner et al., 1998; Berry et al., 2005). Everard et al. (2007) suggest this unconformity may have formed during regional extension associated with the early stages of Togari Group deposition. Although originally interpreted to reflect the Whickham Orogeny (e.g., Turner et al., 1998), the emplacement of A-type granites on King Island, uplift of these granites during development of a regional unconformity, and their subsequent erosion into sedimentary basins such as the Oonah Formation and Togari Group are all likely expressions of continental rifting in western Tasmania (Li et al., 2003; Holm et al., 2003; Berry et al., 2005; Everard et al., 2007). We suggest this rifting event initiated with felsic magmatism on King Island (*ca.* 780 Ma) and continued during deposition of the lower Togari Group between *ca.* 730 Ma (Oonah Formation and Forest Conglomerate and Quartzite) and *ca.* 640 Ma (minimum age of the Black River Dolomite).

Basaltic rocks within the Oonah Formation have alkalic geochemistry typical of mafic magmatism during the early stages of continental rifting (Crawford & Berry, 1992). The alkalic geochemistry of basalts emplaced during incipient rifting reflects relatively minor lithospheric extension, which results in a low degree of mantle melting and significant contamination by a thick crustal column prior to eruption (e.g., McKenzie & Bickle 1988; Baldridge et al., 1991). Basin formation and low-volume alkalic basaltic volcanism in the Oonah Formation is interpreted to represent a phase of relatively minor lithospheric extension that did not lead to successful continental breakup. We therefore suggest that magmatism, extension, and basin formation at *ca.* 780—640 Ma in Tasmania represents a failed rifting event. A second phase of late Neoproterozoic magmatism in Tasmania is recorded by emplacement of voluminous rift-tholeiites at *ca.* 580 Ma in the upper Togari Group and correlative strata (Fig. 5.2), and is interpreted to represent a major rifting event that led to the successful separation of Tasmania from surrounding continents (e.g., Direen & Crawford, 2003).

5.6.3 Refining Tasmania's late Neoproterozoic position in Rodinia

The timing of late Neoproterozoic continental rifting recorded by the Oonah Formation-lower Togari Group overlaps with the early stages of the breakup of the supercontinent Rodinia (Li et al., 2008). Many paleogeographic reconstructions of Rodinia juxtapose the combined Australia-Antarctica landmass with the western margin of Laurentia, possibly with intervening smaller blocks such as South China (Fig. 5.10A; e.g., Dalziel, 1991; Moores, 1991; Karlstrom et al., 1999; Burrett & Berry, 2001; Goodge et al., 2008; Li et al., 2008). Although Tasmania probably occupied the broad rift zone between Australia-Antarctica and Laurentia during the breakup of Rodinia, its exact location in the Neoproterozoic remains uncertain.

Despite the uncertainty in the Neoproterozoic position of Tasmania, its late Neoproterozoic geology is generally interpreted in the context of the rifting history of the southeastern margin of Australia during the breakup of Rodinia (e.g., Calver, 1998; Calver and Walter, 2000; Holm et al., 2003; Direen & Crawford, 2003; Li et al., 2008; Cooper et al., 2011; Yonkee et al., 2014). These interpretations are based partly on correlation of the late Neoproterozoic geology of Tasmania with the Adelaide Rift Complex of southeast Australia (Figs. 5.10A and 5.10B). For example, Calver (1998) correlated the Black River Dolomite (lower Togari Group, Fig. 5.2) with the *ca.* 790 Ma Skillogalee Dolomite (middle Burra Group) in the Adelaide Rift Complex (Preiss, 2000; Preiss et al., 2009) on the basis of lithological similarities and similar δC^{13}_{Carb} values, which are mostly between +2 and +6 $^{0}/_{00}$ (Fig. 5.10B). The close lithological similarities of the Cryogenian Sturtian and Marinoan (Elatina) glacial deposits of the Adelaide Rift Complex and Tasmania (e.g., Calver et al., 2004, 2013b; Hoffman et al., 2009) led Calver and Walter (2000) to suggest lateral continuity of strata between southeast Australia and Tasmania.

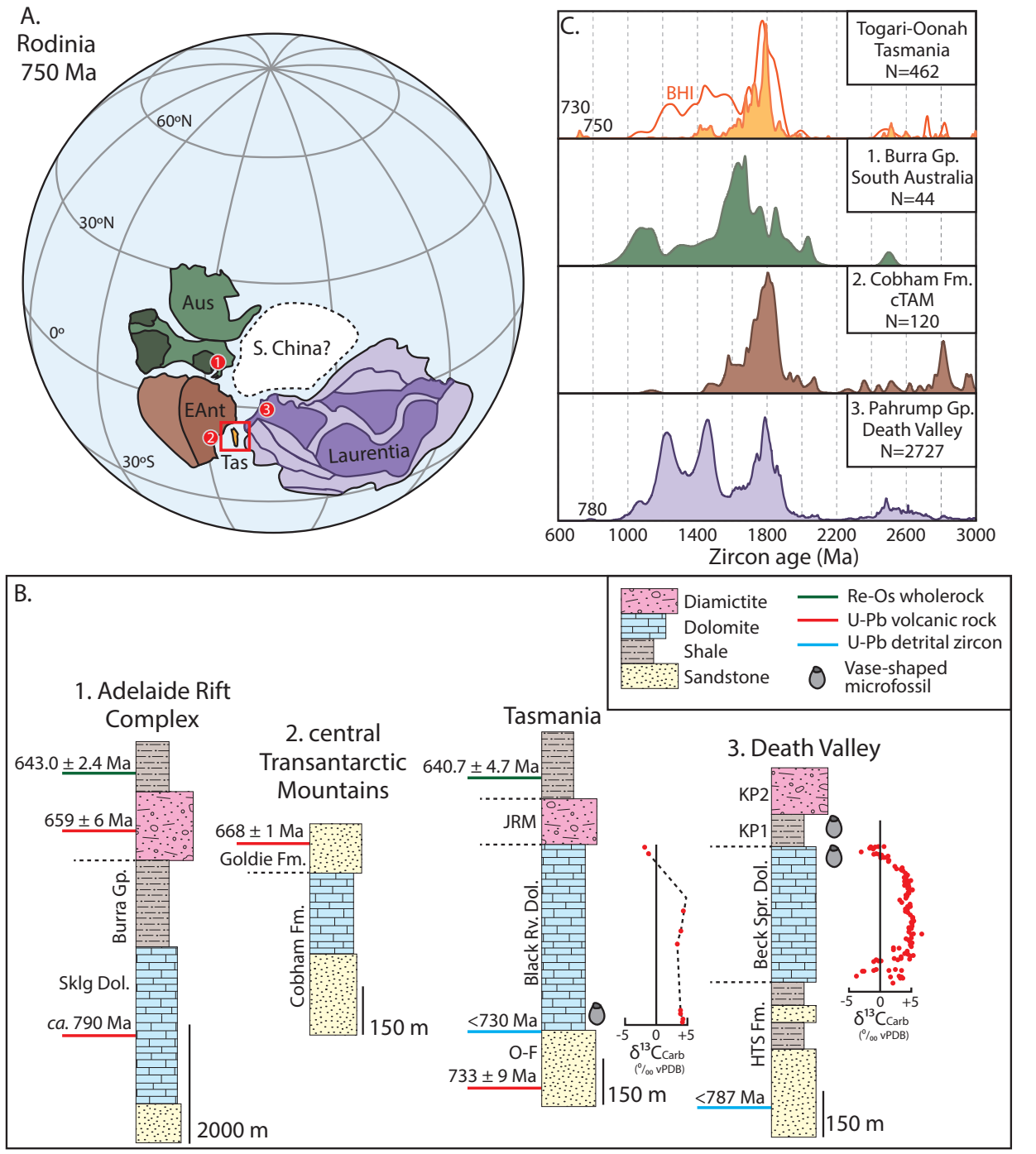

Figure 5.10: Comparison of late Neoproterozoic strata in Tasmania to nearby continents within Rodinia. A: Paleomagnetically-viable reconstruction of Rodinia at 750 Ma from Li and Evans (2011) with locations of (1) Adelaide Rift Complex, (2) Cobham Formation, and (3) Pahrump Group. Note that the position of Tasmania is not constrained by paleomagnetic data and follows e.g., Berry et al. (2008) and Moore et al. (2015). (B) Simplified stratigraphic logs of possible correlatives of Oonah Formation-Togari Group. Adelaide Rift Complex log and age constraints from Preiss et al. (2009) and Kendall et al. (2009), Sklg Dol. = Skillogalee Dolomite. Central Transantarctic Mountains log and age constraints from Laird et al. (1971) and Goodge et al. (2002). Tasmanian log and age constraints are from this study, Calver et al. (2014), and Kendall et al. (2009). The δC^{13}_{Carb} values of the Black River Dolomite are from Calver (1998), JRM = Julius River Member, O-F = Oonah Formation-Forest Conglomerate and Quartzite. Death Valley (Pahrump Group) log and age constraints from Mahon et al. (2014a,b) and Smith et al. (2015), δC^{13}_{Carb} values of Beck Spring Dolomite are from Smith et al. (2015), HTS = Horse Thief Spring Formation. (C) Detrital zircon data from possible correlatives of Oonah Formation-lower Togari Group. The Oonah Formation in the Badger Head inlier contains abundant *ca.* 1240 Ma detrital zircons and is plotted separately (BHI). Data are compiled from: Tasmania: this study, Black et al. (2004), Cumming et al. (2016), Adelaide Rift Complex: Ireland et al. (1998), Cobham Formation: Goodge et al. (2002, 2004), Pahrump Group: Mahon et al. (2014a) and Smith et al. (2015). cTAM= central Transantarctic Mountains.

Although there are some stratigraphic similarities between late Neoproterozoic Tasmania strata in Tasmania and the Adelaide Rift Complex, the revised *ca.* 730 Ma age for base of the Togari Group does not support correlation of the conformably overlying Black River Dolomite with the significantly older Skillogalee Dolomite in the Adelaide Rift Complex. Furthermore, detrital zircon age spectra from the Burra Group include abundant 1650—1500 Ma and 1200—1000 Ma detrital zircons, which are uncommon in the Oonah Formation-lower Togari Group and suggest these two sequences did not share a source region (Fig. 5.10C). Although Cryogenian glacial diamictites in Tasmania are lithologicaly similar to those in the Adelaide Rift Complex (Calver and Walter, 2000), given the possible global-extent of Cryogenian glaciations (Hoffman et al., 1998; Macdonald et al., 2010), the presence these glacial deposits in Tasmania and southeast Australia does not necessarily imply proximity of these areas in the Neoproterozoic. Calver and Walter (2000) argue that differences in the Ediacaran (635—541 Ma) evolution of Tasmania (mafic magmatism and shallow carbonate sedimentation) relative to the Adelaide Rift Complex (predominantly fine-grained siliciclastic sedimentation) indicate that Tasmania was not part of the southeastern margin of Australia at this time. In summary, we suggest that the differences in age, stratigraphy, and detrital zircon provenance of late Neoproterozoic strata in Tasmania and the Adelaide Rift Complex argue against group-scale correlation between these regions. These differences are consistent with the interpretation that Tasmania was not in its present-day position with respect to mainland Australia during the late Neoproterozoic.

A Proterozoic position for Tasmania further south along the margin of Australia-Antarctica was favoured by Berry et al. (2008), who suggest Tasmania was located adjacent to the Transantarctic Mountains of East Antarctic based on the similar Mesoproterozoic geology of these regions (see also Halpin et al., 2014; Moore et al., 2015; Mulder et al., 2015a). Neoproterozoic strata exposed along the length of the Transantarctic Mountains are interpreted to record formation of a rifted margin during the breakup of Rodinia (Goodge et al., 2002; 2004). The earliest stages of rift margin development in East Antarctica are recorded by the >668 Ma Cobham Formation in the central Transantarctic Mountains, which comprises a lower quartzite-rich succession and an upper marble-rich succession (Laird et al., 1971; Goodge et al., 2002, 2004). The association of lower siliciclastic-dominant strata overlain by carbonate-dominant strata exposed in the Cobham Formation is broadly similar to the stratigraphy of the Oonah Formation-lower Togari Group (Fig. 5.10B; Moore et al., 2015). Detrital zircons from the Cobham Formation include abundant 1850—1650 Ma ages and smaller distributions between 1500 and 1400 Ma, which is similar to the detrital zircon age distribution of the Oonah Formation and Forest Conglomerate and Quartzite (Fig. 5.10C), although the Cobham Formation lacks the minor 780—730 Ma and *ca.* 1250—1000 Ma zircons observed in Tasmanian sequences (Fig. 5.10B). Together the similarities in age, stratigraphy, and detrital zircon provenance of the Cobham Formation and the Oonah Formation-lower Togari Group are consistent with these sequences being broadly correlative, which supports a late Neoproterozoic position for Tasmania adjacent to the central Transantarctic Mountains.

In the paleomagnetically-viable reconstruction of Rodinia shown in Figure 5.10A (Li & Evans, 2011), the southwest margin of Laurentia is placed adjacent to the Transantarctic Mountains and the inferred position of Tasmania at *ca.* 750 Ma (*c.f.* Goodge et al., 2008). Late Neoproterozoic strata are also exposed along the southwest margin of Laurentia in the Pahrump Group of Death Valley, California (Mahon et al., 2014a,b; Smith et al., 2015). Late Neoproterozoic strata in the Pahrump Group include the predominantly siliciclastic Horse Thief Springs Formation, the Beck Spring Dolomite, and the diamictite-bearing Kingston Peak Formation (Mahon et al., 2014a; Smith et al., 2015). The Beck Spring Dolomite is a shallow marine dolostone-rich unit deposited between *ca.* 787 Ma and 717 Ma (Fig. 5.10B; Mahon et al., 2014b; Smith et al., 2015) and is similar in lithology and age to the *ca.* 730—640 Ma Black River Dolomite in the lower Togari Group of Tasmania. Vase-shaped microfossils in both the Beck Spring Dolomite and Black River Dolomite also suggest these sequences are time-equivalent. The δC^{13}_{Carb} chemostratigraphy of the Beck Spring Dolomite and Black River Dolomite are both characterised by relative uniform δC^{13}_{Carb} values of +3 to +5 in the lower and middle parts of these units followed by a shift to negative values below their overlying diamictite intervals (Fig. 5.10B; Calver, 1998; Smith et al., 2015). Detrital zircon ages from the Pahrump Group include prominent populations at *ca.* 1800 Ma, *ca.* 1450 Ma, and *ca.* 1250 Ma, and include youngest grains at ca. 780 Ma (Fig. 5.10B). This detrital zircon age distribution is similar to that observed in the Oonah Formation-lower Togari Group, although *ca.* 1250 Ma zircons in the Oonah Formation are only common in the Badger Head inlier (Fig. 5.10B). On the basis of similarities in age, lithostratigraphy, chemostratigraphy, and detrital zircon provenance, we suggest the Horse Thief Spring Formation, Beck Spring Dolomite, and lower parts of the Kingston Peak Formation are correlative with the Oonah Formation-lower Togari Group in Tasmania. This correlation and the similarities between late Neoproterozoic strata in Tasmania and the central Transantarctic Mountains, supports a late Neoproterozoic position for Tasmania between southwest Laurentia and East Antarctica.

5.7 Conclusions

New U-Pb dates from apatite in syn-sedimentary mafic sills in the Oonah Formation indicate that this thick sequence of turbidites and mafic volcanic rocks was deposited at *ca.* 730 Ma. Maximum depositional ages inferred from detrital zircon (730 Ma) and detrital monazite (750 Ma) also support a late Neoproterozoic age for the Oonah Formation. Detrital zircon and monazite data are consistent with the Oonah Formation being derived from recycling of Mesoproterozoic sedimentary sequences in western Tasmania and from Neoproterozoic granites on King Island. On the basis of similar ages and detrital zircon provenance, the Oonah Formation is interpreted to a lateral-equivalent of the Forest Conglomerate and Quartzite, which forms the base of the Togari Group in western Tasmania. Alkalic mafic volcanic rocks within the Oonah Formation record the initial stages of late Neoproterozoic basin formation in Tasmania, leading to the deposition of the Oonah Formation and lower Togari Group, but were associated with relatively minor lithospheric extension. The revised depositional age of late Neoproterozoic strata in Tasmania does not support previous correlation with the Adelaide Rift Complex, implying that Tasmania was not a part of southeast Australia at this time. Accordingly, the record of late Neoproterozoic rifting in Tasmania should not be considered

as representative of the rifting history of southeastern Australia during the breakup of Rodinia. Instead, the age, stratigraphy, and detrital zircon provenance of the Oonah Formation-lower Togari Group are similar to the Pahrump Group in Death Valley and the Cobham Formation of the central Transantarctic Mountains, which supports a late Neoproterozoic position for Tasmania between southwest Laurentia and East Antarctica

5.8 Acknowledgements

We thank Grace Cumming for assistance in the field and Karsten Goemann, Sandrin Feig, and Jay Thompson for analytical assistance. ARC Centre of Excellence in Ore Deposits (CODES) provided funding for this research. We thank Clive Calver and Solomon Buckman for reviews and Anita Andrew for editorial handling. This is a contribution to IGCP Project 648.

5.9 References

Adams, C. J., Black L. P., Corbett K. D., and Green G. R. (1985). Reconnaissance isotopic studies bearing on the tectonothermal history of Early Palaeozoic and Late Proterozoic sequences in western Tasmania. Australian Journal of Earth Sciences, 32, 7–36.

Baker, J., Peate, D., Waight, T., and Meyzen, C. (2004). Pb isotopic analysis of standards and samples using a Pb-207–Pb-204 double spike and thallium to correct for mass bias with a double-focusing MC-ICP-MS. Chemical Geology, 211, 275–303.

Baldridge, W. S., Perry, F. V., Vaniman, D. T., Nealey, L. D., Leavy, B. D., Laughlin, A. W., Kyle, P., Bartov, Y., Steinitz, G., Gladney, E. S. (1991). Middle to late Cenozoic magmatism of the southeastern Colorado Plateau and central Rio Grande rift (New Mexico and Arizona, USA): a model for continental rifting. Tectonophysics, 197, 327–354.

Barfod, G. H., Krogstad, E. J., Frei, R., and Albarède, F. (2005). Lu-Hf and PbSL geochronology of apatites from Proterozoic terranes: A first look at Lu-Hf isotopic closure in metamorphic apatite: Geochimica Et Cosmochimica Acta, 69, 1847–1859.

Berry, R.F. (1989). Microstructural evidence for a westward transport direction during Middle Cambrian obduction in Tasmania. Geological Society of Australia Abstracts.

Berry, R.F. (2014). Cambrian tectonics. In: Corbett, K.D., Quilty, P.G., Calver, C.R. (Eds.). Geological Evolution of Tasmania Geological Society of Australia Special Publication 24. Geological Society of Australia (Tasmania Division).

Berry R. F., and Crawford, A. J. (1988). The tectonic significance of Cambrian allochthonous mafic-ultramafic complexes in Tasmania. Australian Journal of Earth Sciences, 35, 523–533.

Berry R. F., and Gray D. R. (2001). The structure of the coastal section from Goat Island to Ulverstone, northwestern Tasmania (Field guide Vol. 10). Geological Society of Australia Specialist Group in Tectonics and Structural Geology Field Guide 10, Centre for Ore Deposit Research and School of Earth Sciences, University of Tasmania, and Mineral Resources Tasmania.

Berry, R.F., Holm, O.H., and Steele, D. A. (2005). Chemical U-Th-Pb monazite dating and the Proterozoic history of King Island, southeast Australia. Australian Journal of Earth Sciences, 52, 461–471.

Berry R. F., Chmielowski, R. M., Steele D. A., and Meffre, S. (2007). Chemical U-Th-Pb monazite dating of the Cambrian Tyennan Orogeny, Tasmania. Australian Journal of Earth Sciences, 54, 757–771.

Berry, R. F., Steele, D. A., and Meffre, S. (2008). Proterozoic metamorphism in Tasmania: implications for tectonic reconstructions. Precambrian Research, 166, 387–396.

Black, L.P., and Gulson, B. L. (1978). The age of the Mud Tank carbonatite, Strangways Range, Northern Territory. BMR Journal of Australian Geology & Geophysics 3, 227–232.

Black, L. P., Seymour, D. B., Corbett, K. D., Cox, S. E., Streit, J. E., Bottrill, R. S., Calver, C. R., Everard, J. L., Green, G. R., McClenaghan, M. P., Pemberton, J., Taheri, J., and Turner, N. J. (1997). Dating Tasmania's oldest geological events. Australian Geological Survey Organisation Record 1997/15.

Black, L. P., Kamo, S. L., Allen, C. M., Aleinikoff, J. N., Davis, D. W., Korsch, R. J., and Foudoulis, C. (2003). TEMORA 1: a new zircon standard for Phanerozoic U–Pb geochronology. Chemical Geology, 200, 155–170.

Black, L. P., Calver, C. R., Seymour, D. B., and Reed, A. (2004). SHRIMP U-Pb detrital zircon ages from Proterozoic and Early Palaeozoic sandstones and their bearing on the early geological evolution of Tasmania. Australian Journal of Earth Sciences, 51, 885–900.

Black L. P., Everard J. L., McClenaghan, M. P., Korsch, R. J., Calver, C. R., Fioretti, A. M., Brown, A. V., and Foudoulis, C. (2010). Controls on Devonian-Carboniferous magmatism in Tasmania, based on inherited zircon age patterns, Sr, Nd and Pb isotopes, and major and trace element geochemistry. Australian Journal of Earth Sciences, 57, 933–968.

Blissett, A. H. (1962). Geological Atlas 1 Mile Series, Zeehan. Tasmania Geological Survey Tasmania.

Brown, A. V. (1986). Geology of the Dundas-Mt. Lindsay-Mt. Youngbuck region. Geological Survey of Tasmania Bulletin, 62, 221p.

Burrett, C., and Berry, R.(2000). Proterozoic Australia–Western United States (AUSWUS) fit between Laurentia and Australia. Geology, 28, 103–106.

Calver, C. R. (1998). Isotope stratigraphy of the Neoproterozoic Togari Group, Tasmania. Australian Journal of Earth Sciences, 45, 865–874.

Calver, C.R., and Walter, M.R. (2000). The late Neoproterozoic Grassy Group of King Island, Tasmania: correlation and palaeogeographic significance. Precambrian Research, 100, 299–312.

Calver, C. R., and Everard, J. L. (2014). The Surprise Bay Formation (~1300 Ma) and related rocks of western King Island. Tasmanian Geological Survey Record 2014/01.

Calver, C. R., Black, L. P., Everard, J. L., and Seymour, D. B. (2004). U-Pb zircon age constraints on late Neoproterozoic glaciation in Tasmania. Geology, 32, 893–896.

Calver, C. R., Grey, K., and Laan, M. (2010). The 'string of beads' fossil (Horodyskia) in the mid-Proterozoic of Tasmania. Precambrian Research, 180, 18–25.

Calver, C. R., Meffre, S., and Everard, J. L. (2013a). Felsic porphyry sills in Surprise Bay Formation near Currie, King Island, dated at ~775 Ma (LA-ICPMS, U-Pb on zircon). Tasmanian Geological Survey Record, 2013/04.

Calver C. R., Crowley J. L., Wingate M. T. D., Evans, D. A. D., Raub T. D. and Sschmitz M. D. (2013b). Globally synchronous Marinoan deglaciation indicated by U_Pb geochronology of the Cottons Breccia, Tasmania, Australia. Geology, 41, 1127–1130.

Calver, C. R., Everard, J. L., Berry, R. F., Bottrill, R. S., and Seymour, D. B. (2014). Proterozoic Tasmania. In: Corbett, K. D., Quilty, P. G., Calver, C. R. (Eds.). Geological Evolution of Tasmania. Geological Society of Australia, Special Publication 24. Geological Society of Australia (Tasmania Division), pp. 34–94.

Chew, D. M., Sylvester, P. J., and Tubrett, M. N. (2011). U-Pb and Th-Pb dating of apatite by LA-ICPMS: Chemical Geology, 280, 200–216.

Chew, D.M., Petrus, J.A., and Kamber, B.S. (2014). U–Pb LA-MC-ICP-MS dating using accessory mineral standards with variable common Pb. Chemical Geology, 363, 185–199.

Chmielowski, R. M., and Berry, R. F. (2012). The Cambrian metamorphic his- tory of Tasmania: The metapelites. Australian Journal of Earth Sciences, 59, 1007–1019.

Cooper A. F., Maas R., Scott J. M. and Barber A. J. W. (2011). Dating of volcanism and sedimentation in the Skelton Group, Transantarctic Mountains: implications for the Rodinia-Gondwana transition in southern Victoria Land, Antarctica. Geological Society of America Bulletin, 123, 681–702.

Cox, S. F. (1989). Cape Wickham. In: Burrett, C. F., and Martin, E. L. (Eds.). Geology and Mineral Resources of Tasmania. Geological Society of Australia Special Publication, 15, 154–181.

Crawford, A. J., and Berry, R. F. (1992). Tectonic implications of Late Proterozoic-Early Palaeozoic igneous rock associations in western Tasmania. Tectonophysics, 214, 37–56.

Crook, K. A. W. (1979). Tectonic implications of some field relations of the Adelaidean Cooee Dolerite Tasmania. Australian Journal of Earth Sciences, 26, 353–361.

Cumming, G., Everard, J. L., and Meffre, S. (2016). Age constraints and provenance of the Mount Bischoff inlier and the Luina Group: evidence from LA-ICPMS U-Pb dating of detrital zircon. Tasmanian Geological Survey Record UR2016/04.

Dalziel, I. W. D. (1991). Pacific margins of Laurentia and East Antarctica–Australia as a conjugate rift pair: evidence and implications for an Eocambrian supercontinent. Geology, 19, 598–601.

Davidson, G.J., Paterson, H., Meffre, S., and Berry, R.F. (2007). Characteristics and origin of the oak dam East Breccia-hosted, iron oxide Cu-U-(Au) deposit: Olympic Dam region, Gawler Craton, South Australia. Economic Geology, 102, 1471–1498.

Everard, J. L. (2005). Reconnaissance geology of the Norfolk Range-Sandy Cape area, northwest Tasmania. Tasmanian Geological Survey Record 2005/02. Mineral Resources Tasmania, 82p.

Everard, J. L., Seymour, D. B., Reed, A. R., McClenaghan, M. P., Green, D. C., Calver, C. R., and Brown, A. V. (2007). Regional Geology of the southern Smithton Synclinorium: Explanatory Report for the Roger, Sumac and Dempster 1:25,000 map sheets, far northwestern Tasmania. 1:25,000 Scale Digital Geological Map Series Explanatory Report 2. Mineral Resources Tasmania, Hobart, 237p.

Foster, D. A., Gray, D. R., and Spaggiari, C. (2005). Timing of subduction and exhumation along the Cambrian East Gondwana margin, and the formation of Paleozoic backarc basins. Geological Society of America Bulletin, 117, 105–116.
Gee, R. D. (1977). Geological Atlas 1 Mile Series Explanatory Report, Burnie. Tasmania Geological Survey Tasmania.

Gee R. D., and Legge P. J. (1979). Geological Atlas 1:63 360 Series, Sheet 30 (8215N) Beaconsfield. Map and Explanatory Notes (2nd edition). Tasmania Department of Mines, Hobart.

Gehrels, G. E., Valencia, V. A., and Ruiz, J. (2008). Enhanced precision, accuracy, efficiency, and spatial resolution of U-Pb ages by laser ablation-multicollector-inductively coupled plasma mass spectrometry. In: Geochemistry Geophysics Geosystsystems, 9.

Gonçalves, G.O., Lana, C., Scholz, R., Buick, I.S., Gerdes, A., Kamo, S.L., Corfu, F., Marinho, M.M., Chaves, A.O., Valeriano, C., and Nalini Jr., H.A. (2016). An assessment of monazite from the Itambé pegmatite district for use as U–Pb isotope reference material for microanalysis and implications for the origin of the "Moacyr" monazite. Chemical Geology, 424, 30–50.

Goodge, J. W., Myrow, P., Williams, I. S., and Bowring, S., 2002, Age and provenance of the Beardmore Group, Antarctica: Constraints on Rodinia supercontinent breakup: Journal of Geology, 110, 393–406.

Goodge, J. W., Williams, I. S., and Myrow, P. (2004). Provenance of Neoproterozoic and lower Paleozoic siliciclastic rocks of the central Ross orogen, Antarctica: Detrital record of rift-, passive-, and active-margin sedimentation. Geological Society of America Bulletin, 116, 1253–1279.

Goodge, J. W., Vervoort, J. D., Fanning, C. M., Brecke, D. M., Farmer, G. L., Williams, I. S., Myrow, P. M., and DePaolo, D. J. (2008). A positive test of East Antarctica–Laurentia juxtaposition within the Rodinia supercontinent: Science, 321, 235–240.

Halpin, J. A., Jensen, T., McGoldrick, P., Meffre, S., Berry, R. F., Everard, J. L., Calver, C. R., Thompson, J., Goemann, K., and Whittaker, J. M. (2014). Authigenic monazite and detrital zircon dating from the Proterozoic Rocky Cape Group, Tasmania: Links to the Belt-Purcell Supergroup, North America. Precambrian Research, 250, 50–67.
Henson, P. (2002). Geology of the Port Sorell Formation. BSc Honours thesis (unpubl.). University of Tasmania.

Hoffman, P. F., Kaufman, A. J., Halverson, G. P., and Schrag, D. P. (1998). A Neoproterozoic snowball Earth: Science, 281, 1342–1346.

Hoffman, P. F., Calver, C. R., and Halverson, G. P. (2009). Cottons Breccia of King Island, Tasmania: Glacial or non-glacial, Cryogenian or Ediacaran?: Precambrian Research, 172, 311– 322.

Hong, W., Cooke, D. R., Huston, D. L., Maas, R., Meffre, S., Zhang, L., and Fox, N. (2017). Ceochronological, geochemical and Pb isotopic compositions of Tasmanian granites (southeast Australia): Controls on petrogenesis, geodynamic evolution and tin mineralization. Gondwana Research, 46, 124–140.

Holm, O. H. (2003). Structural and metamorphic evolution of the Arthur Lineament, north-west Tasmania, Australia. PhD thesis (unpubl.). University of Tasmania.

Holm, O.H., and Berry, R.F. (2002). Structural history of the Arthur Lineament, northwest Tasmania: An analysis of critical outcrops. Australian Journal of Earth Sciences, 49, 167–185.

Holm O. H., Crawford A. J. and Berry R. F. (2003). Geochemistry and tectonic settings of meta-igneous rocks in the Arthur Lineament and surrounding area, northwest Tasmania. Australian Journal of Earth Sciences, 50, 903–918.

Ireland T. R., Flöttmann T., Fanning C. M., Gibson G. M. and Preiss W. V. (1998). Development of the early Paleozoic Pacific margin of Gondwana from detrital-zircon ages across the Delamerian orogen. Geology, 26, 243–246.

Jackson, S. E., Pearson, N. J., Griffin, W. L., and Belousova, E. A. (2004). The application of laser ablation-inductively coupled plasma-mass spectrometry to in situ U–Pb zircon geochronology. Chemical Geology, 211, 47–69.

Kamenetsky, V., Lygin, A., Foster, J., Meffre, S., Maas, R., Kamenetsky, M., Goemann, K., and Beresford, S. (2016). A story of olivine from the McIvor Hill complex (Tasmania, Australia): clues to the origin of Avebury metasomatic Ni sulfide deposit. American Mineralogist, 101, 1321–1331.

Karlstrom, K. E., Williams, M. L., Mclelland, J., Geissmanm J. W. and Ahall, K. (1999). Refining Rodinia: geologic evidence for the Australia–western U.S. connection in the Proterozoic. GSA Today, 9, 1–7.

Kendall, B., Creaser, R. A., Calver, C. R., Raub, T. D., and Evans, D. A. D. (2009). Correlation of Sturtian diamictite successions in southern Australia and northwestern Tasmania by Re-Os black shale geochronology and the ambiguity of "Sturtian"-type diamictite—cap carbonate pairs as chronostratigraphic marker horizons. Precambrian Research, 172, 301–310.

Laird, M. G., Mansergh, G. D., and Chappell, J. M. A. (1971). Geology of the central Nimrod Glacier area, Antarctica. New Zealand Journal of Geology and Geophysics, 14, 427–468.

Li, Z. -X., and Evans, D. A. D. (2011). Late neoproterozoic 40° intraplate rotation within Australia allows for a tighter-fitting and longer-lasting Rodinia. Geology, 39, 39–42.

Li, Z. -X., Li, X. H., Kinny, P. D., Wang, J., Zhang, S., and Zhou, H. (2003). Geochronology of Neoproterozoic syn-rift magmatism in the Yangtze Craton South China and correlations with other continents: evidence for a mantle superplume that broke up Rodinia. Precambrian Research, 122, 85–109.

Li, Z. -X., Bogdanova, S. V., Collins, A. S., Davidson, A., De Waele, B., Ernst, R. E., Fitzsimons, I. C. W., Fuck, R. A., Gladkochub, D. P., Jacobs, J., Karlstrom, K. E., Lu, S., Natapov, L. M., Pease, V., Pisarevsky, S. A., Thrane, K., Vernikovsky, V. (2008). Assembly, configuration, and break-up history of Rodinia: a synthesis. Precambrian Research, 160, 179–210.

Ludwig, K. R., 2003, Isoplot 3.00: A geochronological toolkit for Microsoft Excel. Berkeley, California, Berkeley Geochronological Centre Special Publication 4, 74p.

Macdonald, F. A., Schmitz, M. D., Crowley, J. L., Roots, C. F., Jones, D. S., Maloof, A. C., Strauss, J. V., Cohen, P. A., Johnston, D. T., and Schrag, D. P. (2010). Calibrating the Cryogenian: Science, 327, 1241–1243.

Mahon, R. C., Dehler, C. M., Link, P. K., Karlstrom, K. E., and Gehrels, G. G. (2014a) Detrital zircon provenance and paleogeography of the Pahrump Group and overlying strata, Death Valley, California: Precambrian Research, 251, 102–117.

Mahon, R. C., Dehler, C. M., Link, P. K., Karlstrom, K. E. and Gehrels, G. E. (2014b). Geochronologic and stratigraphic constraints on the Mesoproterozoic and Neoproterozoic Pahrump Group, Death Valley, California: a record of the assembly, stability, and breakup of Rodinia. Geological Society of America Bulletin, 126, 652–664.

McDougall I. and Leggo P. J. (1965). Isotopic age determinations on granitic rocks from Tasmania. Australian Journal of Earth Sciences, 12, 295–332.

McKenzie, D., and Bickle, M. J. (1988). The Volume and Composition of Melt Generated by Extension of the Lithosphere. Journal of Petrology, 29, 625–679.

Meschede, M. (1986). A method of discriminating between different types of mid-ocean ridge basalts and continental tholeiites within the Nb-Zr-Y diagram. Chemical Geology, 56, 207–218.

Meffre, S., Berry, R. F., and Hall, M. (2000). Cambrian metamorphic complexes in Tasmania: tectonic implications. Australian Journal of Earth Sciences, 47, 972–985.

Meffre, S., Direen, N. G., Crawford, A. J., and Kamenetsky, V. (2004). Mafic volcanic rocks on King Island, Tasmania: evidence for 579 Ma break-up in East Gondwana. Precambrian Research, 135, 177–191.

Meffre, S., Large, R.R., Scott, R., Woodhead, J., Chang, Z., Gilbert, S.E., Danyushevsky, L.V., Maslennikov, V., and Hergt, J.M. (2008). Age and pyrite Pb-isotopic composition of the giant Sukhoi Log sediment-hosted gold deposit, Russia. Geochimica et Cosmochimica Acta ,72, 2377–2391.

Moore, D. H., Betts, P. G. and Hall, M. (2015). Fragmented Tasmania: the transition from Rodinia to Gondwana. Australian Journal of Earth Sciences, 62, 1–35.
Moores, E.M. (1991). Southwest U.S.–East Antarctic (SWEAT) connection: a hypothesis. Geology, 19, 425–428.

Mulder, J. A., Halpin, J. A., and Daczko, N. R. (2015a). Mesoproterozoic Tasmania: Witness to the East Antarctica-Laurentia connection within Nuna. Geology, 43, 759–762.

Mulder, J. A., Berry, R. F., and Scott, R. J. (2015b). The structure and metamorphism of the Red Point Metamorphic Complex– A newly discovered high-pressure metamorphic complex from the south coast of Tasmania. Australian Journal of Earth Sciences, 62, 969–983.

Mulder, J. A., Berry, R. F., Meffre, S., and Halpin, J. A. (2016). The metamorphic sole of the western Tasmanian ophiolite: New insights into the Cambrian tectonic setting of the Gondwana Pacific margin. Gondwana Research, 38, 351–369.

Preiss, W. V. (2000). The Adelaide Geosyncline of South Australia and its significance in Neoproterozoic continental reconstruction. Precambrian Research, 100, 21–63.

Preiss, W. V., Drexel, J. F., and Reid, A.J. (2009). Definition and age of the Kooringa Member of the Skillogalee Dolomite: host for Neoproterozoic (c. 790 Ma) porphyry-related copper mineralization at Burra. MESA Journal, 55, 19–33.

Rubatto, D., Williams, I. S., and Buick, I. S. (2001). Zircon and monazite response to prograde metamorphism in the Reynolds Range, central Australia. Contributions to Mineralogy and Petrology, 140, 458–468.

Saito, Y., Tiba, T., and Matsubara, S. (1998). Precambrian and Cambrian cherts in northwestern Tasmania. Bulletin of the Natinal Science Museum, Tokyo, Series C, 14, 59–70.

Seymour D. B. and Calver C. R. (1998). Time space diagram for Tasmania (2nd edition). Mineral Resources Tasmania and Australian Geological Survey Organisation. Hobart Tas.

Seymour, D. B., McClenaghan, M. P., Green, G. R., Everard, J. L., Berry, R. F., Callaghan, T., Davidson, G. J., and Hills, P. B. (2014). Mid-Paleozoic orogenesis, magmatism and mineralization. In: Corbett, K.D., Quilty, P.G., Calver, C.R. (Eds.), Geological Evolution of Tasmania. Geological Society of Australia Special Publication 24. Geological Society of Australia (Tasmania Division).

Schoene, B., and Bowring, S. A. (2006) U-Pb systematics of the McClure Mountain syenite: Thermochronological constraints on the age of the 40Ar/39Ar standard MMhb: Contributions to Mineralogy and Petrology, 151, p. 615–630.

Sláma, J., Košler, J., Condon, D. J., Crowley, J. L., Gerdes, A., Hanchar, J. M., Horstwood, M. S. A., Morris, G. A., Nasdala, L., Norberg, N., Schaltegger, U., Schoene, B., Tubrett, M. N., and Whitehouse, M. J. (2008). Plesŏvice zircon – a new natural reference material for U–Pb and Hf isotopic microanalysis. Chemical Geology, 249, 1–35.

Smith, E. F., Macdonald, F. A., Crowley, J. L., Hodgin, E. B., and Schrag, D.P. (2015). Tectonostratigraphic evolution of the c. 780–730 Ma Beck Springs Dolomite: Basin formation in the core of Rodinia, in Li, Z. -X., Evans, D. A.D, and Murphy, J. B., (Eds.), Supercontinent Cycles Through Earth History: Geological Society of London Special Publication 424, 213–239.

Spry A. H. (1962). The Precambrian rocks. In: Spry A. H. and Banks M. R. (Eds.) The Geology of Tasmania. Australian Journal of Earth Sciences, 9.

Strauss, J. V., Rooney, A. D., Macdonald, F. A., Brandon, A. D. and Knoll, A. H. (2014). 740 Ma vase-shaped microfossils from Yukon, Canada: implications for Neoproterozoic chronology and biostratigraphy. Geology, 42, 659–662.

Thompson, J., Meffre, S., Maas, R., Kamenetsky, V., Kamenetsky, M., Goemann, K., Ehrig, K., and Danyushevsky, L. (2016). Matrix effects in Pb/U measurements during LA-ICP-MS analysis of the mineral apatite. Journal of Analytical Atomic Spectrometry, 31, 1206–1215.

Turner N. J., 1993. K-Ar geochronology in the Arthur Metamorphic Complex, Ahrberg Group and Oonah Formation, Corinna district. Mineral Resources Tasmania Report 1993/12.

Turner, N. J., and Bottrill, R. S. (2001). Blue amphibole, Arthur Metamorphic Complex, Tasmania: composition and regional tectonic setting. Australian Journal of Earth Sciences, 48, 167–181.

Turner, N. J., Black, L. P., and Kamperman, M. (1998). Dating of Neoproterozoic and Cambrian orogenies in Tasmania. Australian Journal of Earth Sciences, 45, 789–806.

Vicary, M. J. (2004). Digital Geological Atlas 1:25 000 series. Sheet 4045. Burnie. Mineral Resources Tasmania.

Wiedenbeck, M., Alle, P., Corfu, F., Griffin, W. L., Meier, M., Oberli, F., Vonquadt, A., Roddick, J. C., and Speigel, W. (1995). 3 Natural Zircon Standards for U–Th–Pb, Lu–Hf, trace-element and REE analyses. Geostandards Newsletter, 19, 1–23.

Yonkee, W. A., Dehler C. D., Link, P. K., Balgord, E. A., Keeley, J. A., Hayes, D. S., Wells, M. L., Fanning, C. M., and Johnston, S. M. (2014). Tectonostratigraphic framework of Neoproterozoic to Cambrian strata, west-central U.S.: Protracted rifting, glaciation, and evolution of the North American Cordilleran margin. Earth-Science Reviews, 136, 59–95.

Appendix 5.1: Cooee Dolerite geochemical data	Digital Appendix
Appendix 5.2: Apatite U-Pb age data	Digital Appendix
Appendix 5.3: Sample locations	Digital Appendix
Appendix 5.4: Detrital zircon U-Pb age data	Digital Appendix
Appendix 5.5: Detrital monazite U-Pb age data	Digital Appendix

Chapter 6

The metamorphic sole of the western Tasmanian ophiolite: New insights into the Cambrian tectonic setting of the Gondwana Pacific margin

Gondwana Research, v. 38, 351–369

Jacob A. Mulder[1], Ron F. Berry[1], Sebastien Meffre[1], Jacqueline A. Halpin[1]

[1]ARC Centre of Excellence in Ore Deposits (CODES), School of Physical Sciences, University of Tasmania, Private Bag 79, TAS 7001, Australia

6.0 Abstract

The Cambrian Ross–Delamerian Orogeny records the first phase of accretional tectonics along the eastern margin of Gondwana following breakup of the supercontinent Rodinia. Western Tasmania represents a key area for understanding the Cambrian tectonic setting of the eastern margin of Gondwana as it is one of the few places where a Tethyan-type ophiolite is preserved and contains the only known exposures of a sub-ophiolitic metamorphic sole associated with the Ross–Delamerian Orogen. This paper presents an integrated study of the field, petrographic, geochemical, and metamorphic characteristics of the metamorphic sole to the western Tasmanian ophiolite. The structurally highest levels of the metamorphic sole consist of granulite–upper amphibolite facies metacumulates and metagabbros. A transition to amphibolite and epidote–amphibolite facies conditions is recorded by metadolerites and metabasalts towards the base of the metamorphic sole. Kinematic indicators in mylonitic amphibolites suggest the metamorphic sole formed in an east-dipping subduction zone located to the east of the Proterozoic continental crust of Tasmania. Major and trace element whole rock and relict igneous spinel geochemistry indicates that the protoliths to the metamorphic sole formed at a back arc basin spreading centre. Our new data supports a model in which east-dipping subduction in Tasmania was driven by collapse of a back arc basin developed above an earlier west-dipping subduction zone outboard of the eastern margin of Gondwana. The proposed model may help to resolve a controversy related to apparent along-strike variations in subduction zone polarity during the Ross-Delamerian Orogeny and suggests a complex geodynamic setting had developed along the eastern margin of Gondwana by the Middle Cambrian. This study highlights the importance of considering the role of multiple subduction zones in generating metamorphic soles and emplacing ophiolites, which are key events associated with the construction of many orogenic belts worldwide.

6.1 Introduction

Understanding how large fragments of oceanic lithosphere (ophiolites) are emplaced onto continental margins is critical to unravelling the complex tectonic evolution of many orogenic belts. Tethyan-type ophiolites are relatively intact ophiolites that have been emplaced onto continental margins or arc terranes (Moores and Macgregor, 1972). The emplacement of Tethyan-type ophiolites represent important periods in the evolution of orogenic systems that provide key insights into the wider geodynamic setting of orogenesis and the processes by which orogenic belts are constructed.

At the base of many Tethyan-type ophiolites are thin sheets of high-grade, highly deformed metamorphic rocks known as metamorphic soles (e.g. Williams and Smyth, 1973; Jamieson, 1986). Metamorphic soles are thought to form at the subduction zone interface where material from the down-going plate is "welded" onto the hot mantle section of the overriding plate (e.g. Boudier et al., 1988; Hacker and Gnos, 1997). Many metamorphic soles preserve pressure conditions corresponding to depths that far exceed the thickness of the overlying ophiolite, implying significant exhumation of the metamorphic sole prior to ophiolite emplacement (e.g. Wakabayashi and Dilek, 2003; Van Hinsbergen et al., 2015). As metamorphic soles represent the first material accreted to the base of the upper plate and are an integral part of many obducted ophiolite complexes, they represent a unique record of the history of an ophiolite from subduction initiation to emplacement.

The late Neoproterozoic–early Paleozoic Ross–Delamerian Orogen of East Antarctica and southeast Australia records the earliest stages of convergent tectonics along the eastern margin of Gondwana following breakup of the supercontinent Rodinia (e.g. Cawood, 2005; Boger, 2011). Tethyan-type ophiolites emplaced during the Ross–Delamerian Orogeny are rare (Spaggiari et al., 2003), with the best-preserved example exposed in western Tasmania (southeast Australia, Fig. 6.1). The significance of Cambrian orogenesis in Tasmania (Tyennan Orogeny) in the context of the Ross–Delamerian Orogeny has long been problematic due to evidence for east-dipping subduction in Tasmania being synchronous with west-dipping subduction beneath the margin of Gondwana to the north (southeast Australia) and south (East Antarctica). The polarity of subduction along various segments of the Ross–Delamerian Orogen is still debated (e.g. Crawford et al., 2003; Cayley, 2011; Gibson et al., 2011; Rocchi et al., 2011) as it has important implications for understanding the Cambrian tectonic history of eastern Gondwana and subsequent orogenic events along the margin (e.g. Cayley, 2011; Moresi et al., 2014).

Mylonitic amphibolites outcropping beneath the western Tasmanian ophiolite have previously been interpreted as a metamorphic sole (Rubenach, 1973; Berry, 1989) but until now have not been studied in detail. These amphibolites represent the only known metamorphic sole associated with the Ross–Delamerian Orogeny. The metamorphic sole preserves important clues into the processes controlling the emplacement of the western Tasmanian ophiolite and hence has the potential to provide unique insights into the tectonic setting of the eastern margin of Gondwana during the early Cambrian.

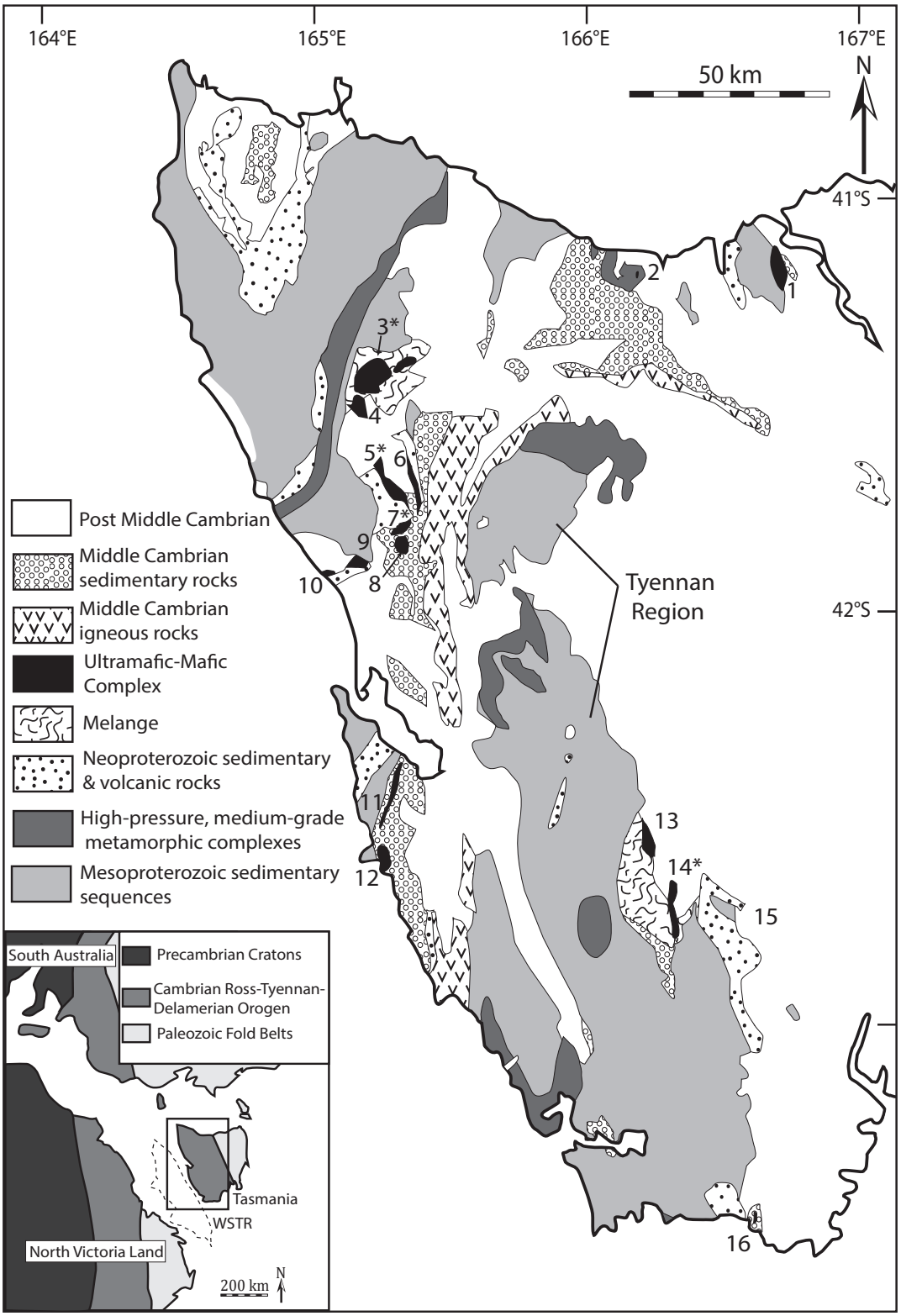

Figure 6.1: Distribution of pre-Late Cambrian rocks in Tasmania, modified after Meffre et al. (2000) and Berry et al. (2007). Inset shows inferred position of Tasmania within the Ross– Delamerian Orogen; dashed outline of the inferred Cambrian position of the Western South Tasman Rise (WSTR) is from Royer and Rollet (1997). Locations of mafic-ultramafic Complexes representing remnants of the western Tasmania ophiolite are modified from Brown (1989). Mafic-ultramafic complexes where metamorphic sole is exposed are marked with an asterisk. 1-Andersons Creek, 2-Forth Metamorphic complex, 3-Heazlewood River complex*, 4-Mt. Stewart, 5-Wilson River*, 6-Huskisson River, 7-Serpentine Hill*, 8-Dundas, 9-McIvors Hill, 10-Trial Harbour, 11-Noddy Creek, 12-Spero Bay, 13-Boyes River, 14-Adamsfield-Gordon River Road*, 15-Styx River area, and 16-Rocky Boat Harbour.

This paper presents an integrated study of the field, microstructural, geochemical, and metamorphic characteristics of the metamorphic sole of the western Tasmanian ophiolite. The new data set supports a detailed assessment of the protoliths to the metamorphic sole rocks and allows us to reconstruct the complex structural and metamorphic history associated with the assembly of a metamorphic sole. Our findings provide new insights into the geodynamic setting of the eastern margin of Gondwana during the Cambrian that may help to resolve the apparent along strike variability in subduction zone polarity during the Ross–Delamerian Orogeny.

6.2 Geological setting

Western Tasmania records a complex geological history reaching back to the Mesoproterozoic. The oldest rocks include the Rocky Cape Group and correlates, which were deposited on a tidal dominated shelf at 1450–1300 Ma (Calver et al., 2014; Halpin et al., 2014). Unconformably overlying the Mesoproterozoic strata are Neoproterozoic volcano-sedimentary sequences recording the formation of an east-facing volcanic passive margin during the break-up of the supercontinent Rodinia (Crawford and Berry, 1992; Meffre et al., 2004). Following Neoproterozoic rifting, Tasmania is interpreted to have been a microcontinental fragment outboard of the eastern margin of Gondwana (Berry et al., 2008; Cayley, 2011; Moore et al., 2013).

In the middle Cambrian the Tasmanian microcontinent collided with an intra-oceanic island arc, initiating the Tyennan Orogeny (Berry and Crawford, 1988; Crawford and Berry, 1992; Turner et al., 1998). The Tyennan Orogeny in Tasmania is synchronous with the Delamerian Orogeny of southeast Australia and the Ross Orogeny of East Antarctica (e.g. Flottmann et al., 1993; Foden et al., 2006; Squire et al., 2006; Boger, 2011), which in turn form part of the larger Neoproterozoic–Paleozoic Terra Australis Orogen developed along the Pacific margin of Gondwana (Cawood, 2005). During the early stages of the Tyennan Orogeny one or more extensive slices of mafic-ultramafic crust and mantle comprising the western Tasmanian ophiolite and mélanges containing allochthonous deep water sedimentary sequences and basaltic rocks, were emplaced over the passive margin. Synchronous with ophiolite emplacement, subduction of the leading edge of the Tasmanian microcontinent resulted in high-pressure, greenschist–eclogite facies metamorphism at *ca*. 510 Ma (Berry et al., 2007; Chmielowski and Berry, 2012). These high-pressure, medium-grade metamorphic rocks are now distributed throughout the structurally complex Tyennan Region (Fig. 6.1).

Relicts of the western Tasmanian ophiolite are preserved as mafic-ultramafic complexes throughout western Tasmania (Fig. 6.1). The mafic-ultramafic complexes are generally in fault contact above Neoproterozoic rift sequences or allochthonous mélanges. Ultramafic rocks in the complexes are orthopyroxene-rich with Cr-rich spinels and mafic rocks include low-Ti tholeiities and boninites (Brown, 1986; Crawford and Berry, 1992). The geochemistry of the mafic-ultramafic complexes is consistent with formation in the fore-arc region of an intra-oceanic island arc (Berry and Crawford, 1988; Crawford and Berry, 1992). The timing of ophiolite formation is constrained by a tonalite

interpreted to represent a late-stage intrusion within the Heazlewood River complex dated at 513.6 ± 5 Ma (Turner et al., 1998) and a 516.0 ± 0.9 Ma gabbro within the McIvor Hill complex (Mortenson et al., 2015).

The closing stages of the Tyennan Orogeny are characterised by rapid exhumation of the high-pressure metamorphic rocks at *ca.* 505 Ma (Turner and Bottrill, 2001; Foster et al., 2005) as recorded by structures with dominantly east-verging transport vectors (Berry, 2014) and post-collision volcanism, possibly in response to slab-break off (Chmielowski and Berry, 2012). A final phase of east-verging, upright folding may record the accretion of the Tasmanian microcontinent onto the margin of East Gondwana at *ca.* 495 Ma (Holm and Berry, 2002; Berry et al., 2007; Cayley, 2011).

6.3 Field geology

The metamorphic sole of the western Tasmanian ophiolite is exposed in four locations in western Tasmania (Fig. 6.1). At each location, the metamorphic sole rocks occur as thin (typically ~100 m) exposures dominated by amphibolites that are in fault bounded blocks below strongly serpentinised ultramafic rocks representing the basal portions of the ophiolite and above Neoproterozoic volcaniclastic sedimentary rocks or Early Cambrian mélange units. Brief descriptions of the structural context and lithologies of the four exposures of the metamorphic sole sampled in this study are given below. The locality maps and cross-sections of each of the metamorphic sole exposures are given in Appendix 6.1.

6.3.1 Heazlewood River complex

Three exposures of amphibolite occur on the western and southern margins of the Heazlewood River complex (Rubenach, 1973). The northernmost body near the Nineteen Mile Creek is the best exposed and consists of 100 m of schistose amphibolite separated from volcaniclastic siltstone to the north by approximately 500 m of breccia consisting of blocks of gabbro and fine-grained amphibolite within a sheared serpentinite matrix. The contact between the amphibolite body and massive serpentinite to the south is not exposed. Amphibolites near the breccia zone are generally pale green, fine-grained, and well foliated. Amphibolites near the contact with the massive serpentinite are dark green to black, coarse-grained rocks with a strongly developed foliation and locally developed alternating plagioclase- and amphibole-rich layering. The foliation in the amphibolites dips moderately to steeply (50–90°) to the south and is associated with a shallowly plunging (~10°) east–west trending lineation defined by amphibole.

6.3.2 Wilson River complex

The metamorphic sole of the Wilson River complex occurs as amphibolite bodies exposed along the western side of the complex at Harman River and Ahearne Creek. The exposure at Harman Creek is a 4 m wide body of coarse-grained, foliated or massive amphibolite, which is faulted against

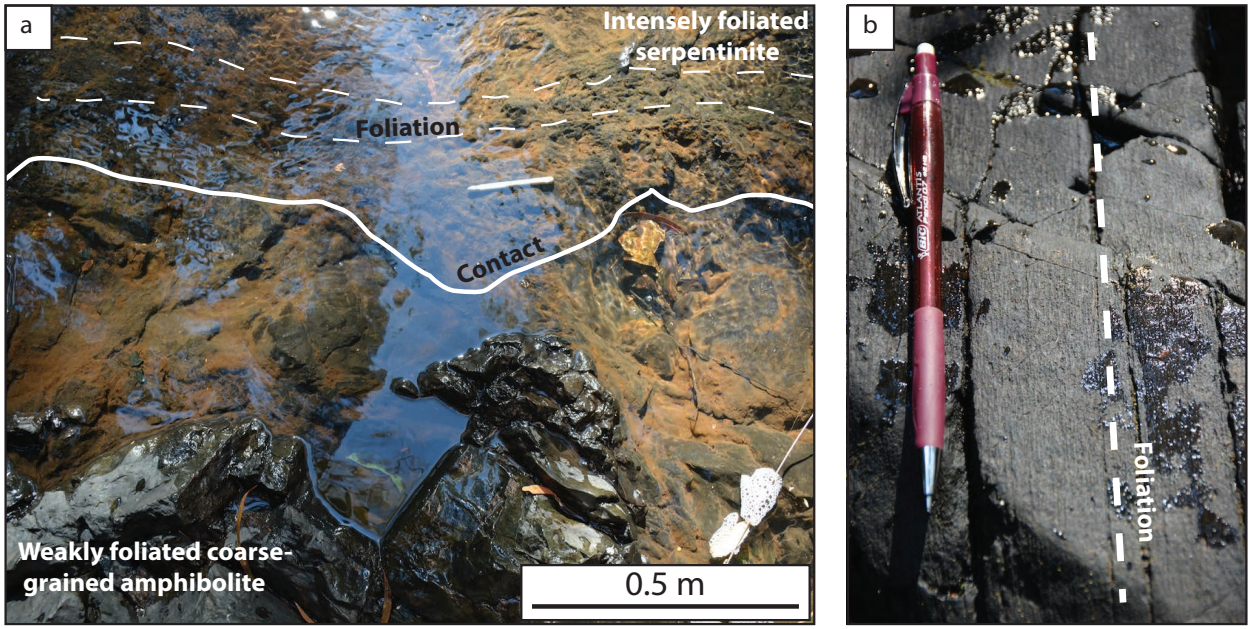

Figure 6.2: Field characteristics of the Tasmanian metamorphic sole exposure at Ahearne Creek. (a) Contact between intensely foliated serpentinite representing the base of the ophiolite and coarse-grained opx–ol amphibolite at the top of the metamorphic sole. Foliation in amphibolite and serpentinite is parallel to the sharp contact. (b) Strongly foliated amphibolites in the lower parts of the metamorphic sole. Aligned amphibole crystals define the foliation.

sheared serpentinite to the east. The contact with the Neoproterozoic rift sequences to the west is not exposed. At Ahearne Creek a 20 m wide amphibolite body is separated from massive serpentine of the Wilson River complex by a 5 m wide zone of extremely hard and intensely foliated serpentinite. The contact between the foliated serpentinite and the amphibolite is sharp, irregular, and dips steeply to the south–southwest (Fig. 6.2a). The intensely developed foliation in the serpentinite is parallel to the contact and locally developed c-s fabrics indicate a top-to-the-west sense of shear. The amphibolites at the contact are coarse-grained, weakly foliated rocks consisting almost entirely of dark green amphibole. Layering is well-developed and is parallel to the contact with the serpentinite. South of the contact the amphibolites are fine–medium-grained, dark green rocks with fine-scale layering defined by variations in amphibole grain size (Fig. 6.2b). These amphibolites have a well-developed, shallowly plunging, east– west or northwest–southeast trending lineation defined by the alignment of the long axes of amphiboles. The amphibolite body is faulted against volcaniclastic sandstone of the Neoproterozoic rift sequences to the south.

6.3.3 Serpentine Hill complex

The metamorphic sole at Serpentine Hill outcrops as a 30 m wide body of amphibolite in a railroad cutting at Argent Tunnel. Zones of intensely sheared serpentinite mark both the northerly and southerly contacts of the amphibolite body. At the northerly contact the amphibolites are coarse-grained, weakly foliated and consist mainly of dark green amphibole. These amphibolites are in fault contact with a complex 2 m wide zone consisting of sheared serpentinite and a steeply dipping, fault-bound slice of phyllite. The sheared serpentinite zone is itself separated from volcaniclastic

siltstones (Neoproterozoic rift sequences) to the north by a steeply south-dipping fault. The southerly contact consists of a steeply dipping, 2 m wide zone of intensely sheared serpentinite separating the amphibolites from massive orthopyroxenite. Amphibolites of the Serpentine Hill complex metamorphic sole have a strongly developed foliation that dips 60°–70° to the south and have a shallowly south–southwest plunging lineation defined by aligned amphibole crystals. The high-angle faults and shear zones defining the contacts of the amphibolite body clearly crosscut the foliation in the amphibolite. A diamond drill hole (DDH-SH1) at Melba Flats, 1 km south of the Argent Tunnel exposure, intersected metamorphic sole amphibolites beneath ultramafic rocks of the Serpentine Hill complex (Brown, 1991; Goscombe, 1991). The drill hole intersected 50 m of retrogressed orthopyroxenite in fault contact above 200 m of amphibolite and epidote–amphibolite, which in turn is faulted above sheared mudstone and volcanic rocks.

6.3.4 Gordon River Road

A 50 m wide exposure of metamorphic sole amphibolites occurs in a road cutting along the Gordon River Road and is in fault contact with a 1.5 × 0.5 km fault-bound body of massive serpentinite to the east. The metamorphic sole is separated from the massive serpentine body by a steeply west-dipping, 2 m wide zone of intensely sheared serpentinite. Amphibolites adjacent to the sheared serpentinite zone are coarse-grained, weakly foliated rocks consisting entirely of dark green amphibole. West of the contact, the amphibolites are very fine—medium-grained and have a strong foliation parallel to compositional layering and to the contact with the sheared serpentinite. A well-developed lineation defined by the alignment of amphiboles plunges steeply to the west–northwest. The amphibolite body is faulted against Cambrian mélange to the west. A second locality in the Gordon River Road area consists of three small bodies of amphibolite within mélange in the upper reaches of the Boyd River, approximately 3 km southwest of the road cutting exposure.

6.4 Methods and materials

Major element concentrations were obtained by X-ray fluorescence (XRF) analysis of glass discs with a Philips PW-1480 X-ray fluorescence spectrometer at the University of Tasmania. The glass discs were prepared by fusing sample powders with a lithium borate flux (sample:flux = 1:10). Rare earth element (REE) and trace element concentrations were measured via laser ablation-inductively coupled plasma mass spectrometry (LA-ICPMS) using a Compex 193 nm Ar–F excimer laser coupled to an Agilent Technologies 7700 series ICPMS at CODES, University of Tasmania. The LA-ICPMS analysis was undertaken on the same XRF fused glass discs used to measure the major element concentrations following a method modified from Yu et al. (2003). Details of the analytical method are described in Appendix 6.3.

6.5 Petrography

The amphibolites from the metamorphic sole exposures are separated into 5 types based on mineralogy and microtexture (Fig. 6.3a–h). A summary of the microstructural kinematic indicators from the amphibolites is presented in Appendix 6.2.

6.5.1 Nematoblastic, orthopyroxene-olivine-hercynite-bearing amphibolites (opx–ol amphibolites)

These rocks have a nematoblastic texture defined by interlocking, 0.2–0.5 mm subidioblastic pale green amphibole (70%–90% modal). Amphibole grains share sharp grain boundaries with 0.05–0.15 mm xenoblastic orthopyroxene grains (5%–10% modal). Olivine occurs as 0.01–0.1 mm xenoblastic grains (up to 5% modal), sharing sharp grain boundaries with adjacent phases and as rare inclusions in amphibole. Spinel (≤5% modal) mostly occurs as dark green 0.01–0.1 mm grains that locally form thin, commonly discontinuous rims around cores of dark brown spinel (Fig. 6.3a). Although we favour the term hercynite to describe these characteristically dark green spinels, many have compositions intermediate between spinel and hercynite and therefore belong to the pleonaste series (Table 6.3).

6.5.2 Granoblastic amphibolites

The granoblastic amphibolites are characterised by 1–2 cm thick amphibole-rich layers separated by ≤ 2 mm thick plagioclase-rich layers, both of which have granoblastic textures (Fig. 6.3b). A subtle elongation of amphibole and plagioclase grains locally defines a layer-parallel foliation. Within the amphibole-rich layers, amphibole (80% modal) occurs as 0.3–1 mm subidioblastic or xenoblastic grains interlocking with 0.1–0.5 mm xenoblastic sericitised plagioclase. The plagioclase-rich layers contain 0.2 mm (average) xenoblastic grains of sericitised plagioclase (60% modal) and 0.3 mm (average) xenoblastic amphibole grains. Clinopyroxene occurs as uncommon 0.5–2.0 mm subidioblastic grains, which are extensively replaced by amphibole and chlorite. Accessory phases include ilmenite and late-stage titanite.

6.5.3 Hornblendites

These amphibolites have a weakly foliated, coarse-grained texture consisting of 1.5–2 mm, subidioblastic amphibole grains (Fig. 6.3c). Subidioblastic dark brown spinel grains are present as a rare accessory phase. The hornblendites are locally interlayered with granoblastic amphibolites at the thin section scale in samples from the Serpentine Hill and Gordon River Road metamorphic sole exposures.

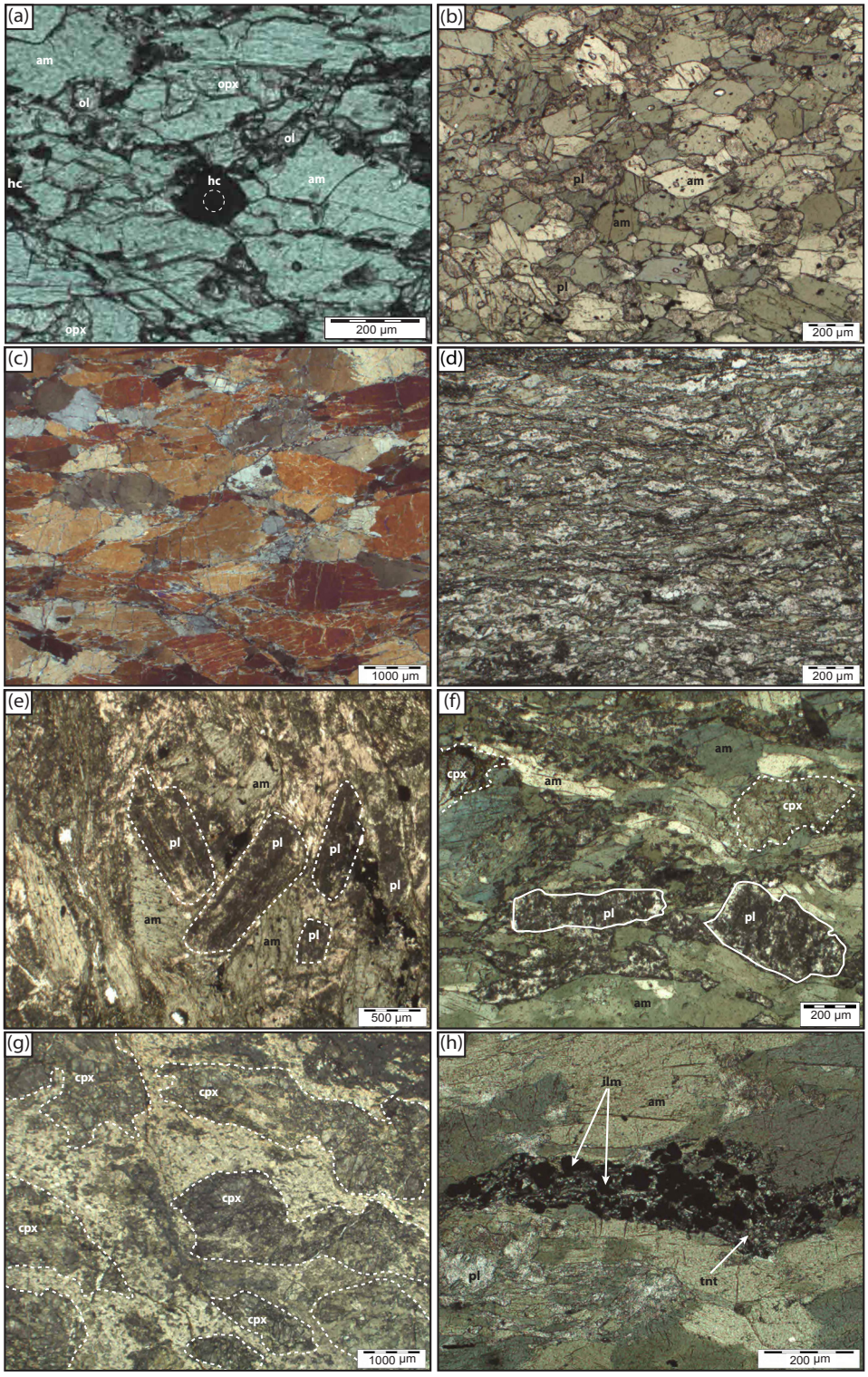

Figure 6.3: Representative photomicrographs of various textural types of metamorphic sole amphibolites. (a) opx–ol amphibolite with olivine (ol), orthopyroxene (opx), amphibolite (am), and herycnite rims (hc) on relict igneous spinel cores (dashed white circle). (b) Granoblastic amphibolite showing typical granoblastic texture consisting of interlocking amphibole and plagioclase (pl). (c) Hornblendite consisting entirely of coarse-grained amphibole. (d) Foliated amphibolite showing well-developed mylonitic textures including c-s fabrics and amphibole (straw and pale green) and plagioclase (colourless) porphyroclasts. (e) Foliated amphibolite showing possible relict ophitic texture defined by large tabular plagioclase grains (white dashed outlines) enclosed by large amphibole grains. (f) Cpx-amphibolite from Heazlewood River complex showing strongly retrogressed clinopyroxene grains (cpx, white dashed outline) and pseudomorphed coarse-grained plagioclase (white solid outline) overprinted by schistose texture defined by amphibole and plagioclase. (g) Cpx-amphibolite showing possible relict gabbroic texture with coarse-grained clinopyroxene grains. (h) Cpx-amphibolite showing retrograde rims of titanite (tnt) on ilmenite (ilm) cores. All photomicrographs are in plain polarised light except for (c), which is in crossed polarised light.

6.5.4 Fine–medium-grained foliated amphibolites (foliated amphibolites)

These amphibolites are fine–medium-grained, strongly foliated rocks with well-developed c-s and porphyroclastic textures (Fig. 6.3d). Amphibole (50%–70% modal) occurs as 0.1–0.2 mm asymmetric augen-shaped porphyroclasts or is concentrated in amphibole-rich bands as subidioblastic elongate grains. Plagioclase occurs as ~0.1 mm augen-shaped porphyroclasts. Layering in the foliated amphibolites is defined by variations in the grain size and abundance of amphibole and locally by ≤1 cm thick bands of epidote. Garnet occurs in one sample (Z346) from Serpentine Hill (Brown, 1991; Goscombe, 1991). Sample 71342 (Boyd River) preserves a possible relict ophitic texture defined by randomly orientated, twinned, tabular plagioclase grains enclosed by large xenoblastic amphibole grains (Fig. 6.3e). Similar relict ophitic textures in metamorphic sole amphibolites from the Heazlewood River complex were noted by Rubenach (1973). In the lower parts of the Serpentine Hill Drill Hole and the Gordon River Road metamorphic sole exposures the foliated amphibolites are very fine-grained and consist of strongly aligned needle-like grains of palest green amphibole (actinolite?) and xenoblastic quartz and plagioclase.

6.5.5 Clinopyroxene-bearing schistose amphibolites (cpx–amphibolites)

Amphibolites from the upper parts of the amphibolite body of the Heazlewood River complex are schistose rocks with ~1 mm thick layers dominated by 0.2–0.5 mm subidioblastic amphibole (60% modal) alternating with plagioclase and quartz-rich layers. Amphibole also occurs in ~0.5 mm wide decussate clots or as single ~0.5 mm spherical grains, both of which are wrapped by the main rock fabric. Plagioclase and quartz-rich layers (28% modal) contain ~0.1 mm xenoblastic slightly elongate sericitised or saussuritised plagioclase grains and rare unaltered twinned plagioclase. Quartz grains have a similar texture to plagioclase. Ghosts of twinned, idioblastic plagioclase grains up to 1.5 mm are common and are typically wrapped by the main rock fabric (Fig. 6.3f). Clinopyroxene (5%–10% modal) occurs as xenoblastic to subidioblastic, randomly orientated grains, which are extensively replaced by amphibole both along cleavage planes and the rims of grains (Fig. 6.3f). In Sample H14, clinopyroxene (40% modal) occurs as coarse grains, which may reflect an originally gabbroic texture (Fig. 6.3g). Ilmenite occurs as clusters of ~0.1 mm xenoblastic grains, which are strung out into the main foliation and are commonly rimmed by titanite (Fig. 6.3h).

The spatial zonation of the different types of amphibolite in each of the metamorphic sole exposures are summarised in idealised logs in Fig. 6.4. A key feature of most of the metamorphic sole exposures is the presence of a 5–50 m thick zone dominated by opx–ol amphibolites at the top of the sole, which are locally interlayered with granoblastic amphibolites and hornblendites. The most complete sections of the metamorphic sole (Serpentine Hill Drill hole, Gordon River Road) are characterised by an upper zone dominated by opx–ol amphibolites with foliated amphibolites making up the majority of the middle–lower parts of the sole. The foliated amphibolites show a notable decrease in grain size and increase in epidote abundance down through the sole.

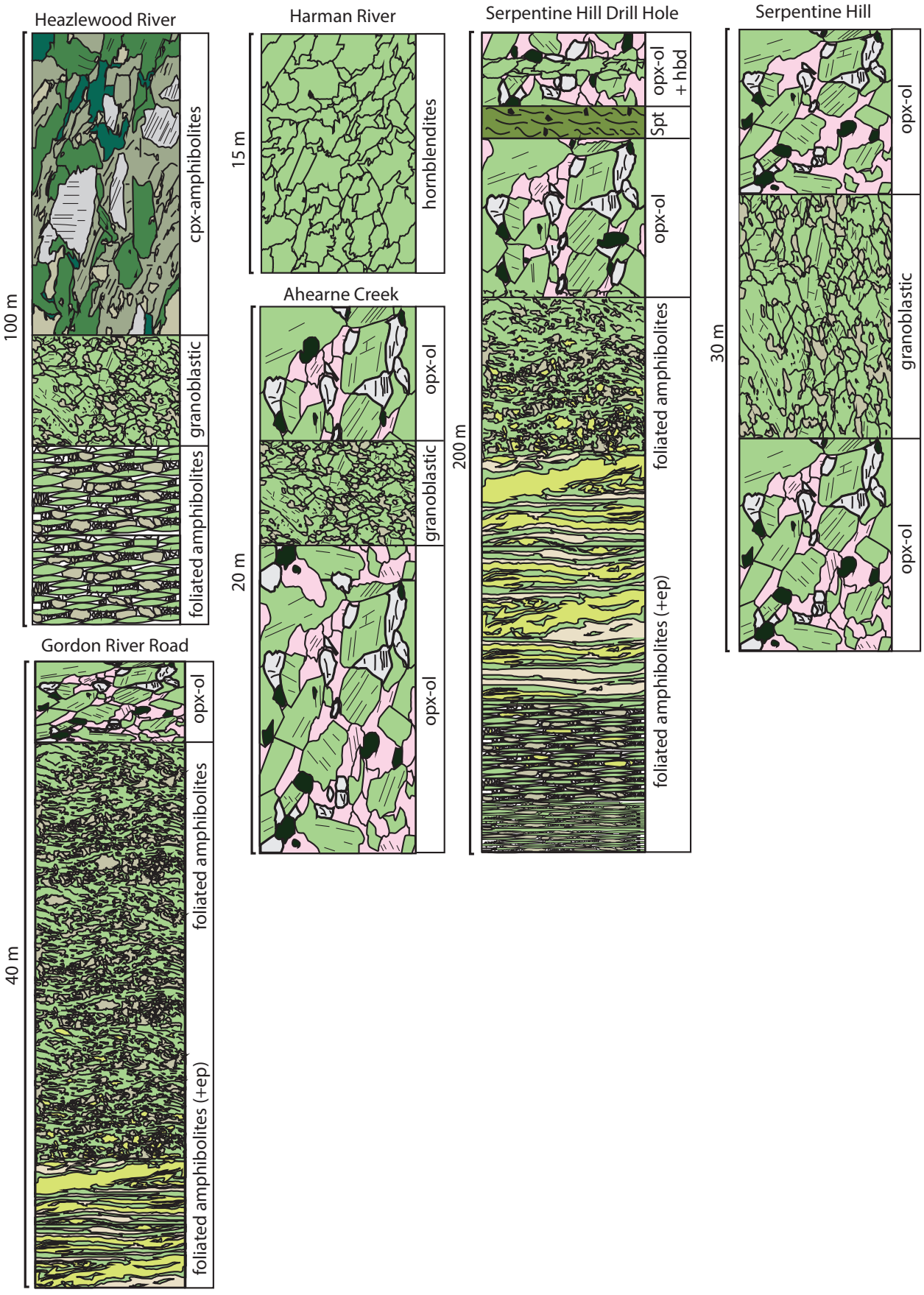

Figure 6.4: Schematic lithological logs for exposures of the Tasmanian metamorphic sole. Textural types shown schematically and labeled on side of logs. Hbd = hornblendite, Spt = serpentinite, ep = epidote.

The Heazlewood River complex exposure is unique in that it lacks opx–ol amphibolites and instead has cpx-amphibolites in the top parts of the sole. Similar to other exposures, the lower parts of the Heazlewood River complex metamorphic sole are dominated by foliated amphibolites.

6.6 Geochemistry

6.6.1 Major elements

The representative major and trace element data of all textural types of amphibolites, including samples from each of the metamorphic sole locations are summarised in Table 6.1. Given the complex syn- and post-metamorphic history of the amphibolites, both major and trace element data are utilized to investigate the geochemistry of the metamorphic sole protoliths.

The SiO_2 (44.26%–45.18%) and MgO (17.98%–21.52%) contents of the opx–ol amphibolites are typical of picro-basalts or cumulate rocks. The opx–ol amphibolites are also characterised by generally low TiO_2 (0.12%–0.58%), K_2O (0.03%–0.11%), and Na_2O (0.82%–1.72%) with high Ni (799–1414 ppm) and Cr (2179–2757 ppm). All remaining amphibolite types have basaltic SiO_2 contents (44.39%–48.02%) with the foliated amphibolites generally having the highest SiO_2 values (46.93–48.02%). On major element variation diagrams (Fig. 6.5), the amphibolites define generally smooth trends characterised by increasing FeO*, Al_2O_3, TiO_2, Na_2O, and K_2O and decreasing Cr_2O_3 with decreasing Mg# (MgO/ MgO + FeO* × 100) from the opx–ol amphibolites (highest Mg#), through the granoblastic amphibolites and hornblendites, followed by the foliated amphibolites and the cpx–amphibolites (lowest Mg#).

6.6.2 Trace elements

The trace element geochemistry of the various types of amphibolite are summarised on chondrite normalized REE plots (Fig. 6.6), and spider diagrams normalised to N-MORB (Fig. 6.7). The opx–ol amphibolites have strongly LREE-depleted patterns ($Ce/Lu_{[N]}$ = 0.06–0.23). The remaining amphibolite types can be separated into two groups based on their REE patterns. The granoblastic and cpx–amphibolites have LREE-depleted patterns similar to that of N-MORB (Sun and Mcdonough, 1989) whereas the hornblendites and foliated amphibolites have LREE-enriched patterns ($Ce/Sm_{[N]}$ = 1.07–1.55) and variably developed negative Eu anomalies indicative of plagioclase fractionation.

On N-MORB normalised trace element spider diagrams (Fig. 6.7), the opx–ol amphibolites are strongly depleted in REE and high field strength elements (HFSE; Ti, Zr, Hf, and Y) and have strong enrichments in fluid mobile elements such as Cs, Rb, Ba, U, K, Pb, which are tens, to hundreds of times higher than typical N-MORB. The opx–ol amphibolites display variably developed negative Ti anomalies and half the samples contain large negative Nb anomalies (Fig. 6.7). The trace element patterns of a retrogressed opx–ol amphibolite sample (2SH5, dashed line Figs. 6.6, 6.7) are similar to those of the fresh opx–ol amphibolite samples. The remaining amphibolite types have depleted REE

Table 6.1: Major and trace element geochemistry of metamorphic sole amphibolites from western Tasmania

Textural Type	opx-ol amphibolite							Granoblastic amphibolite			Hornblendite		Foliated amphibolite			cpx-amphibolite		
Location	GRR	AH	AH	AH	AH	SH	SH	AH	AH	AH	HR	HR	GRR	HZ	HZ	HZ	HZ	HZ
Sample Name	88SG1	A2*	A5	38850a/b	W5	SH3*	2SH5	A4*	W8	2SH2*	W9	W1*	88SG7	71339	H9	H11	H11-2	H12
SiO_2	45.04	44.52	45.18	44.26	44.76	44.85	44.71	46.14	46.06	44.39	45.19	45.24	48.02	47.25	46.93	46.18	44.17	47.17
TiO_2	0.15	0.58	0.14	0.35	0.12	0.3	0.35	0.53	0.62	0.38	0.55	0.5	0.92	0.63	1.57	1.04	1.07	1.03
Al_2O_3	8.78	11.59	10.04	11.37	8.88	11.19	11.40	13.97	14.81	12.23	12.31	12.33	12.88	13.28	15.13	15.27	15.67	14.18
Fe_2O_3*	8.56	10.34	9.60	10.13	9.62	10.16	9.43	10.45	11.18	10.63	10.78	10.73	12.52	11.34	13.06	13.04	14.07	13.95
MnO	0.12	0.15	0.17	0.16	0.21	0.28	0.18	0.17	0.20	0.2	0.19	0.18	0.20	0.20	0.21	0.16	0.28	0.22
MgO	21.18	18.82	21.26	19.76	21.52	17.98	18.99	10.83	9.72	17.36	15.64	16.21	9.34	11.22	5.6	8.09	8.03	7.6
CaO	9.89	9.02	8.26	9.44	8.34	9.48	9.27	12.43	10.17	9.56	11.05	10.39	10.44	9.97	10.16	10.68	10.82	10.6
Na_2O	0.98	1.44	0.82	1.06	0.87	1.72	1.04	2.16	1.61	2.12	1.46	1.37	2.92	2.34	4.01	2.64	2.34	2.75
K_2O	0.06	0.06	0.03	0.04	0.03	0.11	0.05	0.3	1.57	0.13	0.09	0.21	0.27	0.55	0.78	0.92	0.93	1.1
P_2O_5	0.01	0.03	0.01	0.01	0.01	0.02	0.01	0.03	0.05	0.02	0.03	0.05	0.05	0.06	0.16	0.05	0.08	0.11
LOI	4.75	3.76	4.05	2.95	5.19	3.49	4.16	2.73	3.85	3.12	2.58	2.84	2.57	2.87	2.04	1.58	2.36	1.62
Total	99.52	100.31	99.56	99.53	99.55	99.58	99.59	99.74	99.85	100.14	99.87	100.05	100.12	99.70	99.65	99.65	99.82	100.3
Cr	2520	2309	2721	2353	2904	2179	2339	632	922	2015	1556	1647	294	1127	116	248	288	321
Ni	1336	946	1113	1457	1291	799	1482	238	2656	738	725	604	491	656	41	122	395	76
Cs	0.74		3.48	0.36/0.39	0.74		0.31		3.13		0.11		0.10	0.29			0.71	
Rb	1.78		2.33	0.92/0.97	1.24		0.91		54.05		1.17		3.11	13.00			23.65	
Ba	19.84		5.50	5.47/5.20	6.97		9.28		1146.94		19.5		54.20	159.46			353.69	
Th	0.16		0.01	0.03/0.03	0.02		0.05		0.10		0.56		0.64	1.40			0.18	
U	0.09		0.01	0.12/0.06	0.02		0.03		0.05		0.11		0.13	0.37			0.22	
Nb	0.28		0.06	0.46/0.54	0.11		0.90		1.57		4.96		4.56	3.97			1.99	
Ta	0.04		0.02	0.03/0.03	0.01		0.05		0.09		0.35		0.36	0.28			0.15	
Ce	0.83		0.22	0.78/0.74	0.33		1.25		3.82		9.01		9.90	11.98			5.20	
Pb	3.96		1.12	1.37/1.41	1.83		1.52		18.77		1.31		2.33	10.62			4.72	
Pr	0.10		0.06	0.16/0.16	0.04		0.22		0.58		1.20		1.43	1.57			0.75	
Sr	21.39		22.12	33.29/32.32	45.36		32.86		393.86		55.76		25.93	81.04			206.88	
Nd	0.56		0.36	1.15/1.87	0.29		1.43		3.18		5.39		6.75	6.72			4.55	
Zr	7.21		5.72	14.62/14.50	4.36		15.65		23.92		42.68		57.72	48.26			46.14	
Hf	0.21		0.15	0.49/0.49	0.13		0.43		0.81		1.19		1.53	1.32			1.47	
Sm	0.30		0.26	0.83/0.76	0.16		0.77		1.40		1.62		2.31	1.93			2.20	
Eu	0.13		0.13	0.38/0.35	0.10		0.35		0.59		0.62		0.78	0.65			0.89	
Gd	0.66		0.62	1.64/1.68	0.46		1.51		2.53		2.46		2.84	2.67			3.72	
Tb	0.13		0.12	0.33/0.32	0.09		0.28		0.47		0.45		0.51	0.49			0.68	
Dy	1.22		1.0	2.52/2.42	0.88		2.21		3.47		3.14		3.68	3.54			5.00	
Y	7.71		7.01	14.52/14.22	5.73		13.13		21.02		16.98		21.35	20.57			27.90	
Ho	0.29		0.26	0.58/0.55	0.24		0.51		0.78		0.67		0.80	0.78			1.06	
Er	0.90		0.90	1.70/1.66	0.69		1.47		2.43		1.95		2.50	2.35			3.22	
Tm	0.14		0.14	0.25/0.24	0.12		0.22		0.35		0.29		0.33	0.35			0.43	
Yb	1.01		0.90	1.62/1.56	0.74		1.47		2.34		1.81		2.36	2.25			2.87	
Lu	0.16		0.17	0.26/0.26	0.13		0.23		0.35		0.28		0.37	0.35			0.45	

*Major element data from Lewis 1991.
Locations: GRR= Gordon River Road, AH= Ahearne Creek (Wilson River Complex), SH= Serpentine Hill Complex, HR=Harman River (Wilson River Complex), HZ= Heazlewood River Complex.

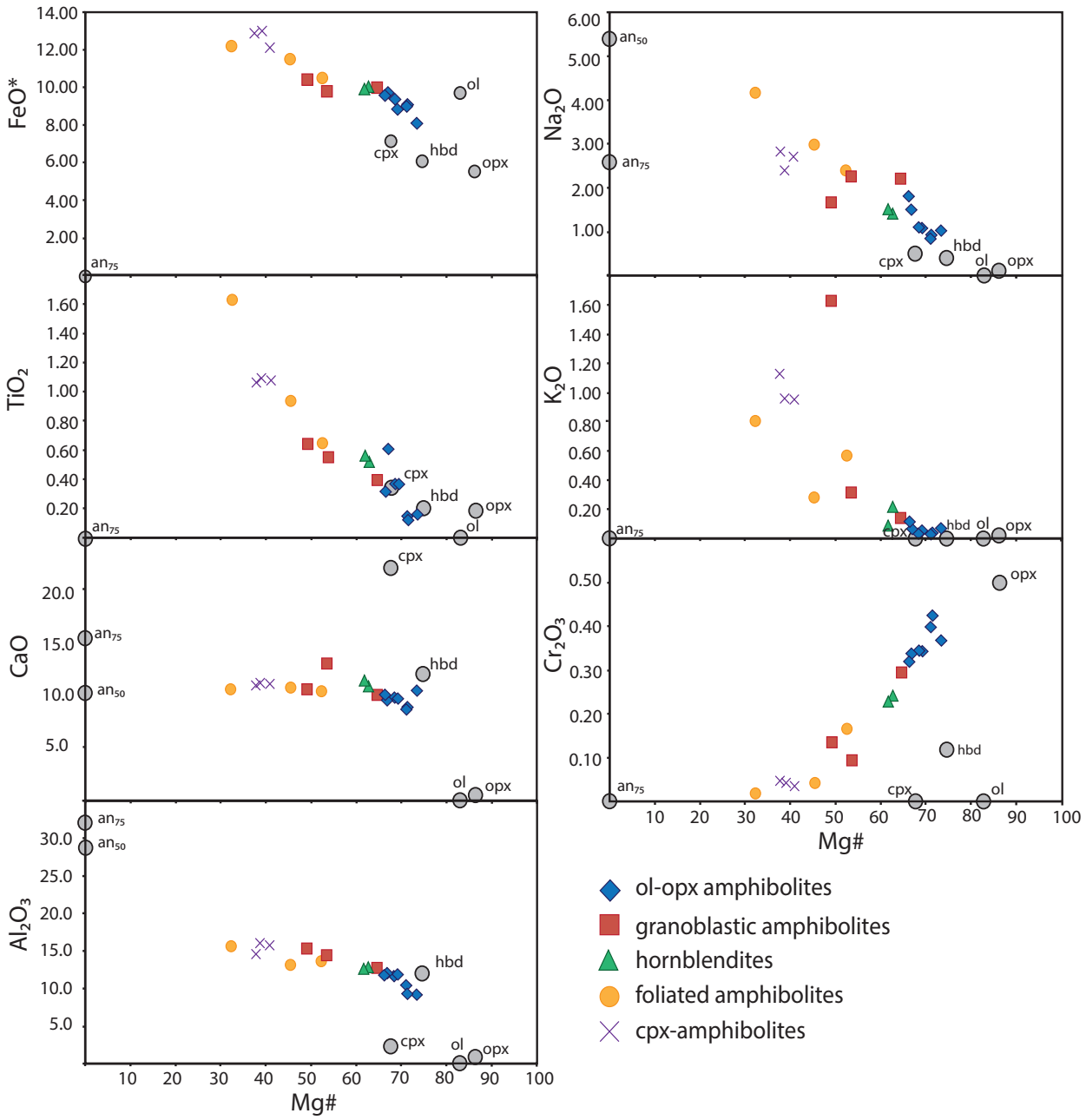

Figure 6.5: Major element variation diagrams plotting major elements (in weight %) against Mg# (Mg + Fe/Mg × 100). Symbols correspond to textural types of amphibolites outlined in petrography section. Also included are possible magmatic composition for olivine (ol), orthopyroxene (opx), clinopyroxene (cpx), plagioclase ($An_{50, 75}$) and a representative hornblende (hbd) composition from a opx-ol amphibolite.

and HFSE contents relative to N-MORB and strong enrichment in fluid mobile elements. Negative Ti anomalies are present in the granoblastic amphibolites and hornblendites and one of the foliated amphibolite samples (88SG7). The hornblendites, foliated amphibolites, and cpx–amphibolites contain negative Nb anomalies, which are absent from the granoblastic amphibolite pattern.

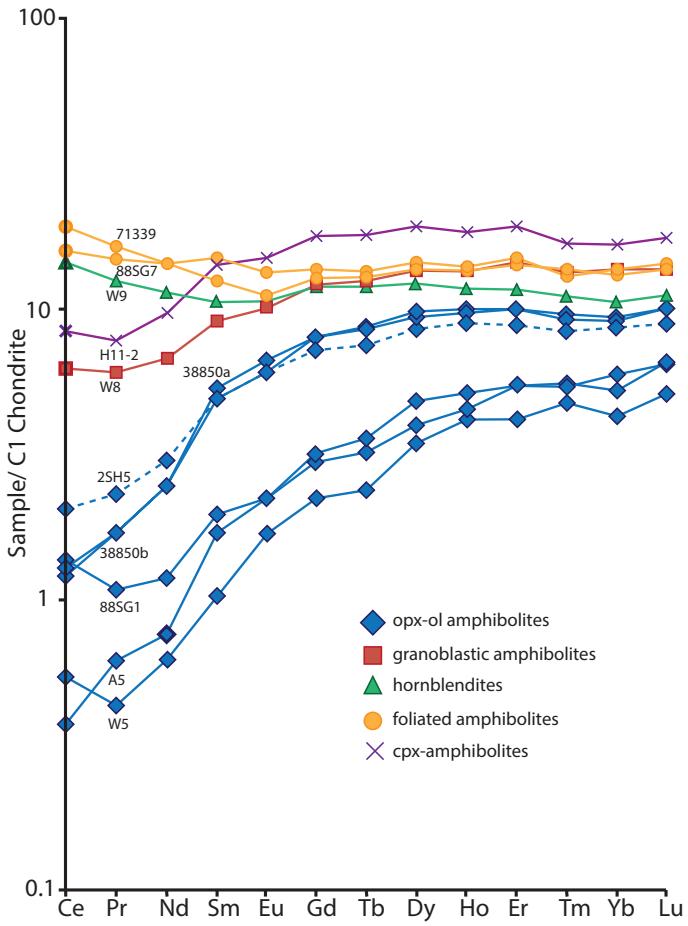

Figure 6.6: REE patterns for various textural types of metamorphic sole amphibolites. Data normalised to C1 chondrite of Sun and Mcdonough (1989). Dashed line represents REE pattern for a retrogressed opx-ol amphibolite sample.

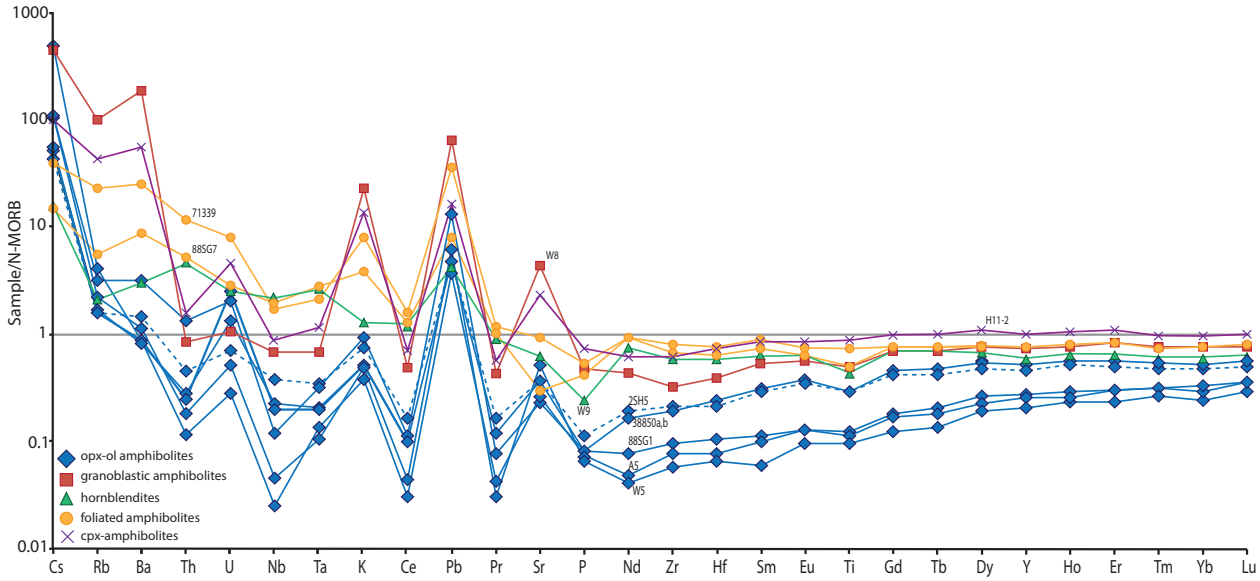

Figure 6.7: N-MORB normalised trace element spider diagram for various textural types of metamorphic sole amphibolites. Dashed line represents trace element pattern for a retrogressed opx-ol amphibolite sample. Diagram constructed using N-MORB normalization factors of Sun and Mcdonough (1989).

6.6.3 Spinel chemistry

The TiO_2 and Al_2O_3 contents of 43 analyses of spinel grains from two samples of opx–ol amphibolite (2SH5 = retrogressed, A5 = fresh) are plotted in Fig. 6.8 to assess the tectonic affinities of the protolith following Kamenetsky et al. (2001). The cores of spinels from both samples are characterised by high Cr_2O_3 (31%–50%), low TiO_2 (~0.2%), and low Al_2O_3 (~15%) contents. The chemical profiles across spinels from sample A5 show an increase in Al_2O_3 and decrease in TiO_2 reflecting an increase in the hercynite component towards the rim. The compositional profiles across spinel grains in sample 2SH5 show an increase in Al_2O_3 and TiO_2 towards aluminian titanomagnetite or titanian picotite compositions. The core composition of spinels from both samples plot in a tight cluster within the boninite/low-Ti arc tholeiite and suprasubduction zone peridotite fields (Fig. 6.8). The spinel compositions from the Neoproterozoic rift sequences in western Tasmania and from ultramafic rocks of the western Tasmanian ophiolite are also included in Fig. 6.8 to assess whether any of these igneous rocks could form the protoliths to the metamorphic sole amphibolites (discussed below).

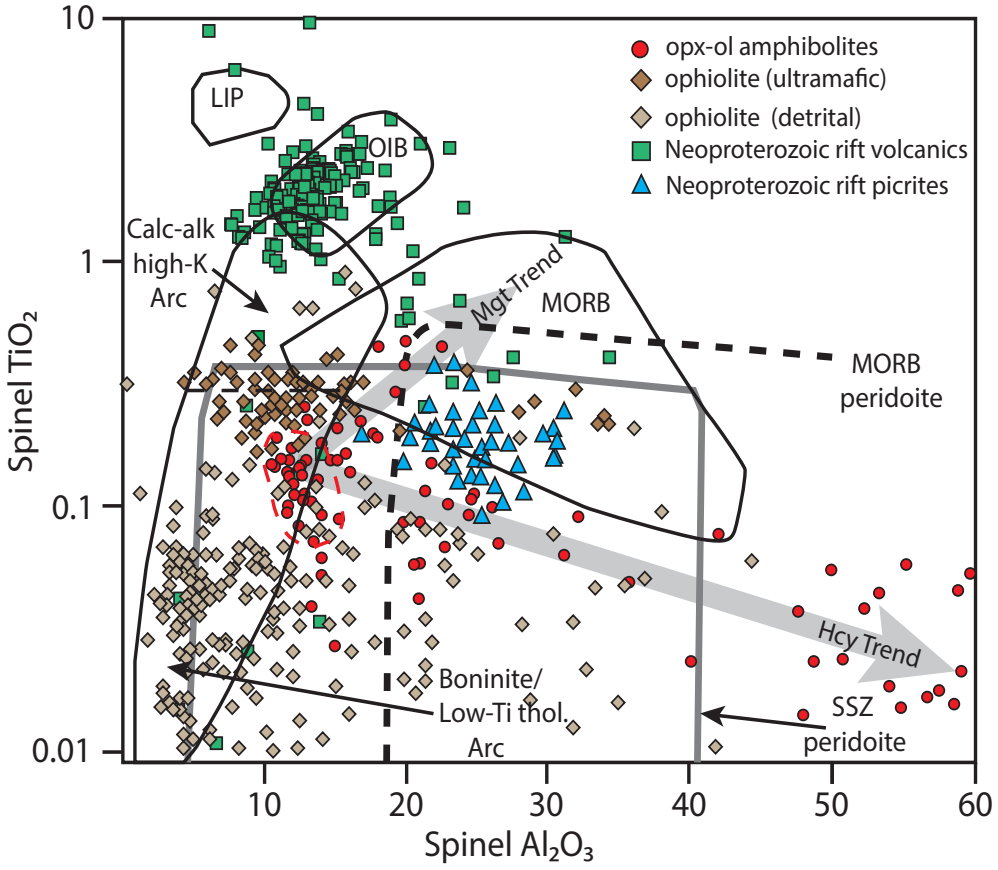

Figure 6.8: Al_2O_3 vs. TiO_2 in spinel tectonic discrimination diagram of Kamenetsky et al. (2001). Red dashed field defines the preferred compositional range of primary igneous spinel compositions from opx–ol amphibolites. Spinels from Neoproterozerzoic rift picrites, volcanics, and detrital spinels derived from the ophiolite are unpublished data of R. F. Berry. Spinel compositions from ultramafic rocks of the ophiolite are unpublished data of J. L. Everard. Two thick grey arrows show different core-rim compositional trends shown by spinels from opx-ol amphibolites (Hcy = hercynite-spinel (pleonaste) rims, Mgt = aluminian titanomagnetite-titanian picotite rims).

6.7 Metamorphism

The pressure–temperature (P–T) history of the metamorphic sole of the western Tasmanian ophiolite is investigated through integrating microtextural observations with conventional thermobarometery (summarised in Table 6.2) and pseudosection modelling. The primary aims of the metamorphic aspect of this study are to explore how the P–T conditions of formation vary between the different textural types of amphibolite and to gain insights into the tectonic setting in which the metamorphic sole formed. Representative mineral chemistries used in the thermobarometric calculations are shown in Table 6.3. A detailed assessment of the chemistry of all major phases present in the amphibolites is available in Appendix 6.4.

6.7.1 Conventional geothermometry

The opx–ol amphibolites contain the equilibrium assemblage olivine, spinel, orthopyroxene allowing application of the olivine–spinel and Al-in-orthopyroxene conventional geothermometers. Both these geothermometers were applied to several mineral pairs from a representative opx–ol amphibolite (sample A5). The Al-in-orthopyroxene thermometer gives temperatures of 770–850 °C, which are generally higher than the 715–770 °C temperature range calculated using the olivine–spinel thermometer.

All remaining types of amphibolite contain amphibole and plagioclase in textural equilibrium allowing application of the hornblende–plagioclase geothermometer (Holland and Blundy, 1994). The hornblende–plagioclase thermometer was applied to mineral pairs from representative samples of granoblastic amphibolite (2SH2), epidote-bearing foliated amphibolite (Z346), and cpx–amphibolite (H12) at pressures of 0.5 GPa and 1.0 GPa. Temperatures for the foliated amphibolite and cpx–amphibolite samples were calculated using the edenite-tremolite equilibria for quartz-bearing rocks, whereas the granoblastic amphibolite sample was assumed to be quartz-free. The foliated amphibolite records temperatures between 655 and 675°C (at 0.5 GPa), which are considerably lower than 775–805°C (at 0.5 GPa) range recorded by the cpx-amphibolite. The anorthite content of the plagioclase used in calculating temperatures for the foliated amphibolite are below the recommended limits for the thermometer, as such these results should be treated with caution. Temperatures could not be calculated for the granoblastic amphibolite sample due to the extremely low anorthite content of the plagioclase, which may reflect late-stage albite replacement.

6.7.2 Pseudosection modelling

Two amphibolites sampled from the upper part of the metamorphic sole directly in contact with the ophiolite were selected for pseudosection modelling in order to estimate the maximum P–T conditions attained by the metamorphic sole rocks. Sample A5 was chosen as it is representative of the opx–ol amphibolites that occur at the top of most exposures of the metamorphic sole and

Table 6.2: Summary of conventional thermobaromtery results for different textural types of metamorphic sole amphibolites.

opx-ol Amphibolites	Olivine-Spinel (Jianping et al., 1995) (°C)	Al-in-orthopyroxene (Witt-Eickschen & Seck 1991) (°C)
Average	740	815
Range	715–770	770–850
Granoblastic Amphibolites	No constraints—extremely low X_{An} in plagioclase and lack of quartz prevents hornblende-plagioclase thermometry	
Hornblendites	No constraints—No suitable mineral assemblages	
Foliated Amphibolites	Hornblende-plagioclase (Holland & Blundy 1994)	
	Temp at 0.5 GPa (°C)	Temp at 1.0 GPa (°C)
Average	665	645
Range	655–675	635–650
cpx-Amphibolites	Hornblende-plagioclase (Holland & Blundy 1994)	
	Temp at 0.5 GPa (°C)	Temp at 1.0 GPa (°C)
Average	795	760
Range	775–805	745–770

has minimal late-stage alteration phases. Sample H12 is typical of the cpx–amphibolites at the top of the Heazlewood River complex metamorphic sole and has only minor late-stage sericite alteration of plagioclase. Pseudosections were constructed using THERMOCALC v3.40 (Powell and Holland, 1988) using an updated version of the Holland and Powell (2011) dataset (ds62, February 2012). Both samples were modelled in the system Na_2O-CaO-FeO-MgO-Al_2O_3-SiO_2-H_2O-TiO_2-O (NCFMASHTO), with H_2O in excess. An assessment of the sensitivity of the predicted stability of the peak metamorphic assemblage to variations in the modelled water content is presented in Appendix 6.5 through construction of T-M(H_2O) sections for each sample. The mineral activity models used in the calculations were: amphibole (Diener and Powell, 2012, updated model from J. Diener pers. Comm. 2014), orthopyroxene (White et al., 2002, 2014), clinopyroxene (Diener and Powell, 2012, updated model from J. Diener pers. Comm. 2014), Spinel (Holland and Powell, 1998, 2011), garnet (White et al., 2007, 2014), plagioclase (Holland and Powell, 2003), epidote (Holland and Powell, 2011), ilmenite (White et al., 2000, 2014), olivine (Holland and Powell, 1998, 2011), and chlorite (White et al., 2014). A melt model suitable for mafic compositions is currently unavailable, therefore many of the high-temperature fields on both pseudosections should be considered metastable with respect to a silicate melt.

The choice of bulk rock Fe^{3+} content can have a dramatic effect on the predicted phase relations in pseudosection modelling, particularly for mafic compositions (e.g. Diener and Powell, 2010). To understand the effect that varying the Fe^{3+} content has on the mineral assemblages predicted by the pseudosections, T-XFe^{3+} (where $XFe^{3+}= Fe^{3+} / [Fe^{3+} + Fe^{2+}]$) sections have been constructed for each sample and are presented and discussed in Appendix 6.6. The pseudosections were constructing using the whole rock XRF data (Table 6.1). Mineral compositional isopleths are calculated for both pseudosections to aid in constraining the P–T history of the amphibolites. The compositional range of isopleths shown in Fig. 6.9a and b correspond to the range in mineral compositions measured in the given sample (Table 6.3, Appendix 6.4).

6.7.2.1 A5

The peak metamorphic assemblage of amphibole, orthopyroxene, olivine is stable over a wide P–T range from 700 to 1000 °C, 0.2–1.3 GPa (Fig. 6.9a). One shortcoming of the pseudosection constructed for sample A5 is the extensive stability field predicted for titanite (sphene), which is not observed as a peak metamorphic phase in any opx-ol amphibolite. The presence of titanite instead of spinel as the main TiO_2-bearing phase may result from the lack of a stabilizing chromium component in the available solution models for spinel. Despite this shortcoming, we consider spinel to be the stable TiO_2-bearing phase across the P–T window shown in Fig. 6.9a, which is consistent with microtextural observations. Fig. 6.9a is constructed assuming $XFe^{3+}= 0.15$ as this best replicates the measured XMg ($Mg/[Mg + Fe^{2+}]$) compositions for orthopyroxene within the peak metamorphic field. The peak P–T estimates for sample A5 have been refined by contouring the peak metamorphic assemblage field with isopleths covering the calculated range of Al on the M1 site of orthopyroxene; other compositional isopleths for orthopyroxene (e.g. XMg and Ca on M2) have similar steep P/T slopes and do not further refine peak pressures or temperatures. The P–T history of sample A5 is further explored by overlaying the diagram with the minimum, maximum, and average estimates from the Al-in-orthopyroxene and olivine-spinel conventional geothermometry results. The olivine–spinel temperature probably reflects resetting during cooling (*c.f.* Fabries, 1979).

6.7.2.2 H12

The pseudosection calculated for H12 suggests the peak assemblage of amphibole, clinopyroxene (diopside), plagioclase, ilmenite, and quartz is stable at 675–850 °C, 0.52–1.02 GPa (Fig. 6.9b). Fig. 6.9b is constructed assuming $XFe^{3+} = 0.10$ and is contoured with isopleths covering the calculated range of Al on the M2 site of amphibole. To further refine the P–T history of sample H12, Fig. 6.9b is overlain by the hornblende–plagioclase conventional geothermometry results.

Table 6.3: Representative mineral chemistries from different textural classes of metamorphic sole amphibolites.

Textural Class	opx-ol amphibolite					Granoblastic amphibolite		Foliated amphibolite				cpx-amphibolite		
Sample Name	A5					2SH3		Z346				H12		
Mineral	Amphibole	Orthopyroxene	Olivine	Chromite	Hercynite	Amphibole	Plagioclase	Amphibole	Plagioclase	Garnet	Epidote	Amphibole	Plagioclase	Clinopyroxene
SiO_2	48.15	54.80	39.56	0.09	0.04	44.07	67.68	43.40	67.23	36.62	37.71	44.88	54.81	51.01
TiO_2	0.19	0.02	0.05	0.13	0.00	1.09	0.00	1.15	0.03	0.13	0.14	0.90	0.05	0.54
Al_2O_3	11.82	3.22	0.01	11.62	58.33	10.40	19.85	11.08	19.96	19.17	23.53	9.48	28.88	3.68
Cr_2O_3	0.25	0.15	0.07	43.89	5.19	0.00	0.00	0.01	0.08	0.01	0.00	0.04	0.00	0.35
$Fe_2O_3^*$	4.25	0.12	0.00	10.87	2.87	5.74	0.27	3.74	0.11	0.00	12.30	3.09	0.24	0.92
FeO	2.19	11.52	17.18	27.04	18.94	13.71	0.00	12.72	0.00	13.4	0.93	14.67	0.00	8.55
MnO	0.13	0.29	0.28	0.38	0.14	0.31	0.00	0.62	0.01	19.57	0.54	0.29	0.00	0.30
MgO	18.18	29.84	43.58	3.84	14.51	9.91	0.00	10.91	0.01	2.35	0.01	10.49	0.00	12.92
CaO	11.91	0.43	0.03	0.00	0.00	11.13	0.29	11.87	0.33	8.03	23.20	11.90	10.53	21.11
Na_2O	1.28	0.00	0.00	0.00	0.00	1.28	10.93	1.14	10.57	0.01	0.00	1.46	5.42	0.55
K_2O	0.00	0.00	0.00	0.00	0.00	0.12	0.04	1.18	0.35	0.02	0.00	0.16	0.03	0.00
Totals	98.36	100.39	100.76	97.86	100.02	97.75	99.06	97.82	98.68	99.31	98.36	97.36	99.96	99.93
Oxygens	23	6	4	4	4	23	8	23	8	12	12.5	23	8	6
Si	6.69	1.93	0.10	0.00	0.00	6.57	2.98	6.47	2.96	2.98	3.00	6.71	2.47	1.91
Ti	0.02	0.00	0.00	0.00	0.00	0.12	0.00	0.13	0.00	0.01	0.01	0.10	0.00	0.02
Al	1.93	0.13	0.00	0.48	1.83	1.83	1.03	1.95	1.05	1.84	2.21	1.67	1.53	0.16
Cr	0.03	0.00	0.00	1.22	0.11	0.00	0.00	0.00	0.00	0.00	0.00	0.01	0.00	0.01
Fe^{3+}	0.44	0.00	0.00	0.29	0.06	0.64	0.01	0.42	0.00	0.00	0.74	0.35	0.01	0.03
Fe^{2+}	0.25	0.34	0.36	0.79	0.42	1.71	0.00	1.59	0.00	0.91	0.06	1.84	0.00	0.27
Mn	0.01	0.01	0.01	0.01	0.00	0.04	0.00	0.08	0.00	1.35	0.04	0.04	0.00	0.01
Mg	3.76	1.57	1.63	0.20	0.58	2.20	0.00	2.42	0.00	0.29	0.00	2.34	0.00	0.72
Ca	1.77	0.02	0.00	0.00	0.00	1.78	0.01	1.90	0.02	0.70	1.98	1.91	0.51	0.85
Na	0.34	0.00	0.00	0.00	0.00	0.37	0.93	0.33	0.92	0.00	0.00	0.42	0.47	0.04
K	0.00	0.00	0.00	0.00	0.00	0.02	0.00	0.22	0.02	0.00	0.00	0.03	0.00	0.00

* Cations calculated using AX (Holland 2005). Ferric iron estimates are those calculated by AX for all minerals except garnet and olivine where all iron is assumed to be Fe^{2+}.

6.8 Discussion

6.8.1 Protolith history

The distinctive textural and geochemical types of amphibolites suggest that protoliths of variable composition were juxtaposed in the formation of the metamorphic sole of the western Tasmanian ophiolite. We interpret the high Mg, Cr, and Ni contents of the opx-ol amphibolites to reflect an olivine- and chromite-bearing protolith. The CaO and Al_2O_3 contents of the opx–ol amphibolites (e.g. Fig. 6.5) suggest the protolith contained plagioclase and possibly clinopyroxene. We therefore interpret the protoliths to opx–ol amphibolites to be cumulates composed mainly of olivine, chromite, and plagioclase, however no relict igneous textures could be recognised in these rocks. A suprasubduction zone setting for the protoliths of the opx–ol amphibolites is inferred by the presence of negative Ti and Nb anomalies, enrichment in fluid mobile elements, and the presence of spinels with low TiO_2 and Al_2O_3 igneous cores— typical of spinels from suprasubduction zone magmas. The spinel geochemistry of the opx–ol amphibolites suggests these rocks were not derived from any of the known Neoproterozoic rift volcanic sequences in Tasmania; including the most primitive picritic lavas (Fig. 6.8).

Major element data including SiO_2, TiO_2, and Mg# for the remaining amphibolite textural types are consistent with derivation from typical basaltic protoliths. Although igneous textures may be expected to be highly modified or even mimicked by deformational and metamorphic processes, the fine–medium grain size of foliated amphibolites may reflect originally basaltic or doleritic protoliths— an interpretation supported by the preservation of apparent relict ophitic textures in these amphibolites (Fig. 6.3e). Similarly, the coarse-grained metamorphic clinopyroxene and ghosts of euhedral plagioclase grains in cpx-amphibolites may reflect originally coarse-grained doleritic or gabbroic textures (Fig. 6.3f, g).

The basaltic amphibolites (e.g. granoblastic amphibolites, hornblendites, foliated amphibolites, and cpx–amphibolites) have REE and HFSE contents less than typical N-MORB implying the protoliths were produced from an already depleted mantle source (Pearce and Stern, 2006). A depleted mantle source is also implied by the presence of negative Ti anomalies in 3 of the 5 basaltic amphibolite samples. Negative Nb anomalies in all basaltic amphibolites except the granoblastic amphibolite sample (W8) may reflect the presence of refractory pargasite or spinel during the generation of the protolith magmas (Bodinier et al., 1996, Tiepolo et al., 2000). The two distinct groups of basaltic amphibolites characterised by LREE-depletion (W8, H11-2) or LREE-enrichment (71339, 88SG7, W9) may represent differences in the degree of fractionation of compositionally similar parental melts rather than two groups of protoliths formed in different tectonic settings. The depleted REE patterns, negative Ti and Nb anomalies, and enrichment in fluid mobile elements displayed by the basaltic amphibolites is characteristic of magmas from suprasubduction settings where a depleted mantle source is re-melted by the addition of fluids derived from a subducting slab. We suggest that the most likely tectonic setting for the metamorphic sole protoliths is a back arc basin, where magma compositions are transitional between N-MORB and typical arc magmas (Pearce and Stern, 2006).

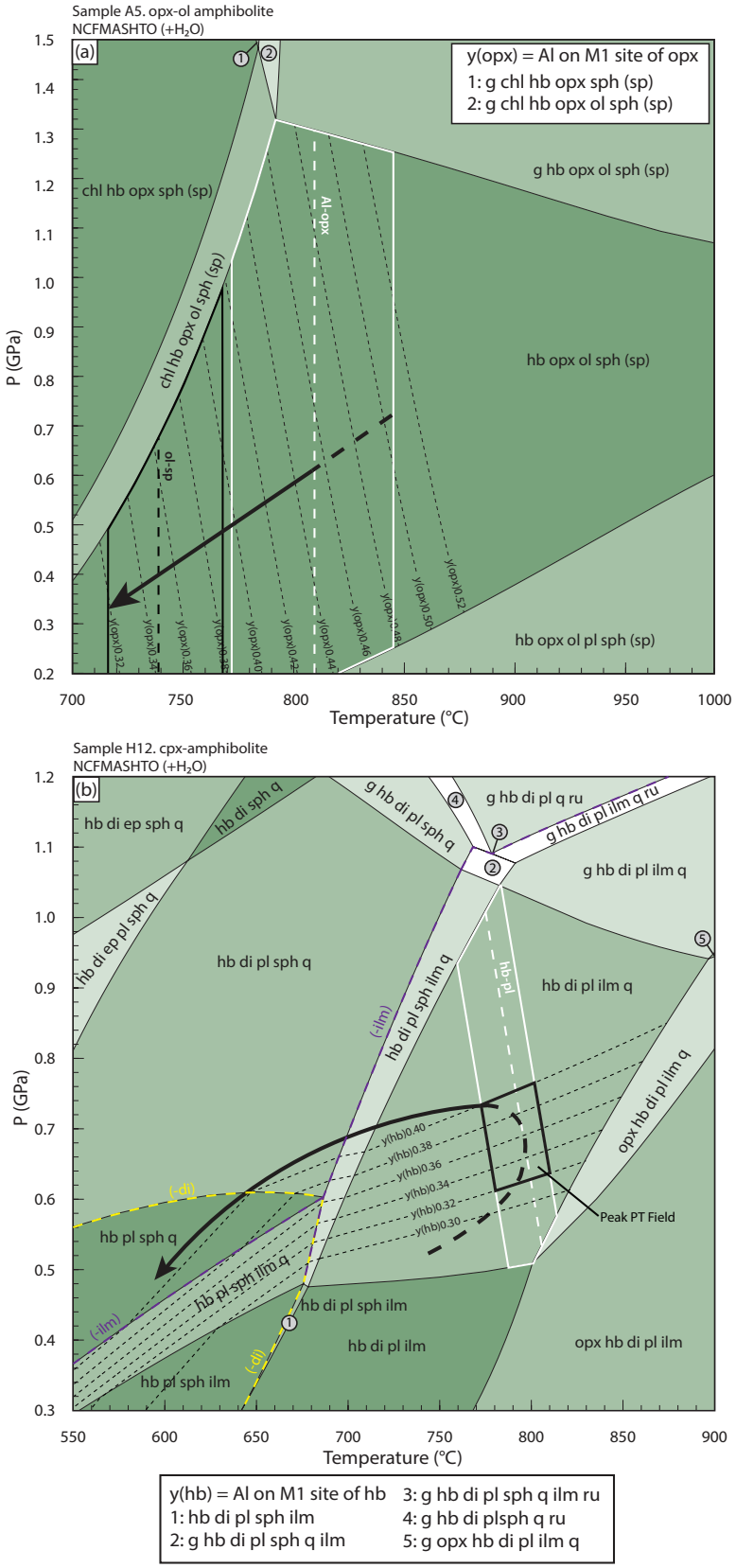

Figure 6.9: Pseudosections for amphibolites from the top of the Tasmanian metamorphic sole. (a) Pseudosection for opx–ol amphibolite (sample A5, Ahearne Creek) overlain by the range of temperatures from Al-in-orthopyroxene (Al–opx) and olivine-spinel (ol–sp) conventional thermometers. Dashed line in centre of ol-sp and Al-opx fields represents the average temperature calculated using these thermometers. Black arrow shows preferred retrograde P–T path. (sp) indicates the interpreted stability of spinel in each field instead of titanite (sph). (b) Pseudosection for cpx-amphibolite (sample H12, Heazlewood River) overlain by range of temperatures calculated with the hornblende–plagioclase (hb–pl) conventional thermometer. Thick dashed lines mark boundary between ilmenite-out (–ilm) and clinopyroxene-out (–di) fields. Black arrow shows preferred P–T path.

The subduction interface at which metamorphic soles form is a complex tectonic environment characterised by high-pressure and temperature metamorphic conditions and high fluid flux (e.g. Bebout, 2007). Formation in such an environment, combined with a complex post-metamorphic, history requires careful consideration of element mobility as a control on the geochemistry of the amphibolites. Post-magmatic alteration or metamorphic processes would be expected to produce significant scatter in the possible fractionation trends observed in the major element variation diagrams of the metamorphic sole amphibolites (Fig. 6.5). With the exception of K_2O and Na_2O, there is relatively little scatter in the major element trends in Fig. 6.5, suggesting that post-magmatic alteration have not significantly affected the compositions of the metamorphic sole protoliths. The similar abundances of the most fluid mobile elements for a retrogressed opx–ol amphibolite (2SH5) relative to fresh opx-ol amphibolite samples (A5, W5, 38850, 88SG1) further supports the interpretation that post-metamorphic alteration has not significantly redistributed elements in the amphibolites (Fig. 6.7). Our interpretation that the Tasmanian metamorphic sole amphibolites largely preserve their original geochemical affinities is consistent with the findings of Ghatak et al. (2012) who suggest that the geochemical signature of the protoliths to metamorphic sole rocks of the Feather River Ultramafic belt were largely preserved during metamorphism.

The trends observed on major element variation diagrams indicate that the protoliths of the various types of amphibolite are basaltic rocks affected by fractionation and possibly cumulate processes. The opx–ol amphibolites may represent olivine–plagioclase–chromite cumulates derived from compositionally similar magmas to those that produced the protoliths to the basaltic amphibolites (Fig. 6.5). Although a rigorous assessment of the petrogenesis of the metamorphic sole protoliths is beyond the scope of this paper, we note that varying degrees of plagioclase, olivine, and possibly clinopyroxene fractionation could produce the generally smooth major element trends in Fig. 6.5.

Possible fractionation trends are also observed in the REE and trace element spider plots where a systematic increase in the absolute abundance of REE and trace elements and a lessening of LREE-depletion is observed between the opx–ol amphibolites and the basaltic amphibolites. Alternatively, many of the major element trends in Fig. 6.5 are consistent with alteration trends from the basaltic amphibolites towards hornblende (e.g. hornblende metasomatism) to produce the opx–ol amphibolite compositions. While there is evidence for extensive mobility of some elements (e.g. Na and K), the trends in less mobile elements are compatible with igneous processes and we favour the interpretation that the protoliths to the metamorphic sole rocks were a suite of related igneous rocks that formed in a similar tectonic setting– possibly at the same spreading centre.

Based on their petrography and geochemistry, the protoliths of the metamorphic sole appear to define an inverted oceanic crustal sequence with cumulates and gabbros occupying the structurally higher parts of the sole and dolerites and basalts comprising the middle and lower parts of the sole. The protoliths defining this oceanic crustal sequence were likely formed at a back arc basin spreading ridge prior to being strongly deformed and metamorphosed at high temperature during assembly of the metamorphic sole.

6.8.2 Metamorphic history

The range of temperatures calculated by conventional geothermometry indicates that the metamorphic sole of the western Tasmanian ophiolite has an inverted metamorphic temperature gradient (Table 6.3). This temperature gradient coincides with changes in the textural type of amphibolites with the highest temperatures recorded by the opx–ol (850 °C) and granoblastic amphibolites (775 °C) at the top of the sole and lower temperatures of ~660 °C recorded by the foliated amphibolites from the lower parts of the metamorphic sole exposures.

Combining the conventional geothermometry results with pseudosection modelling provides additional constraints on the peak metamorphic conditions experienced by the sole amphibolites and allows a partial reconstruction of their prograde and retrograde metamorphic histories. The peak P–T conditions experienced by the opx–ol amphibolites are poorly constrained due to the large stability field of the peak metamorphic assemblage. However, the Al on M1 isopleths for orthopyroxene calculated in Fig. 6.9a suggest that the peak temperatures did not exceed ~ 875 °C, consistent with the results of the conventional Al-in-orthopyroxene geothermometer. The olivine–spinel geothermometer temperatures of ~700 °C may record a portion of the cooling path experienced by sample A5 due to the rapid Mg-Fe exchange rate between olivine and spinel, which often continues below the blocking temperature of other minerals (Fabries, 1979). The absence of pressure sensitive equilibria in the opx-ol amphibolites results in the pressure during all stages of the metamorphic history being poorly constrained to between ~0.2 and 1.3 GPa. We suggest peak pressures for sample A5 may have been similar to those experienced by sample H12 based on a similar position within the upper parts of the metamorphic sole.

The more restricted P–T stability fields for the mineral assemblages in sample H12 allow for a more refined evaluation of the metamorphic history of the highest grade parts of the metamorphic sole than is possible from the opx–ol amphibolites. The preferred peak temperature for sample H12 of ~795 °C is taken as the average hornblende–plagioclase geothermometer temperature (Table 6.2, Fig. 6.9b) and has an uncertainty of ± 40 °C associated with the calibration utilised in this study (Holland and Blundy, 1994). Based on the PT pseudosection modelling, the peak metamorphic assemblage for sample H12 is stable at pressures between ~0.5 and 1.0 GPa (Fig. 6.9b). Peak pressures for sample H12 may be further constrained by the calculated Al on M1 isopleths for amphibole for the bulk composition modelled in Fig. 6.9b, which plot between ~0.55–0.70 GPa on the PT pseudosection and may record a portion of the prograde metamorphic path. Alternatively, the amphibole compositions record a portion of the retrograde path below 650 °C. The isopleth compositions plotted in Fig. 6.9b were measured from the core of amphiboles that are not obviously retrograde (i.e. rimming clinopyroxene); therefore we favour the interpretation that these isopleths record a portion of the prograde metamorphic history approaching peak conditions.

The retrograde path experienced by sample H12 is constrained by microtextural observations including the replacement of clinopyroxene by amphibole (Fig. 6.3f) and the presence of titanite rims on ilmenite (Fig. 6.3h), suggesting a transition to ilmenite- and clinopyroxene-absent fields

during cooling. The decompression path shown in Fig. 6.9b is consistent with the anticlockwise P–T paths calculated for other metamorphic soles (e.g. Hacker, 1991; Hacker and Gnos, 1997; Searle and Cox, 1999; Guilmette et al., 2008), although our data are also permissible of a clockwise P–T path.

The P–T history of the amphibolites from the Tasmanian metamorphic sole shows many features typical of other well-studied metamorphic soles such as an inverted metamorphic gradient and peak granulite facies metamorphism. The metamorphic sole of the western Tasmanian ophiolite probably formed deep within a subduction zone with heat mainly sourced from the mantle section of the overriding plate (e.g. Jamieson, 1986; Hacker, 1991).

6.8.3 Implications for metamorphic sole formation and ophiolite emplacement

Although widely recognised as integral parts of many orogenic belts, the exact mechanisms responsible for the emplacement of ophiolites during collision remain enigmatic (see Agard et al., 2014 for a recent assessment). As subduction zones are intimately linked to the obduction process (e.g. Searle and Cox, 1999; Wakabayashi and Dilek, 2003; Maffione et al., 2015; Van Hinsbergen et al., 2015), metamorphic soles are a key source of information relating to the emplacement of ophiolites as they provide a unique record of the geodynamic setting in which subduction zones initiate. Attempts to understand the relationship between the initiation of subduction, the formation of metamorphic soles, and the emplacement of ophiolites into orogenic belts can generally be assigned to one of three models:

(1) Stern and Bloomer (1992) present the classical model for subduction initiation and ophiolite obduction involving the nucleation of a subduction zone at a transform boundary where younger, buoyant oceanic lithosphere is juxtaposed against older, denser oceanic lithosphere. Spreading in the fore arc above the new subduction zone produces crust with suprasubduction zone geochemical affinities. Following slab roll-back, the suprasubduction zone ophiolite is emplaced over the same subduction zone that it formed above. A key shortcoming of this model is that it cannot account for the formation of metamorphic soles because the plate interface should not be hot enough to produce a metamorphic sole if subduction initiates in old, cold oceanic crust (e.g. Hacker, 1990, 1991; Peacock et al., 1994).

(2) Shervais (2001) proposed a variant of the rollback model of Stern and Bloomer (1992) in which the subduction of a true mid-ocean ridge provides the necessary heat for the generation of a metamorphic sole. In the "ridge subduction" model the protoliths of the metamorphic sole are young basalts with MORB affinities.

(3) Wakabayashi and Dilek (2003) and Wakabayashi et al. (2010) suggest that the generation of suprasubduction zone ophiolites, the formation of metamorphic soles, and ophiolite obduction are all linked through the interactions between two subduction zones. In the "dual subduction zone" model, lithosphere with a suprasubduction zone affinity representing the future ophiolite is formed at a spreading centre above a subduction zone following the model of Stern and Bloomer (1992).

Ophiolite emplacement occurs over a second, later subduction zone that initiates near the axis of the spreading centre above the earlier subduction zone. A metamorphic sole derived from protoliths with suprasubduction zone geochemical affinities is produced in the second subduction zone as crust from the down-going slab comes into contact with the hot mantle section of the upper plate.

The formation of metamorphic soles during the initiation of subduction near a suprasubduction zone spreading axis is supported by thermal modelling that demonstrates that in order to reach the granulite facies conditions recorded in many metamorphic soles, both the upper and lower plates of the subduction system must be hot, and therefore relatively young (Hacker, 1990, 1991; Peacock et al., 1994). Further support for the dual subduction zone model comes from the analogue modelling of Boutelier et al. (2003), which demonstrates that the thermally weakened lithosphere of suprasubduction zone spreading centres are favourable sites for the initiation of new subduction zones.

Any model proposed for the tectonic evolution of the western Tasmanian ophiolite and the formation of its metamorphic sole must account for several key characteristics of the amphibolites identified in this study:

(1) Petrographic observations and geochemical data indicate that the protoliths to the metamorphic sole define an inverted oceanic crustal sequence with metamorphosed cumulates and gabbros at the top of the sole and metabasalts and metadolerites constituting the protoliths to the lower parts of the sole.

(2) The metamorphic sole has an inverted temperature gradient with granulite–upper amphibolite facies conditions in the upper parts of the sole passing down to epidote-amphibolite facies conditions towards the base.

(3) The protoliths of the metamorphic sole have suprasubduction zone affinities and probably formed in a back arc basin.

(4) Microstructures indicate a generally top-to-the-west sense of movement during formation of the metamorphic sole (Appendix 6.2).

We suggest that the dual subduction zone model is best able to account for the lithological, geochemical, and metamorphic characteristics of the metamorphic sole amphibolites presented in this study. The inverted oceanic crustal sequence exhibited by many metamorphic soles (e.g. Jamieson, 1986; Wakabayashi and Dilek, 2003) is difficult to explain with the ridge subduction model of Shervais (2001) as the first rocks accreted to the upper plate would be basalts forming the uppermost crust of the down going plate. A similar problem is encountered with the dual subduction zone model if the second subduction zone initiates directly at the axis of a spreading centre. Conceptually an inverted crustal sequence can be produced by viewing the nascent subduction zone as a lithospheric scale thrust initiated close to, but not directly at the spreading ridge axis. Maffione et al. (2015) and Van Hinsbergen et al. (2015) have recently proposed that inversion of oceanic detachment faults, which trend parallel to spreading centres, are important areas for the initiation of subduction zones and

for forming metamorphic soles. The initial movements on such detachment faults during inversion would bring oceanic lower crustal rocks (e.g. cumulates) of the subducting plate into contact with the mantle section of upper plate. Continual thrusting progressively brings gabbros, dolerites, and basalts into contact with the hanging wall thereby producing the inverted crustal sequence of the metamorphic sole. This model may also explain the inverted metamorphic temperature gradient observed in metamorphic soles as progressive accretion of material to the hanging wall results in a progressive cooling of this heat source (e.g. Hacker, 1991).

A key piece of evidence in favour of applying the dual subduction zone model for the generation and emplacement of the western Tasmanian ophiolite and the formation of its accompanying metamorphic sole is the back arc basin geochemical affinity of the metamorphic sole amphibolites. The formation of the protoliths of the metamorphic sole at a back arc basin spreading centre requires the presence of a pre-existing subduction zone in addition to the one in which the sole was formed (Wakabayashi et al., 2010). Kinematic indicators from the Tasmanian metamorphic sole indicate a general westward emplacement direction for the ophiolite that implies the subduction zone in which the metamorphic sole formed was east-dipping and located to the east of Tasmania in the Cambrian (e.g. Berry and Crawford, 1988). The polarity of the earlier subduction zone above which the back arc basin protoliths of the metamorphic sole rocks formed is poorly unconstrained but we favour a west-dipping scenario based on regional geology considerations (see below).

6.8.4 Geodynamic implications

The results of this study support a growing body of evidence demonstrating that metamorphic soles with suprasubduction zone protoliths are a relatively common feature of ophiolite complexes. Metamorphic soles derived from protoliths with suprasubduction zone affinities have now been described from many temporally and tectonically diverse orogenic belts (e.g. New Caledonia; Cluzel et al., 2012, the Yarlung-Zangbo suture zone; Guilmette et al., 2012, the Fransiscan complex; Wakabayashi et al., 2010, the Philippines; Encarnacion, 2004, and possibly Oman; Ishikawa et al., 2005). As the dual subduction zone model is best able to account for the presence of metamorphic soles derived from protoliths with suprasubduction zone affinities, the interaction between multiple subduction zones appears to have been an important mechanism for generating and emplacing suprasubduction zone ophiolites and forming metamorphic soles in a diverse range of geodynamic settings throughout Earth history (Wakabayashi et al., 2010). Indeed, debates on whether orogenic belts are constructed by a single subduction zone or are influenced by multiple subduction zones of variable polarity have been raised for many orogenic systems worldwide, including some classic localities such as the North American Cordillera (Moores, 1970; Saleeby, 1983), the Oman Mountains (Gray and Gregory, 2000; Searle et al., 2004), and notably the orogenic belt that forms the focus of this study— the Tasmanides (Collins, 2002; Aitchison and Buckman, 2012). The unique insights that metamorphic soles provide into the processes controlling subduction initiation and ophiolite emplacement therefore have important implications for understanding the processes by which ancient collisional belts such as the Ross–Delamerian Orogen are constructed.

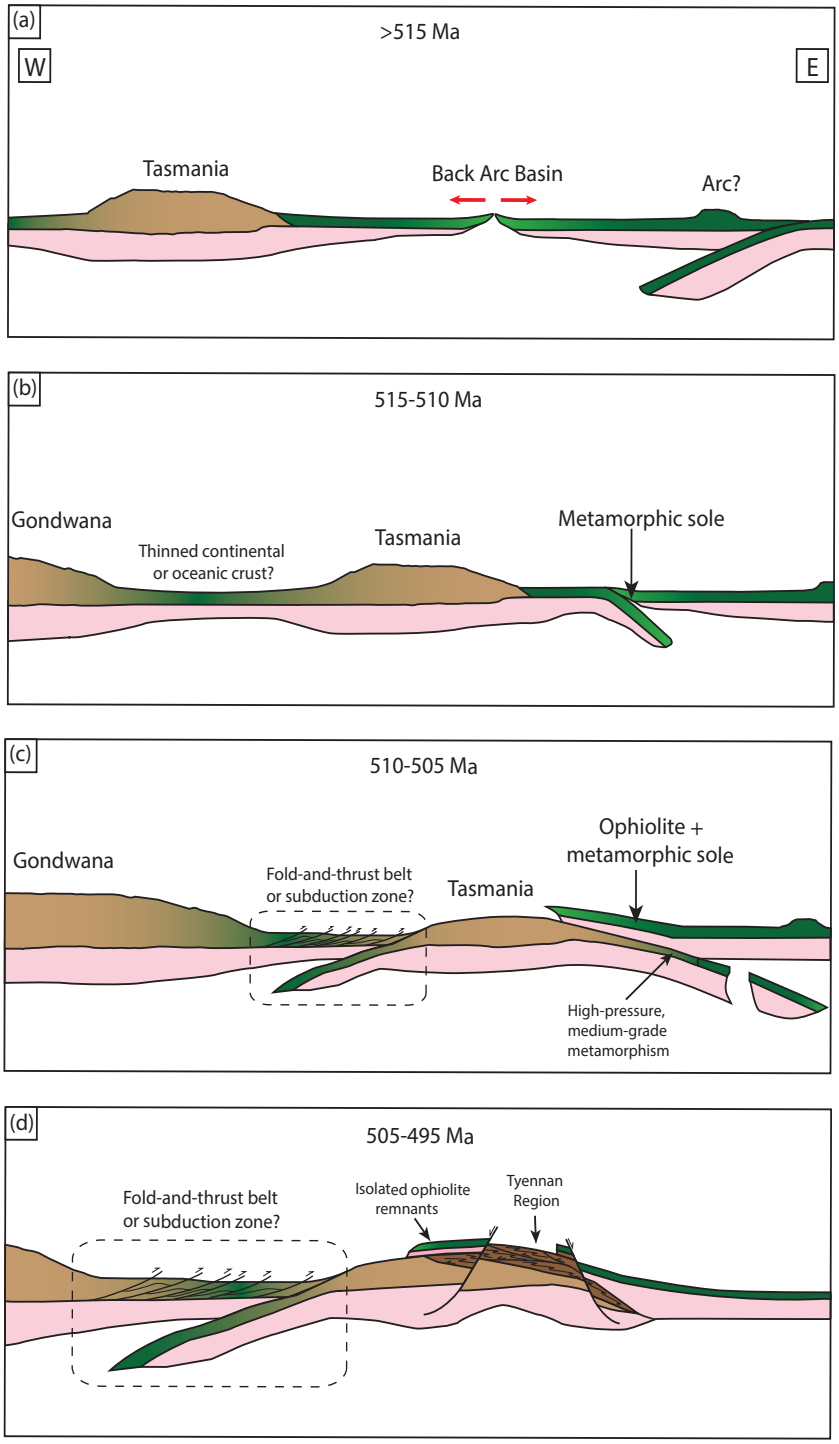

Figure 6.10: Geodynamic scenario proposed for Cambrian evolution of the Tasmania and the eastern margin of Gondwana. (a) Protoliths to the metamorphic sole form in a back arc basin above the west-dipping subduction zone developed along the eastern margin of Gondwana. Tasmania is a microcontinent outboard of the eastern margin of Gondwana. (b) A change in plate kinematics leads to collapse of the back arc basin to form a new east-dipping subduction zone east of Tasmania. The metamorphic sole to the western Tasmanian ophiolite forms in the new east-dipping subduction zone as hot, young back arc basin crust is accreted to the hanging wall of the upper plate. (c) The Tasmanian microcontinent is drawn into the east-dipping subduction zone initiating the main phase of the Tyennan Orogeny. Parts of the microcontinent are subducted and undergo high-pressure metamorphism coincident with obduction of the western Tasmanian ophiolite. Blocking of the east-dipping subduction zone drives convergence to be taken up west of Tasmania causing the eventual accretion of the Tasmanian microcontinent onto the eastern margin of Gondwana during the late Cambrian. (d) Deeply subducted crust (represented by the medium-grade metamorphic complexes) is rapidly exhumed following slab break-off and forms a complex stack of medium-grade metamorphic rocks interleaved with low-grade metamorphic rocks throughout the Tyennan Region. Erosion of ophiolite during uplift contributes to the isolation of the mafic-ultramafic complexes throughout Tasmania. Panel (d) modified from Chmielowski and Berry (2012).

The tectonic setting of the Ross–Delamerian Orogeny has generally been considered within the context of a single, long-lived, continent-dipping subduction zone (e.g. Cawood, 2005; Bradshaw et al., 2009; Boger, 2011; Cayley, 2011; Palmeri et al., 2011). The Cambrian tectonic history of Tasmania has been problematic in many tectonic models of East Gondwana due to the evidence of east-dipping subduction in Tasmania being synchronous with west-dipping subduction elsewhere along the margin. Previous attempts to incorporate Tasmania within the Cambrian tectonic setting of East Gondwana either: consider east-dipping subduction recorded in Tasmania to be representative of the subduction polarity elsewhere along the margin (Meffre et al., 2000; Crawford et al., 2003; Foster et al., 2005), move Tasmania outboard of the main west-dipping subduction zone and view the east-dipping subduction recorded in Tasmania as a local event (e.g. Cayley, 2011), or invoke west-dipping subduction in Tasmania (e.g. Foden et al., 2006; Rocchi et al., 2011).

Our new data from the metamorphic sole of the western Tasmanian ophiolite hint at the presence of two subduction zones east of Tasmania during the Cambrian. One possibility is that the earlier subduction zone (above which the protoliths to the metamorphic sole rocks formed in a back arc basin) was the same west-dipping subduction zone interpreted elsewhere along the Pacific margin of Gondwana at this time (Fig. 6.10a). East-dipping subduction in Tasmania may have initiated by collapse of a back arc basin east of Tasmania in response to a local blocking of the main west-dipping subduction zone or be related to a short-lived phase of contraction recorded elsewhere along the eastern margin of Gondwana at 515–510 Ma (Fig. 6.10b, Squire and Wilson, 2005; Paulsen et al., 2007). Several lines of evidence suggest that Tasmania is exotic with respect to the local basement of Gondwana and cannot simply have been attached to the Gondwanan margin during the Cambrian but instead was likely an outboard microcontinent (e.g. Berry et al., 2008; Cayley, 2011; Halpin et al., 2014; Mulder et al., 2015a). High-pressure metamorphism recorded in the medium-grade metamorphic complexes of Tasmania at 510 Ma (Fig. 6.1, Berry et al., 2007) likely reflects burial of the Tasmanian microcontinent as it was dragged into the east-dipping subduction zone (Fig. 6.10c, Chmielowski and Berry, 2012; Mulder et al., 2015b). Blocking of the east-dipping subduction zone may have caused convergence to be taken up west of Tasmania in the form of either a west-dipping subduction zone or a fold-and-thrust belt (Fig. 6.10c). Much of the area occupied by the hypothesised subduction zone or fold-and-thrust belt is now represented by the poorly known geology of the Western South Tasman Rise (Fig. 6.1, *c.f.* Berry et al., 1997), which was displaced southwards from west of Tasmania during the opening of the Southern Ocean (e.g. Royer and Rollet, 1997). The closing stages of the Tyennan Orogeny involved rapid uplift of the high-pressure metamorphic rocks, which were shedding detritus into sedimentary basins by *ca.* 505 Ma (Turner and Bottrill, 2001, see also Foster et al., 2005). Uplift of the deeply buried continental margin resulted in erosion and deformation of the overlying ophiolite sheet and may have contributed to the isolation of the ophiolite remnants as the various mafic-ultramafic complexes throughout Tasmania (Fig. 6.10d). Convergence west of Tasmania eventually incorporated the microcontinent into Gondwana, which may be recorded by east-verging folding in western Tasmania at *ca.* 495 Ma (Fig. 6.10c, d, Holm and Berry, 2002; Cayley, 2011).

The new geodynamic model presented here may help resolve the apparent along strike differences in subduction zone polarity associated with the Ross–Delamerian Orogeny by viewing the period of east-dipping subduction in Tasmania as a local event driven by collapse of a back arc basin inboard of the main west-dipping subduction zone developed elsewhere along this margin. We suggest a complex geodynamic environment existed along the Pacific margin of Gondwana during the Cambrian that was characterised by microcontinental fragments, marginal basins, and transient subduction zones of variable polarity inboard of a long-lived, west-dipping subduction zone — a tectonic setting similar to that of the modern southwest Pacific. Our findings reinforce the importance of considering the role of multiple subduction zones in generating metamorphic soles and emplacing ophiolites, which are key events associated with the construction of many orogenic belts.

6.9 Conclusions

Highly deformed amphibolites found structurally beneath the Cambrian ophiolite of western Tasmania show many features typical of metamorphic soles. Field relationships demonstrate that the metamorphic sole rocks occur in fault contact below the overlying mantle section of the western Tasmanian ophiolite and above Neoproterozoic rift sequences or Early Cambrian mélanges. The amphibolites of the metamorphic sole can be assigned to 5 distinct textural types including orthopyroxene–olivine–hercynite-bearing amphibolites, granoblastic amphibolites, hornblendites, fine-medium-grained foliated amphibolites, and clinopyroxene-bearing schistose amphibolites. At many exposures of the metamorphic sole, a systematic distribution of amphibolite textural types is observed with orthopyroxene–olivine–hercynite-bearing amphibolites occurring at the structurally highest levels and fine–medium-grained foliated amphibolites typically constituting the middle–lower parts of the sole. Mylonitic amphibolites preserve kinematic indicators recording a top-to-the-west emplacement direction of the western Tasmanian ophiolite, suggesting the metamorphic sole formed in an east-dipping subduction zone. Possible relict igneous textures are locally preserved in the amphibolites and suggest the protoliths included basalts, dolerites, and gabbros. Major and trace element geochemistry indicate that olivine-plagioclase-chromite-rich cumulates and rocks with typical basaltic compositions constitute the protoliths to the metamorphic sole amphibolites. We suggest these protoliths were a suite of related igneous rocks that likely formed in a back arc basin setting. The structurally highest parts of the metamorphic sole record peak granulite–upper amphibolite facies conditions of up to 875 °C, 0.8 GPa and record a cooling and decompression path through low-P amphibolite facies conditions. An inverted metamorphic temperature gradient is indicated by temperature estimates of ~660 °C recorded by epidote-bearing amphibolites in the middle–lower parts of the metamorphic sole. We suggest the protoliths to the metamorphic sole formed in a back arc basin above a west-dipping subduction zone that was active along the eastern margin of Gondwana during the Cambrian. The metamorphic sole protoliths were strongly deformed and metamorphosed in an east-dipping subduction zone that initiated near the spreading centre of the back arc basin. Our new geodynamic model suggests a complex southwest Pacific-style tectonic setting had developed along the Pacific margin of Gondwana during the Cambrian and highlights the importance of the role multiple subduction zones may play in the construction of orogenic belts.

6.10 Acknowledgements

We thank P. H. Olin and L. V. Danyushevsky for analytical assistance and advice on the geochemical aspects of this paper and J. L. Everard for providing unpublished spinel chemistry data. We also thank R. Powell for advice with the phase equilibria modelling and for providing THERMOCALC a-x datafiles. D.H. Green is thanked for insightful discussions on subduction zone processes. Two anonymous reviewers are thanked for their detailed and encouraging comments that greatly improved the final manuscript and Sanghoon Kwon for editorial handling. This research was funded by the ARC Centre of Excellence in Ore Deposits (CODES), School of Physical Sciences, University of Tasmania.

6. 11 References

Agard, P., Zuo, X., Funiciello, F., Bellahsen, N., Faccenna, C., Savva, D., 2014. Obduction: why, how and where. clues from analog models. Earth and Planetary Science Letters 393, 132–145.

Aitchison, J.C., Buckman, S., 2012. Accordion vs. quantum tectonics: insights into continental growth processes from the Paleozoic of Eastern Gondwana. Gondwana Research 22, 674–680.

Bebout, G.E., 2007. Metamorphic chemical geodynamics of subduction zones. Earth and Planetary Science Letters 260, 373–393.

Berry, R.F., 1989. Microstructural evidence for a westward transport direction during Middle Cambrian obduction in Tasmania. Geological Society of Australia Abstracts.

Berry, R.F., 2014. Cambrian tectonics. In: Corbett, K.D., Quilty, P.G., Calver, C.R. (Eds.), Geological Evolution of TasmaniaGeological Society of Australia Special Publication 24. Geological Society of Australia (Tasmania Division).

Berry, R.F., Crawford, A.J., 1988. The tectonic significance of Cambrian allochthonous mafic ultramafic complexes in Tasmania. Australian Journal of Earth Sciences 35, 523–533.

Berry, R.F., Meffre, S., Kreuzer, H., 1997. Metamorphic rocks from the southern margin of Tasmania and their tectonic significance. Australian Journal of Earth Sciences 44, 609–619.

Berry, R.F., Chmielowski, R.M., Steele, D.A., Meffre, S., 2007. Chemical U–Th–Pb monazite dating of the Cambrian Tyennan Orogeny, Tasmania. Australian Journal of Earth Sciences 54, 757–771.

Berry, R.F., Steele, D.A., Meffre, S., 2008. Proterozoic metamorphism in Tasmania: implications for tectonic reconstructions. Precambrian Research 166, 387–396.

Bodinier, J.L., Merlet, C., Bedini, R.M., Simien, F., Remaidi, M., Garrido, C.J., 1996. Distribution of niobium, tantalum, and other highly incompatible trace elements in the lithospheric mantle: the spinel paradox. Geochimica et Cosmochimica Acta 60, 545–550.

Boger, S.D., 2011. Antarctica— before and after Gondwana. Gondwana Research 19, 335–371.

Boudier, F., Ceuleneer, G., Nicolas, A., 1988. Shear zones, thrusts and related magmatism in the Oman ophiolite— initiation of thrusting on an oceanic ridge. Tectonophysics 151, 275–296.

Boutelier, D., Chemenda, A., Burg, J.P., 2003. Subduction versus accretion of intra-oceanic volcanic arcs: insight from thermo-mechanical analogue experiments. Earth and Planetary Science Letters 212, 31–45.

Bradshaw, J.D., Gutjahr, M., Weaver, S.D., Bassett, K.N., 2009. Cambrian intra-oceanic arc accretion to the austral Gondwana margin: constraints on the location of proto- New Zealand. Australian Journal of Earth Sciences 56, 587–594.

Brown, A.V., 1986. Geology of the Dundas-Mt. Lindsay-Mt. Youngbuck region. Geological Survey of Tasmania Bulletin 62, 221.

Brown, A.V., 1989. In: Burrett, C.F., Martin, E.L. (Eds.), Geology and Mineral Resources of TasmaniaSpecial Publication 15. Geological Society of Australia.

Brown, A.V., 1991. Revocation report on the Melba Flats Exempt Area, SR 1987, No 216 of 11 km2. Division of Mines and Mineral Resources Report 1991/10. Tasmania Depart- ment of Resources and Energy.

Calver, C.R., Everard, J.L., Berry, R.F., Bottrill, R.S., Seymour, D.B., 2014. Proterozoic Tasmania. In: Corbett, K.D., Quilty, P.G., Calver, C.R. (Eds.), Geological Evolution of Tasmania Geological Society of Australia Special Publication 24. Geological Society of Australia (Tasmania Division).

Cawood, P.A., 2005. Terra Australis Orogen: Rodinia breakup and development of the Pacific and Iapetus margins of Gondwana during the Neoproterozoic and Paleozoic. Earth-Science Reviews 69, 249–279.

Cayley, R.A., 2011. Exotic crustal block accretion to the eastern Gondwanaland margin in the Late Cambrian-Tasmania, the Selwyn Block, and implications for the Cambrian-Silurian evolution of the Ross, Delamerian, and Lachlan orogens. Gondwana Research.

Chmielowski, R.M., Berry, R.F., 2012. The Cambrian metamorphic history of Tasmania: the metapelites. Australian Journal of Earth Sciences 59, 1007–1019.

Cluzel, D., Jourdan, F., Meffre, S., Maurizot, P., Lesimple, S., 2012. The metamorphic sole of New Caledonia ophiolite: Ar-40/Ar-39, U–Pb, and geochemical evidence for subduction inception at a spreading ridge. Tectonics 31.

Collins, W.J., 2002. Nature of extensional accretionary orogens. Tectonics 21. Crawford, A.J., Berry, R.F., 1992. Tectonic implications of Late Proterozoic-Early Palaeozoic igneous rock associations in western Tasmania. Tectonophysics 214, 37–56.

Crawford, A.J., Meffre, S., Symonds, P.A., 2003. 120 to 0 Ma Tectonic evolution of the southwest Pacific and analgous geological evolution of the 600 to 220 Ma Tasman Fold Belt System. In: Hillis, R., Müller, R.D. (Eds.), The Evolution and Dynamics of the Australian Plate. Geological Society of Australia Special Publication 22 and Geological Society of America Special Paper 372.

Diener, J.F.A., Powell, R., 2010. Influence of ferric iron on the stability of mineral assemblages. Journal of Metamorphic Geology 28, 599–613.

Diener, J.F.A., Powell, R., 2012. Revised activity-composition models for clinopyroxene and amphibole. Journal of Metamorphic Geology 30, 131–142.

Encarnacion, J., 2004. Multiple ophiolite generation preserved in the northern Philippines and the growth of an island arc complex. Tectonophysics 392, 103–130.

Fabries, J., 1979. Spinel–olivine geothermometry in peridotites from ultramafic complexes. Contributions to Mineralogy and Petrology 69, 329–336.

Flottmann, T., Gibson, G.M., Kleinschmidt, G., 1993. Structural continuity of the Ross and Delamerian orogens of Antarctica and Australia along the margin of the paleo- Pacific. Geology 21, 319–322.

Foden, J., Elburg, M.A., Dougherty-Page, J., Burtt, A., 2006. The timing and duration of the Delamerian orogeny: correlation with the Ross Orogen and implications for Gondwana assembly. Journal of Geology 114, 189–210.

Foster, D.A., Gray, D.R., Spaggiari, C., 2005. Timing of subduction and exhumation along the Cambrian East Gondwana margin, and the formation of Paleozoic back arc basins. Geological Society of America Bulletin 117, 105–116.

Ghatak, A., Basu, A.R., Wakabayashi, J., 2012. Elemental mobility in subduction metamorphism: insight from metamorphic rocks of the Franciscan complex and the Feather River ultramafic belt, California. International Geology Review 54, 654–685.

Gibson, G.M., Morse, M.P., Ireland, T.R., Nayak, G.K., 2011. Arc–continent collision and orogenesis in western tasmanides: insights from reactivated basement structures and formation of an ocean-continent transform boundary off western Tasmania. Gondwana Research 19, 608–627.

Goscombe, B.D., 1991. Structural analysis of amphibolite zone, Serpentine Hill DDH No. 1 (SH1). Division of Mines and Mineral Resources - Report 1991/09. Tasmania Depart- ment of Resources and Energy.

Gray, D.R., Gregory, R.T., Miller, J.M., 2000. A new structural profile along the Muscat–Ibra transect, Oman: implications for emplacement of the Samail ophiolite. Geological So- ciety of America Special Paper 349, 513–523.

Guilmette, C., Hebert, R., Dupuis, C., Wang, C.S., Li, Z.J., 2008. Metamorphic history and geodynamic significance of high-grade metabasites from the ophiolitic melange beneath the Yarlung Zangbo ophiolites, Xigaze area, Tibet. Journal of Asian Earth Sciences 32, 423–437.

Guilmette, C., Hebert, R., Dostal, J., Indares, A., Ullrich, T., Bedard, E., Wang, C.S., 2012. Discovery of a dismembered metamorphic sole in the saga ophiolitic melange, South Tibet: assessing an Early Cretaceous disruption of the Neo-Tethyan supra-subduction zone and consequences on basin closing. Gondwana Research 22, 398–414.

Hacker, B.R., 1990. Simulation of the metamorphic and deformational history of the metamorphic sole of the Oman ophiolite. Journal of Geophysical Research-Solid Earth and Planets 95, 4895–4907.

Hacker, B.R., 1991. The role of deformation in the formation of metamorphic gradients — ridge subduction beneath the Oman ophiolite. Tectonics 10, 455–473.

Hacker, B.R., Gnos, E., 1997. The conundrum of Samail: explaining the metamorphic history. Tectonophysics 279, 215–226.

Halpin, J.A., Jensen, T., Mcgoldrick, P., Meffre, S., Berry, R.F., Everard, J.L., Calver, C.R., Thompson, J., Goemann, K., Whittaker, J.M., 2014. Authigenic monazite and detrital zircon dating from the Proterozoic Rocky Cape Group, Tasmania: links to the Belt- Purcell Supergroup, North America. Precambrian Research 250, 50–67.

Holland, T., 2005. AX-Activity-Composition Software. Department of Earth Sciences, University of Cambridge.

Holland, T.J.B., Blundy, J., 1994. Nonideal interactions in calcic amphiboles and their bearing on amphibole–plagioclase thermometry. Contributions to Mineralogy and Petrol- ogy 116, 433–447.

Holland, T.J.B., Powell, R., 1998. An internally consistent thermodynamic data set fro phases of petrological interest. Journal of Metamorphic Geology 16, 309–343.

Holland, T.J.B., Powell, R., 2003. Activity-composition relations for phases in petrological calculations: an asymmetric multicomponent formulation. Contributions to Mineralogy and Petrology 145, 492–501.

Holland, T.J.B., Powell, R., 2011. An improved and extended internally consistent thermodynamic dataset for phases of petrological interest, involving a new equation of state for solids. Journal of Metamorphic Geology 29, 333–383.

Holm, O.H., Berry, R.F., 2002. Structural history of the Arthur Lineament, northwest Tasmania: An analysis of critical outcrops. Australian Journal of Earth Sciences 49, 167–185.

Ishikawa, T., Fujisawa, S., Nagaishi, K., Masuda, T., 2005. Trace element characteristics of the fluid liberated from amphibolite-facies slab: inference from the metamorphic sole beneath the Oman ophiolite and implication for boninite genesis. Earth and Planetary Science Letters 240, 355–377.

Jamieson, R.A., 1986. P–T Paths from high-temperature shear zones beneath ophiolites. Journal of Metamorphic Geology 4, 3–22.

Jianping, L., Kormprobst, J., Vielzeuf, D., Fabries, J., 1995. An improved experimental calibartion of the olivine–spinel geothermometer. Chinese Journal of Geochemistry 14, 68–77.

Kamenetsky, V.S., Crawford, A.J., Meffre, S., 2001. Factors controlling chemistry of mag- matic spinel: an empirical study of associated olivine, Cr-spinel and melt inclusions from primitive rocks. Journal of Petrology 42, 655–671.

Lewis, R. 1991. Structure and metamorphic petrology of the Forth Metamorphic Complex. Bsc. (Hons) Thesis (unpubl.), University of Tasmania, Hobart.

Maffione, M., Thieulot, C., Van Hinsbergen, D.J.J., Morris, A., Plumper, O., Spakman, W., 2015. Dynamics of intraoceanic subduction initiation: 1. Oceanic detachment fault inversion and the formation of supra-subduction zone ophiolites. Geochemistry, Geophysics, Geosystems 16, 1753–1770.

Meffre, S., Berry, R.F., Hall, M., 2000. Cambrian metamorphic complexes in Tasmania: tectonic implications. Australian Journal of Earth Sciences 47, 971–985.

Meffre, S., Direen, N.G., Crawford, A.J., Kamenetsky, V., 2004. Mafic volcanic rocks on King Island, Tasmania: evidence for 579 Ma break-up in East Gondwana. Precambrian Research 135, 177–191.

Moore, D.H., Betts, P.G., Hall, M., 2013. Towards understanding the early Gondwanan margin in Southeastern Australia. Gondwana Research 23, 1581–1598.

Moores, E.M., 1970. Ultramafics and orogeny, with models of US Cordillera and Tethys. Nature 228, 837–842.

Moores, E.M., Macgregor, I.D., 1972. Types of alpine ultramafic rocks and their implica- tions for fossil plate interactions. Geological Society of America Memoirs 132, 209–224.

Moresi, L., Betts, P.G., Miller, M.S., Cayley, R.A., 2014. Dynamics of continental accretion. Nature 508, 245.

Mortenson, J.K., Gemmell, J.B., Mcneil, A.W., Friedman, R.M., 2015. High-precision U–Pb zircon chronostratigraphy of the Mount Read Volcanic Belt in Western Tasmania, Australia: implications for VHMS deposit formation. Economic Geology 110, 445–468.

Mulder, J.A., Halpin, J.A., Daczko, N.R., 2015a. Mesoproterozoic Tasmania: witness to the East Antarctica-Laurentia connection within Nuna. Geology 43, 759–762.

Mulder, J.A., Berry, R.F., Scott, R.J., 2015b. The structure and metamorphism of the Red Point Metamorphic Complex –A newly discovered high-pressure metamorphic complex from the south coast of Tasmania. Australian Journal of Earth Sciences 62 (8), 969–983.

Palmeri, R., Talarico, F.M., Ricci, C.A., 2011. Ultrahigh-pressure metamorphism at the lanterman range (Northern Victoria Land, Antarctica). Geological Journal 46, 126–136.

Paulsen, T.S., Encarnacion, J., Grunow, A.M., Layer, P.W., Watkeys, M., 2007. New age constraints for a short pulse in Ross orogen deformation triggered by East–West Gondwana suturing. Gondwana Research 12, 417–427.

Peacock, S.M., Rushmer, T., Thompson, A.B., 1994. Partial melting of subducting oceanic-crust. Earth and Planetary Science Letters 121, 227–244.

Pearce, J.A., Stern, R.J., 2006. Origin of back-arc basin magmas: trace element and isotope perspectives. Back-Arc Spreading Systems. Geological, Biological, Chemical, and Physical Interactions 166, 63–86.

Powell, R., Holland, T.J.B., 1988. An internally consistent dataset with uncertainties and correlations: 3. Applications to geobarometry, worked examples and a computer program. Journal of Metamorphic Geology 6, 173–204.

Rocchi, S., Bracciali, L., Di Vincenzo, G., Gemelli, M., Ghezzo, C., 2011. Arc accretion to the early Paleozoic Antarctic margin of Gondwana in Victoria Land. Gondwana Research 19, 594–607.

Royer, J.Y., Rollet, N., 1997. Plate-tectonic setting of the Tasmanian region. Australian Journal of Earth Sciences 44, 543–560.

Rubenach, M.J., 1973. The Tasmanian Ultramafic-Gabbro and Ophiolite Complexes (PhD) University of Tasmania.

Saleeby, J.B., 1983. Accretionary tectonics of the North-American Cordillera. Annual Review of Earth and Planetary Sciences 11, 45–73.

Searle, M., Cox, J., 1999. Tectonic setting, origin, and obduction of the Oman ophiolite. Geological Society of America Bulletin 111, 104–122.

Searle, M.P., Warren, C.J., Waters, D.J., Parrish, R.R., 2004. Structural evolution, metamorphism and restoration of the Arabian continental margin, Saih Hatat region, Oman Mountains. Journal of Structural Geology 26, 451–473.

Shervais, J.W., 2001. Birth, death, and resurrection: the life cycle of suprasubduction zone ophiolites. Geochemistry, Geophysics, Geosystems 2.

Spaggiari, C.V., Gray, D.R., Foster, D.A., 2003. Tethyan- and Cordilleran-type ophiolites of Eastern Australia: implications for the evolution of the tasmanides. Ophiolites in Earth History 218, 517–539.

Stern, R.J., Bloomer, S.H., 1621–1636. Subduction zone infancy: Examples from the Eocene Izu-Bonin-Mariana and Jurassic California arcs. Geological Society of America Bulletin 104, 1992.

Squire, R.J., Wilson, C.J.L., 2005. Interaction between collisional orogenesis and convergent-margin processes: evolution of the Cambrian proto-Pacific margin of East Gondwana. Journal of the Geological Society 162, 749–761.

Squire, R.J., Wilson, C.J.L., Dugdale, L.J., Jupp, B.J., Kaufman, A.L., 2006. Cambrian back arc- basin basalt in Western Victoria related to evolution of a continent-dipping subduction zone. Australian Journal of Earth Sciences 53, 707–719.

Sun, S.S., Mcdonough, W.F., 1989. Chemical and Isotopic Systematics of Oceanic Basalts: Implications for Mantle Composition and Processes. Geological Society Special Publication.

Tiepolo, M., Vannucci, R., Oberti, R., Foley, S., Bottazzi, P., Zanetti, A., 2000. Nb and Ta incorporation and fractionation in titanian pargasite and kaersutite: crystal-chemical constraints and implications for natural systems. Earth and Planetary Science Letters 176, 185–201.

Turner, N.J., Bottrill, R.S., 2001. Blue amphibole, Arthur Metamorphic Complex, Tasmania: composition and regional tectonic setting. Australian Journal of Earth Sciences 48, 167–181.

Turner, N.J., Black, L.P., Kamperman, M., 1998. Dating of Neoproterozoic and Cambrian orogenies in Tasmania. Australian Journal of Earth Sciences 45, 789–806.

Van Hinsbergen, D.J.J., Peters, K., Maffione, M., Spakman, W., Guilmette, C., Thieulot, C., Plumper, O., Gurer, D., Brouwer, F.M., Aldanmaz, E., Kaymakci, N., 2015. Dynamics of intraoceanic subduction initiation: 2. Suprasubduction zone ophiolite formation and metamorphic sole exhumation in context of absolute plate motions. Geochemistry, Geophysics, Geosystems 16, 1771–1785.

Wakabayashi, J., Dilek, Y., 2003. What constitutes ‘emplacement’ of an ophiolite?: mechanisms and relationship to subduction initiation and formation of metamorphic soles. Ophiolites in Earth History 218, 427–447.

Wakabayashi, J., Ghatak, A., Basu, A.R., 2010. Suprasubduction-zone ophiolite generation, emplacement, and initiation of subduction: a perspective from geochemistry, metamorphism, geochronology, and regional geology. Geological Society of America Bulletin 122, 1548–1568.

White, R.W., Powell, R., Holland, T.J.B., Worley, B., 2000. The effect of TiO2 and Fe2O3 on metapelitic assemblages at greenschist and amphibolite facies conditions: mineral equilibria calculations in the system K2O–FeO-MgO–Al2O3–SiO2–H2O–TiO2– Fe2O3. Journal of Metamorphic Geology 18, 497–511.

White, R.W., Powell, R., Clarke, G.L., 2002. The interpretation of reaction textures in Fe- rich metapelitic granulites of the Musgrave block, Central Australia: constraints from mineral equilibria calculations in the system K2O-FeO-MgO-Al2O3-SiO2-H2O- TiO2-Fe2O3. Journal of Metamorphic Geology 20, 41–55.

White, R.W., Powell, R., Holland, T.J.B., 2007. Progress relating to calculation of partial melting equilibria for metapelites. Journal of Metamorphic Geology 25, 511–527.

White, R.W., Powell, R., Holland, T.J.B., Johnson, T.E., Green, E.C.R., 2014. New mineral activity-composition relations for thermodynamic calculations in metapelitic systems. Journal of Metamorphic Geology 32, 261–286.

Williams, H., Smyth, W.R., 1973. Metamorphic aureoles beneath ophiolite suites and alpine peridotites— tectonic implications with West Newfoundland examples. American Journal of Science 273, 594–621.

Witt-Eickschen, G., Seck, H.A., 1991. Solubility of Ca and Al in Ortho-pyroxene from spinel peridotite— an improved version of an empirical geothermometer. Contributions to Mineralogy and Petrology 106, 431–439.

Yu, Z.S., Norman, M.D., Robinson, P., 2003. Major and trace element analysis of silicate rocks by XRF and laser ablation ICP-MS using lithium borate fused glasses: Matrix effects, instrument response and results for international reference materials. Geo- standards Newsletter— The Journal of Geostandards and Geoanalysis 27, 67–89.

Appendix 6.1: Locatility maps of metamorphic sole exposures

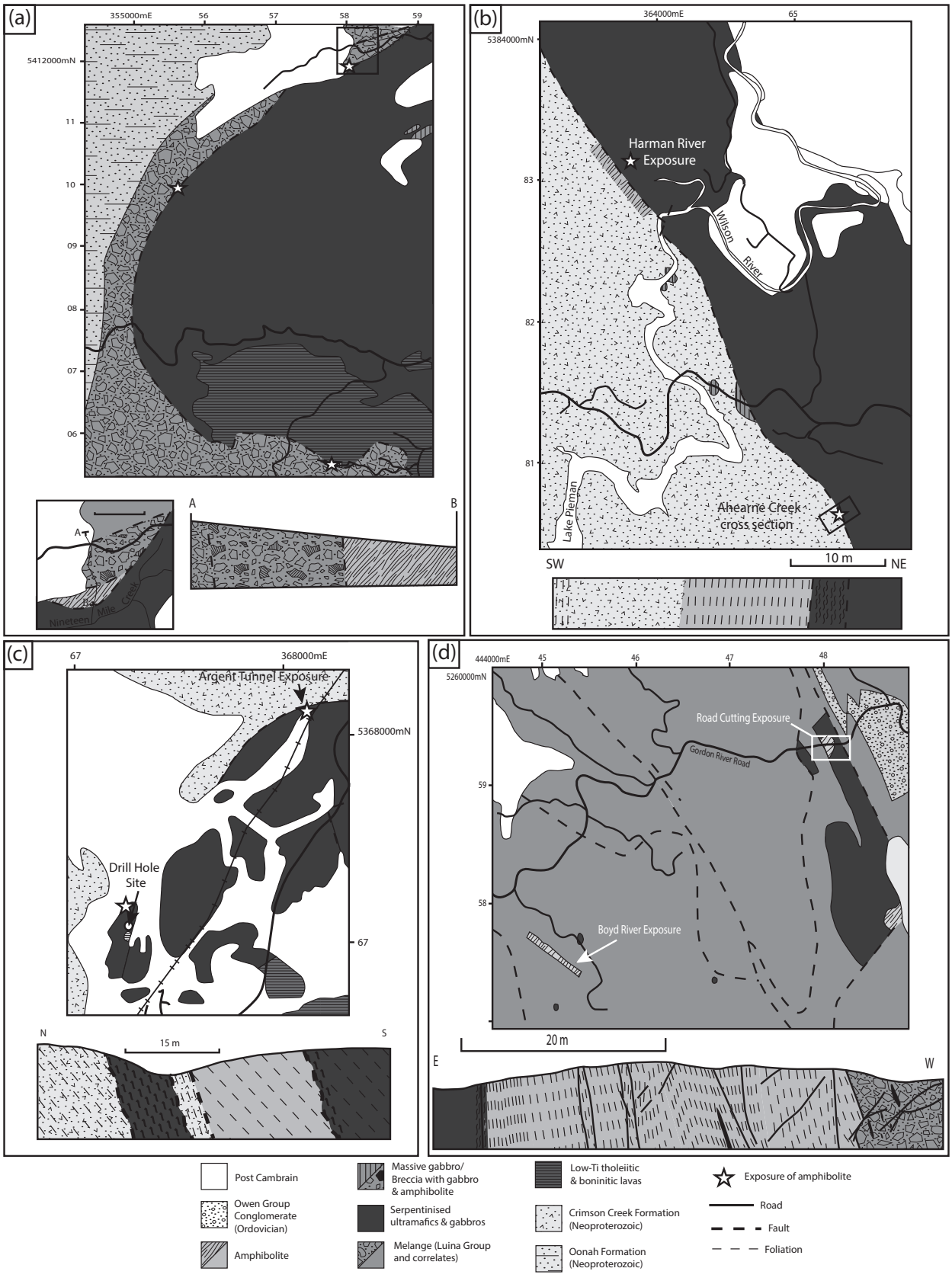

Appendix 6.1: Field maps and cross sections of the metamorphic sole to the western Tasmania ophiolite. (a) Heazlewood River Complex, (b) Wilson River Complex, (c) Serpentine Hill Complex, (d) Gordon River Road exposure (Adamsfield Complex).

Appendix 6.2: Summary of kinematic indicators

The kinematics during formation of the metamorphic sole was investigated using microstructural evidence from orientated thin sections. Thin sections were prepared from orientated samples from each of the metamorphic sole exposures. The thin sections were cut parallel to the dominant stretching lineation and perpendicular to the main foliation. All foliation orientations are presented as dip (two numbers)/dip direction (three numbers) and lineations are presented either a pitch direction on the main foliation surface or as plunge (two numbers) and trend (three numbers). Sense of shear orientations are reported after rotating the schistosity to horizontal and returning the local fold axes to horizontal.

Microstructures used in the kinematic study included: Shearband fabrics (i.e. C-S or C'-S fabrics), Sigma-type porphyroclasts, mineral fish (typically amphibole), and boudinaged crystals. Sense of shear indicators were identified from the opx-ol amphibolites, foliated amphibolites, and the cpx-amphibolites. Sense of shear indicators were identified in multiple samples from each of the metamorphic sole exposures studied. Descriptions of the microstructures and sense of shear are presented below for representative samples from each of the metamorphic sole exposures that show the most unambiguous microstructures.

Gordon River Road

Sample 88SG10 is a representative foliated amphibolite from the exposure of the metamorphic sole along the Gordon River Road that shows well-developed shear bands fabrics and contains abundant sigma-type poprhyroclasts.
The main fabric for this sample is a well-developed schistosity orientated at 78°/215° with a prominent stretching lineation defined by aligned amphibole pitching at 69° north on this surface. Both the sigma-type porphyroclasts and shear band fabrics indicate a top to the northwest sense of shear.

Serpentine Hill

Sample 2SH5 is a foliated amphibolite from the argent tunnel exposure of the metamorphic sole at Serpentine Hill contains sigma-type porphyroblasts locally developed shear band fabrics. A mineral stretching lineation defined by aligned amphibole pitches 40° northeast on the main schistosity in this sample which is orientated at 68°/145°. The sigma-type porphyroclasts and shear band fabrics indicate a top to the southwest sense of shear.

Heazlewod River

Sample H11-2 is a cpx-amphibolite from the Heazlewood River Complex contains common mineral (amphibole) fish and rare boudinaged grains. A strong mineral stretching lineation defined by aligned amphibole pitches 10° east on the surface of the strongly developed schistosity orientated at 85/006. The microstructures in this sample indicate a top to the west sense of shear.

Appendix 6.2: Summary of kinematic indicators

Wilsons River Complex

The only samples from the Wilsons River Complex preserving sense of shear indicators are the nematoblastic hornblendites from the Ahearne Creek exposure of the metamorphic sole. The sense of shear associated with these samples is ambiguous with only sense of shear indicators identified being mineral (amphibole) fish, which in all samples show both dextral (top south) and sinistral (top north) sense of shear. To increase the confidence in the results from this area, all the mineral fish that could be identified were counted in three sections, the results are summarised in table A1.

Table A1: summary of sense of shear indicators from opx-ol amphibolites.

Sample	Orientation of main foliation	Orientation of stretching lineation	Total mineral fish counted	Number of dextral mineral fish	Number of sinistral mineral fish	Interpreted sense of shear
A1 +	87/082	05→172	44	31	14	Top south-southwest
A2	70/264	00→355	100	82	18	Top south
A3	90/076	10→346	78	65	13	Top south-southeast

Mineral fish showing a dextral sense of shear (top south or south-southeast) were dominant in each of the three samples and a top to the south sense of shear is tentatively interpreted for the metamorphic sole from the Wilson River Complex.

Appendix 6.3: Trace element analysis methods - See digital appendix

Appendix 6.4: Amphibolite mineral chemistry - See digital appendix

Appendix 6.5: Assessment of varying H_2O content on P-T pseudosection

Figure A5a shows that the key effect of reducing the water content of sample A5 at 0.65 Gpa is to reduce the stability of chlorite-bearing assemblages. Figure A5a demonstrates that changing the water content for sample A5 at 0.65 Gpa may stabilize the observed peak metamorphic mineral assemblage to lower temperatures (<700°C), however this result is not considered significant as the peak temperatures are constrained to ~800°C by the Al-in-orthopyroxene thermometer.

The T-H2O section for sample H12 (Fig. A5b) shows that garnet- and orthopyroxene-bearing assemblages become stabilized at 0.65 Ga at water-undersaturated conditions. Figure A5b also demonstrates that titanite-bearing fields become unstable across most of the modeled temperature range at 0.65 Gpa. At the preferred peak temperatures for sample H12 (form the hornblende-plagioclase conventional thermometer) of ~800°C, the absence of garnet or orthopyroxene in the observed mineral assemblages argues against water-undersaturated conditions. Although Fig. A5b shows that the water-undersaturated observed peak metamorphic assemblage is stabilized to temperatures <700°C at 0.65 Gpa, we suggest the peak metamorphic temperatures from the hornblende-plagioclase thermometer and the absence of titanite-bearing fields argue against water-undersaturated conditions during peak metamorphism.

Appendix 6.5: Assessment of varying H_2O content on P-T pseudosection

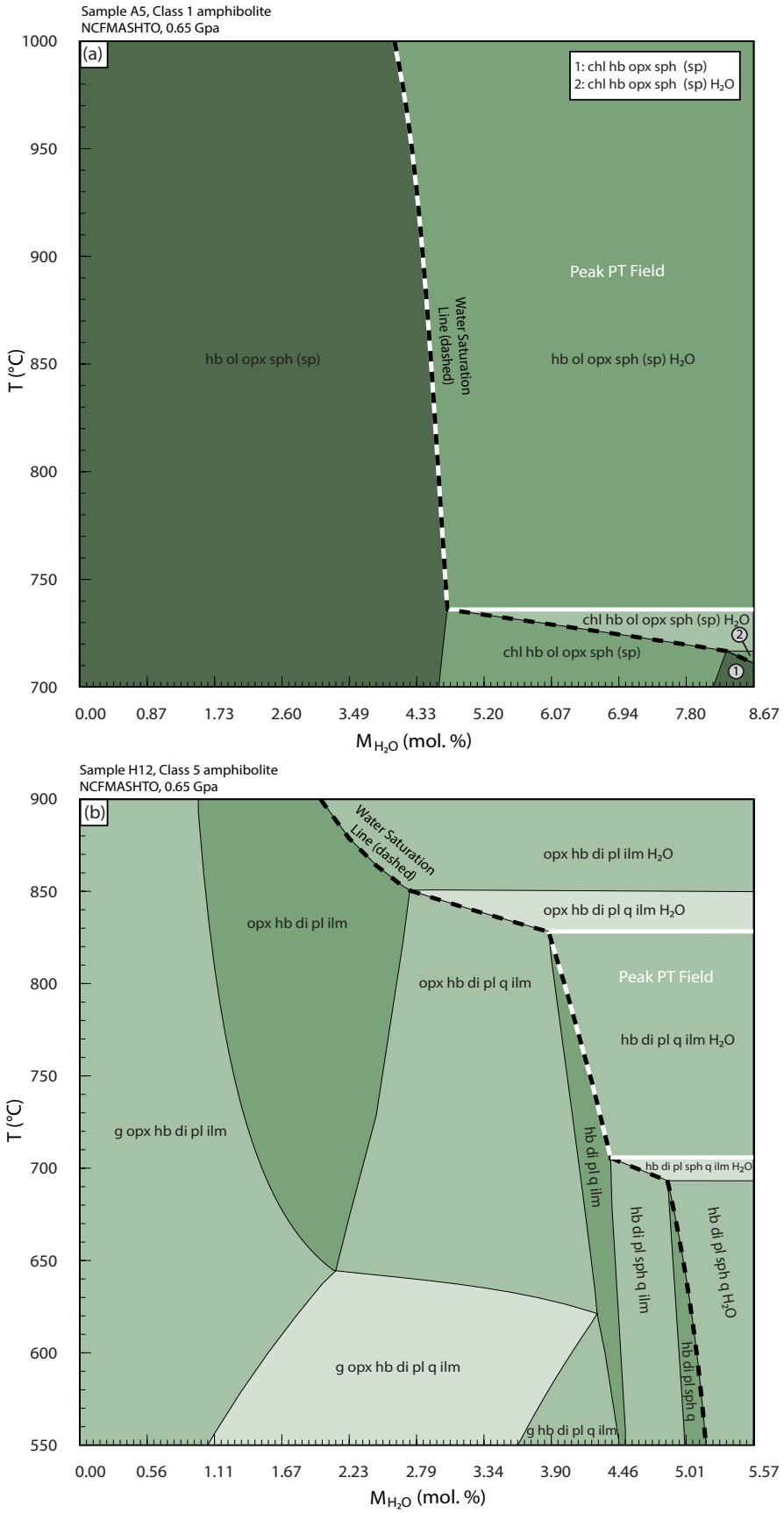

Fig. A5: T-M(H_2O) sections constructed for (a) Sample A5 and (b) Sample H12. Both diagrams contructed at 0.65 GPa across the same temperature range used in the PT pseduosections (Fig. 6.9a and b). Thick solid white line outlines inferred peak PT field (from PT pseudosection) and the thick dashed black line separates water-saturated fields from water-undersaturated fields.

Appendix 6.6: Assessment of varying Fe^{3+} content on P-T pseudosection

Figure A6a

This section demonstrates that altering the Fe^{3+} content used to construct the PT pseudosection for sample A5 (XFe^{3+} = 0.15) does not have a significant effect on the predicted temperature range for the peak metamorphic assemblage. PT pseudosections calculated at variable XFe^{3+} (0.05—0.20, not shown) demonstrate the predicted pressure stability of the peak metamorphic assemblage is also insensitive to changing Fe^{3+} content.

Figure A6b

Figure A6b shows that the peak metamorphic assemblage of sample H12 is shifted to increasing temperatures as XFe^{3+} is increased at 0.65 Gpa. PT pseudosections calculated at variable XFe^{3+} (0.05—0.20, not shown) show that the major effect of altering Fe^{3+} is to shift the position of the quartz-in line separating the amphibole-clinopyroxene-plagioclase-ilmenite and amphibole-clinopyroxene-plagioclase-ilmenite-quartz fields. Reducing the estimated XFe^{3+} by 0.05 acts to shift the quartz-in line up pressure by ~0.5 GPa and *visa versa.* We suggest XFe^{3+} = 0.10 is an appropriate minimum estimate of the ferric iron content of this sample as a lower ferric iron content (e.g. XFe^{3+} = 0.05) would stabilize orthopyroxene, which is not observed at the peak temperatures inferred from the hornblende-plagioclase thermometry results. We note that a maximum estimate for the ferric iron content of sample H12 is poorly constrained, which may result in the predicted P and T conditions for the peak metamorphic assemblage as shown on Fig. 9b to be underestimated.

Appendix 6.6: Assessment of varying Fe^{3+} content on P-T pseudosection

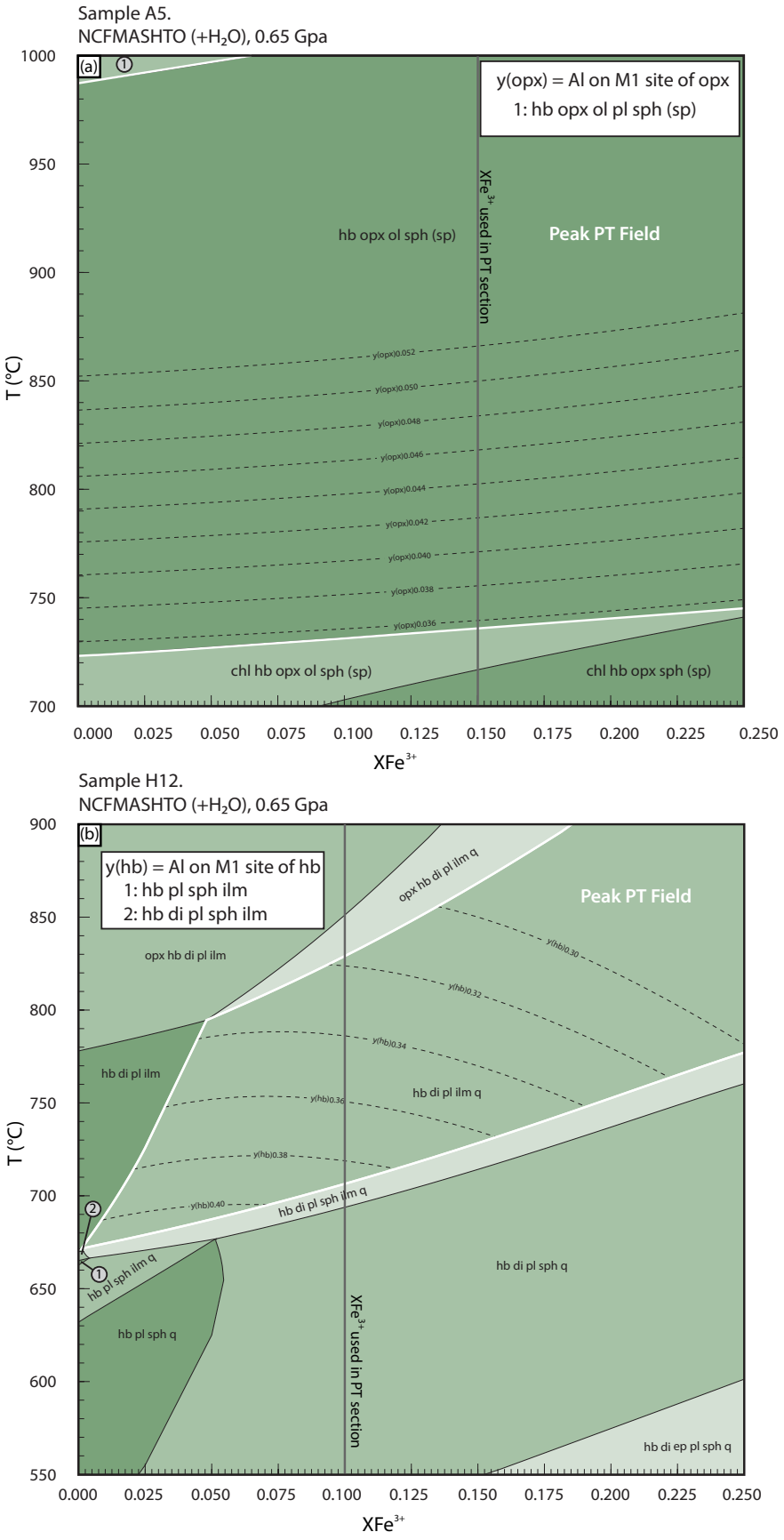

Fig. A6: T-XFe^{3+} sections constructed for (a) Sample A5 and (b) Sample H12. Thick white solid lineoutlines inferred peak PT field (from PT pseudosection). Both samples are calculated at 0.65 GPa with H_2O in excess across the temperature range modeled for the respective pseudosections in Fig. 6.9.

Chapter 7

Synthesis

7.0 Introduction

This study aims to better understand the tectonic setting of Tasmania in the context of the supercontinents Nuna, Rodinia, and Gondwana. Section 7.1 summarises the progress made towards achieving this aim and forms the basis of a new model for the Mesoproterozoic to early Paleozoic evolution of Tasmania presented in Section 7.2 and a discussion of future avenues of research on the Proterozoic of Tasmania in Section 7.3.

7.1 Summary and significance of findings

7.1.1 Chapter 2: Mesoproterozoic Tasmania: Witness to the East Antarctica-Laurentia connection within Nuna

This chapter used the detrital zircon provenance of the 1450—1300 Ma lower-middle Rocky Cape Group to understand the position and tectonic setting of Tasmania in the context of Nuna.

Detrital zircons from the lower-middle Rocky Cape Group form age populations and have Hf isotopic compositions consistent with a provenance in basement terranes of southwest Laurentia and the southern Mawson Continent (East Antarctica). The detrital zircon provenance and basin architecture of the lower-middle Rocky Cape Group are consistent with it representing the east-facing passive margin of the southern Mawson Continent produced during the breakup of Nuna. The position of Tasmania along the margin of the Mawson Continent and the southwest Laurentia provenance of the lower-middle Rocky Cape Group support a southwest Laurentia-East Antarctica (SWEAT) configuration for Nuna.

The rifting history leading to separation of Australia-Antarctica and Laurentia during the break up of Nuna is poorly understood. Pisarevsky et al. (2014a) interpret the northward younging of mafic magmatism from *ca.* 1450 Ma in the Belt-Purcell Group to *ca.* 1380 Ma in the Hart River area to record the progressive south-to-north (present-day coordinates) rifting of Australia-Antarctica from western Laurentia. In contrast, the new data from Tasmania support a connection between southwest Laurentia and East Antarctica during deposition of the lower-middle Rocky Cape Group at 1450—1300 Ma, which implies that the rift separating Australia-Antarctica from western Laurentia during the breakup of Nuna propagated from north-to-south.

7.1.2 Chapter 3: The syn-orogenic sedimentary record of the Grenville Orogeny in southwest Laurentia

This chapter explored the relationship between late Mesoproterozoic intracontinental sedimentation and convergence and collision along the southern margin of Laurentia during the Grenville Orogeny. The new model for late Mesoproterozoic basin formation in southwest Laurentia provides tectonic context for correlative strata of the upper Rocky Cape Group in Tasmania (Chapter 4).

The earliest phase of syn-orogenic sedimentation in southwest Laurentia is recorded in the lower Pahrump and Apache Groups, which are remnants of a 1340—1320 Ma distal back arc basin system that pre-dated the Grenville orogenic cycle. The 1255—1230 Ma lower Unkar Group and correlates represent back arc basin deposits that were sourced in part from a 1280—1230 Ma continental arc along the southern margin of Laurentia prior to continent-continent collision. The overlying disconformable 1150—1100 Ma upper Unkar Group and correlates are distal foreland basin deposits sourced from the structurally high parts of the Grenville orogen during the early stages of continent-continent collision. The Hazel Formation represents the youngest episode of late Mesoproterozoic sedimentation in southwest Laurentia and is a proximal foreland basin that formed during the final continent-continent collisional phase of the Grenville Orogeny.

The late Mesoproterozoic strata in southwest Laurentia preserve similar stratigraphy and detrital zircon provenance across a regionally extensive basin system. This distinctive basin system represents a promising 'piercing point' for refining the paleogeography of Rodinia as it is truncated by the late Neoproterozoic western rift margin of Laurentia and hence could be preserved on formerly adjacent continents.

7.1.3 Chapter 4: Rodinian devil in disguise: Correlation of 1.25—1.10 Ga strata between Tasmania and Grand Canyon

This chapter proposed correlation of the upper Rocky Cape Group with late Mesoproterozoic strata in southwest Laurentia and refined the position of Tasmania within Rodinia.

New detrital zircon data from the upper Rocky Cape Group refine the maximum depositional age of its two disconformity-bound units to <1260 Ma (Irby Siltstone) and <1170 Ma (Jacob Quartzite). Striking similarities in age, stratigraphy, and detrital zircon provenance support correlation of the upper Rocky Cape Group with late Mesoproterozoic strata in southwest Laurentia. This correlation implies that the upper Rocky Cape Group was a part of the extensive syn-orogenic basin system that developed inboard of the Grenville orogen and supports a late Mesoproterozoic position for Tasmania along the southwest margin of Laurentia. East-directed paleocurrents in the Jacob Quartzite show that the upper Rocky Cape Group was sourced in part from terranes west of Laurentia. A concealed late Mesoproterozoic orogen in the central Transantarctic Mountains (East Antarctica) has a similar detrital zircon age signature to the upper Rocky Cape Group and is interpreted to be

the westerly source of Jacob Quartzite. The late Mesoproterozoic position of Tasmania along the southwest margin of Laurentia and the East Antarctic provenance of the upper Rocky Cape Group support a SWEAT connection within Rodinia at *ca.* 1150 Ma. The connection between southwest Laurentia, Tasmania, and East Antarctica within Rodinia is very similar to the configuration of these blocks within Nuna (Section 7.1.1).

7.1.4 Chapter 5: Depositional age and correlation of the Oonah Formation: Refining the timing of late Neoproterozoic basin formation in Tasmania

This chapter refined the depositional age of the enigmatic Oonah Formation and explored its relationship to Proterozoic sequences in Tasmania and on continents adjacent to Tasmania within Rodinia.

New U-Pb dates from syn-sedimentary mafic volcanic rocks and detrital zircon and detrital monazite from turbiditic strata refine the deposition age of Oonah Formation to *ca.* 730 Ma. Correlation of the Oonah Formation and lower Togari Group in western Tasmania is supported by similarities in age and detrital zircon provenance. The Oonah Formation and lower Togari Group were deposited during failed continental rifting between 780—640 Ma and are correlated with parts of the Pahrump Group in southwest Laurentia on the basis of similar stratigraphy, carbon isotope chemostratigraphy, and detrital zircon provenance. This correlation, together with broad similarities in age and detrital zircon provenance of the Oonah Formation-lower Togari Group to the Cobham Formation in the central Transantarctic Mountains, support a late Neoproterozoic position for Tasmania between southwest Laurentia and East Antarctica during the early stages of Rodinia breakup.

The timing of final separation of Australia-Antarctica from western Laurentia during the breakup of Rodinia is controversial. Paleomagnetic data imply breakup of a SWEAT configuration for Rodinia by 650 Ma (Li & Evans, 2011). However, the tectonostratigraphic record of western Laurentia shows that final continental rifting and developement of a passive margin occurred after 580 Ma (e.g., Yonkee et al., 2014). Tasmania's position between Australia-Antarctica and western Laurentia makes it as a key location for better understanding the breakup history of Rodinia. The late Neoproterozoic evolution of Tasmania is characterised by failed continental rifting at 780—640 Ma, which was followed by a major rift event at *ca.* 580 Ma that likely represents the separation of Tasmania form surrounding continents. The late Neoproterozoic tectonostratigraphic record of Tasmania is similar to that of the western margin of Laurentia and supports final separation of Tasmania from surrounding continents after *ca.* 580 Ma.

7.1.5 Chapter 6: The metamorphic sole of the western Tasmanian ophiolite: New insights into the Cambrian tectonic setting of the Gondwana Pacific margin

This chapter developed a new model for the formation and emplacement of an ophiolite in Tasmania during the middle Cambrian Tyennan Orogeny and explored the wider tectonic setting in which the Tasmanian microcontinent was incorporated into Gondwana.

Integrated field mapping, metamorphic phase equilibria modelling, and microstructural analysis of the high-grade metamorphic sole of the Tasmanian ophiolite show that it formed in an east-dipping subduction zone to the east of Tasmania. Based on the geochemistry of the metamorphic sole, this east dipping subduction zone initiated during the collapse of a back arc basin. This back arc basin is interpreted to have formed inboard of the west-dipping subduction zone active along the Pacific margin of Gondwana in the latest Neoproterozoic to Cambrian. The early Paleozoic tectonic evolution of Tasmania demonstrates that a complex geodynamic setting analogous to the modern southwest Pacific had developed along the Pacific margin of Gondwana following the breakup of Rodinia.

7.2 From Nuna to Gondwana: A new model for the early tectonic evolution of Tasmania

The key findings of this study are integrated into a new model for the tectonic evolution of Tasmania between the Mesoproterozoic and early Paleozoic, which is outlined below and summarised in Figures 7.1—7.3.

The oldest geological event recorded in Tasmania is the deposition of the lower-middle Rocky Cape Group between 1450 and 1300 Ma (Fig. 7.1A). The lower-middle Rocky Cape Group was deposited in one of a series of basins throughout eastern Australia-Antarctica and western Laurentia between 1500 and 1300 Ma during the breakup of Nuna (e.g., Betts & Giles 2006; Jones et al., 2015). The lower-middle Rocky Cape Group initiated within an intracontinental basin during regional extension between southwest Laurentia and East Antarctica and may have evolved into a passive margin as a north-to-south-propagating rift system separated Australia-Antarctica from western Laurentia (Fig. 7.1A). Paleomagnetic data suggest that Australia-Antarctica and western Laurentia were widely separated by *ca.* 1200 Ma (Pisarevksy et al., 2014b), which marks the end of the Nuna supercontinent cycle (Fig. 7.1B). Following the breakup of Nuna, two locations for Tasmania are consistent with the geology of the Rocky Cape Group. Tasmania either (1) formed part of the southern Mawson Continent (East Antarctica), which is consistent with the interpretation of the lower-middle Rocky Cape Group as an east-facing passive margin (Fig. 7.1B), or (2) remained part of the southwest margin of Laurentia, which is supported by correlation of the upper Rocky Cape Group with late Mesoproterozoic strata in southwest Laurentia.

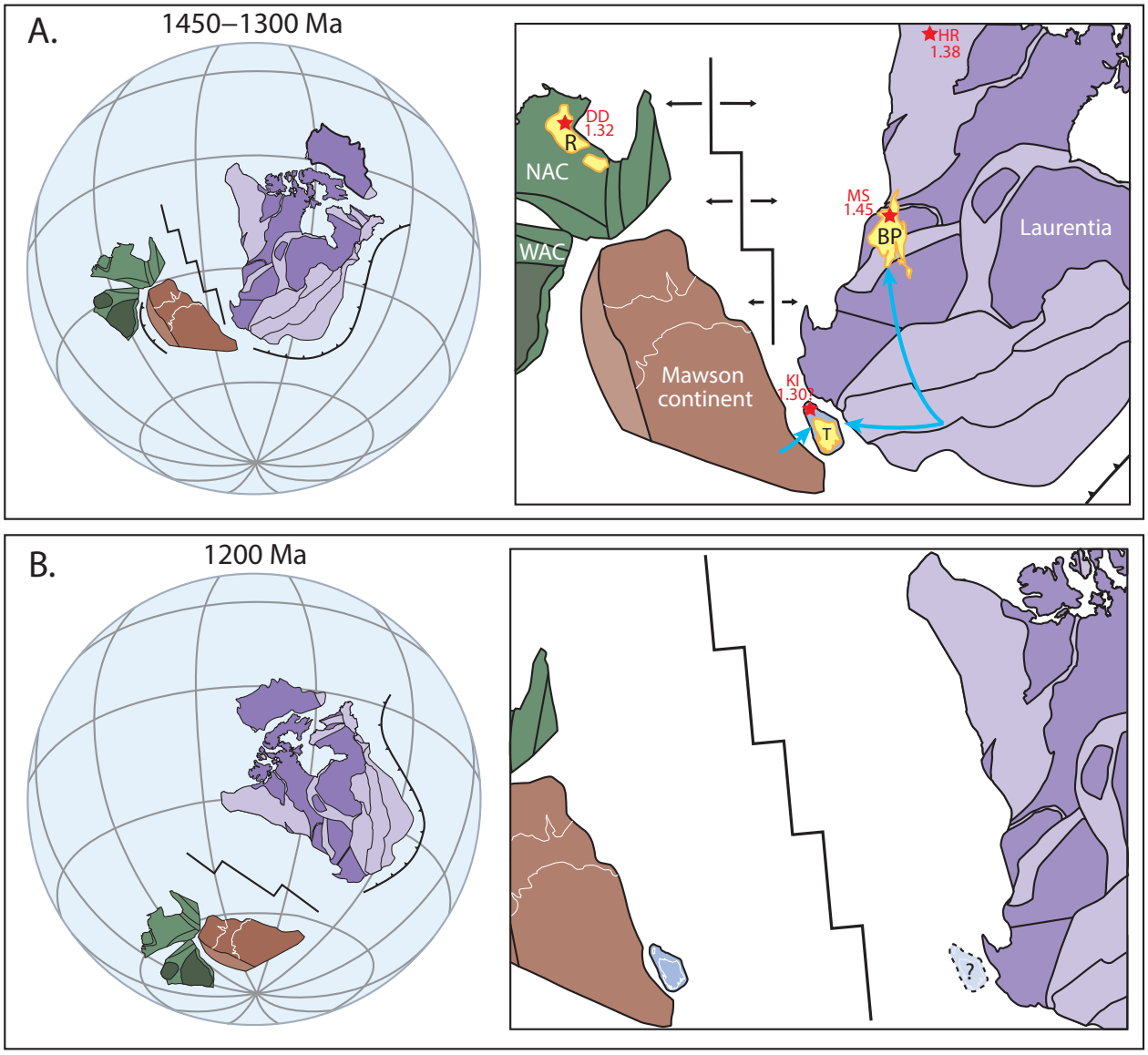

Figure 7.1: Paleogeographic context and tectonic model for the evolution of Tasmania during the breakup of Nuna. Reconstructions on the left show paleomagnetically-constrained positions of Australia-Antarctica and Laurentia. Panels on the right show more detail of the tectonic setting of Tasmania with geology of Australia-Antarctica from Aitken et al. (2016) and Laurentia from Whitmeyer and Karlstrom (2007).

(A) Reconstruction for 1450—1300 Ma. The lower-middle Rocky Cape Group forms in an extensional basin between the southern Mawson Continent and southwest Laurentia as a north-to-south-propagating rift separates Australia-Antarctica from western Laurentia during the breakup of Nuna. Sedimentary basins that are time-equivalent to the lower-middle Rocky Cape Group (T) include the Roper Group (R) and upper Belt-Purcell Group (BP). Blue arrows show sediment transport directions into lower-middle Rocky Cape Group. Mafic magmatism possibly associated with the breakup of Nuna is marked with red stars with age (in Ga) and includes the Derim Derim Dolerite (DD), Hart River Sill (HR), Moyie Sills (MS), and dolerite dykes on King Island (KI). WAC—West Australia Craton; NAC—North Australia Craton. Paleomagnetically-constrained reconstruction from Pisarevsky et al. (2014a).

(B) Reconstruction for 1200 Ma showing the complete separation of Australia-Antarctica from western Laurentia marking the end of the Nuna supercontinent cycle. Tasmania is either located along the eastern margin of the Mawson Continent or the southwestern margin of Laurentia. Paleomagnetically-constrained reconstruction from Pisarevsky et al. (2014b).

The tectonic evolution of Tasmania during the transition from Nuna to Rodinia remains uncertain. Geological and paleomagnetic data are consistent with a SWEAT configuration for both Nuna and Rodinia. A comparison of paleomagnetic poles from Australia and Laurentia implies a complex interaction between these continents between their wide separation at *ca.* 1200 Ma until *ca.* 750 Ma when a SWEAT configuration had been reestablished (Li & Evans, 2011; Pisarevksy et al., 2014b). The provenance of the Rocky Cape Group demonstrates that Tasmania was located between southwest Laurentia and East Antarctica during the breakup of Nuna at 1450—1300 Ma and occupied a similar position during the assembly of Rodinia at *ca.* 1250—1150 Ma. The affinity of the late Neoproterozoic geology of Tasmania to southwest Laurentia and East Antarctica further strengthens the ties between these three blocks within an assembled Rodinia. There is little evidence for regional orogenesis in Tasmania that could reflect the closure of a major ocean basin separating southwest Laurentia and East Antarctica between 1200 Ma and 750 Ma as implied by paleomagnetic data. The closure of such an ocean basin could have been accommodated by an orogenic belt adjacent to Tasmania such as the Jiangnan orogen of South China, which may record Mesoproterozoic to early Neoproterozoic convergence between Australia-Antarctica and western Laurentia (e.g., Li et al., 1995, 2002, 2008; Yao et al., 2017, but see Cawood et al., 2013 for a different interpretation). An alternative hypothesis is that southwest Laurentia and East Antarctic blocks failed to separate during the breakup of Nuna with the SWEAT connection persisting into Rodinia.

Regardless of the model favoured for the Nuna—Rodinia transition, by the late Mesoproterozoic Tasmania was located in the foreland of an orogenic belt developed along the southern margin of Laurentia and continuing into East Antarctica (Fig. 7.2A). The shallow marine carbonate-shale sequences of the Irby Siltstone (upper Rocky Cape Group) in Tasmania were deposited in an extensive continental back arc basin system developed above a north-dipping subduction zone to the south. Continent-continent collision along the Grenville orogen and its extension into East Antarctica resulted in the deposition of distal foreland basin deposits of the Jacob Quartzite at *ca.* 1150 Ma (Fig. 7.2A). Following the assembly of Rodinia, Tasmania was located in a tectonically stable environment within the core of the supercontinent.

The early stages of the breakup of Rodinia are recorded in Tasmania by the emplacement of anorogenic granites on King Island between 780—750 Ma. As breakup proceeded, Tasmania occupied a broad rift zone between Australia-Antarctica and western Laurentia (Fig. 7.2B). Basin formation and mafic volcanism in Tasmania at 730—640 Ma reflects minor lithospheric extension and is interpreted to represent a failed rift event. Continental rifting in Tasmania at *ca.* 580 Ma records the separation of Tasmania from southwest Laurentia and East Antarctica and its isolation as a microcontinent in the paleo-Pacific Ocean (Fig. 7.3A). Between the latest Neoproterozoic and late Cambrian, the Tasmanian microcontinent occupied a complex geodynamic setting outboard of the Pacific margin of Gondwana in which it collided with an intraoceanic island arc before eventually being accreted onto the margin of southeast Australia (Fig. 7.3B).

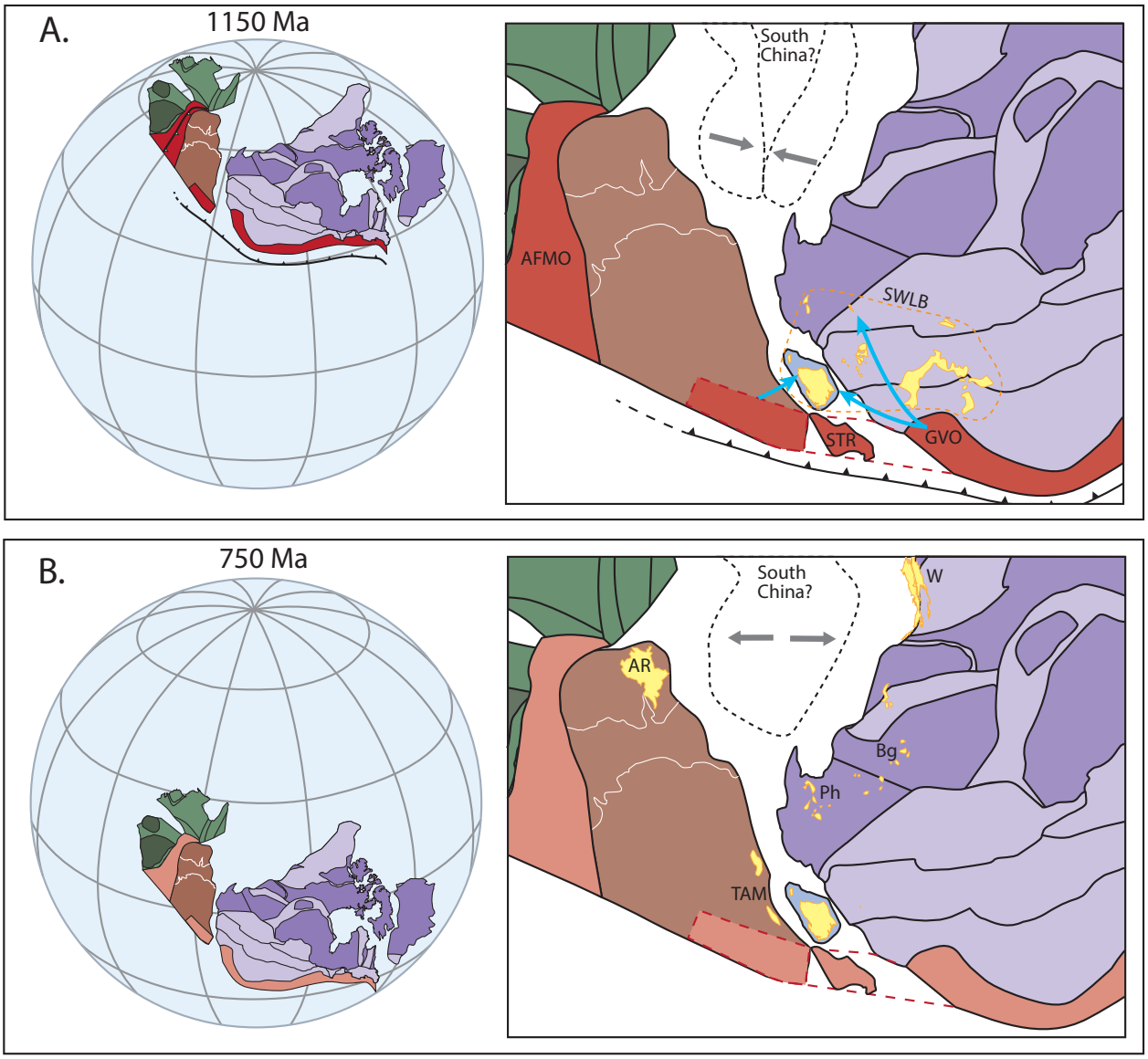

Figure 7.2: Paleogeographic context and tectonic model for the evolution of Tasmania during the assembly and breakup of Rodinia. Reconstructions on the left show paleomagnetically-constrained positions of Australia-Antarctica and Laurentia. Panels on the right show more detail of the tectonic setting of Tasmania with geology of Australia-Antarctica from Aitken et al. (2016) and Preiss (2000) and Laurentia from Whitmeyer and Karlstrom (2007) and Yonkee et al. (2014).

(A) Reconstruction for 1150 Ma. Tasmania is located in the foreland of the Grenville orogen in southern Laurentia and its extension into East Antarctica. Blue arrows show transport of sediment into the syn-orogenic upper Rocky Cape Group. SWLB—southwest Laurentian syn-orogenic basin system, GVO—Grenville orogen, STR—South Tasman Rise, AFMO— Albany-Fraser-Musgrave orogen. Paleomagnetically-constrained reconstruction from Pisarevsky et al. (2014b).

(B) Reconstruction for 750 Ma. Late Neoproterozoic basins in Tasmania, Transantarctic Mountains (TAM), Adelaide Rift Complex (AR), Windemere Supergroup (W), Brigham Group and correlates (Bg), and Pahrump Group (Ph) record the early stages of Rodinia breakup. Paleomagnetically-constrained reconstruction from Li and Evans (2011).

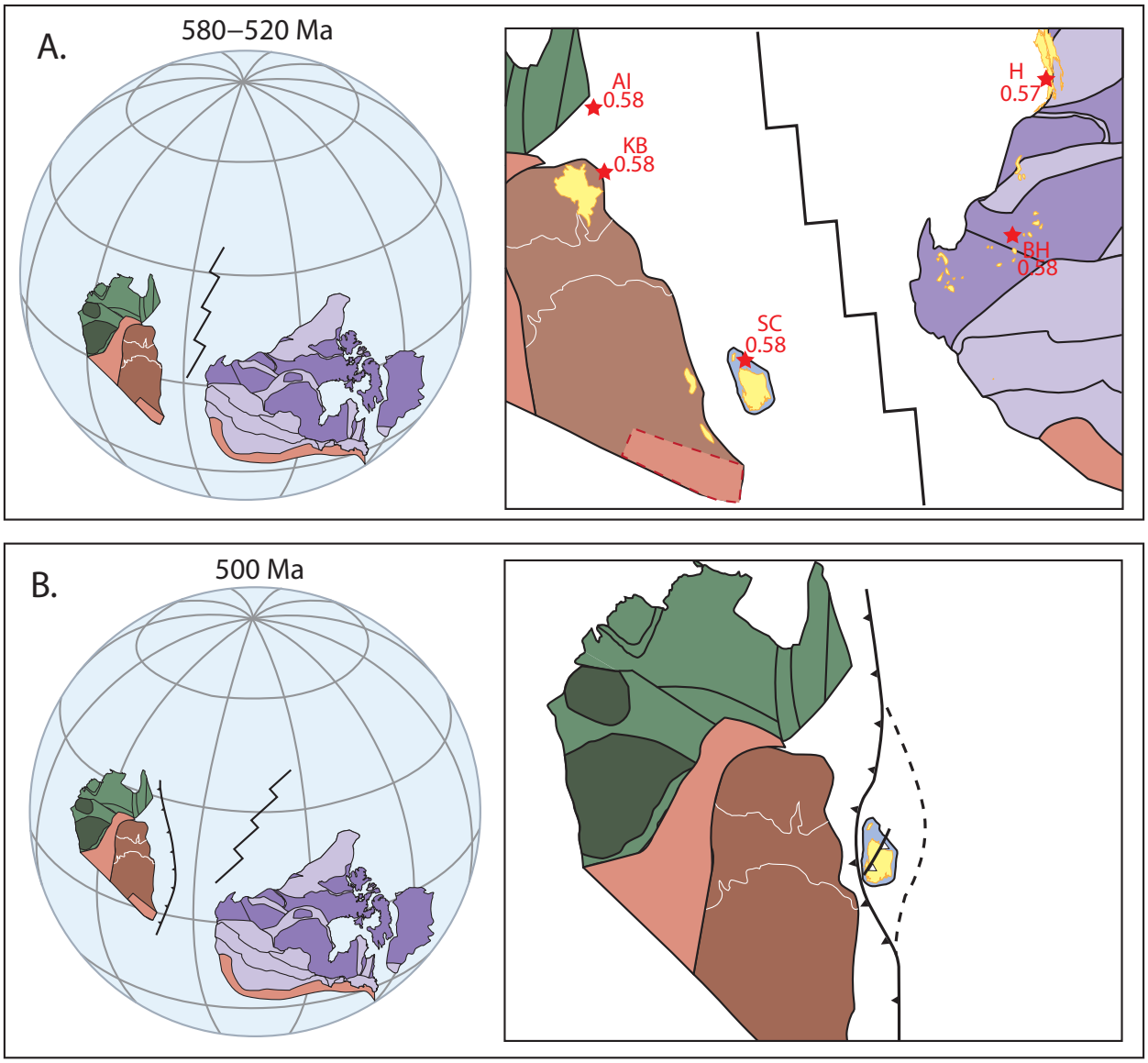

Figure 7.3: Paleogeographic context and tectonic model for the evolution of Tasmania during the final breakup of Rodinia and the assembly of Gondwana. Reconstructions on the left show paleomagnetically-constrained positions of Australia-Antarctica and Laurentia. Panels on the right show more detail of the tectonic setting of Tasmania with geology of Australia-Antarctica from Aitken et al. (2016), Preiss (2000) and Laurentia from Whitmeyer and Karlstrom (2007) and Yonkee et al. (2014).

(A) Reconstruction for 580—520 Ma showing final break up of Rodinia. Tasmania is isolated as a microcontinent in the paleo-Pacific Ocean outboard of the margin of East Gondwana. Mafic magmatism interpreted to mark final breakup shown as red stars with age (in Ga) and includes Anakie Inlier (AI), Koonenberry Belt (KB), Spinks Creek Volcanics and correlatives (SC), Browns Hole Formation (BH), Hamil Group (H). Paleomagnetically-constrained reconstruction from Merdith et al. (2017).

(B) Reconstruction for 500 Ma. Tasmanian microcontinent collides with intraoceanic island arc and is subsequently accreted onto the Pacific margin of Gondwana. Dashed line to the right of Tasmania shows approximate position of west-dipping subduction zone prior to Tyennan Orogeny. Solid line with open triangles marks limit of ophiolite obduction associated with an east-dipping subduction zone to the east of Tasmania. Paleomagnetically-constrained reconstruction from Merdith et al. (2017).

7.3 Future Research

This study presents the first tectonic model for the Mesoproterozoic to early Paleozoic evolution of Tasmania within the paleogeographic framework of the supercontinents Nuna, Rodinia, and Gondwana. Although significant progress has been made towards refining the age, stratigraphy, and tectonic setting of Tasmania's Proterozoic rocks, further work is required to test the new model for the early tectonic evolution of Tasmania. Key questions arising from this study that could test the new model and warrant further research include:

(1) What is the basement to Tasmania?

The unexposed basement to the Rocky Cape Group is assumed to be Paleoproterozoic on the basis of 1800—1600 Ma Nd model ages calculated from late Neoproterozoic to Cambrian intrusive rocks in western Tasmania (Meffre et al., 2004; Berry et al., 2008). A promising opportunity to directly date Tasmania's basement is presented by gneissic and granitic xenoliths entrained in Tertiary basalts throughout the state (Everard, 2001), which may represent fragments of the lower crust. Understanding the age of Tasmania's basement would significantly improve the constraints on its Proterozoic position along the margin of Laurentia where the distribution of basement provinces is relatively well established (e.g., Whitmeyer & Karlstrom, 2007).

(2) Was rifting between East Antarctica and southwest Laurentia during the breakup of Nuna successful?

The geological record of Tasmania is consistent with a connection between East Antarctica and southwest Laurentia between the middle Mesoproterozoic and late Neoproterozoic. However, there is little evidence in Tasmania for the closure of a major ocean basin between these continents implied by paleomagnetic data during the late Mesoproterozoic Nuna to Rodinia transition. A persistent connection between East Antarctica and southwest Laurentia during the transition from Nuna to Rodinia could be further tested by:

(A) Additional high-quality paleomagnetic data from Australia-Antarctica between 1500 and 1000 Ma, particularly from the Mawson Continent, which is paleomagnetically unconstrained during this interval.

(B) A detailed study of the architecture of the 1450—1300 Ma basin in Tasmania. The lower-middle Rocky Cape Group can be interpreted as an east-facing passive margin based on the distribution of sedimentary facies and paleocurrent information. However, the distribution of sedimentary facies in the lower-middle Rocky Cape Group may reflect the geometry of a sub-basin within a larger basin system. Understanding the relationship of strata correlative with the lower-middle Rocky Cape Group on King Island and in the Tyennan Region and Clark Group of southwest Tasmania could

help resolve the geometry of the 1450—1300 Ma basin in Tasmania and test its interpretation as an east-facing passive margin produced during the breakup of Nuna.

(3) What is the tectonic setting of Mesoproterozoic metamorphism on King Island and early Neoproterozoic metamorphism on the South Tasman Rise?

Middle Mesoproterozoic (*ca.* 1290 Ma) and early Neoproterozoic (*ca.* 920 Ma) metamorphic rocks on King Island and the South Tasman Rise respectively have been interpreted as fragments of orogenic belts related to the assembly of Rodinia (Fioretti et al., 2005; Berry et al., 2005; Li et al., 2008). These interpretations are based largely on the age of these metamorphic rocks, which overlap with Rodinia-forming orogens globally. However, a detailed study of the pressure-temperature-time history of these metamorphic events is required to demonstrate that they record collisional processes. A better understanding of the regional tectonic setting of late Mesoproterozoic (1120—1050 Ma) magmatic rocks from the South Tasman Rise could also be achieved through a detailed geochemical study including Hf isotopic analysis of zircon, which would help to clarify whether these rocks formed in an arc, collisional, or anorogenic environment. Further work towards understanding these Mesoproterozoic and early Neoproterozoic metamorphic and magmatic events could provide further insight into the position and wider tectonic setting of Tasmania during the transition from Nuna to Rodinia.

(4) Was late Neoproterozoic rifting in Tasmania progressive or sequential?

Late Neoproterozoic rifting in Tasmania is interpreted in this study to be a progressive event that initiated at 780 Ma and led to continental breakup at *ca.* 580 Ma as Australia-Antarctica separated from western Laurentia. The late Neoproterozoic evolution of Tasmania may instead reflect two distinct rift-drift events, with early rifting at 780—640 Ma recording separation of Australia-Antarctica from western Laurentia (e.g., Li & Evans, 2011) and later rifting at *ca.* 580 Ma reflecting the separation of Tasmania from either Australia-Antarctica of Laurentia. A key test of the progressive versus sequential rifting models for the late Neoproterozoic separation of Australia-Antarctica from western Laurentia would be to identify rift-related activity in Tasmania at 640—580 Ma. Plausible targets include mafic lava flows in the Robbins Creek Formation that underlie 580 Ma basalts in the Grassy Group, volcaniclastic units in the Success Creek and Crimson Creek Groups, and the numerous Proterozoic mafic dyke suites in northwest Tasmania, which are mostly undated. Refining the duration of late Neoproterozoic rifting in Tasmania would provide important constraints on the timing of final separation of Australia-Antarctica from western Laurentia and a better understanding of the tectonic evolution of Tasmania during the transition from Rodinia to Gondwana.

7.4 References

Aitken, A. R. A., Betts, P. G., Young, D. A., Blankenship, D. D., Roberts, J. L., and Siegert, M. J., 2015. The Australo-Antarctic Columbia to Gondwana transition. Gondwana Research, v. 29, 136–152.

Betts, P. G., and Giles, D., 2006. The 1800—1100 Ma tectonic evolution of Australia. Precambrian Research, v.144, 92—125.

Berry, R. F., Holm, O. H., and Steele, D. A., 2005. Chemical U-Th-Pb monazite dating and the Proterozoic history of King Island, southeast Australia. Australian Journal of Earth Science, v. 52, 461–471.

Berry, R. F., Steele, D. A., and Meffre, S., 2008. Proterozoic metamorphism in Tasmania: implications for tectonic reconstructions. Precambrian Research, v. 166, 387–396.

Cawood, P. A., Wang, Y., Xu, Y., Zhao, G., 2013, Locating South China in Rodinia and Gondwana: A fragment of greater India lithosphere? Geology, v. 41, 903–906.

Everard, J. L., 2001: inclusions of high pressure origin in Tasmanian Cenozoic basalts: A catalogue of localities. Tasmanian Geological Record 2001/9.

Fioretti, A. M., Black, L. P., Foden, J., and Visonà, D., 2005. Grenville-age magmatism at the South Tasman Rise (Australia): a new piercing point for the reconstruction of Rodinia. Geology, v. 33, 769–772.

Jones, J. V., Daniel, C. G., and Doe, M. F., 2015. Tectonic and sedimentary linkages between the Belt-Purcell basin and southwestern Laurentia during the Mesoproterozoic, ca. 1.60–1.40 Ga. Lithosphere, v. 7, 465–472.

Li, Z. -X., and Evans, D. A. D., 2011. Late neoproterozoic 40° intraplate rotation within Australia allows for a tighter-fitting and longer-lasting Rodinia. Geology, v. 39, 39–42.

Li, Z. -X., Zhang, L., and Powell, C. McA., 1995. South China in Rodinia: Part of the missing link be- tween Australia–East Antarctica and Laurentia? Geology, v. 23, 407–410.

Li, Z. -X., Li, X. H., Zhou, H., and Kinny, P. D., 2002. Grenvillian continental collision in south China: New SHRIMP U-Pb zircon results and implications for the configuration of Rodinia: Geology, v. 30, 163–166.

Li, Z. -X., Bogdanova, S. V., Collins, A. S., Davidson, A., De Waele, B., Ernst, R. E., Fitzsimons, I. C. W., Fuck, R. A., Gladkochub, D. P., Jacobs, J., Karlstrom, K. E., Lu, S., Natapov, L. M., Pease, V., Pisarevsky, S. A., Thrane, K., and Vernikovsky, V., 2008. Assembly, configuration, and break-up history of Rodinia: a synthesis. Precambrian Research v. 160, 179–210.

Meffre, S., Direen, N. G., Crawford, A. J., and Kamenetsky, V., 2004. Mafic volcanic rocks on King Island, Tasmania: evidence for 579 Ma break-up in East Gondwana. Precambrian Research, v. 135, 177–191.

Merdith, A. S., Collins, A. S., Williams, S. E., Pisarevsky, S., Foden, J. D., Archibald, D. B., Blades, M. L., Alessio, B. L., Armistead, S., Plavsa, D., Clark. C., Müller, R. D., 2017. A full-plate global reconstruction of the Neoproterozoic. Gondwana Research, In Press.

Pisarevsky, S. A., Elming, S. Å., Pesonen, L. J., and Li, Z. -X., 2014a. Mesoproterozoic paleogeography: supercontinent and beyond. Precambrian Research, v. 244, 207–225.

Pisarevsky, S. A., Wingate, M. T. D., Li, Z. -X., Wang, X. C., Tohver, E., and Kirkland, C. L., 2014b. Age and paleomagnetism of the 1210 Ma Gnowangerup–Fraser dyke swarm, Western Australia, and implications for late Mesoproterozoic paleogeography. Precambrian Research, v. 246, 1–15.

Preiss, W. V., 2000. The Adelaide Geosyncline of South Australia and its significance in Neoproterozoic continental reconstruction. Precambrian Research, v.100, 21–63

Whitmeyer, S. J., and Karlstrom, K. E., 2007. Tectonic model for the Proterozoic growth of North America. Geosphere, v. 3, 220–259.

Yao, W., Li, Z. -X., Li, W. X., and Li, X. H., 2017. Proterozoic tectonics of Hainan Island in supercontinent cycles: New insights from geochronological and isotopic results. Precambrian Research, v. 290, 86–100.

Yonkee, W. A., Dehler, C. M., Link, P. K., Balgord, E. A., Keeley, J., Hayes, D. S., Fanning, C. M., Wells, M. L., and Johnston, S. M., 2014. Tectono-stratigraphic framework of Neoproterozoic to Cambrian strata, west-central U.S.: Protracted rifting, glaciation, and evolution of the North American Cordilleran margin: Earth-Science Reviews, v. 136, 59–95.